

Printed May 1985

Compatibility of Refractory Metals with Sodium in the Presence of Oxygen and UO_2

Frank J. Zanner, William F. Hammett, John E. Gronager,
William A. Averill, Roy C. Feber

Prepared by
Sandia National Laboratories
Albuquerque, New Mexico 87185 and Livermore, California 94550
for the United States Department of Energy
under Contract DE-AC04-76DP00789



Issued by Sandia National Laboratories, operated for the United States Department of Energy by Sandia Corporation.

NOTICE: This report was prepared as an account of work sponsored by an agency of the United States Government. Neither the United States Government nor any agency thereof, nor any of their employees, nor any of their contractors, subcontractors, or their employees, makes any warranty, express or implied, or assumes any legal liability or responsibility for the accuracy, completeness, or usefulness of any information, apparatus, product, or process disclosed, or represents that its use would not infringe privately owned rights. Reference herein to any specific commercial product, process, or service by trade name, trademark, manufacturer, or otherwise, does not necessarily constitute or imply its endorsement, recommendation, or favoring by the United States Government, any agency thereof or any of their contractors or subcontractors. The views and opinions expressed herein do not necessarily state or reflect those of the United States Government, any agency thereof or any of their contractors or subcontractors.

Printed in the United States of America
Available from
National Technical Information Service
U.S. Department of Commerce
5285 Port Royal Road
Springfield, VA 22161

NTIS price codes
Printed copy: A12
Microfiche copy: A01

SAND85-0850
Unlimited Release
Printed April 1985

Distribution
Category UC-25

Compatibility of Refractory Metals With
Sodium in the Presence of Oxygen and UO_2^*

Frank J. Zanner
Process Metallurgy Division

William F. Hammetter
Inorganic Materials Chemistry Division

John E. Gronager
Severe Accident Source Terms Division

William A. Averill
Battery Development Division

Sandia National Laboratories
Albuquerque, NM 87185

Roy C. Feber
Materials Science and Technology Division
Los Alamos National Laboratories
Los Alamos, NM 87545

*This work was supported by the United States Nuclear Regulatory Commission; the Joint Research Centre Euratom, Ispra Establishment; and the Japanese Power Reactor and Nuclear Fuel Development Corporation, and performed at Sandia National Laboratories which is operated for the United States Department of Energy under contract number DE-AC04-76DP00789.

Intentionally Left Blank

Abstract

Compatibility of Ta-10W, Ta-8W-2Hf, Mo, Mo-13Re, Mo-26Re, Mo-41Re, TZM, Re, and Re-5W alloys with Na and UO_2 were studied in two temperature regimes. In the first regime Yates order experiments with three independent variables $300 \leq T \leq 800^\circ C$, $10 \leq t \leq 130$ hours, and $2 \leq [O] \leq 100$ ppmw oxygen potentials in Na were used to evaluate responses such as ultimate tensile strength, fracture energy, weight gain, and hardness. Samples were exposed to Na in individual crucibles with a fixed amount of oxygen. In the second regime, $\sim 600 \leq T \leq 2000^\circ C$, tubes fabricated from the refractory alloys were loaded with UO_2 and Na containing 400 ppmw [O]. The bottom of the tube was heated to $2000^\circ C$ and the top was allowed to cool naturally. A reflux condition was created in the tube and gradients approaching $250^\circ C/cm$ were obtained on the walls of the tube.

All of the materials were found to be compatible with Na in the low temperature regime and Ta-10W, Ta-8W-2Hf, and Mo-41Re were found to be compatible in the high temperature regime. Re and Re-5W exhibited grain boundary failure when subjected to the high temperature test conditions. Re additions were found to enhance the tensile properties of Mo but did not significantly improve the fracture toughness as inferred from the fractography. The mechanical properties of the Ta alloys were found to be very sensitive to the impurities in the Na. Fracture initiation was found to control the tensile ductility and fracture energy (defined as the area under the load-displacement curve of the tensile test divided by the original area at the root of the notches) of the Mo, Mo-Re, and Re alloys.

Intentionally Left Blank

Acknowledgments

A project of this magnitude requires the assistance of many people and the integration of many services. A large number of personnel at SNLA and LANL were involved at one time or another in the completion of this work and the authors are grateful for their efforts.

The authors are particularly grateful for the assistance of R. W. Fisher, J. P. Maroone, C. Robertson, and A. Netz (all SNLA), who together served as the nucleus and were involved in all phases of the coordination and execution of this work.

In addition, significant contributions were made by C. Hills (SNLA): TEM; M. Sturm (SNLA): SEM; P. Hatch (SNLA): mechanical testing; S. Weissman, M. Gonzales, S. Hallett, and R. Bild (all SNLA): analytical chemistry; M. McAllister and M. Yost (all SNLA): metallography; D. Hull (LANL): induction heating; and D. Hoffman and V. Sandoval (all LANL): assistance with the high temperature tests.

J. Van Den Avyle, F. Braaten, D. Powers (all SNLA), and J. Weeks, (Brookhaven National Laboratory) deserve special acknowledgment for the support that they provided with fractography, crucible fabrication, thermodynamics, and technical assistance, respectively.

Lastly, supervisory personnel including N. Magnani, J. Walker, M. Davis, R. Whan, J. Jellison, T. Schmidt, R. Quinn, P. Conlon, and N. Brown (all SNLA) provided assistance in the allocation of personnel and resources.

Intentionally Left Blank

Contents

	<u>Page</u>
Introduction	25
Experimental	28
Low Temperature Regime	29
Experimental Details	29
Material Evaluation	38
Mechanical Properties	38
Microstructural Properties	39
Physical Properties	39
Statistical Analysis Techniques	40
High Temperature Regime	41
Test Parameters	42
Test Apparatus	42
Specimen Preparation	43
Specimen Evaluation	45
Results	45
Low Temperature Test Results Overview	46
Ta Alloys	47
Mo and TZM	53
Mo-Re Alloys	55
Re and Re-5W	58
Tungsten	61
High Temperature Test Results	62
Radiography	62
Surface Appearance	62
Hardness	63
Metallography	63
First Test Series	63
Second Test Series	65
Discussion	65

Contents (Continued)

	<u>Page</u>
Low Temperature Experiments	65
General	65
Ta Alloys	67
Mo and Mo Alloys	72
Re Materials	75
High Temperature Tests	77
Summary	78
Recommendations	79
Conclusions	82
Bibliography	84

Illustrations

<u>Figure</u>		<u>Page</u>
1	Schematic Illustration of PAHR Experiment	89
2	Low Temperature Refractory Metal-Na Compatibility Experiments	90
3	Equilibrium Chemical Potential of [O] in Na as a Function of Temperature.	91
4	Specimen Design	92
5	Low Temperature Crucible Assembly.	93
6	Solubility of Oxygen in Na as a Function of Temperature	94
7	Sodium Charging Apparatus	95
8	Exposure Furnace and Loading Racks	96
9	High Temperature Reflux Test Apparatus	97
10	High Frequency Induction Heating System	98
11	Temperature Locating Device for Reflux Tests	99
12	Typical Temperature Profile for Reflux Tests	100
13	Stainless Steel Collar-Tube Assembly	101
14	Tube Closure Assembly	102
15	Average Fracture Energy of As-Received Specimens	103
16	Average Ultimate Tensile Strength of As-Received Specimens	104
17	Average Fracture Energy After Na Exposure	105
18	Average Notched Ultimate Strength After Na Exposure	106
19	Average Hardness of As-Received Specimens	107
20	Average Hardness of Specimens After Na Exposure	108

Illustrations (Continued)

<u>Figure</u>		<u>Page</u>
21	Average Weight Change of Specimens After Na Exposure	109
22	Summary of Typical Load-Elongation Curves and Mechanical Properties for Ta-10W Alloy	110
23	Summary of Typical Load-Elongation Curves and Mechanical Properties for T-111 Alloy	111
24	Metallographic Structure of Selected Ta-10W Alloy Specimens	112
	a. As-Received	
	b. +++	
	c. ---	
25	Metallographic Structure of Selected T-111 Alloy Specimens	113
	a. As-Received	
	b. +++	
	c. ---	
26	Surface Attack of Ta-10W Exposed at 800°C for 130 Hours in Na with 100 ppmw [O].	114
27	Transmission Electron Micrographs of Ta-10W Alloy .	115
	a. As-Received	
	b. Recrystallized	
	c. 000	
28	Transmission Electron Micrographs of Ta-10W Alloy .	116
	a. ---	
	b. +- -	
	c. + - -	
	d. +- -	
29	Transmission Electron Micrographs of Ta-10W Alloy .	117
	a. - - +	
	b. - + +	
	c. + - +	
	d. + + +	
30	Transmission Electron Micrographs of T-111 Alloy . .	118
	a. As-Received	
	b. ---	
	c. 000	
	d. +++	

Illustrations (Continued)

<u>Figure</u>		<u>Page</u>
31	Low Magnification Fractographic Montage of Ta-10W Alloy Specimens	119
32	Low Magnification Fractographic Montage of T-111 Alloy Specimens	120
33	High Magnification Fractographs of Ta-10W Alloy Specimens	121
	a. As-Received	
	b. As-Received Smooth	
	c. ++- Unrecrystallized	
	d. ++-	
34	High Magnification Fractographs of Ta-10W Alloy Specimens	122
	a. +--	
	b. -+-	
	c. ---	
	d. ooo	
35	High Magnification Fractographs of Ta-10W Alloy Specimens	123
	a. +++	
	b. +-+	
	c. -++	
	d. ---+	
36	High Magnification Fractographs of T-111 Alloy Specimens	124
	a. As-Received	
	b. As-Received Smooth	
	c. ++- Unrecrystallized	
	d. ++-	
37	High Magnification Fractographs of T-111 Alloy Specimens	125
	a. +--	
	b. -+-	
	c. ---	
	d. ooo	
38	High Magnification Fractographs of T-111 Alloy	126
	a. +++	
	b. +-+	
	c. -++	
	d. ---+	

Illustrations (Continued)

<u>Figure</u>		<u>Page</u>
39	Ta-10W Fracture Energy Model Response as a Function of Temperature and Oxygen Potential for 10-hour Exposures	127
40	Ta-10W Fracture Energy Model Response as a Function of Temperature and Oxygen Potential for 70-hour Exposures	128
41	Ta-10W Fracture Energy Model Response as a Function of Temperature and Oxygen Potential for 130-hour Exposures	129
42	Ta-10W Ultimate Notched Tensile Strength Model Response as a Function of Temperature and Oxygen Potential for 10-hour Exposures	130
43	Ta-10W Ultimate Notched Tensile Strength Model Response as a Function of Temperature and Oxygen Potential for 70-hour Exposures	131
44	Ta-10W Ultimate Notched Tensile Strength Model Response as a Function of Temperature and Oxygen Potential for 130-hour Exposures	132
45	T-111 Fracture Energy Model Response as a Function of Temperature and Oxygen Potential for 10-hour Exposures	133
46	T-111 Fracture Energy Model Response as a Function of Temperature and Oxygen Potential for 70-hour Exposures	134
47	T-111 Fracture Energy Model Response as a Function of Temperature and Oxygen Potential for 130-hour Exposures	135
48	T-111 Ultimate Notched Tensile Strength Model Response as a Function of Temperature and Oxygen Potential for 10-hour Exposures	136
49	T-111 Ultimate Notched Tensile Strength Model Response as a Function of Temperature and Oxygen Potential for 70-hour Exposures	137
50	T-111 Ultimate Notched Tensile Strength Model Response as a Function of Temperature and Oxygen Potential for 130-hour Exposures	138

Illustrations (Continued)

<u>Figure</u>		<u>Page</u>
51	Inside Surface and Cross Section of a 316 Stainless Steel Crucible After Exposure to Sodium . . . a. SEM Photomicrograph of Inside Surface b. Photomicrograph of Cross Section	139
52	Summary of Typical Load-Elongation Curves and Mechanical Properties for Mo (Source 1)	140
53	Summary of Typical Load-Elongation Curves and Mechanical Properties for Mo (Source 2)	141
54	Summary of Typical Load-Elongation Curves and Mechanical Properties for TZM (Source 1)	142
55	Summary of Typical Load-Elongation Curves and Mechanical Properties for TZM (Source 2)	143
56	Metallographic Structure of Selected Mo (Source 1) Specimens a. As-Received b. +++ c. ---	144
57	Metallographic Structure of Selected Mo (Source 1) Specimens a. As-Received b. +++ c. ---	145
58	Metallographic Structure of Selected TZM (Source 1) Specimens a. As-Received b. +++ c. ---	146
59	Metallographic Structure of Selected TZM (Source 2) Specimens a. As-Received b. +++ c. ---	147
60	Low Magnification Fractographic Montage of Mo (Source 1) Specimens	148
61	Low Magnification Fractographic Montage of Mo (Source 2) Specimens	149

Illustrations (Continued)

<u>Figure</u>		<u>Page</u>
62	Low Magnification Fractographic Montage of TZM (Source 2) Specimens	150
63	Low Magnification Fractographic Montage of TZM (Source 2) Specimens	151
64	Typical High Magnification Fractographs for Mo and TZM Alloy a. Lamellar Mode b. Quasi Cleavage c. Intergranular	152
65	Mo (Source 2) Weight Change Model Response as a Function of Temperature and Oxygen Potential for 10-hour Exposures	153
66	Mo (Source 2) Weight Change Model Response as a Function of Temperature and Oxygen Potential for 70-hour Exposures	154
67	Mo (Source 2) Weight Change Model Response as a Function of Temperature and Oxygen Potential for 130-hour Exposures	155
68	TZM (Source 2) Alloy Weight Change Model Response as a Function of Temperature and Oxygen Potential for 10-hour Exposures	156
69	TZM (Source 2) Alloy Weight Change Model Response as a Function of Temperature and Oxygen Potential for 70-hour Exposures	157
70	TZM (Source 2) Alloy Weight Change Model Response as a Function of Temperature and Oxygen Potential for 130-hour Exposures	158
71	Summary of Typical Load-Elongation Curves and Mechanical Properties for Mo-13Re Alloy	159
72	Summary of Typical Load-Elongation Curves and Mechanical Properties for Mo-26Re (Source 1) Alloy	160
73	Summary of Typical Load-Elongation Curves and Mechanical Properties for Mo-26Re (Source 2) Alloy	161

Illustrations (Continued)

<u>Figure</u>		<u>Page</u>
74	Summary of Typical Load-Elongation Curves and Mechanical Properties for Mo-41Re (Source 1) Alloy	162
75	Summary of Typical Load-Elongation Curves and Mechanical Properties for Mo-41Re (Source 2) Alloy	163
76	Metallographic Structure of Selected Mo-13Re Specimens a. As-Received b. +++ c. ---	164
77	Metallographic Structure of Selected Mo-26Re (Source 1) Specimens a. As-Received b. +++ c. ---	165
78	Metallographic Structure of Selected Mo-26Re (Source 2) Specimens a. As-Received b. +++ c. ---	166
79	Metallographic Structure of Selected Mo-41Re (Source 1) Specimens a. As-Received b. +++ c. ---	167
80	Metallographic Structure of Selected Mo-41Re (Source 2) Specimens a. As-Received b. +++ c. ---	168
81	Low Magnification Fractographic Montage of Mo-13Re Specimens	169
82	Low Magnification Fractographic Montage of Mo-26Re (Source 1) Specimens	170
83	Low Magnification Fractographic Montage of Mo-26Re (Source 2) Specimens	171

Illustrations (Continued)

<u>Figure</u>		<u>Page</u>
84	Low Magnification Fractographic Montage of Mo-41Re (Source 1) Specimens	172
85	Low Magnification Fractographic Montage of Mo-41Re (Source 2) Specimens	173
86	Typical High Magnification Fractographs for Mo-26Re Alloy a. Cleavage b. Intergranular c. Lamellar	174
87	Specimen Surface Appearance as a Function of Na Exposure for the Mo-41Re Alloy (Source 1) a. As-Received b. Na Exposed	175
88	Fracture Initiation for Selected Exposures for the Mo-41Re Alloy (Source 1) a. As-Received b. +-- c. +++ d. ooo	176
89	Mo-13Re Alloy Weight Change Model Response as a Function of Temperature and Oxygen Potential for 10-hour Exposures	177
90	Mo-13Re Alloy Weight Change Model for 70-hour Exposures	178
91	Mo-13Re Alloy Weight Change Model for 130-hour Exposures	179
92	Mo-41Re (Source 1) Alloy Weight Model for 10-hour Exposures	180
93	Mo-41Re (Source 1) Alloy Weight Model for 70-hour Exposures	181
94	Mo-41Re (Source 1) Alloy Weight Model for 130-hour Exposures	182
95	Summary of Typical Load-Elongation Curves and Mechanical Properties for Wrought Re	183
96	Summary of Typical Load-Elongation Curves and Mechanical Properties for CVD Re	184

Illustrations (Continued)

<u>Figure</u>		<u>Page</u>
97	Summary of Typical Load-Elongation Curves and Mechanical Properties for CVD Re-5W Alloy	185
98	Metallographic Structure of Selected Wrought Re Specimens a. As-Received b. +++ c. ---	186
99	Metallographic Structure of Selected CVD Re Specimens a. As-Received b. +++ c. ---	187
100	Metallographic Structure of CVD Re-5W Alloy Specimens a. As-Received b. +++ c. ---	188
101	Low Magnification Fractographic Montage of Wrought Re Specimens	189
102	Low Magnification Fractographic Montage of CVD Re and CVD Re-5W Specimens a. CVD Re b. CVD Re-5W	190
103	Typical High Magnification Fractographs for Wrought Re, CVD Re and CVD Re-5W Specimens a. Wrought Re b. CVD Re c. CVD Re-5W	191
104	Surface Characterization of Selected CVD Re Specimens as a Function of Na Exposure a. As-Received b. +++ c. +++	192
105	CVD Re-5W Alloy Fracture Energy Model Response as a Function of Temperature and Oxygen Potential for 10-hour Exposures	193
106	CVD Re-5W Alloy Fracture Energy Model Response as a Function of Temperature and Oxygen Potential for 70-hour Exposures	194

Illustrations (Continued)

<u>Figure</u>		<u>Page</u>
107	CVD Re-5W Alloy Fracture Energy Model Response as a Function of Temperature and Oxygen Potential for 130-hour Exposures	195
108	Wrought Re Weight Change Model Response as a Function of Temperature and Oxygen Potential for 10-hour Exposures	196
109	Wrought Re Weight Change Model Response as a Function of Temperature and Oxygen Potential for 70-hour Exposures	197
110	Wrought Re Weight Change Model Response as a Function of Temperature and Oxygen Potential for 130-hour Exposures	198
111	CVD Re Weight Change Model Response as a Function of Temperature and Oxygen Potential for 10-hour Exposures	199
112	CVD Re Weight Change Model Response as a Function of Temperature and Oxygen Potential for 70-hour Exposures	200
113	CVD Re Weight Change Model Response as a Function of Temperature and Oxygen Potential for 130-hour Exposures	201
114	Typical W Fractography a. Quasi Cleavage b. Intergranular	202
115	Contact Radiographs of Load Tubes After Testing .	203
116	Outside Surface Appearance of Tubes After Testing	204
117	Inside Surface Appearance of Tubes After Testing .	205
118	Ta-10W Alloy Tube Metallographic Sections	206
119	Ta-10W Alloy Tube Metallographic Sections	207
120	Ta-10W Alloy Tube TEM Microstructures	208
121	Ta-10W Alloy Tube TEM Microstructures	209
122	T-111 Alloy Tube Metallographic Sections	210

Illustrations (Continued)

<u>Figure</u>		<u>Page</u>
123	T-111 Alloy Tube Metallographic Sections	211
124	Mo-41Re Alloy Tube Metallographic Sections	212
125	Mo-41Re Alloy Tube Metallographic Sections	213
126	CVD Re Tube Metallographic Sections	214
127	CVD Re Tube Metallographic Sections	215
128	CVD Re-5W Alloy Tube Metallographic Sections	216
129	CVD Re-5W Alloy Tube Metallographic Sections	217
130	Typical Metallographic Sections for Second Ta-10W Alloy Tube	218
131	Typical Metallographic Sections for Second Mo-41Re Alloy Tube	219
132	Average Oxygen Concentration of Selected Ta-10W and T-111 Alloy Specimens as a Function of Fracture Energy	220
133	Effect of Re Additions on the Fracture Energy of Mo	221

Tables

<u>Table</u>		<u>Page</u>
1	Material Chemistry Analysis	222
2	Recrystallization Conditions	223
3	Average Notch Specimen Fracture Energy for All Material Exposed to Na and for Material in the As-Received Condition	224
4	Average Notch Ultimate Tensile Strength for All Material Exposed to Na and for Material in the As-Received Condition	225
5	Comparison of Notched and Smooth Specimen Fracture Energy Before Exposure to Na	226
6	Comparison of Notched and Smooth Specimen Ultimate Tensile Strength	227
7	Average Rockwell A Hardness for All Na Exposure Conditions and for As-Received Material	228
8	Average Weight Change for All Na Exposure Conditions	229
9	Fracture Energy Regression Survey	230
10	Notched Ultimate Tensile Strength Regression Survey	231
11	Hardness Regression Survey	232
12	Weight Change Regression Survey	233
13	Fracture Energy as a Function of Oxygen Potential Normalized to Recrystallized Fracture Energy	234
14	Ta-10W Alloy Mechanical Properties and Weight Change as a Function of Exposure to Na at Different Oxygen Potentials	235
15	T-111 Alloy Mechanical Properties and Weight Change as a Function of Exposure to Na at Different Oxygen Potentials	236

Tables (Continued)

<u>Table</u>		<u>Page</u>
16	Hydrogen Concentration of Selected Ta-10W Specimens	237
17	Carbon Concentration of Selected Ta-10W Specimens.	238
18	Oxygen Concentration of Selected Ta-10W and T-111 Alloy Specimens	239
19	Ta-10W and T-111 Ultimate Notched Tensile Strength and Fracture Energy as a Function of Crucible Material	240
20	Mo Mechanical Properties and Weight Change as a Function of Exposure to Na at Different Oxygen Potentials (Source 1)	241
21	Mo Mechanical Properties and Weight Change as a Function of Exposure to Na at Different Oxygen Potentials (Source 2)	242
22	TZM Alloy Mechanical Properties and Weight Change as a Function of Exposure to Na at Different Oxygen Potentials (Source 1)	243
23	TZM Alloy Mechanical Properties and Weight Change as a Function of Exposure to Na at Different Oxygen Potentials (Source 2)	244
24	Mo-13Re Alloy Mechanical Properties and Weight Change as a Function of Exposure to Na at Different Oxygen Potentials	245
25	Mo-26Re Alloy Mechanical Properties and Weight Change as a Function of Exposure to Na at Different Oxygen Potentials (Source 1)	246
26	Mo-26Re Alloy Mechanical Properties and Weight Change as a Function of Exposure to Na at Different Oxygen Potentials (Source 2)	247
27	Mo-41Re Alloy Mechanical Properties and Weight Change as a Function of Exposure to Na at Different Oxygen Potentials (Source 1)	248

Tables (Continued)

<u>Table</u>		<u>Page</u>
28	Mo-41Re Alloy Mechanical Properties and Weight Change as a Function of Exposure to Na at Different Oxygen Potentials (Source 2)	249
29	Oxygen Concentration of Selected Mo and Mo Alloy Specimens	250
30	Wrought Re Mechanical Properties and Weight Change as a Function of Exposure to Na at Different Oxygen Potentials	251
31	CVD Re Mechanical Properties and Weight Change as a Function of Exposure to Na at Different Oxygen Potentials	252
32	CVD Re-5W Alloy Mechanical Properties and Weight Change as a Function of Exposure to a at Different Oxygen Potentials	253
33	W Mechanical Properties and Weight Change as a Function of Exposure to Na at Different Oxygen Potentials	254
34	Posttest Hardness of Tube Outer Surface as a Function of Distance and Temperature From the Bottom	255

Compatibility of Refractory Metals with Sodium in the Presence of Oxygen and UO₂

Introduction

One accident scenario for a Liquid Metal Fast Breeder Reactor (LMFBR) assumes that the reactor core has suffered catastrophic disassembly with the rubble of reactor fuel and cladding covered with liquid metal coolant on some structural or core-catcher material. An important, yet unanswered question, is then how much heat must be extracted from the rubble to keep this mass from causing structural damage to the core catcher. A specific, in-pile experiment in this Post Accident Heat Removal (PAHR) program has been designed to measure the one-dimensional heat flow from a debris bed of enriched UO₂ particles covered with molten sodium at different temperatures. A schematic illustration of the experiment is shown in Figure 1.

The double-walled crucible shown in Figure 1 contains 8 kg of UO₂ particles which are submerged in 4 to 5 kg of sodium which is contained in stainless steel, nominally maintained at a temperature of 800°C. Five temperature excursions are planned which will cause a maximum temperature of ~2000°C to occur at a point on the inner wall with a gradient along the wall of ~200°C/cm. Because of unplanned reactor "scrams," the experiment could be cooled rapidly at any time. The planned duration of the in-pile test is 100 hours, of which 5 hours will be at 2000°C. Initial pressure will be set at one atmosphere absolute with a cover gas of argon. The experiment will be sealed and the initial oxygen content of the sodium will be ~2 ppmw (parts per million by weight). Based on "worst case" estimates of (1) leaks during the test; (2) adsorption of O₂ or H₂O on the fixtures or components during assembly; (3) the presence of impurities of easily reduced oxides (i.e., Fe); and

(4) the possible presence of hyperstoichiometric UO_{2+x} , the content of dissolved oxygen could reach 400 ppmw during the test. However, the addition of oxygen through leaks during the test has been shown to be negligible.⁽¹⁾ Thus, once sealed, the total amount of oxygen within the experiment will be fixed.

The double-walled crucible must be constructed of a material which is able to maintain sufficient mechanical integrity in the above operational conditions at elevated temperatures. No such material selection is obvious. It is known that refractory metals are moderately inert to molten alkali metals with low concentrations of dissolved impurities (O_2 , H_2 , N_2 , and C).⁽²⁾ As the concentration of impurities in Na (principally O_2) increases, the refractory metals may be subject to attack. Numerous studies report on the interaction of a refractory metal with molten alkali metals with fixed oxygen potentials.⁽³⁻⁶⁾ No report covers the wide range of conditions nor the extremely harsh conditions envisioned for this planned in-pile experiment. Also, due to the nature of the in-pile experiment, an evaluation of a candidate material must be done, not at fixed oxygen potential, but with a fixed amount of oxygen present as an impurity.

Three major problem areas were perceived to be dominant from a material survivability standpoint:

1. Since temperature may be cycled through the recrystallization temperature of the material, refractory metals, or alloys with a ductile-to-brittle transformation temperature (DBTT) lower than $25^\circ C$ are preferred;
2. High oxygen potentials which may occur in the sodium liquid will cause embrittlement in refractory metals or alloys which have a high solubility for oxygen, namely Ta alloys;

3. Refractory metal transport may occur in regions of steep temperature gradients. (This phenomenon has been observed when using Ta in lithium environments.)⁽⁷⁾

The DBTT constraint and the need for sufficient strength at 2000°C limit crucible candidate materials to Mo-Re alloys, Re, Re-W alloys, and Ta alloys. The specific materials evaluated for fabrication of the double-walled crucible were wrought Ta-10W, Ta-8W-2Hf, Mo-41Re, Mo-26Re, Mo-13Re, Re, Mo, TZM (Mo-0.5Ti-0.07Zr), W, and chemically vapor deposited (CVD) Re and Re-5W. In several instances, materials from three sources were evaluated. Molybdenum, TZM, and W were evaluated, even though their DBTT is high in the event that the other candidate materials would not be acceptable and a composite coated crucible would be required.

Compatibility testing was divided into two temperature regimes: (1) $300^{\circ}\text{C} \leq T \leq 800^{\circ}\text{C}$ and (2) $\sim 600^{\circ}\text{C} \leq T \leq 2000^{\circ}\text{C}$. Specimens were submerged in liquid Na for all low temperature tests. In high temperature tests the specimens are subjected to both liquid and vapor attack.

The evaluation strategy for the low temperature tests was based on a Yates Order experimental matrix⁽⁸⁾ with three independent variables (1) temperature (300-800°C), (2) time (10-130 hours), and (3) sodium oxygen content (2-100 ppmw). This experimental matrix defines a cubic factor space. Experiments were made at the vertices and the midpoint of this space. The material characteristics (dependent variables) evaluated were room temperature notched-tensile properties, hardness, weight change, fractography, and microstructure.

High temperature ($\sim 600^{\circ}\text{C} \leq T \leq 2000^{\circ}\text{C}$) evaluations were essentially engineering proof tests of some candidate materials, selected on the basis of the low temperature results. The candidate materials were fabricated into thin-walled cylindrical tubes, filled with sodium (400 ppmw oxygen), and UO_2 , sealed and heated (to

~2100°C) near one end. Because of the steep temperature gradient (250°C/cm), a reflux condition existed such that the candidate material was exposed to sodium in both the liquid and vapor states. General appearance, hardness, metallography and transmission electron microscopy (TEM) were used to assess survivability of the candidate materials under these more extreme conditions.

The purpose of this report is to document the results of experiments conducted to evaluate the compatibility of refractory metal alloys in high temperature environments consisting of liquid and gaseous Na and uranium fuel. Materials which demonstrate compatibility in this environment will be selected as candidates for fabrication of the double-walled crucible to be used in the PAHR test described above. This combination of materials also finds wide application in components for the LMFBR and for parts in high-energy reactors for terrestrial and extraterrestrial application. Examples include high temperature instrumentation and heat pipes.

The experimental strategy and details of the methods used to evaluate the candidate materials will be described in the next section. The results will be presented in two subsections: low temperature results and high temperature results. Finally, a ranking of the candidate materials for fabrication of the crucible will be presented based on the results of the evaluation.

Experimental

Compatibility tests were divided into two temperature regimes: (1) $300^{\circ}\text{C} \leq T \leq 800^{\circ}\text{C}$ and (2) $\sim 600^{\circ}\text{C} \leq T \leq 2000^{\circ}\text{C}$. In each regime the candidate materials were exposed to oxygen-bearing sodium in closed containers. The choice of a "static" test, rather than exposure in a "dynamic" recirculating liquid sodium loop with fixed oxygen potential, was dictated by the design of the in-pile experiment. Once the in-pile experiment is assembled and sealed, a fixed amount of oxygen is available to interact with the crucible

and other components of the experiment. The oxygen potential will change depending on the nature and extent of the interaction with each component. To accurately evaluate crucible candidate materials under these conditions of changing oxygen potential (where the nature and magnitude of the change depends strongly on the particular candidate material), a closed or static test must be used. Most of the materials evaluated herein would suffer severe attack when exposed to Na with fixed oxygen potentials of the order of 100 ppmw.

To ensure a valid evaluation when using a closed test, the test must be scaled such that the amount of oxygen initially available to interact with the sample of candidate material is the same as the amount of oxygen which is available to interact with the crucible. Also, the containers for the evaluated oxygen potential tests must not alter the oxygen potentials seen by the samples and the initial oxygen content must be identical in each of the containers for the different candidate materials. The term "selected" is used throughout this paper in reference to selection of specimens for analysis. Since this study involved hundreds of specimens with replicates at each trial it was necessary for economic reasons to select specimens from trials for further analysis. However, in no instance was the selection process used to bias the results.

Low Temperature Regime

Experimental Details

For evaluation in the low temperature regime, notched tensile samples of each material were exposed to environments as shown by the factor space cube in Figure 2. Two samples of each material were exposed to the conditions at each corner point with four samples exposed to conditions at the center of the factor space cube. Each specimen was sealed in an individual crucible with a measured amount of Na having the prescribed oxygen potential.

Evaluations in this regime were essentially isothermal, with samples being exposed to oxygen-bearing sodium liquid only.

At temperatures of 550°-600°C, the kinetics for sodium uranate formation from molten sodium, dissolved oxygen, and UO_2 are rapid relative to the duration of the exposures. The formation of Na_3UO_4 will buffer the equilibrium oxygen chemical potential to extremely low levels (see Figure 3). However, since it was felt necessary to evaluate the crucible candidate materials at high oxygen potentials throughout this temperature regime, no UO_2 was included in the low temperature evaluation experiments.

A standard three-symbol notation is used for identification of exposure conditions throughout this test. For example, exposure at 800°C for 130 hours in Na at 100 ppmw [O] is designated +++, respectively and exposure at 300°C for 10 hours in Na at 2 ppmw [O] is designated---, respectively. The center point in the factor space, 550°C, 70 hours, 50 ppmw [O] is designated 000. Thus, the first symbol represents temperature; + = 800°C, 0 = 550°C, - = 300°C, the second symbol represents time; + = 130 hours, 0 = 70 hours, - = 10 hours, and the third symbol represents oxygen potential of the Na; + = 100 ppmw [O], 0 = 50 ppmw [O], and - = 2 ppmw [O].

Thirty-five to forty notched tensile specimens and two smooth gage section specimens of each material (in annealed condition) were procured in one lot from each source in accordance with the design specifications illustrated in Figure 4. Chemistry certifications, were available, are also included in Table 1. Upon delivery, all specimens were numbered with a vibratory stencil and 22 samples from each lot were recrystallized according to the conditions listed in Table 2. For all samples except W, recrystallization was carried out in a liquid nitrogen trapped, Mo element, vacuum furnace at pressures less than 6.7×10^{-4} Pa (5×10^{-6} torr). Tungsten specimens were recrystallized in a similar W element furnace at pressures less than 6.7×10^{-4} Pa. All the Ta alloy specimens were loosely wrapped in 0.03 mm-thick Ta foil and then placed on a

Ta foil covered high purity corrugated MgO hearth in order to minimize interstitial contamination during recrystallization. All Mo and Mo alloy specimens were placed open to the furnace atmosphere on a Ta foil covered corrugated MgO plate.

After recrystallization, all specimens were weighed in a calibrated 0.0001 g resolution balance, measured for thickness at the notched region with a calibrated micrometer (0.003 mm resolution), and measured for width at the notch roots with an optical comparator (0.003 mm resolution). Next, the hardness of at least six each specimens, each randomly sampled from as received and recrystallized material from each source was measured using a calibrated hardness testor and the applicable indenter and load.

After exposure the specimens were cleaned with successive alcohol rinses commencing immediately after the specimens were removed from the Na.

The selection of materials for crucibles and the Na charging apparatus were based on thermodynamic arguments, as well as availability and fabricability. Figure 3⁽⁹⁾ shows the equilibrium chemical potential of oxygen in sodium as a function of temperature for several, fixed oxygen concentrations. Also shown in Figure 3 are the temperature variations of the oxygen potentials in equilibrium with (1) Ni-NiO; (2) Na(l), dissolved oxygen, and Cr as would be present in stainless steel; and (3) Na(l), dissolved oxygen and UO_2 .

From Figure 3 it is seen that nickel would be an excellent choice as a container material for all exposure conditions. It is known that nickel is resistant to interaction with molten sodium containing as much as 500 ppmw dissolved oxygen to 900°C.⁽¹⁰⁾ However, 316 stainless steel crucibles were used for all low oxygen potential exposures to ensure low oxygen potential by utilizing the $NaCrO_2$ reaction and to test the compatibility of stainless steel in the system. The latter is important because the outer container

and low temperatures hardware for the in-pile tests are fabricated from stainless steel. Nickel A200 tubing was used as a container for all exposures in Na at elevated oxygen potentials (> 2 ppmw [O]).

The interaction of molten sodium, dissolved oxygen, and chromium from the stainless steel to form sodium chromite, $\text{NaCrO}_2^{(11)}$ will cause the equilibrium oxygen potential to be buffered at the level shown in Figure 3. If excess dissolved oxygen is available, formation of NaCrO_2 will limit the available oxygen content to the levels shown throughout this low temperature regime. For high oxygen exposures (> 10 ppmw dissolved oxygen), this buffering would lower the oxygen potential experienced by the test coupon. However, at low dissolved oxygen exposures, the quantity of available oxygen is insufficient to form NaCrO_2 at 800°C , while at 300°C the buffering due to NaCrO_2 formation will only decrease the oxygen content of the sodium below the ~ 2 ppmw level if the kinetics of formation are rapid relative to the duration of the exposure. Each crucible consisted of four parts: bottom cap, tube side wall, top cap, and evacuation tube. A dimensioned assembly drawing with weld preps is illustrated in Figure 5. The end cap welds and the evacuation tube-to-cap weld are autogeneous and were made on an automated GTA welder. Each weld was individually He-leak checked and certified to be leak free at 1×10^{-7} STDCC/S He.

After the top cap weld was completed, the crucible and contents were evacuated to 0.133 Pa (1×10^{-3} torr) with a diffusion pump and the evacuation tube was sealed by pinch welding. A resistance weld was simultaneously made over the pinched areas to ensure a leaktight crucible.

All crucibles were identified with both a vibratory stenciled number on the crucible and a drilled number stamped stainless steel disc secured to the stub of the evacuation tube. Next, each crucible was wrapped in a steel foil bag to minimize oxidation of the crucible. In order to insure Na with a low oxygen potential all 316 stainless steel crucibles also contained a ~ 0.5 g chunk of

pure V. Na oxygen potential for low oxygen potential exposures is assumed to be 2 ppmw. However, due to the presence of stainless steel and V in these exposures, the true oxygen potential for these tests probably fell very quickly to less than 2 ppmw.⁽¹²⁾

All stainless steel parts were cleaned according to the following procedure:

1. Vapor degrease
2. Clean with 20 percent by weight NaOH
3. Tap water rinse
4. Clean with 50 percent by volume HCl
5. Tap water rinse
6. Deionized water rinse

All Ni parts were cleaned with a vapor degrease.

Each crucible was filled with sodium from a "master" batch. This was to ensure that the different candidate materials were initially exposed to an identical oxygen concentration at each exposure condition. The master batch was prepared from high purity sodium (< 2 ppmw oxygen) obtained from a recirculating sodium purification loop. Master batches of approximately 4 kg of the high-purity sodium were drawn into welded type 316 stainless steel containers 13.97 cm ID.; 30.48 cm high and 0.32 cm wall thickness after each can was "seasoned" on the Na loop with flowing Na for periods in excess of 48 hours. Sodium metal was then burned in a dryroom (< 300 ppm H₂O) atmosphere producing NaO₂ + Na₂O₂. The freshly prepared oxide powder was immediately added to the master can through a valve arrangement and back filled with argon. The dissolved oxygen concentration of the master batch was fixed using the well-established relationship between oxygen solubility in liquid sodium and temperature as shown in Figure 6.⁽¹³⁾ This figure shows that to fix the oxygen concentration at 100 ppmw, the upper limit of dissolved oxygen content in the low temperature regime, and the sodium must be equilibrated at 300°C ± 5°C. The

master batch of Na-Na₂O was equilibrated at the temperature necessary ($\pm 5^\circ\text{C}$) to fix the oxygen content at the desired level for not less than 48 hours. For tests requiring low oxygen potential Na, a can containing clean Na was connected to the transfer system and equilibrated at 150°C for 48 hours.

The Na temperature within the can was monitored with high impedance devices connected to two type K 304 stainless steel sheathed thermocouples which were also used as feedback to an automatic temperature control device.

Sodium was loaded into individual crucibles by forcing Na from the 4 l heated can with high purity argon (see Figure 7). Flow was controlled with a heated metering valve and the amount of sodium loaded into each crucible was monitored with a precision electronic balance. Fifteen grams ± 0.1 g of Na was loaded into each crucible. After loading with Na, each crucible was placed within a liquid nitrogen cooled Al chill block to quench the Na. This cooled block also served the purpose of lowering the dew point within the glove box. Next, a specimen was loaded into each crucible, a cap and tube assembly was slid into the crucible, and crucible assemblies in lots of 10 were loaded into Ziploc[®]-sealed plastic bags for immediate transfer to the welding dry box.

The quantity of Na₂O added to the master batch was not less than four times the amount necessary to equilibrate at the highest oxygen concentration desired (100 ppmw for the low temperature evaluations; 400 ppmw for the high temperature tests). This was to ensure availability of an excess of Na₂O and to counteract any depletion of oxygen due to formation of NaCrO₂ as previously discussed. An estimate of the rate at which oxygen is depleted from the saturated sodium-oxygen solution was made by assuming that the rate controlling step in the reaction of liquid sodium, dissolved oxygen, and chromium from the stainless steel is diffusion of chromium to the inner surface of the master can. For a thin-walled

cylinder of ID = 2a and OD = 2b, initial uniform concentration of C_0 and surface concentration at $r = a$ and $r = b$ of C_1 ; Crank⁽¹⁴⁾ relates the quantity of diffusing substance leaving the hollow cylinder through each surface, M_t , to time and material parameters as:

$$\frac{M_t}{M_\infty} = 1 - \frac{4}{b^2 - a^2} \sum_{n=1}^{\infty} \frac{J_0(a\alpha_n) - J_0(b\alpha_n)}{\alpha_n^2 \{J_0(a\alpha_n) = J_0(b\alpha_n)\}} \cdot \exp(-D\alpha_n^2 t) \quad [1]$$

where M_∞ is the initial quantity of diffusing substance; the α_n 's are the positive roots of

$$J_0(a\alpha_n)Y_0(b\alpha_n) - J_0(b\alpha_n)Y_0(a\alpha_n) = 0 \quad [2]$$

the J_0 and Y_0 are zero order Bessel functions of the first and second kind respectively; D the diffusion coefficient, and t the time. The amount of chromium in the 316 stainless steel master can, M_∞ , is ~18 w/o or ~780 g (assuming a density of 8 g/cm³ for stainless steel). The amount of chromium necessary to deplete the sodium-oxygen solution of 0.40 g (100 ppmw) of dissolved oxygen by formation of NaCrO₂ (48.60 w/o Cr; 29.91 w/o O; 21.49 w/o Na) is 0.65 g. Using $M_t = 0.65$ g and $M_\infty = 780$ g, the ratio $M_t/M_\infty = 8.33 \times 10^{-4}$ and from Figure 5.10 of Crank $\{Dt/(b-a)^2\}^{1/2} = 3.62 \times 10^{-4}$. Eq [1] assumes that the diffusing substance was initially at a constant, uniform concentration and leaves the cylinder through both the inner and outer surfaces. To comply with these boundary conditions, we consider the inner surface area of our master can to be divided between the inside and outside surfaces of a "pseudo" can of inside radius a'; outside radius b'; a height equivalent to the master can and twice the wall thickness. This can be expressed mathematically as:

$$2\pi ah = 2\pi a'h + 2\pi(a'+0.64 \text{ cm})h \quad [3]$$

With $a = 6.99$ cm, we calculate $a' = 3.18$ cm and $b' = 3.81$ cm. The diffusion coefficient of chromium in 316 stainless steel at 300°C has been reported to be very small: 10^{-17} - 10^{-23} cm^2/sec .⁽¹⁵⁾ Using the largest available value of D ; the values of a' and b' determined above and the relationship of

$$\left\{ \frac{Dt}{(b-a)^2} \right\}^{1/2} = 3.62 \times 10^{-4} \quad , \quad [4]$$

the time required to deplete the oxygen content of the sodium-oxygen solution of 100 ppmw of dissolved oxygen by formation of NaCrO_2 is approximately 1.44×10^6 hours at 300°C and 1.44×10^3 hours at 400°C . These times are long compared to the actual equilibration times used, and thus depletion of oxygen in the master batch due to the formation of NaCrO_2 was not significant. In addition, since the cans were "seasoned" for at least 48 hours in flowing Na, the actual amount of Cr available for reaction is probably considerably less than the amount assumed above.

The amount of sodium-oxygen solution added to each sample container was scaled to the following ratios:

1. Weight of Sodium Present
Surface area of crucible exposed to sodium in the in-pile test.
2. Weight of Sodium Present
Volume of crucible for in-pile test.

For the in-pile test, these ratios are 3.43 g Na/ cm^2 of crucible material and 34.3 g Na/ cm^3 of crucible material, respectively. The notched-tensile samples are the same size for each material.

With 15 g of sodium-oxygen solution added to each sample container the ratios:

1. Weight of Sodium

Surface area of
Sample

2. Weight of Sodium

Volume of Sample

ranged from 4.08 to 6.05 g Na/cm² of refractory alloy and 34.4 to 132 g Na/cm³ of refractory alloy, respectively. These ratios are comparable with those of the in-pile test, thus assuring that the same relative amount of oxygen will be available to interact with the sample of candidate material as will be present for the in-pile experiment under "worst case" assumptions.

Each foil-wrapped crucible was stacked vertically in a stainless steel rack holding up to 36 crucibles. A typical run consisted of exposing three racks at one time in an electric element air furnace having a hot zone 940 mm high, 1220 mm wide, and 940 mm deep (see Figure 8). The racks were placed at fixed locations within the furnace. Individual crucible location within each rack was noted, and a type K thermocouple was attached to both the front and back of each rack. An additional thermocouple was attached to the center of the centrally located rack within the furnace. Output from each thermocouple was recorded on a multichannel recorder for each run. Temperature uniformity within the furnace was better than $\pm 5^{\circ}\text{C}$. After each run the racks were removed from the hot furnace and air-cooled with a large fan.

In summary, for the low temperature regime, notched-tensile samples of each candidate material were exposed separately to each condition noted on the factor space cube of Figure 2. Nickel containers were used for all high (> 2 ppmw dissolved oxygen) oxygen exposures while 316 stainless steel was used for exposures at

2 ppmw dissolved oxygen. No UO_2 was included for the low temperature evaluations. The amount of oxygen available to interact with the tensile sample was determined to be similar to the amount of oxygen available to interact with the crucible for the in-pile test. The oxygen content of the sodium was set by using the well-established relationship between oxygen solubility and temperature.

Material Evaluation

The performance of all materials was evaluated by:

- A. Mechanical property measurements
- B. Microstructural property measurements
- C. Physical property measurements

A. Mechanical Properties--In order to obtain baseline properties with which to compare changes created by exposure, duplicate notched specimens, as well as smooth specimens in the as-received condition, were fractured in tension on an MTS[®] Systems machine at a constant cross-head velocity of 0.25 mm/sec. Load versus cross-head displacement was recorded on chart paper, and all fracture surfaces were coated with Krylon[®] immediately after testing. An extensometer was also mounted on the smooth bar specimens and strain versus load curves were recorded on chart paper. All notched Na-exposed specimens were tested in the same fashion.

Mechanical properties derived from this test include yield strength at 0.2 percent offset (for smooth specimens only), ultimate tensile strength (maximum load/original area), A_0 , and fracture energy. Fracture energy is defined in this work as the area under the load-displacement curve divided by A_0 , the cross sectional area of the specimen at the root of the notches. The area under the load displacement curve was measured with a calibrated planimeter. Fracture mode of selected specimens was evaluated with a scanning electron microscope (SEM). Hardness was measured on all exposed specimens except CVD Re and Re-5W. These specimens were too thin for a valid hardness measurement.

B. Microstructural Properties--Microstructural properties of specimens in the as-received condition as well as specimens exposed at 800°C, 130 hours, 100 ppm [O] and 300°C, 10 hours, 2 ppm [O] were evaluated by optical metallography. In each case the samples were mounted in plastic and polished through one micron diamond abrasive using standard metallographic techniques.

All Ta alloy samples were etched with a solution of 30 ml Hf, 30 ml H₂SO₄, 30 ml H₂O, and three to five drops of H₂O₂. Following standard preparation, all Mo and Mo alloy samples were chemically polished using a diluted potassium ferricyanide solution and then chemically etched in Murakanis reagent (10 g K₃Fe(CN)₆, 10 g KOH, 100 ml H₂O). All Re base materials were examined using Nomarski interference techniques.

Selected Ta-10W and T-111 specimens were also examined using transmission electron microscopy (TEM). Specimens were thinned by hand grinding through 600 grit SiC paper and then Jet electro-polished in an ice bath at 10 v and 100 mA in an electrolyte comprised of 20 percent H₂SO₄ and 80 percent methyl alcohol. The thinned samples were examined with a Jeol 200 CX electron microscope at 200 kV acceleration. Electron diffraction and x-ray spectroscopy were also employed to identify microstructural features.

C. Physical Properties--All specimens were weighed before and after exposure and the weight change was utilized as a dependent variable. In addition, bulk oxygen content was determined in selected specimens with a LECO oxygen analyzer. The cleaning procedure for Ta alloy samples included:

1. Immersion in an ultrasonic cleaner containing one (1) part HF and four (4) parts HNO₃ for 2 minutes at 20°C.
2. Rinsed two (2) times with deionized water in an ultrasonic cleaner.
3. Rinsed in acetone and dried at 110°C.
4. Store under argon immediately after drying.

The cleaning procedure for the Mo alloy samples included:

1. Immersion in one (1) part HF acid and four (4) parts HNO₃ acid for 10 seconds at 120°C.
2. Arrest reaction by immersion in 36 percent HCl.
3. Rinse three (3) times in deionized H₂O.
4. Rinse three (3) times in methanol, then dry at 110°C.
5. Store under argon immediately after drying.

The surface of selected specimens was examined utilizing SEM augmented with a x-ray spectrometer and Auger ESCA spectroscopy.

Statistical Analysis Techniques

Data sets for exposed samples of each alloy lot were grouped by dependent variable, and each group was surveyed for significant correlations with a multiple regression computer program.⁽¹⁶⁾ The first order terms plus all cross products and one second order term, [O]², were forced in the regression by using a backward procedure with a significance criterion of 1.0. This survey procedure produced a total of 56 multiple regressions with the dependent variables, UTS, fracture energy, hardness, and specimen weight change.

If significant correlations were found in the survey regressions (as determined by the magnitude of the "t value" of the coefficients and the "F value" for the regression⁽¹⁷⁾), the model was refined by deleting the terms whose coefficients had low "t values" and recomputing the regression. In this application the Student t test is used to test the validity of the hypothesis that a regression coefficient is not zero. For example, at 18 degrees of freedom, if the t value is greater than 2.1 the hypothesis can be accepted with 95 percent confidence.

Contour plots were computed for the significant models by solving the regression 10⁴ times at a constant exposure time within the ranges 300°C < T < 800°C and 2 ppm < [O] < 100 ppm.

Arbitrarily chosen contour levels (a constant value for the dependent variable) were retrieved from the 10^4 solutions and plotted as a function of temperature and oxygen potential. This plotting technique enables the experimentalist to quickly summarize and evaluate all responses within the experimental factor space.

Average values of each property and standard deviations for all dependent variables were computed by the regression program and were used to rank each alloy.

High Temperature Regime

High temperature compatibility evaluations were essentially engineering proof tests of candidate materials which "survived" the low temperature test matrix. The planned high temperature excursions of the in-pile test will cause environments (steep temperature gradients, multiple phases, unequal potential gradients, etc.) near the crucible which cannot easily be predicted. Thus, the high temperature evaluations were designed to simulate the conditions of the in-pile experiment as closely as possible, and to simply observe whether the crucible candidate material would survive the resulting environment.

The candidate materials were fabricated into cylindrical tubes, closed at one end. The tubes were filled with 85 g of depleted UO_2 of the particle size distribution to be used for the in-pile experiment and 12 g of sodium with 400 ppm dissolved oxygen. A stainless steel plug with attached evacuation tube was welded to a stainless steel collar which had previously been brazed to the refractory metal tube. The tubes were evacuated, backfilled with argon to a room temperature pressure of ~4 psia and sealed. This initial pressure was calculated to yield approximately one atmosphere at the maximum test temperature. The tubes were heated at the bottom end by a focused induction coil to ~2000°C, while the top

of the tube was allowed to cool naturally. Gradients of $\sim 250^{\circ}\text{C}/\text{cm}$ were attained near the heated end. This gradient caused a reflux condition along the length of the tube which closely simulates the "dry out" condition of the in-pile test. The candidate material will be in contact with the sodium vapor in the heated portion and sodium liquid in the cooler portion.

Based on the low temperature test results Ta-10W, T-111, Mo-41Re, Re/CVD, and Re-5W/CVD tubes were selected for the reflux tests.

Test Parameters

In the first series of tests, each tube received five hours of exposure to 2000°C . Specifically, the bottom 17.5 mm of each tube was heated to 2000°C for 1 hour, cooled to $< 700^{\circ}\text{C}$, and then reheated to 2000°C ; this procedure was repeated four times and was usually completed in a single day. In some instances, the tube was allowed to cool to room temperature overnight once at the convenience of laboratory scheduling.

After the first series was completed and evaluated, a second series of tests was conducted with Ta-10W and Mo-41Re tubes. Each tube was tested for 18 hours with a bottom temperature of 1000°C . The 18-hour interval was interrupted once by cooling to room temperature to facilitate scheduling. This test was followed by 6 hours of operation with bottom temperatures ranging from 800°C to 1500°C in four cycles of 1.5 hours each, all completed in a single day. The 1500°C maximum temperature was maintained for approximately 80 minutes of each cycle.

Test Apparatus

The vacuum chamber containing the high-temperature reflux tests is illustrated in Figure 9. During each test the chamber pressure was less than 10^{-2} Pa with a chamber leak rate < 0.20 Pa/min. Evacuation was accomplished with an oil diffusion pumped system.

The end of the tube was heated by a focused high-frequency induction heating system as illustrated in Figure 10. A small hole was drilled in the concentrator in order to directly observe the heated side wall of the tube with a PYRO Automatic optical pyrometer. The instruments were calibrated through a 1-inch thick quartz window (as provided for viewing on the vacuum chamber) against a standard lamp traceable to the National Bureau of Standards. Pyrometer readings were corrected to true temperatures with normal spectral emittances from the literature⁽¹⁸⁾ and checked in the case of Mo by surface and black body measurements on the end of a Mo tube at 2000°C.

Temperatures were measured up the side wall of the tube with an optical pyrometer, and registry was maintained with a stainless steel device as illustrated in Figure 11. A typical temperature profile for tests with a 2000°C zone is shown in Figure 12. A type K stainless steel sheathed thermocouple was embedded in a closed end hole at the top of the tube and the temperature was continuously monitored to detect instabilities.

Specimen Preparation

All as-received tubes were proof tested for mechanical integrity by heating the bottom 15 mm to 1000°C for 20 minutes using the apparatus discussed above. After heating they were inspected ultrasonically in immersion with a 10 MHz shear wave in both circumferential and longitudinal directions. Next the tubes were contact radiographed from two 90° offset longitudinal views. After the tubes were cut to length (178 mm), a 304L stainless steel collar (see Figure 13) was vacuum brazed to the open end of the tube.⁽¹⁹⁾ This collar provided a simple means of tube closure by welding and enabled secure fastening and locating in the heating apparatus as well as qualifying a braze for future experimental use. All braze joints were vacuum leak tested to 1×10^{-7} STDcc/s He.

Ta-10W and T-111 tubes were fabricated by rolling and welding annealed 1.5 mm-thick sheet. Thus, the finished tube had a longitudinal autogeneous electron beam weld and a circumferential weld to fasten a 1.5 mm-thick end plug. All tubes were 19 mm outside diameter. The Mo-41 Re tubes were produced by gun drilling 19 mm diameter bar stock produced by a powder metallurgy process.

The Re and Re-5W tubes were produced by chemical vapor depositing (CVD) over a Mo mandrel. After completing the deposit the mandrel was etched away and the tube O.D. ground to 19 mm diameter. These CVD tubes had a 9.5 mm radius on the bottom closure. The wall thickness of all tubes was 1.5 mm.

After a cleaning in methanol, the tubes were loaded with 12 ± 0.1 g of Na equilibrated to 400 ppmw [O] using the same apparatus and techniques that were used for the Ni crucibles. The tubes were then encapsulated in plastic Ziploc[®] bags which were in turn placed in an O-ring-sealed stainless steel tube before removal from the glove box. The plastic bags were stored in the glove box. The sealed assembly was transported to another glove box (maximum elapsed time of six hours), loaded with 85 ± 0.01 g of depleted UO_2 having a particle size distribution ranging from 30 to 2000 μm , resulting in a void fraction of 32 percent when loosely packed. The depleted UO_2 loaded in all tubes originated from one lot and it was high fired in hydrogen at 2275°C for 6 hours and placed in a sealed container until used. The stoichiometry of the UO_2 was 2.002 as determined by x-ray diffraction.

After the UO_2 was added, a 304L stainless steel cap containing a 304L stainless steel 3.18 mm diameter, 0.25 mm wall thickness tube was inserted into the stainless steel collar brazed to the refractory tube. The collar was heat sunked with a Cu ring and the cap was autogeneously welded to the collar utilizing the GTA process. See Figure 14, illustrating the weld prep and assembly. Next, a Swagelock[®] stainless steel bellows valve was connected to the evacuation tube, closed, and the assembly was removed from the glove

box. Immediately after removal, the assembly was evacuated and helium-leak tested to 10^{-6} STDcc/s He. While on the same manifold the assembly was backfilled with 4 psia of high purity He and sealed with the valve.

After testing, each tube assembly was photographed and contact radiographed and the stainless steel cap was cut off with a lathe. Immediately afterward, the tube was placed in a glove box heated to 140°C, and the contents were poured into a welded stainless steel crucible which was then sealed shut by GTA welding and archived. The empty tube was removed from the glove box and cleaned in alcohol. Each tube was then slit longitudinally along the axis with a carbide wheel or by an EDM process.

Specimen Evaluation

The hardness of each tube was measured, starting at the bottom, at 3.2 mm intervals. Next, the half section was cut into 50 mm-long segments. The bottom two segments were mounted in plastic and polished through 1 mm diamond abrasive using standard metallographic techniques. The specimens were etched, as described previously, and examined with a metallograph.

Results

For convenience and clarity an overview of the low temperature results is presented first, and average properties before and after sodium exposure are compared for all alloys. This subsection is followed by more specific reporting for individual alloys and alloy groups. The high temperature results are grouped by observational technique (i.e., radiography, microstructure, etc.).

Low Temperature Test Results Overview

All alloys are ranked by fracture energy and ultimate tensile strength in the as received condition in Figures 15 and 16, respectively. Next the same materials are ranked by the same variables for global average properties after Na exposure in Figures 17 and 18, respectively. Only data from recrystallized specimens are presented in Figures 17 and 18. Similar rankings using average hardness for as received material and average hardness and weight change for recrystallized sodium, exposed material are presented in Figures 19, 20, and 21, respectively. A more complete tabular form of all the above data is listed in Tables 3 through 8.

Evaluations of the survey regressions for the dependent variables fracture energy, ultimate tensile strength, hardness, and weight change are summarized in Tables 9, 10, 11, and 12, respectively. All of the model evaluations listed in the above tables are based on 7 independent variables (linear terms of temperature, time, and oxygen potential, linear cross-products, and second order oxygen potential) resulting in 7 degrees of freedom for each regression and 12 degrees of freedom for residual analysis. With 20 observations and seven degrees of freedom, regressions with $F_{(7,20)} > 2.51$ imply a significance of 95 percent.⁽²⁰⁾ The σ reported in the above tables is the standard deviation of the residuals and R^2 is the coefficient of determination⁽²¹⁾ or the correlation coefficient squared. For example, a R^2 of 0.80 implies that there is a 20 percent unexplained variance in the model. High values of R^2 (above 0.90) with a low σ and high F value imply accurate predictive models. Values of R^2 between 0.8 and 0.9 imply models which lack accuracy but provide valuable information on trends.

Fracture energy data for all materials grouped by oxygen potential and normalized to the average fracture energy of recrystallized specimens are presented in Table 13.

Average recrystallized fracture energy is obtained by the expression

$$\frac{\bar{y}[+ + -] \text{ recrystallized}}{\bar{y}[+ + -] \text{ unrecrystallized}} \quad (\bar{y} \text{ as received})$$

where y is fracture energy in joules/cm² and $\bar{y}[+-]$ represents the average of two observations at 800°C, 130 hours and 2 ppmw [O].

With the exception of Ta-10W, T-111, Mo from Source 2, and TZM from source 2 all of the materials show an enhancement of fracture energy with Na exposure at low oxygen potential and in general this enhancement becomes greater as oxygen potential is increased.

Ta Alloys

All of the mechanical property and weight change results for Ta-10W and the T-111 alloy are presented in Tables 14 and 15, respectively. Typical load-elongation curves and mechanical properties are summarized in Figures 22 and 23 for Ta-10W and T-111, respectively. Typical optical metallographic sections of as received material and recrystallized material exposed to Na at 800°C, 130 hours, 100 ppmw [O] and 300°C, 10 hours, 2 ppmw [O] for both Ta-10W and T-111 are presented in Figures 24 and 25, respectively. A higher magnification photomicrograph of a selected area of the Ta-10W specimen exposed at 800°C, 130 hours, 100 ppmw [O] is illustrated in Figure 26. The coating or deposit on the surface of this specimen appears to penetrate the grain boundaries and an analysis of this utilizing the SEM with a energy dispersive x-ray technique (EDS) indicated a Ta rich compound. The elements Na, Ni, and W were not detected in this coating. Lesser amounts of this coating were detected on the T-111 specimen exposed to the same conditions. A surface coating was not observed on the 300°C, 130 hour, 2 ppmw exposure.

Transmission electron microscopy (TEM) was performed on thinned sections from as received material for Ta-10W and T-111 for all exposures on Ta-10W and for selected exposures on T-111 alloy. The TEM results are illustrated in the selected photomicrographs of Figures 27 through 30.

The matrix material appeared to be clear of precipitates in all cases. In the as received Ta-10W material a thin grain boundary film with halos was present (see Figure 27a) and this film disappeared after recrystallization (see Figure 27b). After exposure at 300°C for 10 hours and low oxygen potential a fine granular precipitate was observed adjacent to the grain boundaries in both Ta-10W and T-111 and a thin film appeared to delineate the grain boundaries (see Figures 28a and 30a, respectively). After 130 hours under the same conditions the precipitate particles in the Ta-10W alloy appeared to elongate and started to condense into a grain boundary film (see Figure 28b). Exposures at 300°C, 10 hours and 130 hours with an oxygen potential of 100 ppm and at the conditions of the experimental midpoint produce clean microstructures (see Figures 29a, 29b, and 27c, respectively). A continuous grain boundary film is present after exposure at 800°C for both 10 and 130 hours in Na with low oxygen potential (see Figures 28c and 28d, respectively). Electron diffraction of the boundary film illustrated in Figure 28d matched the lattice spacings of β TaH and Ta₂C. Since TaH decomposes at 60°C, the thinned foil from specimen A10 (see Figure 28d) was heated in the TEM to 800°C in steps while simultaneously observing the structure. The grain boundary film appeared stable during heating so the film is probably a carbide. Grain boundary films were also observed in specimens exposed at 800°C for 10 hours and 130 hours in Na with 100 ppm oxygen potential (see Figures 29c and 29d, respectively). The longer exposure time produced a thicker film but a clean diffraction pattern could not be obtained from these films because of matrix interactions. However, the films resulting from exposure at high oxygen potential were different in appearance (see Figures 28c, 28d, 29c, and 29d) than those produced by low oxygen potential exposures.

Tensile fracture surfaces of test coupons representing each test condition for both Ta alloys were surveyed by SEM. Low magnification montages illustrating the fracture morphologies for each test condition are presented in Figures 31 and 32 for Ta-10W and T-111, respectively. In general all the specimens failed by a transgranular ductile void mode except for specimens exposed at 300°C, 10 hours, 2 ppmw [O] (A22 and B16); 800°C, 10 hours, 2 ppmw [O] (A4 and B6); and 300°C, 130 hours, 2 ppmw [O] (A1 and B2). The failure mode for these three exposures was mixed with portions of each fracture surface showing evidence of a multimode failure including ductile void, brittle intergranular, and quasi-cleavage. Typical higher magnification fractographs illustrating the modes of fracture for each alloy are presented in Figures 33 through 35 for Ta-10W and in Figures 36 through 38 for T-111.

Regression analysis of the Ta-10W and T-111 alloy data produced statistically significant models for the dependent variables fracture energy, ultimate tensile strength, and weight change. Fracture energy of the Ta-10W alloy is related to the independent variables by the following model:

$$\begin{aligned}
 & \text{Ta-10W} \\
 & \text{Fracture Energy} = + 97.08 \pm 3.25 \qquad \qquad \qquad [5] \\
 & (\text{joules/cm}^2) \qquad - 0.0702 [\text{Temp}] \text{ }^\circ\text{C} \qquad \qquad \qquad t = -13.71 \\
 & \qquad \qquad \qquad - 0.4548 [\text{time}] \text{ hrs} \qquad \qquad \qquad t = -12.60 \\
 & \qquad \qquad \qquad + 2.9756 [O] \text{ ppmw } [O] \qquad \qquad \qquad t = 32.73 \\
 & \qquad \qquad \qquad + 0.0008 [(Temp) * (time)] \qquad \qquad \qquad t = 14.57 \\
 & \qquad \qquad \qquad - 0.0257 [(O) * (O)] \qquad \qquad \qquad t = -29.20 \\
 & \qquad \qquad \qquad \pm 3.33
 \end{aligned}$$

where $R^2 = 0.992$ and $F_{(5, 18)} = 308.4$. The error term listed to the right of the constant term (± 3.25) in [5] is the uncertainty of the constant term and the error term listed at the end of [5] (± 3.33) is the standard error of the residuals. The t values listed to the right of each independent variable in Eq [5] indicate the significance level of each coefficient in the regression.

Contour plots developed from Eq [5] are presented for exposure times of 10 hours, 70 hours, and 130 hours in Figures 39, 40, and 41, respectively. Experimentally determined values of the dependent variables are plotted at the corners of the contour plots for 10 hour and 130 hour exposures and at the center of the contour plot for 70 hour exposure.

Ultimate tensile strength of the Ta-10W alloy is related to the independent variables by the following model:

$$\begin{aligned}
 &\text{Ta-10W} \\
 &\text{Ultimate} \\
 &\text{Tensile Strength} = + 779.87 \pm 6.06 \qquad \qquad \qquad [6] \\
 &(\text{MPa}) \qquad \qquad \qquad - 0.04680 [\text{Temp}] \qquad \qquad \qquad t = -4.43 \\
 &\qquad \qquad \qquad + 1.72415 [0] \qquad \qquad \qquad t = 6.98 \\
 &\qquad \qquad \qquad + 0.00030 [(\text{Temp}) * (\text{time})] \qquad \qquad \qquad t = 3.36 \\
 &\qquad \qquad \qquad - 0.00439 [(\text{time}) * (0)] \qquad \qquad \qquad t = -5.85 \\
 &\qquad \qquad \qquad - 0.01520 [(0) * (0)] \qquad \qquad \qquad t = -6.55 \\
 &\qquad \qquad \qquad \pm 8.79
 \end{aligned}$$

where $R^2 = 0.888$ and $F_{(5,18)} = 18.94$.

Contour plots developed from the Ta-10W strength model are presented for 10, 70, and 130 hour exposure times in Figures 42, 43, and 44, respectively.

Fracture energy of the T-111 alloy is related to the independent variables by the following model:

$$\begin{aligned}
 &\text{T-111} \\
 &\text{Fracture Energy} = + 75.21 \pm 8.09 \qquad \qquad \qquad [7] \\
 &(\text{joules/cm}^2) \qquad \qquad \qquad - 0.05074 [\text{Temp}] \qquad \qquad \qquad t = -4.15 \\
 &\qquad \qquad \qquad - 0.25262 [\text{time}] \qquad \qquad \qquad t = -2.90 \\
 &\qquad \qquad \qquad + 3.26684 [0] \qquad \qquad \qquad t = 16.38 \\
 &\qquad \qquad \qquad + 0.00063 [(\text{Temp}) * (\text{time})] \qquad \qquad \qquad t = 4.72
 \end{aligned}$$

$$\begin{aligned}
& - 0.00150 [(time) * (0)] & t = -2.22 \\
& - 0.02814 [(0) * (0)] & t = -15.18 \\
& \pm 7.96
\end{aligned}$$

where $R^2 = 0.960$ and $F_{(6, 19)} = 51.39$.

Contour plots developed from the T-111 fracture energy model are presented for the standard exposure times in Figures 45, 46, and 47.

Ultimate tensile strength of the T-111 alloy is related to the independent variables by the following model:

$$\begin{aligned}
& \text{T-111} \\
& \text{Ultimate} \\
& \text{Tensile Strength} = + 592.10 \pm 18.42 & [8] \\
& \text{(MPa)} & + 0.14553 [\text{Temp}] & t = 5.34 \\
& & + 0.82185 [\text{time}] & t = 7.23 \\
& & + 4.62675 [0] & t = 8.92 \\
& & - 0.00177 [(\text{Temp}) * (0)] & t = -4.58 \\
& & - 0.00742 [(\text{time}) * (0)] & t = -4.62 \\
& & - 0.02780 [(0) * (0)] & t = -6.32 \\
& & \pm 18.89
\end{aligned}$$

where $R^2 = 0.910$ and $F_{(6, 20)} = 7.51$.

Contour plots developed from the T-111 strength models are presented for the standard exposure times in Figures 48, 49, and 50.

Additional experiments were performed to clarify the unusual response of Ta-10W and T-111 to the exposure conditions. These experiments included hydrogen, oxygen and carbon analyses, and evaluation of the influence of crucible material.

Results of the hydrogen analysis of selected Ta-10W specimens are presented in Table 16. In summary these results show elevated

hydrogen levels in specimens exposed to Na with low oxygen potential except for the 800°C, 130 hour exposure. Hydrogen concentration is very low in the specimen exposed at the midpoint. Specimens exposed at 800°C, 130 hours at both high and low oxygen potential have similar hydrogen concentrations. Results of the carbon analysis of selected Ta-10W specimens are presented in Table 17. The variable results of carbon analysis within a single specimen of unexposed material (A28), brackets the concentration levels obtained from exposed specimens (which also exhibit large within specimen variability). Thus, it is probable that specimen carbon concentration is not influenced by Na exposure.

Results of the oxygen analysis of selected Ta-10W and T-111 specimens are presented in Table 18. In general the oxygen concentration of the T-111 is higher than Ta-10W for each exposure condition. This probably reflects the gettering of the Hf addition in T-111. Within the scatter of the data, oxygen concentration is not affected by exposure to Na at low oxygen potential. Both alloys show a substantial increase in bulk oxygen concentration when exposed under the midpoint conditions. The oxygen concentration of Ta-10W specimens exposed to Na with 100 ppmw oxygen potential for 10 hours is approximately double that for the unexposed material and the 130 hour exposure for both Ta-10W and T-111 yields specimen oxygen concentrations which are approximately equivalent to concentrations in unexposed material (see Table 18). Four Ta-10W samples were also analyzed in the unetched condition. The largest difference in oxygen concentration between etched and unetched samples is found for the 800°C, 130 hour, 100 ppmw [O] exposure of Ta-10W specimens. These data along with the photomicrographs showing surface attack (Figure 26) indicate that substantial surface oxidation occurs at this exposure. The weight change data for these materials (see Tables 14 and 15) also indicate significant weight loss for the 800°C, 130 hour, 100 ppmw [O] exposure for Ta-10W and both 800°C, 100 ppmw [O] exposures for T-111. All of the above data suggest surface oxidation followed by sloughing of the oxide surface layer.

Results of the crucible material study are presented in Table 19. Exposure in 316 stainless steel crucibles results in a decrease in Ultimate Tensile Strength (UTS) and fracture energy for both Ta-10W and T-111 as compared to similar exposures in Ni crucibles.

SEM photomicrographs of the submerged internal surface and a cross-sectional view of the wall of a 316 stainless steel crucible are presented in Figures 51a and 51b, respectively. This crucible contained a Ta-10W specimen exposed to Na with low oxygen potential at 300°C for 130 hours. Both photomicrographs indicate very shallow surface attack selectively occurring at grain boundaries. A sputter profile was obtained normal to the surface shown in Figure 51a over a $100\ \mu\text{m}^2$ area utilizing Auger spectroscopy, and the results show a Cr depletion up to 2 μm below the crucible surface. No change was detected in other elements at this depth.

Mo and TZM

All of the mechanical property and weight change results for Mo and TZM are presented in Tables 20 through 23. Typical load-elongation curves and mechanical properties are summarized in Figures 52, 53, 54, and 55. Typical optical photomicrographs of metallographic sections representing as-received material and recrystallized material exposed to Na at 800°C, 130 hours, 100 ppmw [O] and 300°C, 10 hours, 2 ppmw [O] for all Mo and TZM sources are presented in Figures 56 through 59.

Regions adjacent to the exposed specimen surface were examined at 500X using optical metallographic techniques and the surfaces and adjacent areas appeared to be clean and free from attack. Fracture surfaces of test coupons representing each experimental condition were surveyed by SEM. Low magnification montages illustrating the fracture morphology for each test condition are presented in Figures 60 through 63.

Fracture behavior of these materials ranged from complete brittle quasi cleavage for recrystallized material to brittle quasi cleavage or lamellar fracture with localized ductile bands for material in the unrecrystallized condition. Exposure to Na seemed to have little effect on the fracture morphology.

Typical (for both Mo and TZM) higher magnification fractographs of the quasi cleavage mode and the lamellar fracture mode are illustrated in Figures 64a and 64b, respectively.

Potential models as determined by the regression surveys included Mo source 2 and TZM sources 1 and 2 fracture energy and Mo source 2 and TZM source 2 weight change. Follow up regressions in which low significance coefficients were dropped yielded two statistically significant models; weight change of source 2 Mo and weight change of source 2 TZM alloy. Weight change due to Na exposure for Mo from source 2 is related to the independent variables as follows:

$$\begin{aligned}
 &\text{Mo (Source 2)} \\
 &\text{Weight Change} = + 7.22 \pm 0.62 \qquad \qquad \qquad [9] \\
 &(\text{Milligrams}) \quad - 0.00805 [\text{Temp}] \qquad \qquad \qquad t = 7.84 \\
 &\qquad \qquad \qquad - 0.024460 [\text{time}] \qquad \qquad \qquad t = 3.97 \\
 &\qquad \qquad \qquad + 0.00003 [(\text{Temp}) * (\text{time})] \qquad \qquad t = -2.71 \\
 &\qquad \qquad \qquad + 0.00010 [(\text{Temp}) * (0)] \qquad \qquad \qquad t = -8.83 \\
 &\qquad \qquad \qquad + 0.000175 [(time) * (0)] \qquad \qquad \qquad t = -3.71 \\
 &\qquad \qquad \qquad - 0.000404 [(0) * (0)] \qquad \qquad \qquad t = 5.82 \\
 &\qquad \qquad \qquad \pm 0.56
 \end{aligned}$$

where $R^2 = 0.940$ and $F_{(6, 18)} = 28.5$.

Contour plots developed from the Mo source 2 weight change model are presented in Figures 65, 66, and 67 for the standard exposure times.

Weight change of source 2 TZM alloy is related to the independent variables as follows:

$$\begin{aligned}
 &\text{TZM (Source 2)} \\
 &\text{Weight Change} = + 5.96 \pm 0.40 \qquad \qquad \qquad [10] \\
 &\text{(Milligrams)} \quad - 0.00836 [\text{Temp}] \qquad \qquad \qquad t = -12.23 \\
 &\qquad \qquad \qquad - 0.02971 [\text{time}] \qquad \qquad \qquad t = -7.19 \\
 &\qquad \qquad \qquad + 0.00003 [(\text{Temp} * (\text{time}))] \qquad \qquad \qquad t = 5.29 \\
 &\qquad \qquad \qquad + 0.00009 [(\text{Temp}) * (0)] \qquad \qquad \qquad t = 12.03 \\
 &\qquad \qquad \qquad + 0.00020 [(0) * (\text{time})] \qquad \qquad \qquad t = 6.46 \\
 &\qquad \qquad \qquad - 0.00031 [(0) * (0)] \qquad \qquad \qquad t = -7.05 \\
 &\qquad \qquad \qquad \pm 0.38
 \end{aligned}$$

where $R^2 = 0.972$ and $F_{(6, 20)} = 74.97$.

Contour plots developed from the TZM source 2 weight change model are presented in Figures 68, 69, and 70 for the standard exposure times.

Mo-Re Alloys

Mechanical property and weight change results are summarized in Tables 24 through 28 for all of the Mo-Re alloys. Load-elongation curves and mechanical properties are summarized in Figures 71 through 75. Typical optical photomicrographs of metallographic sections representing as-received material and recrystallized material exposed to Na at 800°C, 130 hours, 100 ppmw [O] and 300°C, 10 hours, 2 ppmw [O] for all the Mo-Re alloys are presented in Figures 76 through 80. All sodium exposed surfaces appeared to be clean and free from attack, as observed by optical metallography. Fracture surfaces of test coupons representing each experimental condition are presented in low magnification montages in Figures 81 through 85.

As shown in the montage of Figure 81 and the typical higher magnification fractographs in Figures 86a and 86b the Mo-13Re alloy

failure mode is brittle. However, two modes are present: failure of as-received material (specimens E74, E76, and E89) is quasi cleavage as shown in Figure 81 and failure of recrystallized specimens is intergranular as illustrated in Figure 81. Exposure to Na did not appear to influence the fracture mode.

Mo-26Re samples from source 1 all failed by a brittle intergranular mode as illustrated in the typical high magnification fractograph of Figure 86b and the low magnification montage of Figure 82. As-received Mo-26Re material from source 2 (specimens F74, F73, and F83 in Figure 83) failed by a lamellar mode with localized ductility as shown in the high resolution fractograph in Figure 86c. However, after recrystallization all of the Mo-26Re source 2 material failed by a brittle intergranular mode as shown in the typical high resolution fractograph in Figure 86b. Thus, all recrystallized Mo-26Re material failed in a brittle manner and the failure mode does not appear to be influenced by Na exposure.

All Mo-41Re material from source 1 failed by brittle mixed mode of quasi-cleavage and intergranular fracture as illustrated in the typical high resolution fractograph shown in Figures 86a and 86b and by the low magnification montage of Figure 84. Unrecrystallized material from source 2 (specimens G85, G73, and G78 in Figure 85) failed in a lamellar mode with localized ductility as illustrated by the typical high resolution fractograph of Figure 86c. All recrystallized specimens from source 2 failed by the same brittle mixed mode illustrated in Figures 86a and 86b for source 1 material. Again Na exposure did not appear to influence the fracture mode.

Fracture initiation studies were performed on fractured notch tensile specimens of the Mo-41Re source 1 material utilizing SEM. Figures 87a and 87b illustrate the appearance of typical specimen surfaces near the notch root before and after Na exposure, respectively. These photomicrographs illustrate the good resistance that these materials possess against general attack. Fracture initiation

for the as-received recrystallized material is illustrated in Figure 88a. Initiation is very brittle and occurs in an intergranular fashion at the surface with crack propagation also occurring in an intergranular fashion through the specimen. After exposure at 800°C for 10 hours in Na with low oxygen potential, there is evidence of surface plasticity, a small number of secondary cleavage cracks occur at the root of the notch, and crack propagation for the first three or four grains from the surface occurs by a combination cleavage and intergranular fracture (see Figure 88b). Specimens exposed at 800°C for 130 hours to Na containing 100 ppmw oxygen exhibited extensive secondary cleavage cracking at the root of the notch, and after initiation at one of these cracks, fracture propagated in a mixed intergranular/cleavage mode for about 25 grains (see Figure 88c). Further in from the surface the crack propagated in an intergranular fashion (not shown in Figure 88c). Extensive secondary cleavage cracks were found at the root of the notch on specimens exposed under midpoint conditions and propagation from the surface occurred by cleavage for the first three or four grains (see Figure 88d). After this point, propagation proceeded in an intergranular fashion.

Further evaluation of regression models for the Mo-Re alloys yielded two models that were statistically significant: Weight change of the Mo-13Re and Mo-41Re source 1 alloys.

Weight change due to Na exposure for the Mo-13Re alloy is related to the independent variables in the following manner:

$$\begin{array}{l}
 \text{Mo-13Re} \\
 \text{Weight Change} = + 6.75 \pm 0.46 \qquad \qquad \qquad [11] \\
 \text{(Milligrams)} \quad - 0.00919 [\text{Temp}] \qquad \qquad \qquad t = -11.70 \\
 \qquad \qquad \qquad - 0.01874 [\text{time}] \qquad \qquad \qquad t = -3.95 \\
 \qquad \qquad \qquad + 0.00003 [(\text{Temp}) * (\text{time})] \qquad t = 3.45 \\
 \qquad \qquad \qquad + 0.00009 [(\text{Temp}) * (0)] \qquad \qquad t = 10.64 \\
 \qquad \qquad \qquad + 0.00009 [(\text{time}) * (0)] \qquad \qquad t = 2.48
 \end{array}$$

$$- 0.00032 [(0) * (0)] \quad t = -6.37$$

$$\pm 0.40$$

where $R^2 = 0.952$ and $F_{(6, 20)} = 43.2$.

Contour plots developed from the Mo-13Re weight change model are presented in Figures 89, 90, and 91 for the standard exposure times.

Weight change due to Na exposure for the Mo-41Re alloy from source 1 is related to independent variables in the following manner:

Mo-41Re (Source 1)

$$\text{Weight Change} = - 6.54 \pm 0.28 \quad [12]$$

(Milligrams)

+ 0.00827 [Temp]	t = 18.63
- 0.01144 [time]	t = -4.37
- 0.05715 [0]	t = -7.95
+ 0.00001 [(Temp) * (time)]	t = 3.35
- 0.00008 [(Temp) * (0)]	t = -15.68
+ 0.00008 [(time) * (0)]	t = 3.76
+ 0.00070 [(0) * (0)]	t = 11.09

$$\pm 0.20$$

where $R^2 = 0.991$ and $F_{(7, 19)} = 176.6$.

Contour plots developed from the Mo-41Re alloy weight change model are presented in Figures 92, 93, and 94 for the standard exposure times.

Oxygen concentrations of selected Mo and Mo alloy specimens are listed in Table 29.

Re and Re-5W

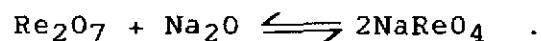
Mechanical property and weight change results for wrought Re, CVD Re, and CVD Re-5W are summarized in Tables 30 through 32, respectively. Typical load-elongation curves and mechanical properties are summarized in Figures 95 through 97. Hardness measurements

were not performed on the thin CVD material because a valid Rockwell A indentation could not be obtained. Typical optical photomicrographs of metallographic sections representing as-received material and recrystallized material exposed to Na at 800°C, 130 hours, 100 ppmw [O] and 300°C, 10 hours, 2 ppmw [O] for the above materials are presented in Figures 98 through 100. All Na exposed specimen surfaces and near surface regions (examined at 500X) appeared to be clean and free from attack.

Low magnification montages illustrating the fracture morphology for each test condition are presented in Figures 101 and 102a and 102b for wrought Re, CVD Re, and CVD Re-5W, respectively.

All Re and Re-5W specimens failed by a ductile intergranular mode and typical high resolution fractographs for wrought Re, CVD Re, and CVD Re-5W are presented in Figures 103a, 103b, and 103c, respectively. Sodium exposure and/or alloy recrystallization did not appear to influence the fracture mode for these materials.

In addition to evaluation of the fracture surface, specimen surfaces near the root of the notch were also examined with SEM. Typically (for all Re base materials) the as received, unexposed, surfaces are characterized by crisp, sharp grain boundary intersections with the specimen surface and in some instances cracks occurred at the grain boundary-surface intersection as shown in Figure 104a. After exposure at 800°C, 130 hours in Na with 100 ppmw [O] these intersecting boundaries have a rounded appearance and the boundaries do not appear to be the site of cracks. In addition, the specimen surface was covered with solidified globules as shown in Figure 104b and 104c. These globules were analyzed with an electron microprobe and found to be rich in Re, Na, and oxygen. It is likely that the particles formed by the reaction



Na ReO₄ melts at 425°C. (22) Potential models as determined by the survey regressions included fracture energy for wrought Re, CVD Re, and CVD Re-5W along with weight change for wrought Re and CVD Re. After low significance coefficients were dropped from the survey models, three statistically significant models remained; CVD Re-5W fracture energy, wrought Re weight change, and CVD Re weight change. Fracture energy of the CVD Re-5W alloy is related to the independent variables by the following model:

CVD Re-5W

$$\begin{aligned} \text{Fracture Energy} &= + 249.37 \pm 12.10 && [13] \\ (\text{joules/cm}^2) & - 0.18001 [\text{Temp}] && t = -8.73 \\ & - 0.84852 [\text{time}] && t = -6.81 \\ & + 0.00103 [(\text{Temp}) * (\text{time})] && t = 4.96 \\ & + 0.00123 [(\text{Temp}) * (0)] && t = 5.77 \\ & + 0.00418 [(time) * (0)] && t = 4.41 \\ & - 0.00329 [(0) * (0)] && t = -2.48 \\ & + 11.4 \end{aligned}$$

where $R^2 = 0.943$ and $F_{(6, 20)} = 36.05$.

Contour plots developed from Eq [13] are presented for exposure times of 10 hours, 70 hours, and 130 hours in Figures 105 through 107.

Weight change due to Na exposure for wrought Re is related to the independent variables by the following model:

Wrought Re

$$\begin{aligned} \text{Weight Change} &= + 4.10 \pm 0.15 && [14] \\ (\text{Milligrams}) & - 0.00473 [\text{Temp}] && t = -20.50 \\ & - 0.00562 [\text{time}] && t = -4.12 \\ & - 0.01477 [0] && t = -4.32 \\ & + 0.00001 [(\text{Temp}) * (\text{time})] && t = 3.02 \\ & + 0.00005 [(\text{Temp}) * (0)] && t = 18.69 \\ & + 0.00005 [(time) * (0)] && t = 4.62 \end{aligned}$$

$$- 0.00007 [(0) * (0)] \quad t = -2.53$$

$$\pm 0.124$$

where $R^2 = 0.984$ and $F_{(7, 20)} = 106.39$.

Contour plots for the wrought Re weight change model are presented for the standard Na exposure times in Figures 108 through 110.

Weight change due to Na exposure for CVD Re is related to the independent variables by the following model:

$$\begin{aligned} &\text{CVD Re} \\ &\text{Weight Change} = + 4.96 \pm 0.22 \quad [15] \\ &\text{(Milligrams)} \quad - 0.00624 [\text{Temp}] \quad t = -16.61 \\ &\quad - 0.00725 [\text{time}] \quad t = -3.17 \\ &\quad + 0.00001 [(\text{Temp}) * (\text{time})] \quad t = 3.20 \\ &\quad + 0.00006 [(\text{Temp}) * (0)] \quad t = 13.24 \\ &\quad + 0.00004 [(time) * (0)] \quad t = 1.91 \\ &\quad - 0.00019 [(0) * (0)] \quad t = -7.53 \\ &\quad \pm 0.20 \end{aligned}$$

where $R^2 = 0.977$ and $F_{(6, 18)} = 77.94$.

Contour plots for the CVD Re weight change model are presented for the standard Na exposure times in Figures 111 through 113.

Tungsten

Mechanical property and weight change data on W are summarized in Table 33. Hardness was not obtained because the material was so brittle that the hardness indenter fractured the specimens. Unrecrystallized specimens failed by intergranular quasi cleavage (see Figure 114a) and recrystallized material failed in a classical intergranular brittle fashion (see Figure 114b). Both tensile

properties and fracture mode did not appear to be influenced by Na exposure and specimen surfaces appeared to be free from attack.

High Temperature Test Results

Radiography

Contact radiographs of each tube for the first test series were made of two views 90° apart and one view for each tube is shown in Figure 115. The radiographs show that the larger particles of UO_2 settle to the bottom of each tube after the temperature cycles.

Surface Appearance

Outer surface appearance of the bottom 75 mm of the tubes after 5 hours exposure at 2000°C is illustrated in Figure 116. The Ta-10W tube surface appears to be thermally etched in the 2000°C zone and grain structure is clearly visible. The surface of the Mo-41Re tube also appears to be thermally etched but not as severely as the Ta-10W. Re-5W and T-111 surfaces do not appear to be visually affected by the high temperature exposure. The surface of the Re tube exhibits what appears to be exfoliation in a region about 75 mm from the bottom of the tube.

Figure 117 illustrates the surface appearance of the inside of the tubes after sectioning along the axis. In general, the surfaces appear discolored as a function of the temperature and location of the tube contents but no gross attack can be discerned at low magnifications. However, the same exfoliation observed on the exterior of the CVD Re tube appears to be present on the inside surface of this tube. The longitudinal welds on the Ta-10W and T-111 tubes are also visible in Figure 117 and as indicated, they appear to be free from cracks and attack along the entire length of the tubes.

Hardness

A summary of the hardness measurements made on the outside surface of each tube as a function of distance and temperature along the tube axis is tabulated in Table 34 for T-111, Ta-10W, Mo-41Re, CVD Re, and CVD Re-5W. In general, each material softened at the hot end with the most pronounced effect occurring in the CVD tubes.

Metallography

First Test Series--Longitudinal sections of each tube were cut into 50 mm long increments, mounted, and polished. The complete length of each section was examined optically at 32 and 300X and the bottom tube section (hot section) was photographed along the entire length at 32X. In all instances the microstructures observed at 50 mm from the tube bottom were typical of the remaining length of the tube.

Figures 118 and 119 are posttest photomicrographs of typical structures on the Ta-10W tube as well as the as-received condition and a cross section of the longitudinal weld. Approximate conditions of exposure are also listed with each photomicrograph. Note that considerable grain growth occurs in the very hot region (Figures 118a and 118b) and the grain size decreases as the exposure temperature is reduced. Note also that the integrity of both the inner and outer surfaces of the tube as well as the weld (see Figure 118) appears to be good even though the weld is not a full penetration weld.

Foils prepared from the 2000°C, ~1800°C, ~1700°C, 1350°C, and 1000°C regions of the Ta-10W tube were evaluated by TEM, and typical photomicrographs of these regions are illustrated in Figures 120 and 121. The herringbone structure (see Figure 113a) from the hottest region was evaluated by electron diffraction and showed no difference in diffraction pattern. A fine unidentified grain boundary precipitate was observed in the 1800°C region (see

Figure 120b) as well as regions of herringbone structure (not shown). The grain boundaries appeared clean in the remaining foils, and as the exposure temperature decreased, the dislocation density appeared to increase.

Figures 122 and 123 are photomicrographs of typical structures in the T-111 tube, as well as the as-received condition and a cross section of the longitudinal weld. Approximate conditions of exposure are also listed with each photomicrograph. Note that there is very little grain growth in this tube probably because the T-111 grain boundaries are stabilized with the 2 percent Hf. Again, the closure weld at the bottom of the tube (see Figure 122b) and the tube surfaces appear to be free from attack even though there is a lack of weld penetration.

Posttest photomicrographs from typical microstructures from the Mo-41Re tube along with the approximate exposure conditions (as well as the as received condition) are presented in Figures 124 and 125. Grain growth is evident in the high temperature regions but there is no evidence of attack by the high temperature exposure to oxygen in Na and UO_2 .

Typical microstructures for various exposure conditions, as well as the as-received condition, are presented in Figures 126 and 127 for the CVD Re tube. These photomicrographs illustrate the massive grain growth in the hot region and extensive grain boundary cracking after the grain growth had occurred.

A similar collection of typical microstructures for the CVD Re-5W tube is presented in Figures 128 and 129. This tube exhibited the same behavior as the CVD Re tube.

It is interesting that both CVD tubes were leak tight at the end of the test even though significant grain boundary separation had occurred. All of the tubes tested appeared to be free from any attack in the region of steep temperature gradient.

Second Test Series--As stated previously, the highest temperature exposure for the second series was 1500°C with a total exposure time at that temperature limited to 320 minutes. This temperature produced full recrystallization in both materials tested (Ta-10W and Mo-41Re) and a small amount of grain growth in the Ta-10W tube. Both tubes were cut longitudinally along the axis and the resulting cross sections were mounted, polished, and inspected by optical metallography at magnifications up to 300X for the entire length of each tube. Both tubes were free of internal attack and surface attack at the internal and external surfaces. Typical optical microstructures from the 1500°C region and from the cooler region of the tube (~75 mm from the bottom) are shown in Figure 130 for Ta-10W and in Figure 131 for Mo-41Re, respectively.

Discussion

Organization of this section will be similar to the previous section on results in that discussion of the results will be ordered by test temperature. In addition, a separate subsection summarizing the discussion will be included.

Low Temperature Experiments

General

Two classes of materials were evaluated in this study:

1. Materials that are not influenced by recrystallization, such as Ta and Re.
2. Materials that are strongly influenced by recrystallization such as Mo, W, and Mo alloys.

Both classes of materials exhibited good resistance to general attack by Na for all exposures within the factor space. Considering the maximum oxygen exposure and a typical sample geometry, the threshold oxygen concentration for significant attack at the temperatures and times evaluated, is above $\sim 0.45 \text{ mg/cm}^2$ of refractory metal and $\sim 4.5 \text{ mg/cm}^3$ of refractory metal. The above numbers are significant from an engineering standpoint because many applications of these materials involve use in closed systems with a fixed supply of oxygen available. However, it is important to stress the necessity for maintaining a sealed system because other investigators⁽²³⁾ have reported substantial attack in 600°C Na in which the oxygen concentration is buffered at 40 ppmw.

In general, hardness and ultimate strength (except for the Ta alloys) were not significantly correlated to exposure conditions for recrystallized materials (see Tables 11 and 12). The reason for this lack of systematic response is possibly due to the brittle nature of these materials and the relatively low interaction rates with oxygen as the diffusion rates of oxygen in these materials is typically low.⁽²⁴⁾ On the other hand, both Ta-10W and T-111 ultimate strengths were highly correlated to exposure conditions (see Tables 9 and 10, respectively) and, on the average, exposure to Na tended to weaken both materials (see Table 4). This systematic response is probably a result of the relatively high diffusion rates for oxygen in Ta.

The histograms which rank alloys by strength and fracture energy should be used with caution because they do not take into consideration fracture toughness. For example, the Mo-41Re alloy ranks very high for both strength and fracture energy. However, after recrystallization the fracture mode of this material is brittle intergranular. This implies a very low fracture toughness. All other Mo-Re alloys, pure Mo, TZM, and W also fail in a brittle intergranular manner after recrystallization.

The histograms of Figures 17 and 18, the SEM fracture evaluations, and the data in Table 13 show that Re and Re-5W exhibit little degradation in properties after recrystallization, tolerate large amounts of oxygen ($\sim 0.6 \text{ mg/cm}^2$ or $\sim 12.9 \text{ mg cm}^3$) (see Tables 30 through 33) are resistant to hydrogen embrittlement,⁽²⁵⁾ and always fail in a ductile intergranular fashion. Disadvantages in utilizing these materials include high cost, poor fabricability because of a large work hardening coefficient ($m = 0.372$ at 10°C)⁽²⁶⁾ due to the hexagonal structure and, as the high temperature tests show, grain boundary separation because of the large grain size of CVD material.

The Re materials are followed in the histogram rankings by the Ta alloys. Like Re, the properties of Ta-10W and T-111 are not influenced by recrystallization. These alloys exhibited the most systematic response to exposures within the factor space probably because of the high diffusion rates for interstitials. With exception of the ductility trough at low oxygen potential, both materials performed well in the test environment.

A detailed discussion of the results pertaining to each alloy family will follow.

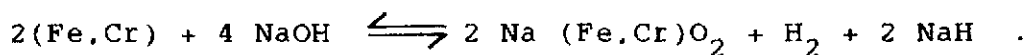
Ta Alloys

The low temperature test trends are in some respect contrary to expectations derived from previous work in buffered experiments. For example, the fracture energies of Ta-10W and T-111 decrease after exposure to Na with low oxygen potential, but after exposure to Na at elevated oxygen potentials, the fracture energy is higher than for the unexposed condition. From the literature, one would expect little change in properties with low oxygen potential exposure⁽²⁷⁾ and a general degradation after exposure at elevated oxygen potentials.⁽²⁸⁾ Explanation of these phenomena is not

straightforward and requires utilization of the extensive chemical and microstructural analysis performed on these systems.

Stainless steel crucibles were used for exposures at low oxygen potentials to evaluate the compatibility of stainless steel in the system and to buffer the oxygen potential in the Na to very low levels by utilizing the NaCrO_2 reaction. The mixed fracture modes and low fracture energies observed at several of the low oxygen exposures (300°C, 10 hours and 130 hours; and 800°C, 10 hours) correlate well with the high hydrogen concentrations presented in Table 16. Exposure at 800°C for 10 hours, 2 ppmw [O] in Ni crucibles produced fracture energies approximately two times higher than those obtained for the same exposure conditions in stainless steel crucibles (see Table 19). Thus, the decrease of fracture energy as a result of exposure to Na at low oxygen potential appears to be related to both elevated hydrogen concentration and crucible material.

The presence of high hydrogen concentrations in the test coupons after certain exposures was unexpected. It is likely that dissolved hydrogen or NaOH is present as a contaminant in the sodium as no specific hydrogen "getter" was included in the purification loop.⁽²⁹⁾ The NaOH can be reduced by Fe or Cr⁽³⁰⁾ present in the stainless steel by the following reaction:



The reduction of NaOH could have occurred either in the stainless steel purification loop, master can or the individual experiment cans. Another, less likely, explanation for the elevated [H] concentration in some of the Ta alloy specimens is H pick-up from the cleaning procedure.⁽³¹⁾ Since the cleaning procedure is the same for specimens tested at all exposures, a surface barrier argument would also have to be applied to explain the variable [H] pick-up.

Grain boundary attack on the submerged 316 stainless steel crucible surface, and depletion of Cr on the surface as observed by Auger spectroscopy is consistent with a reduction of NaOH or with the consumption of dissolved oxygen in excess of that in equilibrium with NaCrO_2 . Whatever the source, dissolved hydrogen could interact quickly with the test coupons as diffusion rates of H in Ta are high ($D = 2.6 \times 10^{-3} \text{ cm}^2/\text{s}$ at 300°C).⁽³²⁾ The low concentration of [H] and the improved properties of the specimens exposed to low oxygen Na at 800°C for 130 hours can be explained by an evaluation of H permeability in stainless steel. Hydrogen permeability in 316 stainless steel is two orders of magnitude higher at 800°C than at 300°C (7.33×10^{-6} as compared to $2.1 \times 10^{-8} \text{ cc/cm-s-atm}^{1/2}$,⁽³³⁾ respectively) resulting in the possibility that it is kinetically favorable for hydrogen to leave both the test coupon and the system via the crucible wall at the 800°C , 130 hours exposure. Using nickel crucibles increases the possibility that any hydrogen contaminant is lost from the system, as the permeability of H through Ni is higher than 316 stainless steel (2.34×10^{-7} at 300°C and $5.24 \times 10^{-5} \text{ cc/cm-s-atm}^{(1/2)}$ at 800°C).⁽³³⁾ Thus hydrogen contamination would only be observed in samples exposed at low temperatures or short times in stainless steel crucibles.

Because of the lack of an observed hydride in the TEM examination of specimens containing elevated H concentrations it is probable that the H is present as an interstitial in solid solution. Several investigators have shown that dissolved hydrogen has a potent effect on the mechanical properties of Ta.^(34,35) The mechanism postulated for creating a fracture mode change includes concentration enhancement of [H] at points of fracture in response to stress concentration.

Bulk carbon analysis indicates C transport between the specimen and the environment does not occur; however, the TEM work shows a considerable redistribution of C within specimens exposed at low

oxygen potential (see Figure 28). It is not surprising that carbides are present since the solubility of C in Ta at room temperature is low, less than 1 ppm at 500°C as extrapolated by Horz et al.⁽³⁶⁾ However, changes in carbide morphology do not appear to correlate with mechanical properties. For example, continuous grain boundary films were observed in both 800°C exposures at low oxygen potential but only specimens exposed for 10 hours failed in a mixed mode of fracture. On the other hand, specimens exposed at 300°C for 10 and 130 hours showed extensive precipitation of carbides adjacent to the grain boundaries and these specimens failed in a mixed mode. One would expect that continuous grain boundary films would degrade properties more than discrete precipitates at the grain boundary. The absence of grain boundary carbide networks at exposures with high oxygen potential also suggests that carbide morphology could be influenced by a C-[H] or C-[O] interaction.

The mechanical property response of the Ta alloys after exposure to Na with elevated oxygen potential could also be a result of interstitial solid solution effects.^(37,38) This response is characterized by a moderate increase in strength coupled with a large increase in fracture energy at midpoint exposures and modest increases in both strength and fracture energy (as compared to unexposed properties) at elevated oxygen potential (see Figures 22 and 23 and Table 13). Fracture mode for all the above conditions is ductile void (see Figures 34d, 35, 37d, and 38).

Plots of average specimen oxygen concentration as a function of average fracture energy for Ta-10W and T-111 are presented in Figure 132. Exposures at 300°C, 130 hours, low oxygen potential were omitted from this plot because of the [H] influence discussed previously. If the outlier point, 800°C, 130 hours, 100 ppm [O], for Ta-10W is disregarded a clear trend exists for both materials wherein fracture energies increase as a function of increasing specimen oxygen concentration. As stated previously, the TEM results on the Ta-10W alloy showed a clear matrix for all exposures

and clean grain boundaries for the midpoint exposure and the 300°C exposures, a light unidentified grain boundary film on the 800°C, 10 hours exposure, and a heavier grain boundary film on the 800°C, 130 hour exposure. Clear microstructures for specimens with high oxygen concentrations suggest that oxygen is present as an interstitial in solid solution. Mitchell and Smialek⁽³⁹⁾ have found that [O] in interstitial solid solution up to concentrations of ~1000 ppmat in Ta causes solid solution hardening which is linearly related to the oxygen concentration at temperatures between 77°K and 450°K. We propose that this solid solution hardening provide the mechanical property enhancement. Mitchell and Smialek suggest a complex explanation for this phenomena which includes long and short-range diffuse interactions between oxygen interstitials and dislocations.

The distribution of oxygen within the microstructure appears to be controlled by unknown factors. This is demonstrated by the observations of (1) a heavy oxide surface film and surface grain boundary attack for the Ta-10W exposed at 800°C, 130 hours and 100 ppmw [O], (2) low matrix oxygen concentration and grain boundary films for both 800°C high oxygen potential exposures, and (3) clean matrix and grain boundaries and elevated oxygen concentrations for the 550°C and 300°C exposures. Since these materials are very susceptible to interaction with interstitial contaminants, the scatter in Figure 132 could be caused by an unevaluated variable such as nitrogen or even a complex interstitial interaction. However, it is important to point out that, in general, properties improve after exposure to Na with elevated oxygen potential within the factor space evaluated.

T-111 alloy specimens have a smaller grain size than Ta-10W as illustrated in the optical photomicrographs of Figures 24 and 25, respectively. This fine grain size is also manifested in the fracture morphology as T-111 has smaller fracture features than Ta-10W (see Figures 36 through 38 and Figures 33 through 35, respectively). Hafnium is added as an oxygen "getter" in T-111 and it

appears that these fine hafnium oxides prevent grain growth. The banded appearance of the T-111 microstructures is also caused by these HfO_2 particles. The generally higher oxygen concentrations obtained for the T-111 alloy are probably a result of the Hf addition.

It is clear from the photomicrographs (Figure 26) which illustrates surface attack that the 800°C , 130 hour, 100 ppmw [O] exposure is close to the threshold for severe attack and possible degradation of base metal properties. The weight loss resulting from this exposure appears to result from sloughing of the oxide film as shown in Figure 26. Tantalum oxide, Ta_2O_5 , is a nonpassivating oxide and, due to the large density difference between the oxide and the metal, it is usually a nonadherent film. Both alloys exhibit excellent corrosion resistance at the other exposure conditions.

Contour plots of fracture energy and ultimate stress for both Ta-10W and T-111 (see Figures 39 through 44 and Figures 45 through 47, respectively) illustrate responses as a function of temperature and oxygen potential. However, there is a hidden hydrogen effect at the low oxygen potential and without the [H] it is likely that the properties would not be degraded in this region of the factor space.

Mo and Mo Alloys

Microstructures as illustrated by the optical photomicrographs show that the following materials were received in the fully recrystallized or partially recrystallized condition:

- Mo source 1, Figure 56a
- Mo-13Re (partial), Figure 77a
- Mo-26Re source 1, Figure 78a
- Mo-41Re source 1, Figure 80a
- TZM source 2, Figure 59a.

Fracture energy decreased by a factor of about two after recrystallization as shown in Table 13 for Mo source 2 (Factor = 2.79), Mo-13Re (2.92), Mo-26Re source 2 (2.05), Mo-41Re source 2 (1.36), and TZM source 1 (3.04). All fully recrystallized Mo and Mo alloys failed by brittle intergranular or cleavage mode. Merrigan and Lundberg⁽⁴⁰⁾ have also observed brittle fractures in the recrystallized Mo-13Re alloy. In general, unrecrystallized material failed in a mixed mode by lamellar tearing with localized ductile void and cleavage regions between the tears (see Figures 61, 62, 81, 83, and 85).

In some instances, unrecrystallized material failed in a cleavage mode. The oscillation between a mixed mode with some ductility and brittle cleavage for the same unrecrystallized material points out the intrinsic brittle nature of these materials.

The brittle fracture morphology observed for the recrystallized Mo-Re alloys was unexpected. Previous work⁽⁴¹⁾ has shown that the ductile-to-brittle transition temperature of recrystallized Mo is substantially lowered and fabricability of ingot material is enhanced by alloying with Re. All the work cited evaluates the DBTT as a function of the Re concentration by the use of slow bend tests. Our work with notched tensile specimens also shows that fracture energies of recrystallized material from source 2 (all alloys from the same supplier) increase with Re concentration while source 1 material (from two suppliers) exhibits an opposite trend (see Figure 133). These results point out the danger of implying good fracture toughness based on tensile and slow bend tests. For many applications, the poor fracture toughness of these materials will rule out their use.

As mentioned previously, all materials used in this investigation were fabricated by state-of-the-art processing. The variability of properties by source indicates the extreme sensitivity of

these materials to processing and emphasizes the importance of instituting elaborate qualification testing and monitoring programs for material used in critical experiments.

The general enhancement of fracture energies after Na exposure, even though all fractures were brittle, is probably related to differences in fracture initiation. For example, it is clear that the fracture initiation illustrated for the unexposed recrystallized Mo-41Re material (see Figure 89c) is more brittle than the fracture initiations observed for specimens exposed to Na (see Figures 89b, 89c, and 89d). Since these materials have high strength and low fracture toughness, subtle changes in fracture initiation can play a large role in influencing fracture energy. For example, this sensitivity is illustrated with the following calculation:

assume $\sigma_{\text{applied}} = 600 \text{ MPa}$ and $K_{\text{IC}} = 347 \text{ MPa} \sqrt{\text{mm}}$ then the critical flaw size to initiate fracture is

$$a = \frac{K_{\text{IC}}^2}{\sigma^2 \pi} = 0.106 \text{ mm} \quad [16]$$

which is a small flaw.

This sensitivity is also responsible for the poor reproducibility of replicate experiments, which, in turn, results in a lack of correlation between the dependent variables and exposure conditions.

With the exception of the TZM alloys, oxygen concentrations of the Mo and Mo alloys are very low and are not influenced by Na exposure (see Table 29). TZM alloy contains 0.5 percent Ti and 0.08 percent Zr, and these elements are probably responsible for the increased oxygen concentration because of their high affinity for oxygen.

In all cases, substantial increases in fracture energies occurred after exposure to the midpoint conditions. As oxygen potential was increased to 100 ppm, fracture energies, on the average, remained unchanged as compared to those obtained from the midpoint exposures (see Table 13). This observation is consistent with the fracture initiation argument presented above. The data in Table 29 show that bulk diffusion of oxygen did not occur (except perhaps in TZM), so initiation conditions were modified with initial exposure to oxygen rich Na and then remained unchanged for higher concentrations and longer exposure times.

The hydrogen effect observed in the Ta alloys exposed to Na at low oxygen potential in stainless steel crucibles is not observed in the Mo alloys. Mo is not embrittled by [H] because of the low solubility of hydrogen in Mo, 0.4 ppmw at 500°C.⁽⁴²⁾

Re Materials

The microstructures (see Figures 91 through 93) show that the CVD Re and Re-5W have much larger grain sizes than the wrought Re specimens. All show evidence of extensive twinning. Recrystallization produced extensive grain growth (approaching the specimen thickness) in the CVD materials and relatively little grain growth in the wrought material. All specimen surfaces examined by optical metallography at ~250X appeared to be free from attack. However, as-received CVD specimens had an irregular surface on one side of the specimen (see Figure 92a), probably created by the CVD process. These surface defects disappeared after exposure to Na.

Load elongation plots for wrought Re, CVD Re, and Re-5W (see Figures 95, 96, and 97, respectively) illustrate the influence of grain size on the shape of the load-displacement tensile curves. Typically, the small grain wrought material curves are characterized by a steep slope with sudden fracture. Large grain material tensile

curves show much more plasticity immediately before fracture as evidenced by decreasing load with increasing displacement or elongation. This behavior is characteristic of necking which was also observed on some of the necked Ta alloy specimens (see Figures 22 and 23).

On the average, the fine grain wrought Re had about 20 percent lower fracture energy in the recrystallized unexposed condition and after exposure to low oxygen potential Na as compared to the CVD material. After exposure to Na at elevated oxygen potential all three materials on the average have nearly identical fracture energies (50 ppmw [O]: wrought Re, 175; CVD Re, 176; and CVD Re-5W, 175; 100 ppmw [O]: wrought Re, 189; CVD Re, 184; and CVD Re-5W, 191 j/cm²) at each exposure condition. At low oxygen exposures average fracture energies were: wrought Re, 107; CVD Re, 127; and CVD Re-5W, 127 j/cm². Typically, the fracture mode for all these materials and exposures is ductile intergranular with a great deal of localized slip (see Figure 103). Bulk oxidation occurs on the Re specimen surface during exposure to Na₂O, the molten NaReO₄ collects into globules, and sharp defects on the specimen surface are smoothed out (see Figures 104b and c). Since all these materials fail in an intergranular fashion, fracture initiation occurs at grain boundaries which intersect the surface. Fracture energies improve dramatically and are roughly equivalent after exposure to Na at elevated oxygen potential, and the reason for this response is the rounding of surface flaws by oxidation (reduction of initiation sites). Grain size appears to control initiation (small grains mean more initiation sites) in the unexposed specimens and specimens exposed at low oxygen potential. However, there is also an improvement in fracture energies, but not equivalence, after exposure to Na at low oxygen potential and this improvement is caused by a small amount of surface oxidation as observed by the SEM.

Contour maps of the fracture energy of Re-5W as a function of oxygen potential and temperature for different exposure times provide a more detailed evaluation of the influence of temperature

and time and the strong interactions between these variables and oxygen potential. The 10-hour plot (see Figure 105) shows that the lowest fracture energies occur at 800°C and low oxygen potential while the highest fracture energies are produced with low temperature exposures. At 70-hour exposures, this trend continues except that oxygen potential becomes a more potent influence because of the time interactions with temperature and oxygen potential (see Figure 106). At 130 hours (see Figure 107) oxygen potential becomes the dominant influence. The trough which occurs at high temperature and low oxygen potential is tied to the low availability of oxygen and fast oxidation kinetics.

The small weight gains observed for these materials indicate that attack is not a problem when a limited supply of oxygen is available. However, it is clear that the formation and sloughing of the molten oxide in systems with an abundant oxygen supply could cause a very rapid catastrophic attack.

High Temperature Tests

As stated previously, the high temperature tests were used as an engineering proof test to economically evaluate crucible compatibility in a multicomponent system. Only materials that showed promise in the low temperature tests were selected for the high temperature tests.

It is significant to note that all of the tubes tested at high temperatures were hermetically tight after the testing sequence. However, the exposure threshold for leaking was very close for the CVD tubes. As also shown in the low temperature experiments, recrystallization of the CVD Re and Re-5W results in massive grain growth (see Figures 126 through 129). Presumably, the thermal cycling causes failure at the boundaries and, in some instances, grains have fallen from the tube. The photomicrographs show that a

layered structure exists in the CVD tubes. This is caused by interruptions in the CVD process and it is significant that thin layers start out with smaller grains which in turn are smaller in diameter after exposure relative to grains in the thicker layers. The columnar grains in the thick layers ripen into large single crystals after exposure (see Figure 126). If delamination of the layers could be prevented, it would probably be better to build up a wall section by successive thin layers. This practice would minimize the possibility of penetrating the entire cross-sectional thickness with a single grain boundary.

Metallographic evaluations of the entire axial cross sections for Ta-10W, T-111, Mo-41Re, CVD Re and CVD Re-5W at magnifications from 32X to 300X show that significant attack did not occur as a result of the test conditions in any of these materials. There was also no evidence of erosion of the side walls by formation of Na-refractory metal oxide compounds or of erosion by refluxing. Substantial refluxing occurred in all of the high temperature tests as evidenced by segregation of the UO_2 bed (larger particles at the bottom of the tube, see Figure 115) and the vibration of the tubes that occurred during each experiment. If Na uranate decomposition occurred in the $\sim 1100^\circ C$ region of the tube and supplied extra oxygen, the decomposition did not appear to influence the tube integrity at the magnifications examined. This is particularly significant because the tubes in the second test series experienced 18-hour exposures at these temperatures.

TEM evaluation of foils taken from five locations within the high temperature Ta-10W tube typically show that both grain boundaries and matrix were free of second phase particles. Thus it appears that the high temperature test environment did not significantly degrade the microstructure of the Ta-10W tube.

Summary

Two classes of materials were evaluated in this study:

1. Materials which generally exhibit ductile transgranular failure modes before and after recrystallization, e.g., Ta alloys.
2. Materials which exhibit intergranular failure modes after recrystallization, e.g., Mo and Re base systems.

For both types of materials the compatibility issues are driven by the purity of the sodium. All systems evaluated appear to be compatible with "pure" Na i.e., < 2 ppmw[O] within the exposure temperatures and times evaluated herein as evidenced by the small weight changes, lack of hardness response, and lack of surface attack as indicated by microstructural observations. However, as impurities (i.e., intentionally added O or the unexpected addition of H) are added to the sodium, the mechanical property response of the refractory metal systems ranged from mixed degradation and enhancement for the Ta systems to general enhancement for the Mo and Re based systems.

All of the mechanical tests and evaluations were made at room temperature in air, whereas applications involve use at elevated temperatures and greatly reduced oxygen potentials. This fact is a particularly important consideration in evaluating the fracture initiation effects previously described. For example, the surface oxidation and subsequent melting of NaReO_4 in the Re base systems may produce "hot shortness" if the mechanical property tests were conducted in situ.

The complexity of the material responses points to the importance of carefully defining the intended use environment before recommending a refractory metal. In most instances the choice will require balancing several trade-offs.

Recommendations

The recommendation of a material to use for the PAHR crucible is driven by the compatibility results obtained in this study and other factors such as material cost, fabricability, and weldability.

For example, in this study Ta-10W was recommended as the best candidate for the in-pile experiment for the following positive reasons:

1. Easy to fabricate.
2. Relatively cheap, ~\$440.00/kg.
3. Easy to braze by conventional brazing.
4. Mechanical properties are not affected by recrystallization.
5. Compatible with UO_2 and 400 ppm oxygen potential Na at 2000°C and in steep temperature gradients.
6. Readily available.
7. Autogenous weld easily.
8. Very good resistance to molten Na at low and high oxygen potentials, provided a fixed, defined supply of oxygen is available.
9. Generally has good fracture toughness.

However, the above advantages for use are balanced against the following disadvantages:

1. Embrittled by hydrogen.
2. Exhibits strain rate sensitivity.
3. Moderate high temperature strength.
4. Exhibits a complex sensitivity to interstitials.

T-111 would also be a successful candidate because of most of the above plus the desirability of Hf stabilization in controlling grain size and oxygen matrix effects, but it is not commercially available.

Mo-Re alloys demonstrated good compatibility but were not recommended because of poor fracture toughness, poor fabricability, and limited availability. A similar list of advantages and disadvantages could be made for the Mo-26Re and Mo-41Re alloys and they would include:

Advantages include:

1. Good resistance to hydrogen.
2. Very good resistance to Na at $2 < [O] < 100$ ppm.
3. Good high temperature strength.
4. Compatible with UO_2 and high oxygen potential Na at $2000^\circ C$ and in steep temperature gradients.
5. Autogenous welds can be made with care.

Disadvantages include:

1. Fracture mode is brittle after recrystallization.
2. Very difficult to fabricate.
3. Very difficult to braze.
4. Possibility of sigma phase formation as Mo depletion occurs.
5. Limited availability.
6. Very expensive ~\$2640.00/kg.

In a similar fashion the Re materials were not recommended because of the propensity for rapid grain growth and high cost.

Advantages for the CVD Re and Re-5W include:

1. Resistant to hydrogen.
2. Mechanical properties are not adversely affected by recrystallization.
3. Very good resistance to molten Na at $2 < [O] < 100$ ppm.
4. Autogenous welds readily.
5. Compatible with UO_2 and high oxygen potential (400 ppm) Na at $2000^\circ C$ and in steep temperature gradients.

6. Fracture mode is ductile after all exposures even though failure is intergranular.
7. Easy to braze by conventional brazing

Disadvantages include:

1. Work hardens very rapidly.
2. Difficult to machine by conventional means.
3. CVD has structural irregularities and large grain size.
4. Very high grain growth.
5. Very expensive ~\$7700.00/kg.
6. Exhibits grain boundary cracking.

Wrought Re could not be considered for this application because it could not be fabricated into the shapes required.

Conclusions

1. All of the materials tested are compatible with Na for the test conditions $300^{\circ}\text{C} < [O] < 800^{\circ}\text{C}$, $10 \text{ hours} < t < 130 \text{ hours}$, and $2 \text{ ppmw} < [O] \leq 100 \text{ ppmw}$.
2. Ta-10W, T-111, and Mo-41Re are compatible with Na and UO_2 for the test conditions $400^{\circ}\text{C} < T \leq 2000^{\circ}\text{C}$, $t \leq 5 \text{ hours}$, and $[O] \leq 400 \text{ ppmw}$.
3. CVD Re, and Re-5W exhibited grain boundary failure when tested under the high temperature conditions listed above.
4. Re additions to Mo enhance tensile properties but do not significantly improve the room temperature fracture toughness as inferred by the fractography.
5. Mechanical properties of Ta-10W and T-111 are very sensitive to impurities in molten Na (i.e., O,H) because of the relatively high diffusion rates of these species in Ta.

6. Fracture initiation controls the tensile ductility and toughness as inferred by the fractography for Mo, Mo-Re, and Re as a function of exposure in Na as measured in postexposure tensile tests conducted at room temperature in air. This response might be completely different in tests conducted in situ.

Bibliography

1. J. Gronager memo dated June 23, 1982 entitled D-10 Parameter List.
2. L. Shreir, ed., Corrosion, Vol. 1, John Wiley & Sons, N.Y., 1963, p. 5.63.
3. C. B. Alcock, M. G. Barker, and G. P. Stavropoulos, "The Corrosion of Ta by Na₂O--Saturated Liquid Sodium," Corrosion Science, Vol. 10, 1970, pp. 105-110.
4. C. C. Addison, M. G. Barker, and D. J. Wood, "The Role of Dissolved Oxygen in the Corrosion of Nb and Ta by Liquid Sodium," J. Chem. Soc., Dalton Trans., 1972, pp. 13-16.
5. R. L. Klueh, "The Effect of Oxygen on Ta-Na Compatibility," Met. Trans., Vol. 3, 1972, pp. 2145-2150.
6. R. W. Harrison, Corrosion of Oxygen Contaminated Ta in NaK, Corrosion by Liquid Metals, J. E. Draley and J. R. Weeks, eds., AIME, Plenum Press, NY, 1970, pp. 151-175.
7. D. Quataert and C. A. Busse, "Investigation of the Corrosion Mechanism in Ta-Li High Temperature Heat Pipes by Ion Analysis," J. of Nuc. Mat., Vol. 46, 1973, pp. 329-340.
8. F. Yates, "The Design and Analysis of Factorial Experiments," Bulletin 35, Imperial Bureau of Soil Science, Harpenden, Herts, England, Hafner (McMillan), 1937.
9. D. R. Stull and H. Prophet, eds., JANAF Thermochemical Tables, 2nd edition, National Bureau of Standards, 1971.
10. W. Z. Friend, Corrosion of Nickel and Nickel-Base Alloys, John Wiley & Sons, 1980.

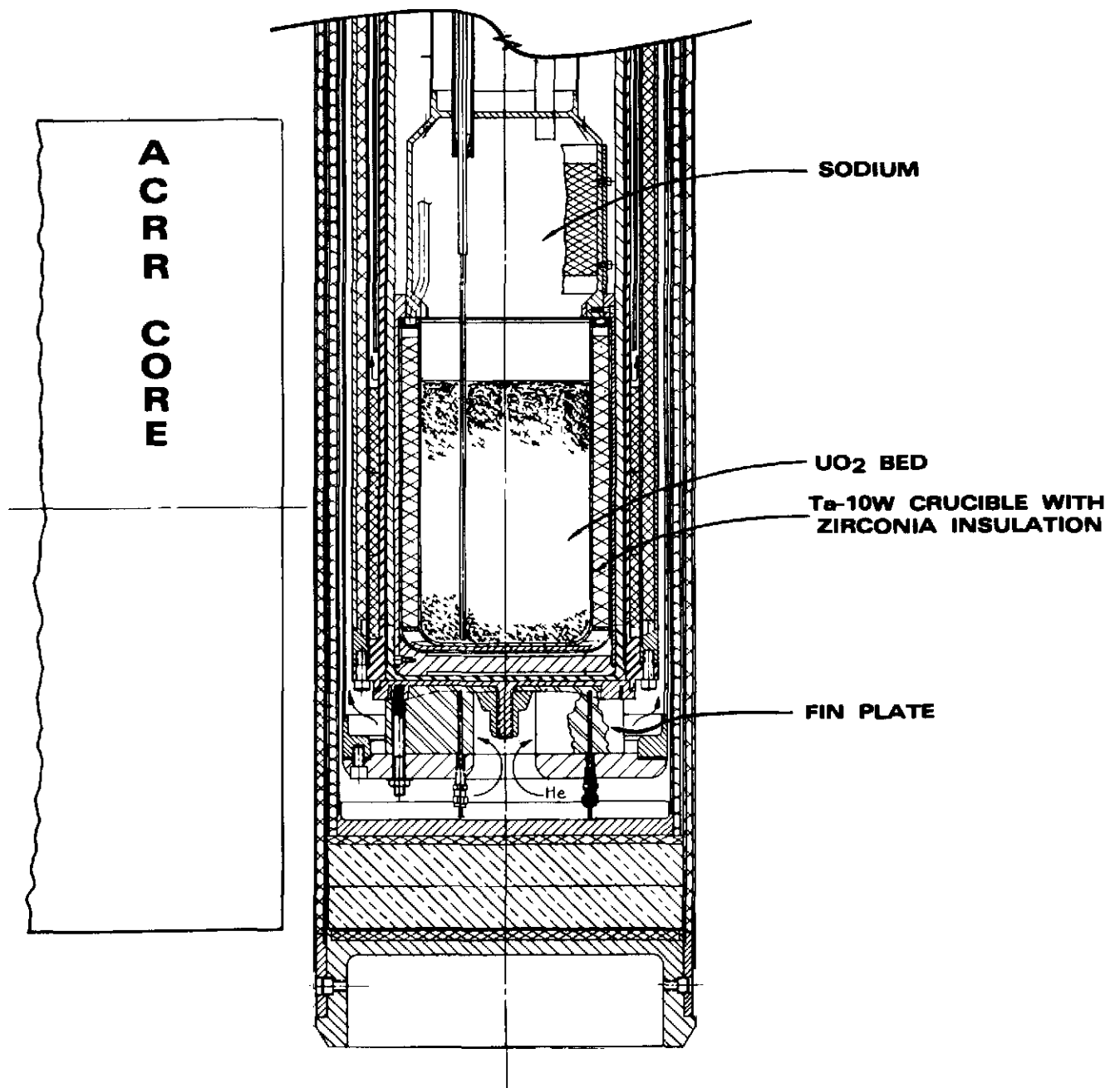
11. O. M. Sreedharan and J. B. Gnanamoorthy, "Oxygen Potentials in Alkali Metals and Oxygen Distribution Coefficients Between Alkali and Structural Metals--An Assessment," J. Nuc. Mat., Vol. 89, 1980, p 121.
12. D. L. Smith, "Investigations of the Thermodynamics of V-O Solid Solutions by Distribution Coefficient Measurements in the V-O-Na System," Met. Trans., Vol. 2, 1971, pp. 579-583.
13. J. D. Noden, "Na-O Equilibria," J. of British Nuc. Energy Soc., Vol. 12, 1973, p. 329.
14. J. Crank, The Mathematics of Diffusion, 2nd Edition, Clarendon Press, London, 1975.
15. J. Askill, Traces Diffusion Data for Metals, Alloys, and Simple Oxides, Plenum Press, N.Y., 1978, p. 51.
16. N. R. Draper and H. Smith, Applied Regression Analysis, John Wiley & Sons, N.Y., 1966, p. 167.
17. ibid., 16, p. 25.
18. Y. E. Touloukian and D. D. DeWitt, "Thermal Radiative Properties: Metallic Elements and Alloys, Thermophysical Properties of Materials," IFI/Vol. 7, Plenum, N.Y., 1970.
19. F. M. Hosking, "Sodium Compatibility of Refractory Metal Alloy-304L Stainless Steel Braze Joints," to appear in Welding Journal, April, 1985.
20. O. L. Davies, ed., The Design and Analysis of Industrial Experiments, 2nd Edition, Hafner Pub., N.Y., 1963, p. 602.
21. ibid., 15, p. 14.

22. N. M. Igumnova, D. V. Drobot, and V. V. Tolokonnikova, "Zh. Neorg. Khm," Vol. 20, 1975, p. 556, English Translation in Russ. J. Inorg. Chem., Vol 20, 1975, p. 310.
23. *ibid.*, 4, p. 13.
24. D. Hull and W. S. Owen, "The Interaction of Interstitial Solute and Substructure in Refractory Metals." The Science and Technology of W, Ta, Mo, and Nb and Their Alloys, N. E. Promisel, ed., Pergamon Press, 1964, p. 99.
25. J. Kish, Personal Communication, Re Alloys, Inc., Elyria, Oh., 44035, Febuary, 1985.
26. E. M. Savitskii, M. A. Tylkina, and K. B. Povarova, Rhenium Alloys, Israel Program for Scientific Translations, Jerusalem, 1970, p. 34
27. *ibid.*, 2, p. 5.63.
28. *ibid.*, 5.
29. *ibid.*, 2, p. 2.85.
30. R. N. Newman, C. A. Smith, and R. J. Smith, "The Corrosion of Steels in Molten NaOH," J. Electrochem. Soc., Vol. 124, 1977, p. 1247.
31. J. H. DeVan, J. R. Distefano, and E. E. Hoffman, "Compatibility of Refractory Alloys with Space Reactor System Coolants and Working Fluids," Proc. of Symp. on Refractory Alloy Technology for Space Nuclear Power Applications, R. H. Cooper and E. E. Hoffman, eds., Oak Ridge, TN, p 79 (Jan. 1984).

32. J. Volk and G. Alefeld, Diffusion in Solids: Recent Developments, A. S. Nowick and J. J. Burton, eds., Acd. Press, NY, 1975, pp. 232-302.
33. E. H. Van Derenter and V. A. Maroni, "Hydrogen Permeability Characteristics of Some Austenitic and Nickel-Base Alloys," J. Nuc. Mat., Vol. 92, p. 103, 1980.
34. A. F. Gad, "Effects of Hydrogen on Strength and Ductility of Ta," Phd. Thesis, Univ. of Houston, Houston, Tx., 1983, p. 152.
35. R. E. Reed-Hill, "Comparison of H and O Slow Strain-Rate Embrittlements," Hydrogen Effects in Metals, 3rd Int. Conf., 1974, p. 877.
36. G. Horz, K. Lindenmaier, and R. Klaiss, "High Temperature Solid Solubility Limit of C in Nb and Ta," J. Less. Comm. Metals, Vol. 35, pp. 97-105, 1974.
37. R. E. Pawel and J. J. Campbell, "The Influence of Alloying Elements on Oxygen Diffusion and Flexure in Ta-Base Alloys," Acta. Met., Vol. 29, 1981, pp. 809-817.
38. M. Weller, J. X. Zhang, G. Y. Li, T. S. Ke, and J. Diehl, "Internal Friction Study on the Existence of Oxygen Pairs in Interstitial Solid Solution of Ta with Oxygen," Acta. Met., Vol. 29, 1981, pp. 1055-1060.
39. T. E. Mitchell and R. L. Smialek, "Interstitial Hardening and the Peierls Stress in Ta," Conf. Proc. Second International Conference on the Strength of Metals and Alloys, Pacific Grove, Calif., 1970, Vol. 1, pp. 73-77.
40. M. Merrigan and L. B. Lundberg, "An Initial Evaluation of Mo-13Re Alloy for Reactor Heat Pipes," Proc. 18th IECEC, Orlando, Fla., August 1983.

41. R. I. Jaffee, C. T. Sims, and J. J. Harwood, "The Effect of Re on the Fabricability and Ductility of Mo and W," Plansee Proc., 3rd Seminar, 1958, Pergamon Press, 1959, pp. 380-411.

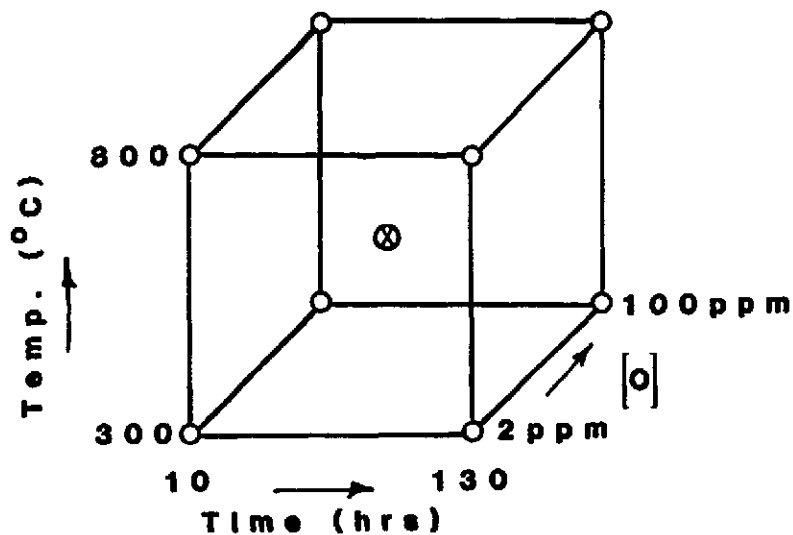
42. C. J. Smithells, Metals Reference Book, Fifth Ed., Butterworths, London, 1976, p. 839.



Schematic Illustration of PAHR Experiment

Figure 1

**LOW TEMPERATURE REFRACTORY METAL
Na COMPATABILITY EXPERIMENTS**

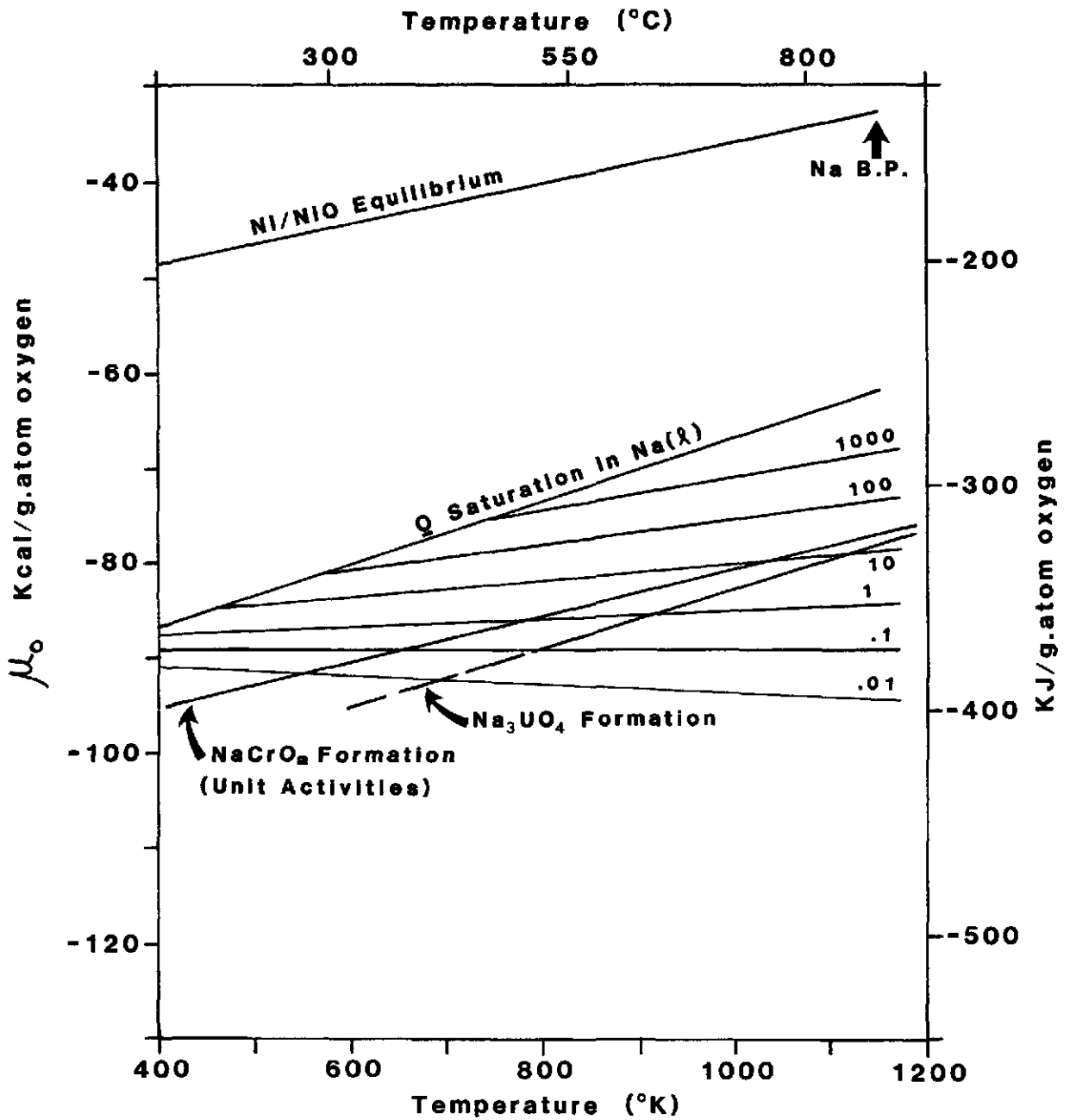


[O] - dissolved Oxygen in Na
 ⊗ 550 °C, 70 hrs, 50 ppm [O]

**Materials: Ta-10W
 Ta-8W-2Hf
 Mo
 Mo-26Re
 Mo-41Re
 W
 W-26Re
 Re
 Re-5W**

Factor Space Cube

Figure 2



Temperature Dependence of the Equilibrium Chemical Potential of Oxygen Dissolved in Sodium (several concentrations shown in parts per million by weight) and the Oxygen Potentials for Formation of NiO, NaCrO₂ and Na₃UO₄

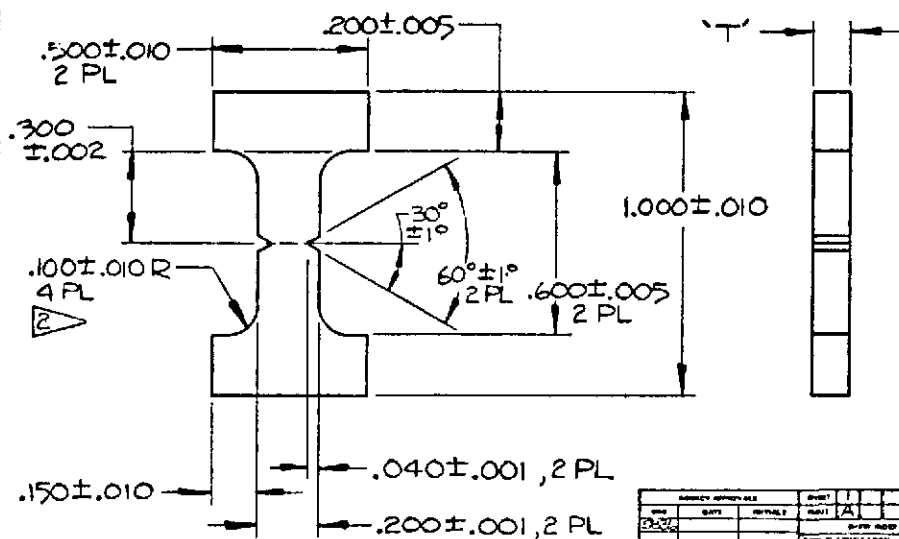
Figure 3

NOTES:

1. GENERAL REQUIREMENTS ARE DEFINED IN 99000000.

2. RADII MUST BE TANGENT WITH $.200 \pm .001$ SURFACES.

FORM 100-100	REV	DATE	BY	CHK
T86986-000	A			
PART NUMBER		REV	DATE	BY
DENGLED 2455 / FISHER 7836				



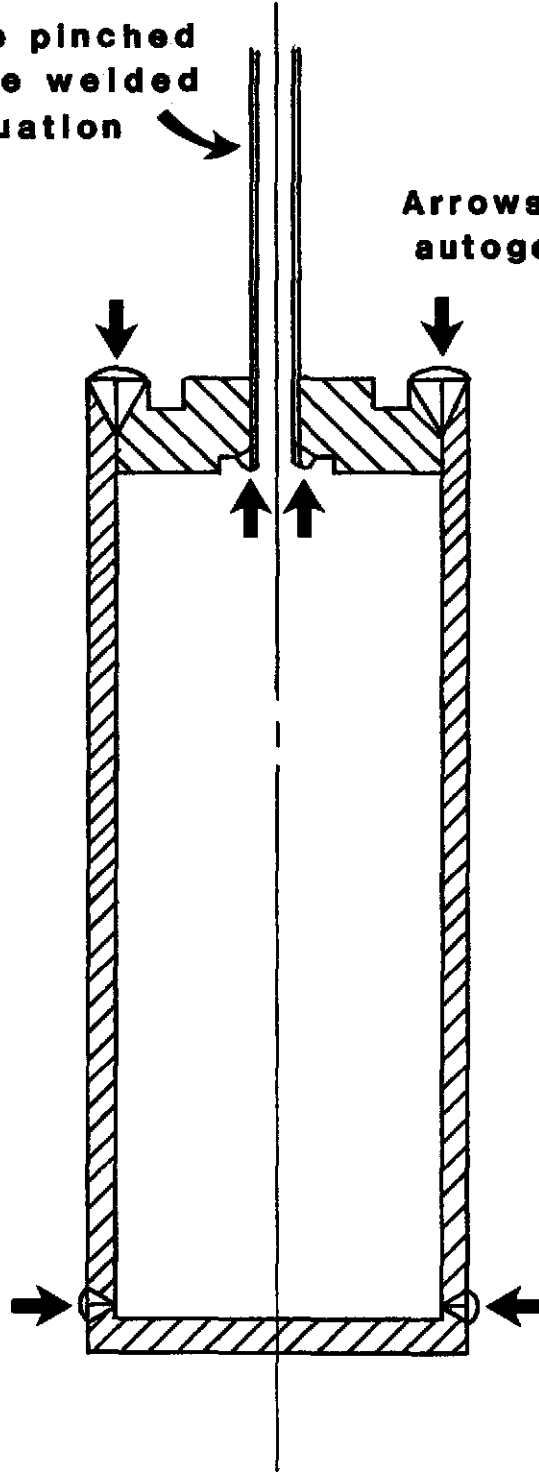
DESIGNED BY		DATE	REV	BY	CHK	TITLE
2455						
CLASSIFICATION		UNCLASSIFIED				SCALE
CLASSIFICATION		UNCLASSIFIED				
DRAWN BY		DATE		REV		PART
14213		T86986				

Metallurgical Test Specimens

Figure 4

**Pumping tube pinched
and resistance welded
after evacuation**

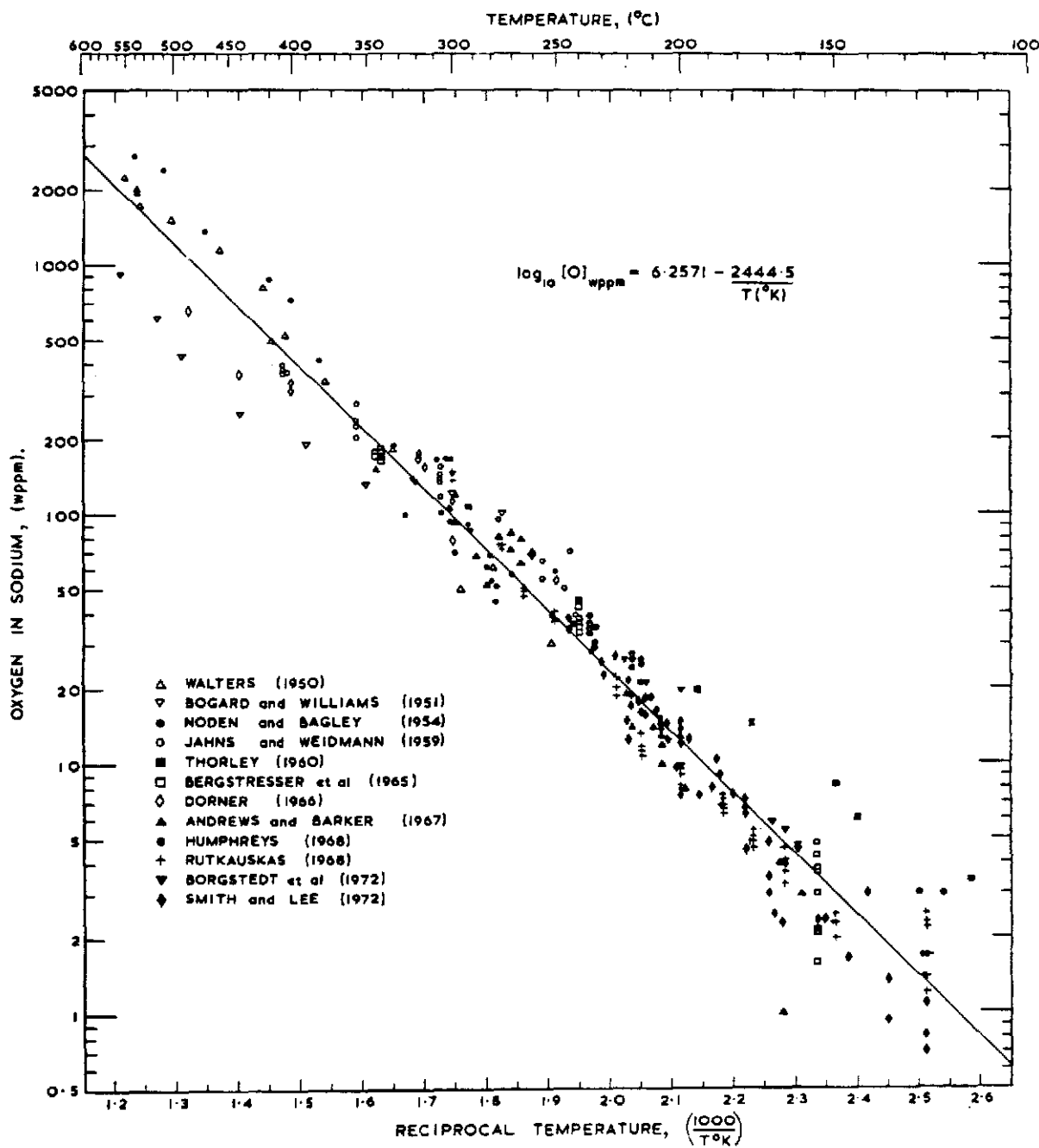
**Arrows indicate GTA
autogenous welds**



**Material either:
A-200 Ni
or
316 SS**

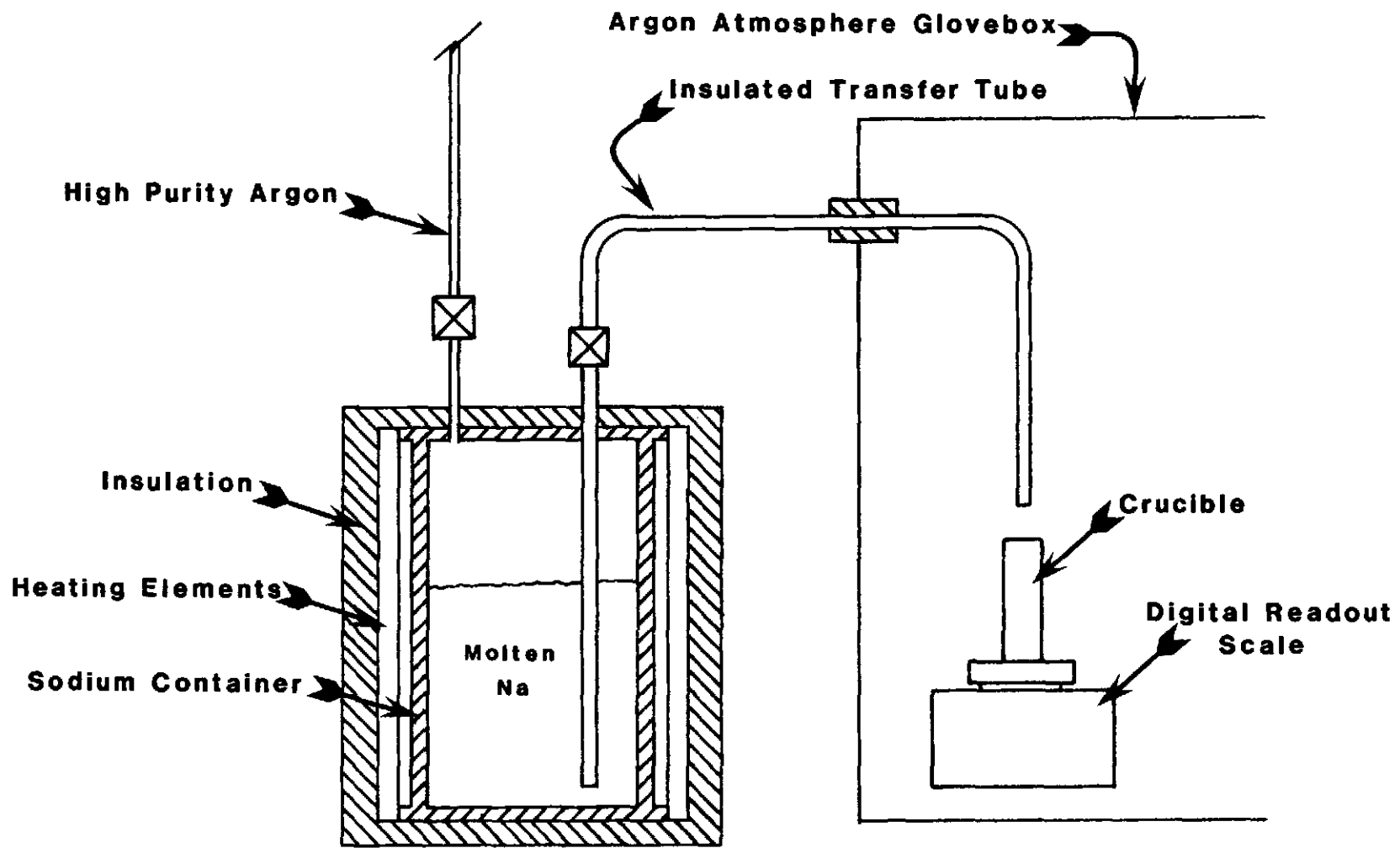
LOW TEMPERATURE CRUCIBLE ASSEMBLY.

Figure 5



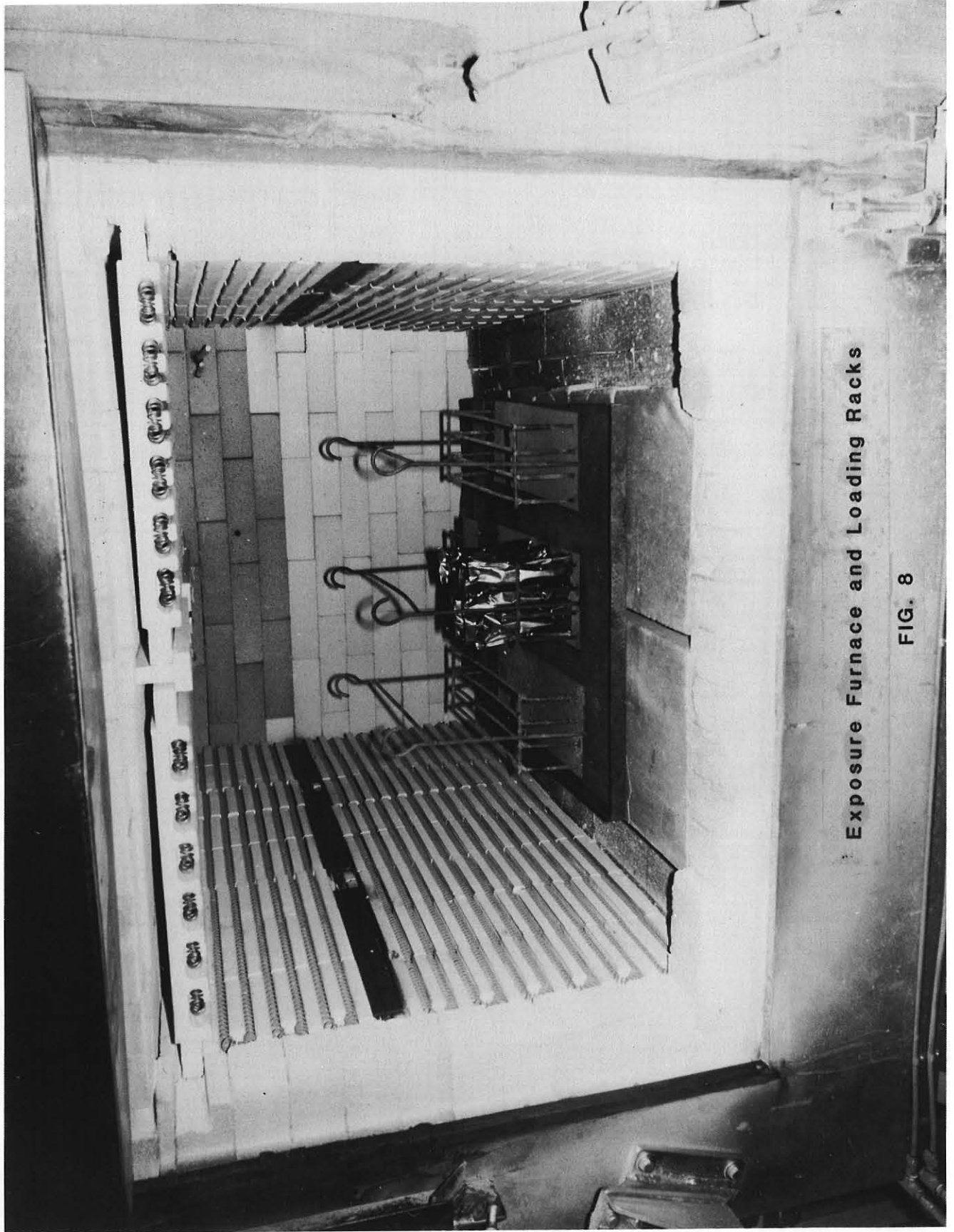
**Temperature Dependence of the Solubility
of Oxygen in Liquid Sodium**

Figure 6



SODIUM CHARGING APPARATUS

Figure 7



Exposure Furnace and Loading Racks

FIG. 8

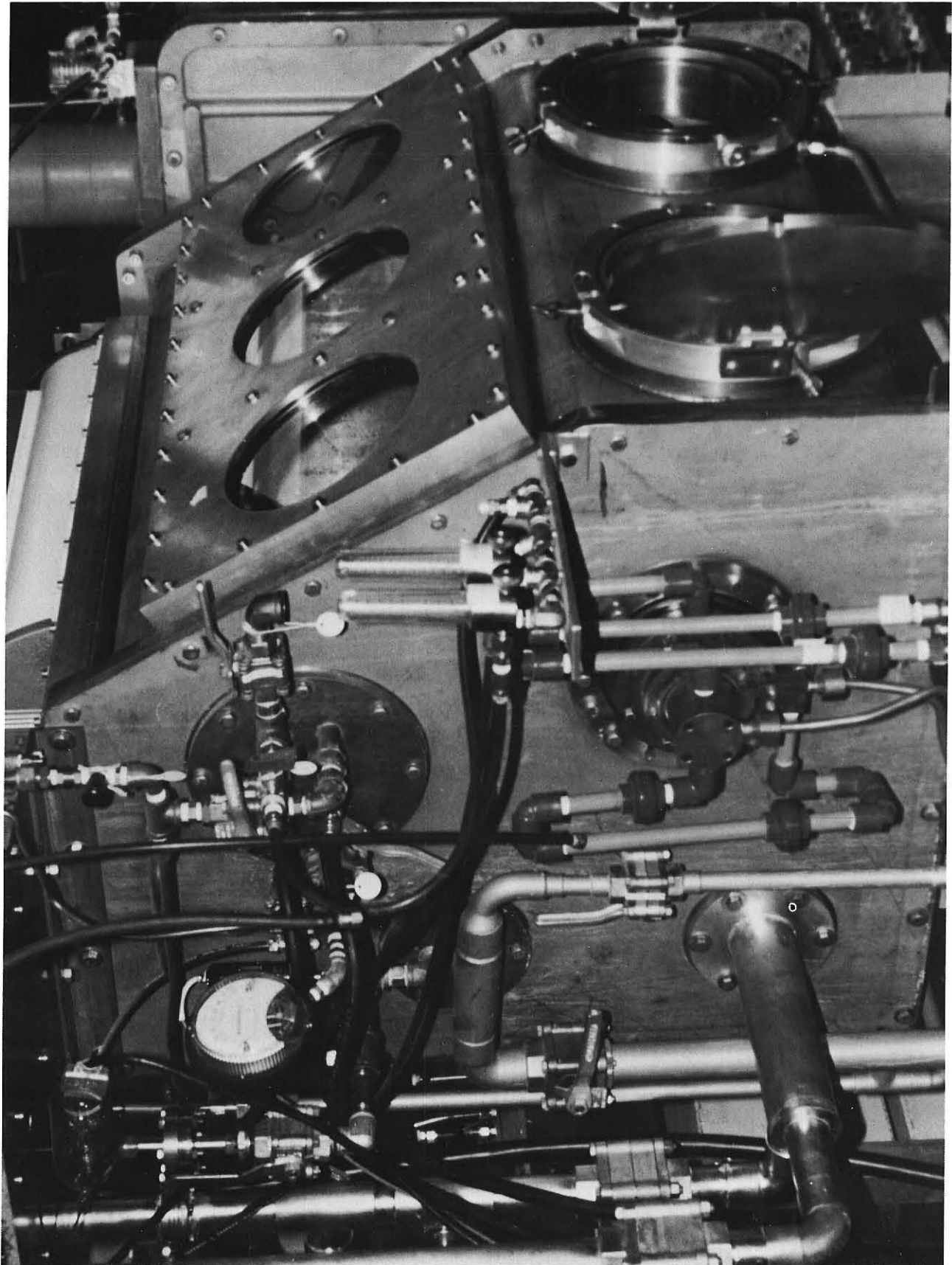
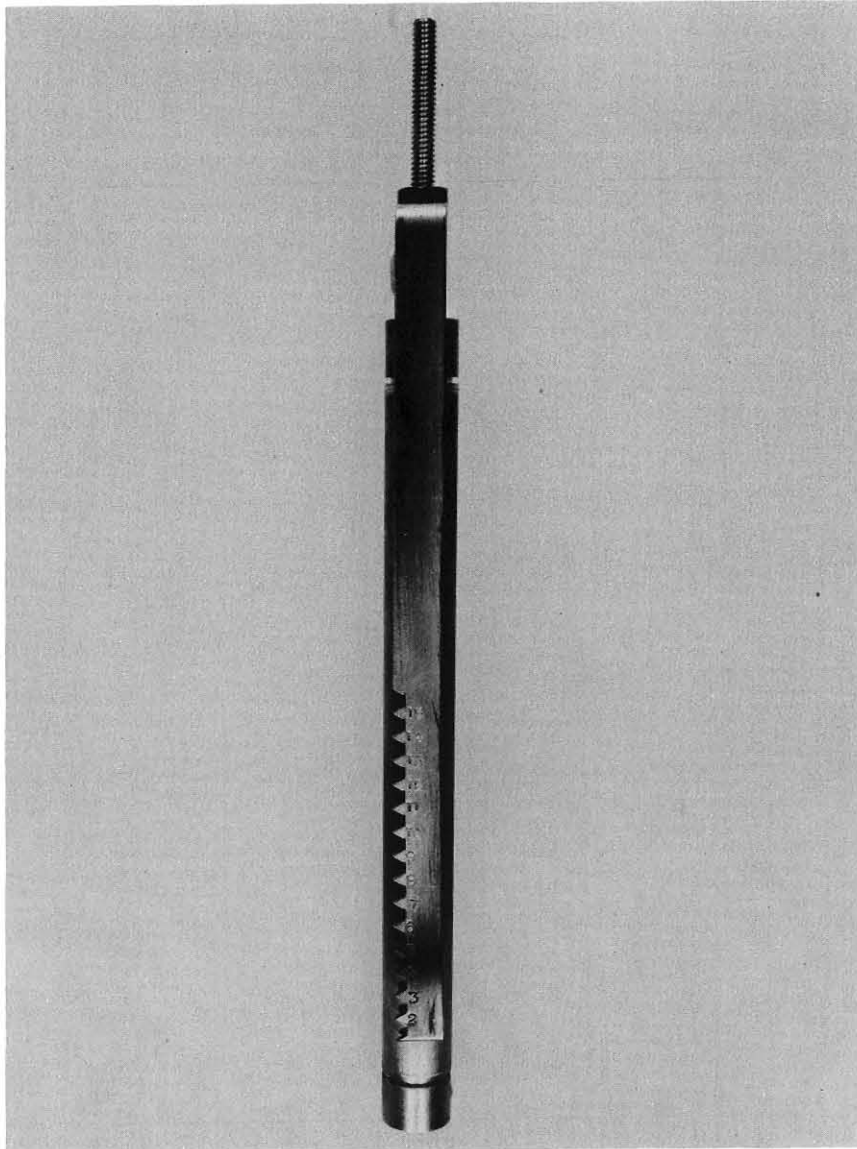


FIG. 9 HIGH TEMPERATURE REFLUX TEST APPARATUS

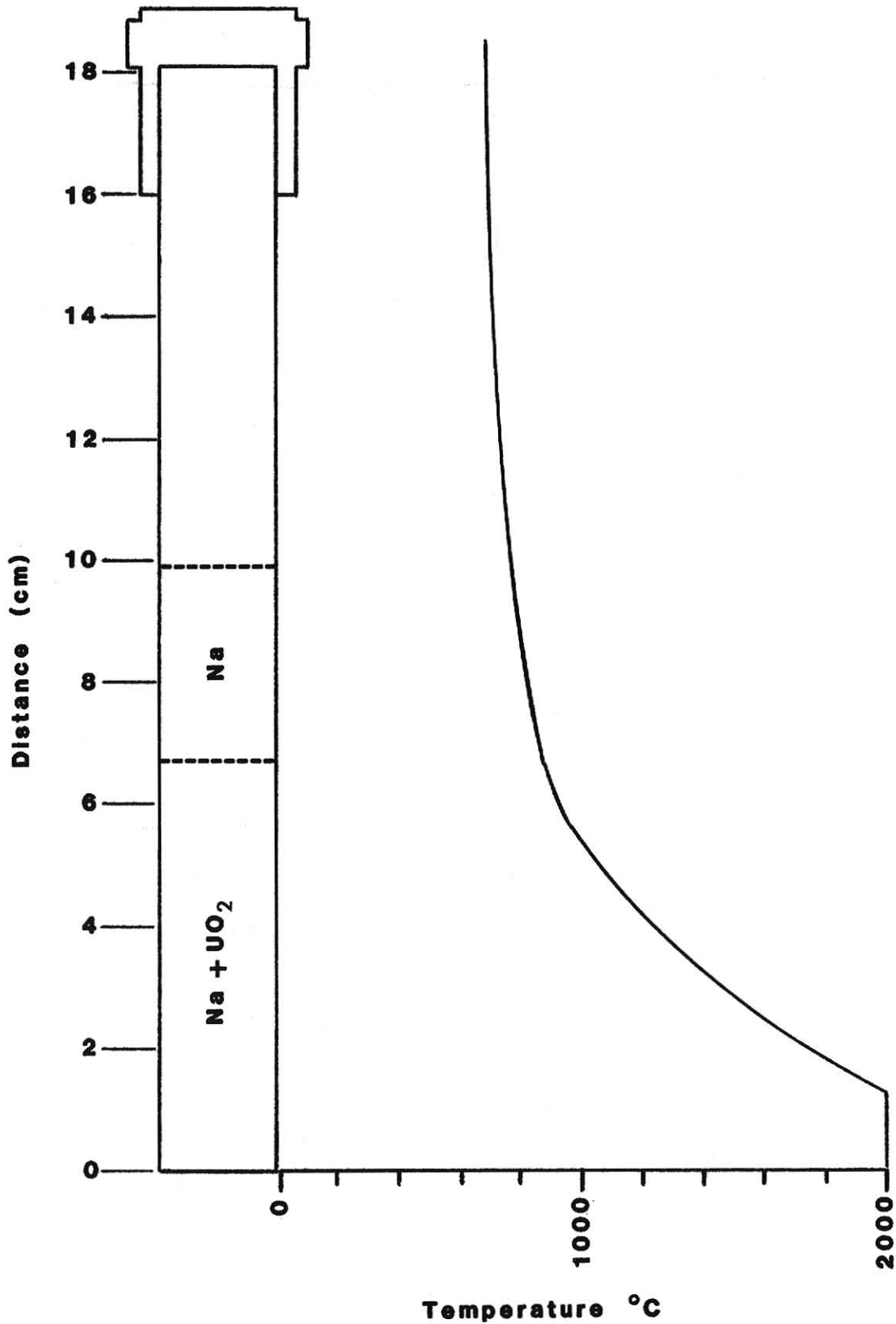


FIG. 10 HIGH FREQUENCY INDUCTION HEATING SYSTEM



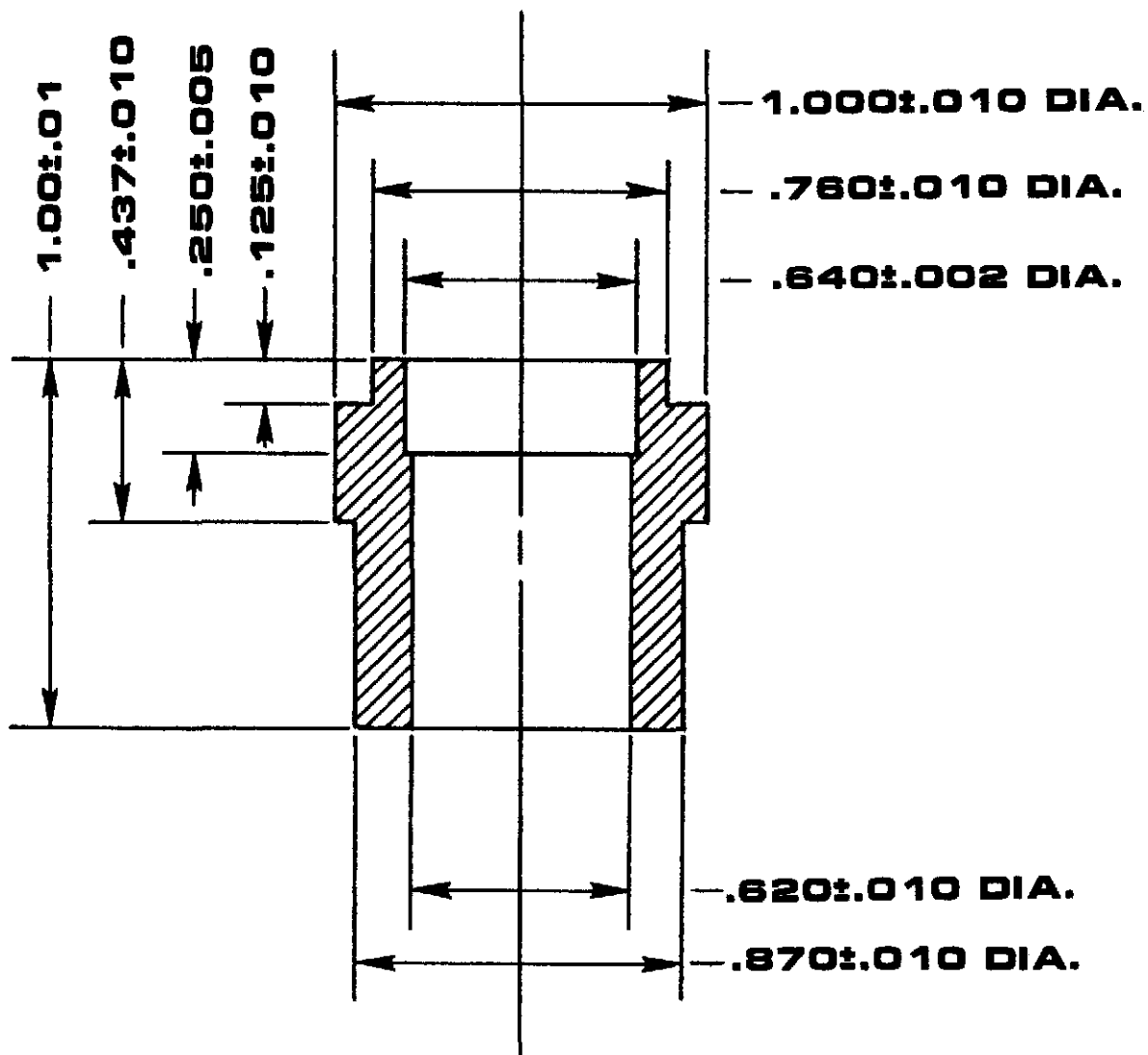
Temperature Locating Device for Reflex Tests

Fig. 11



Typical Temperature Profile for Reflux Tests

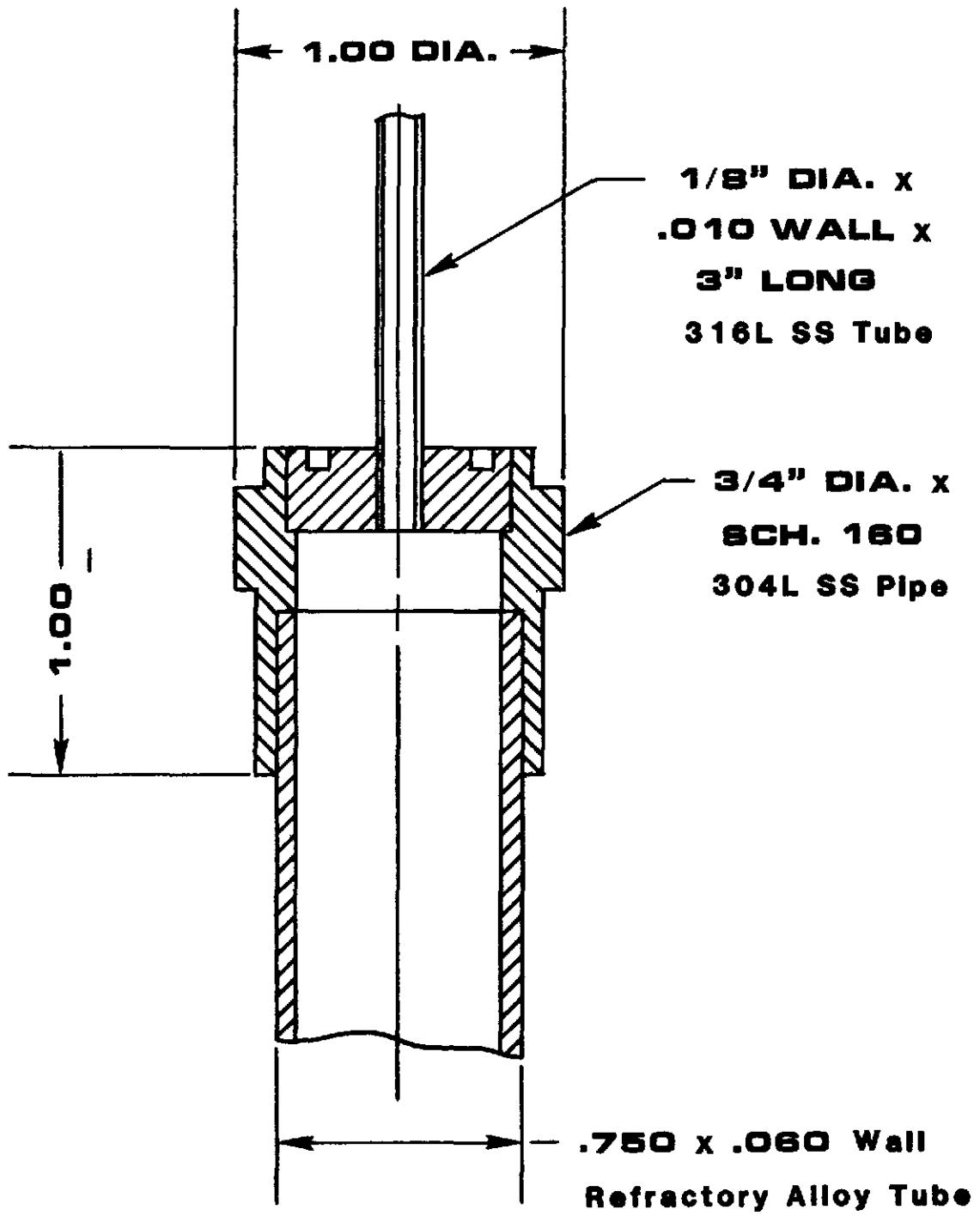
Fig. 12.



Material: 304L SS pipe

STAINLESS STEEL COLLAR-TUBE ASSEMBLY.

Figure 13



TUBE CLOSURE ASSEMBLY.

Figure 14

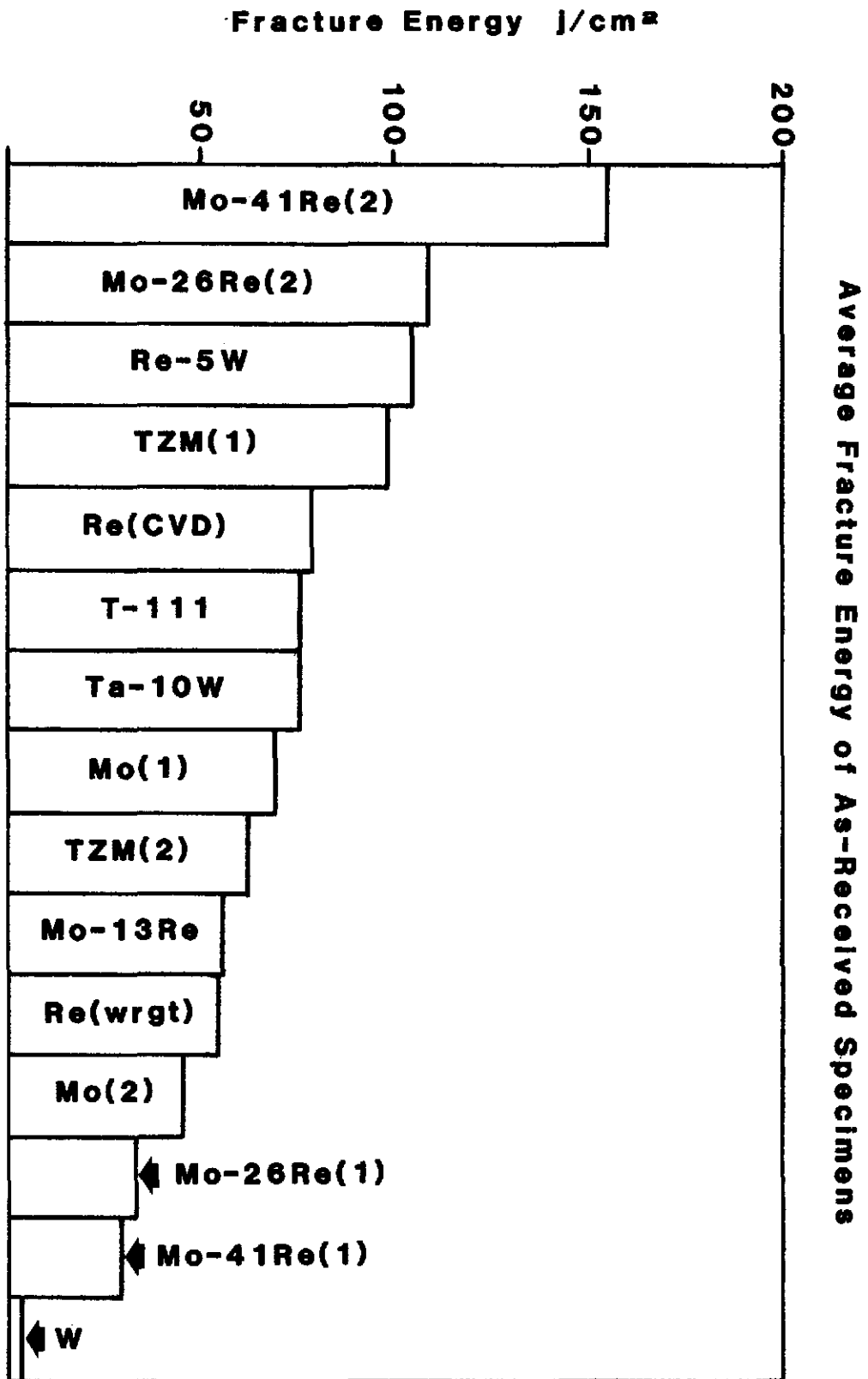


Figure 15

Average Notched Tensile Strength of As-Received Specimens

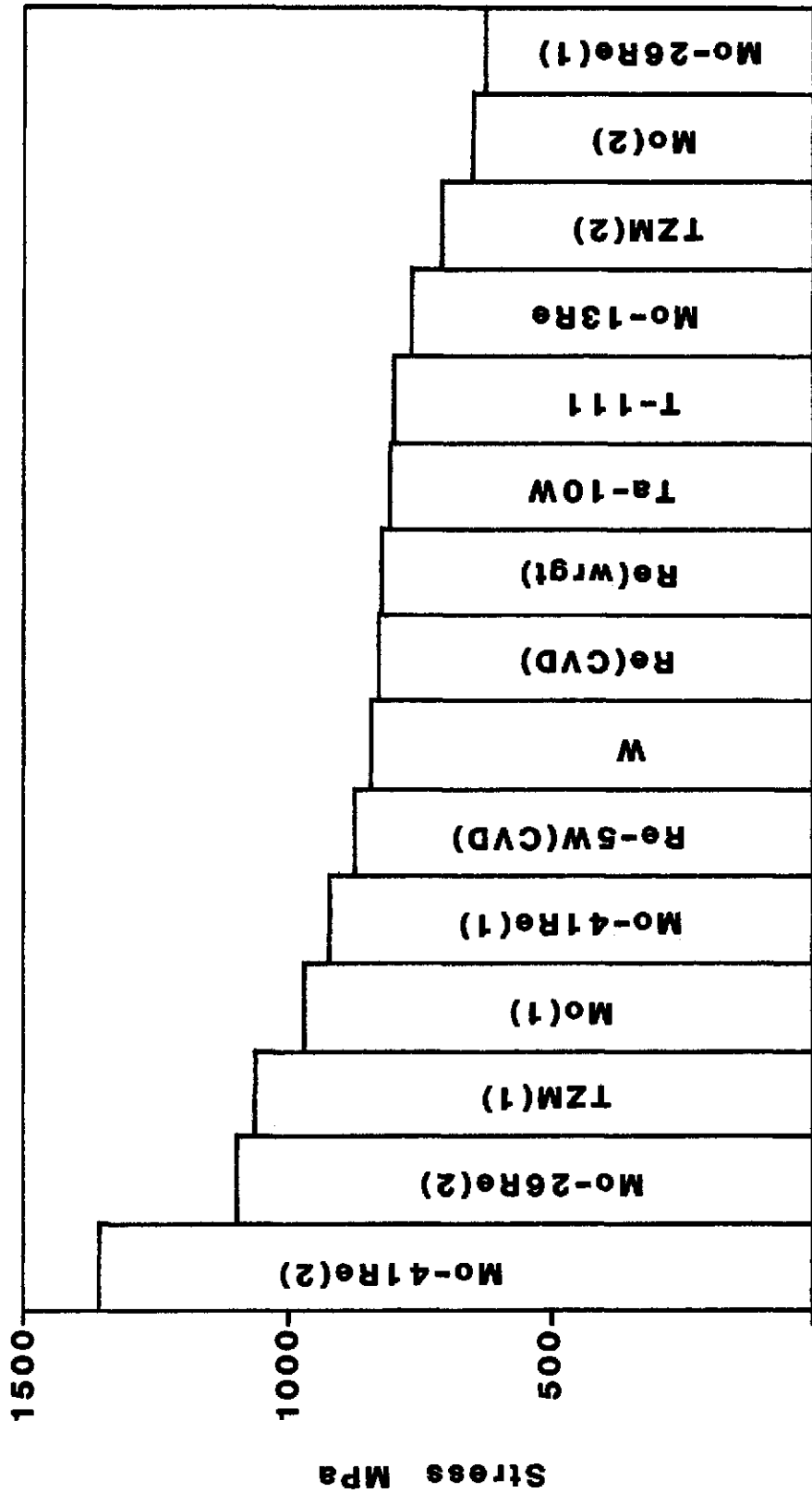


Figure 16

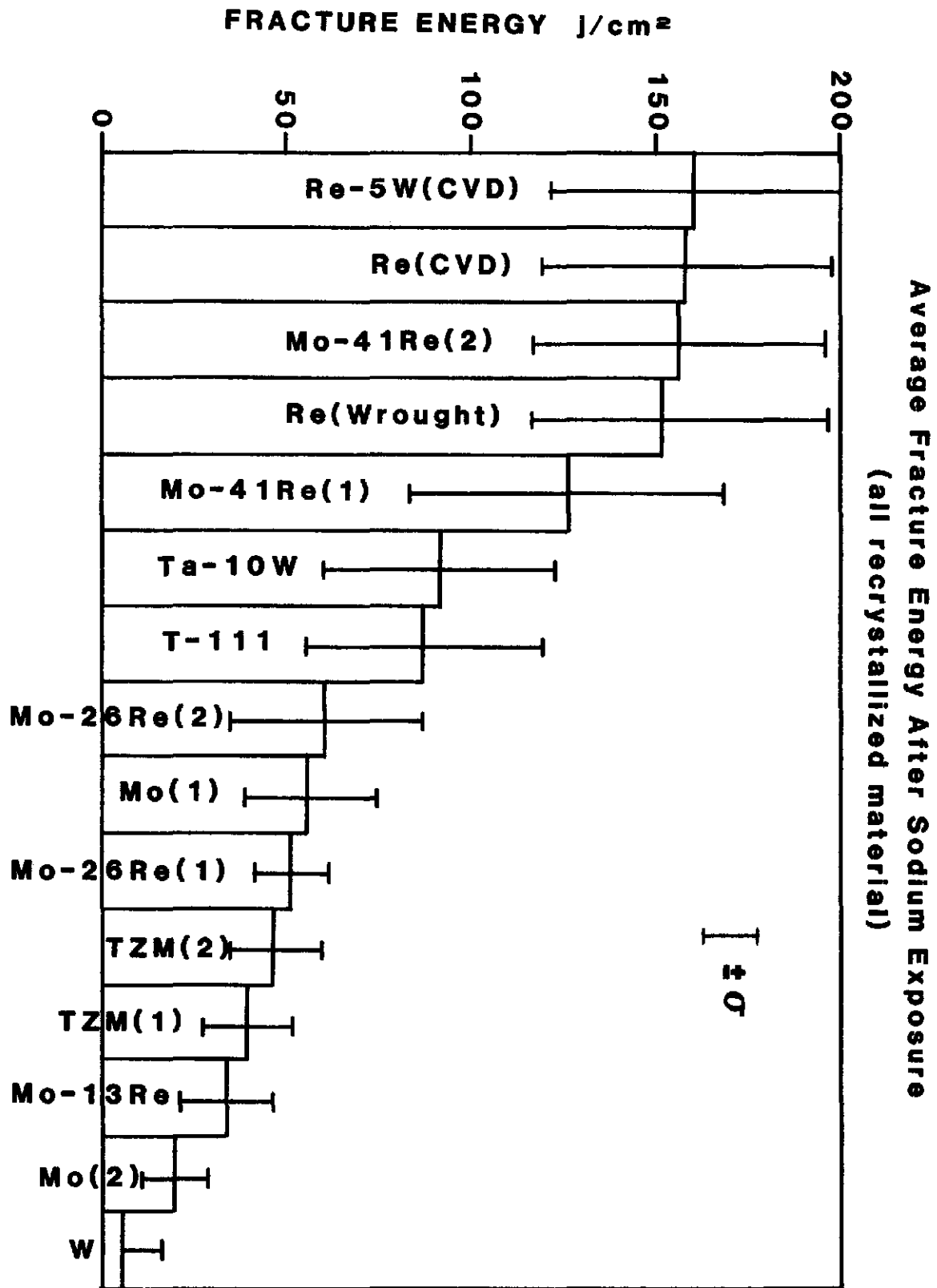


Figure 17

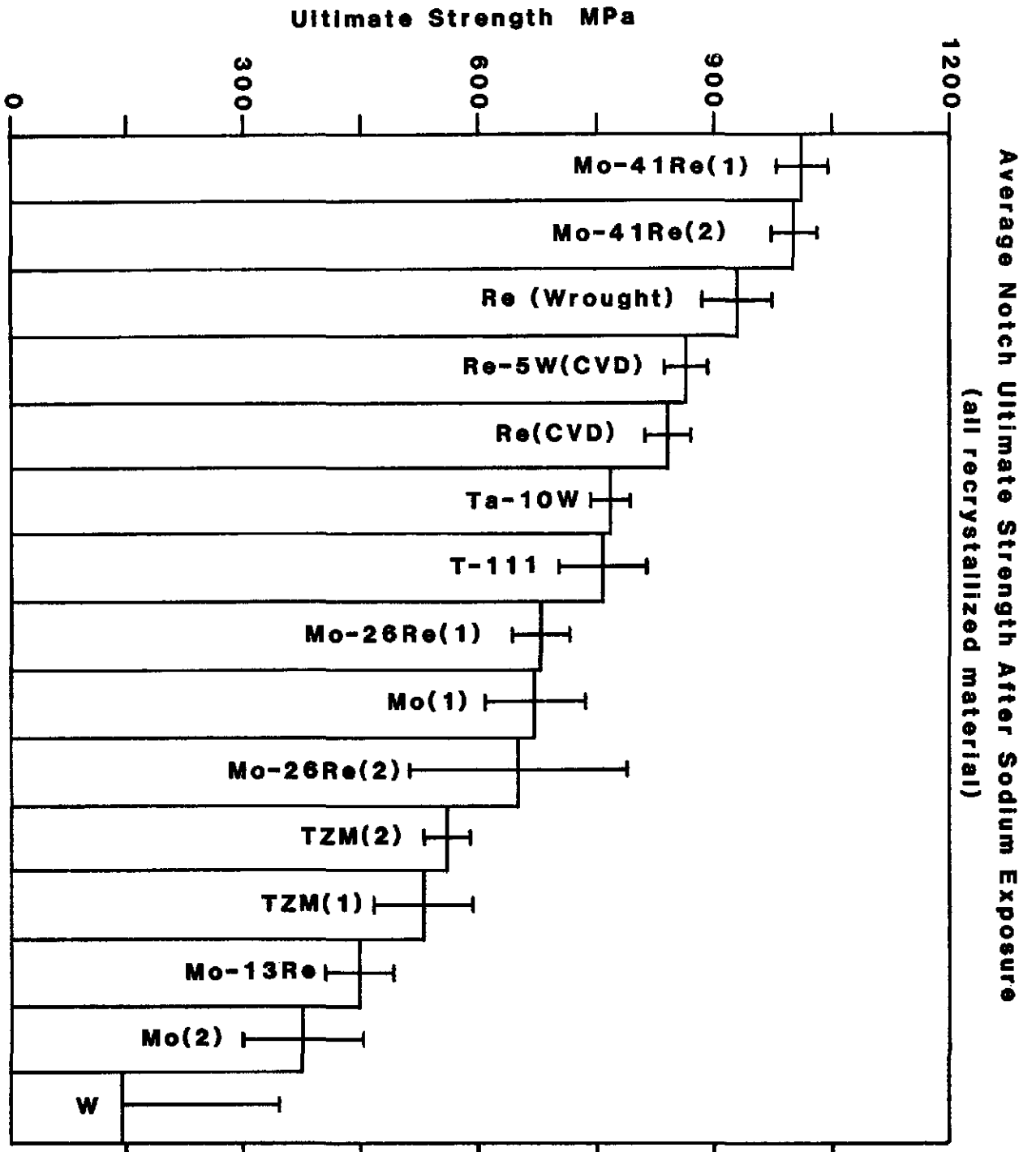


Fig. 18

Average Hardness of As-Received Specimens

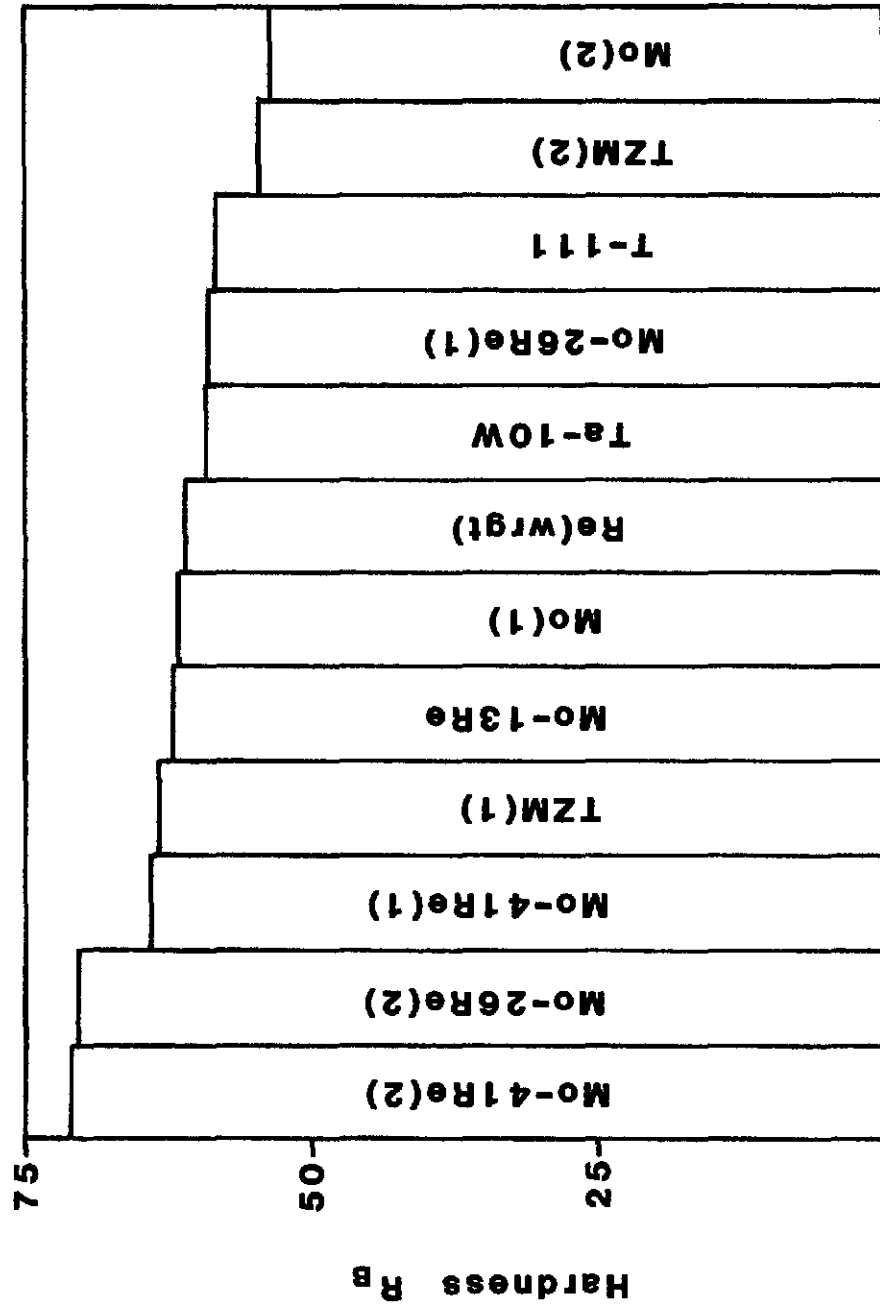


Figure 19

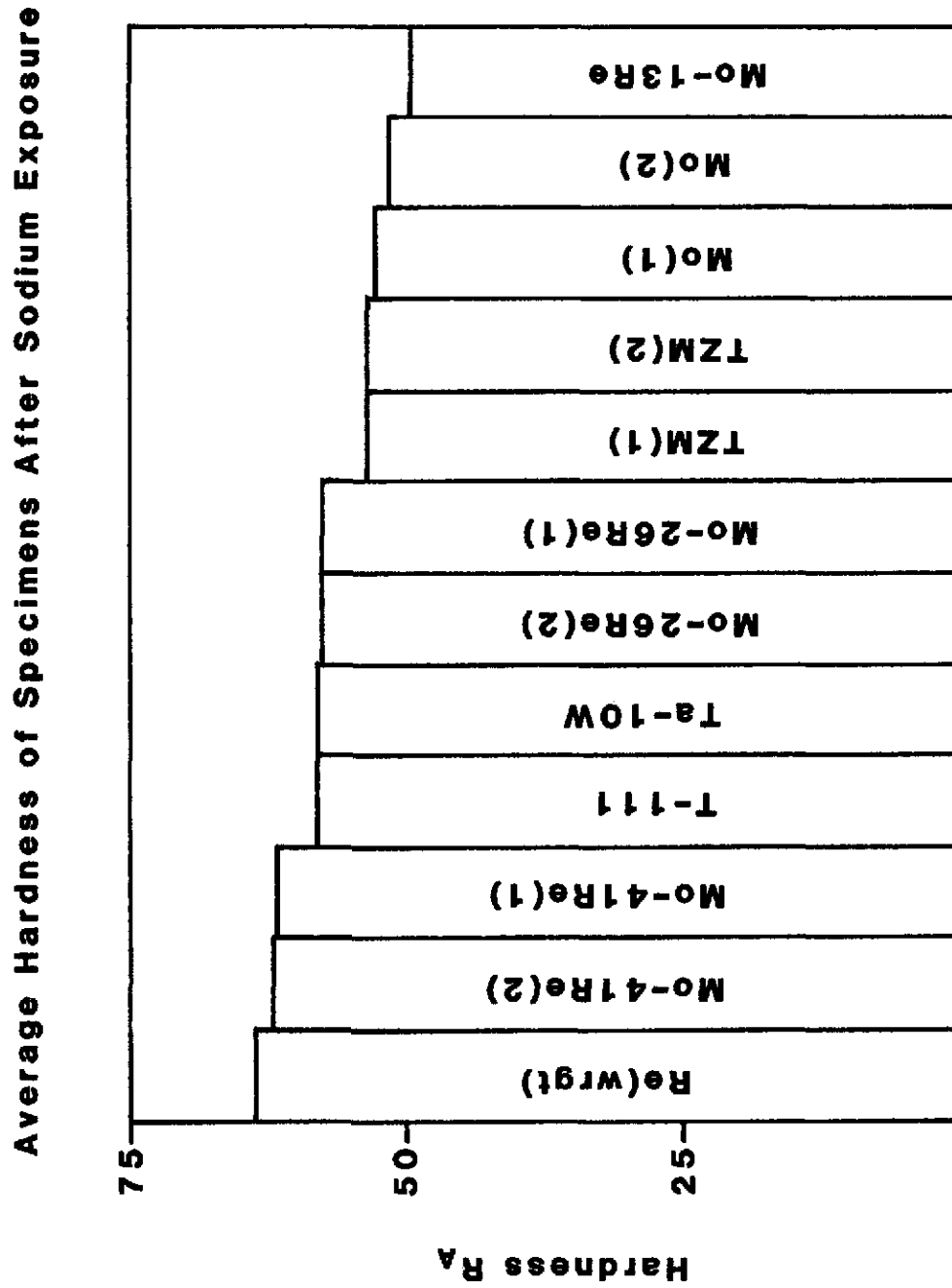


Figure 20

Average Weight Change of Specimens After Sodium Exposure

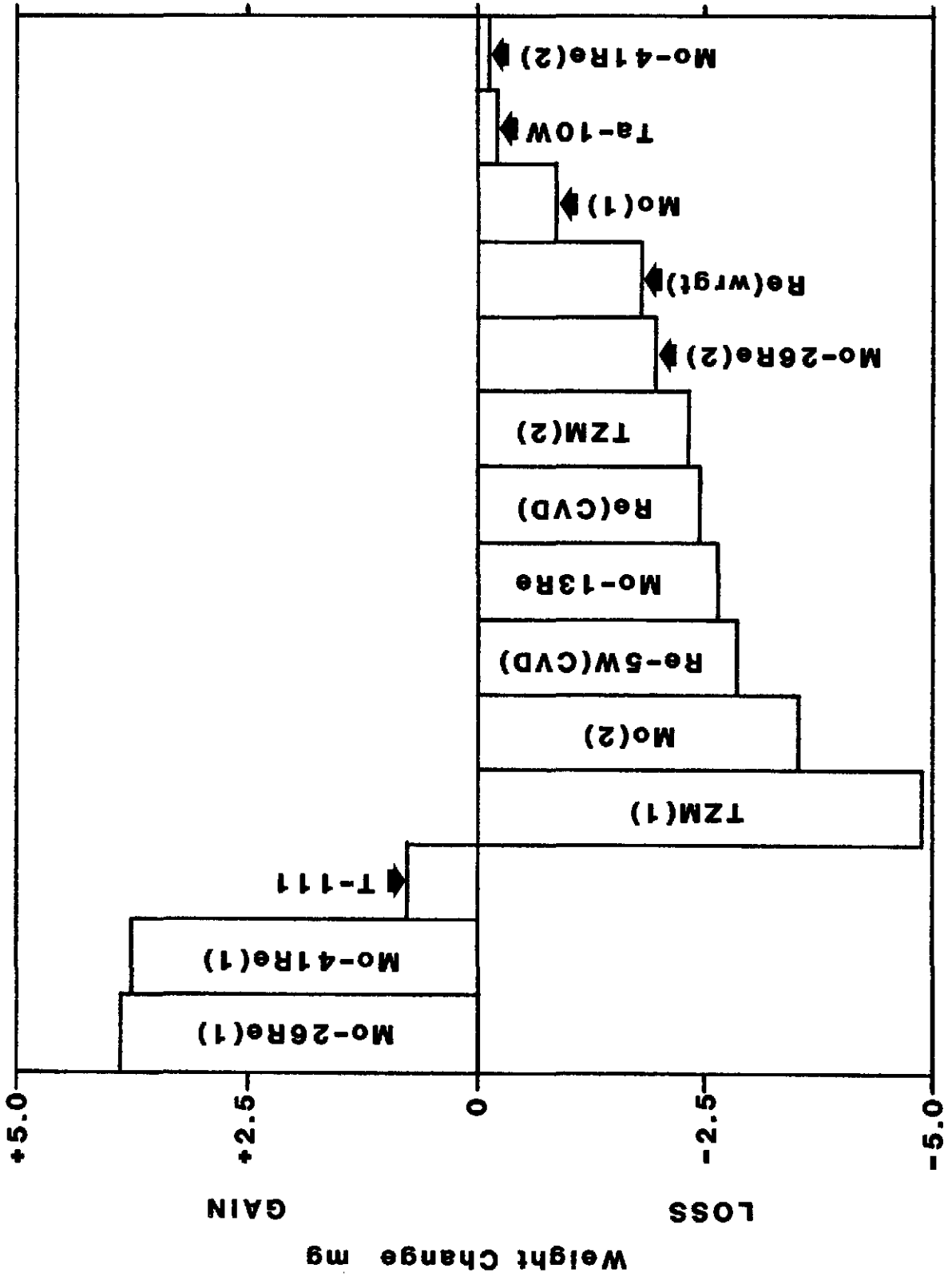
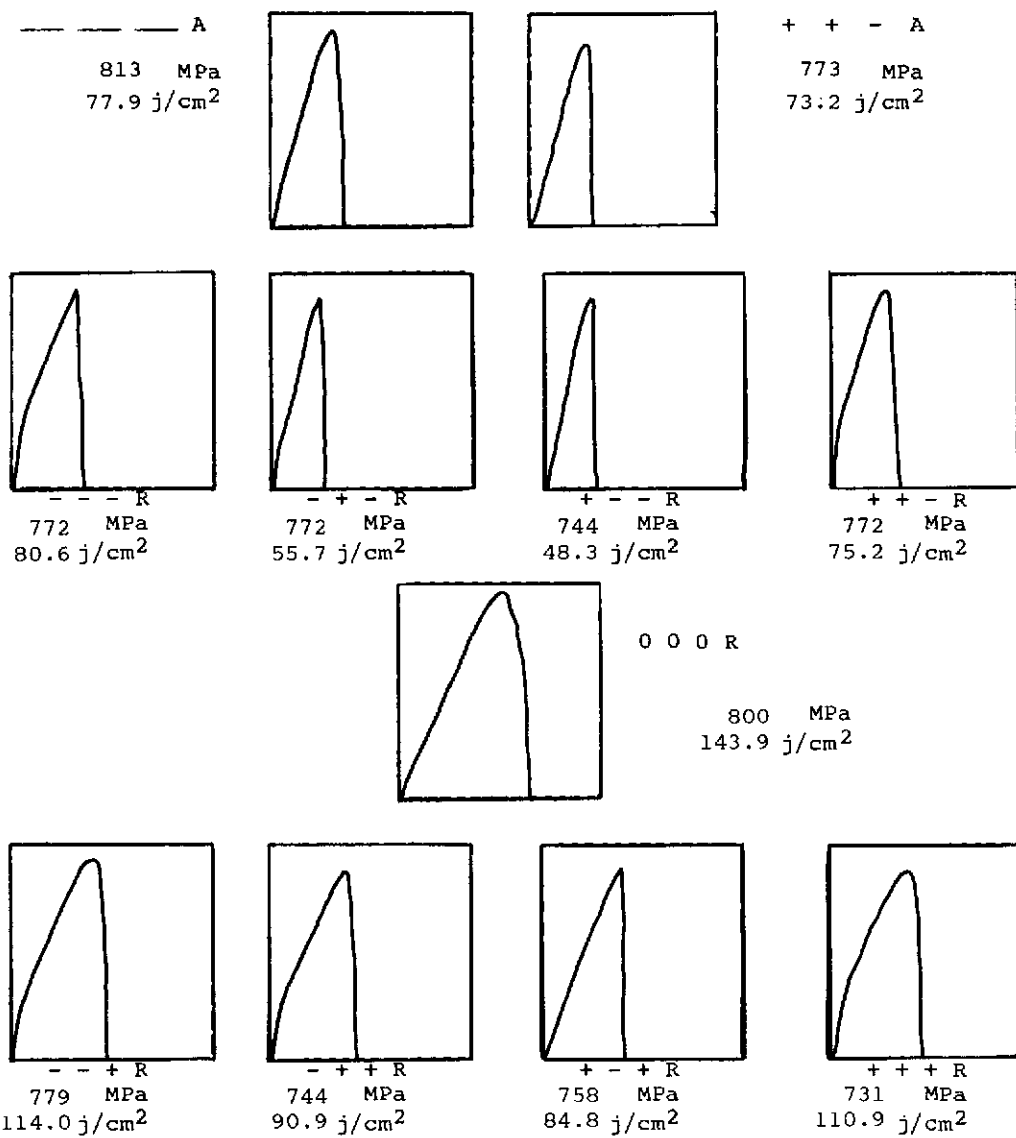


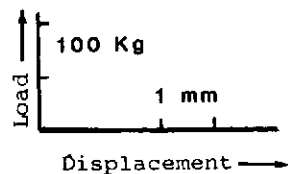
Figure 21

Mechanical Properties of Notched Tensile Coupons as a Function of Exposure Conditions for Ta - 10W



	TEMPERATURE	TIME	[O] POTENTIAL
+	800°C	130 Hrs.	100 ppm
0	550°C	70 Hrs.	50 ppm
-	300°C	10 Hrs.	2 ppm

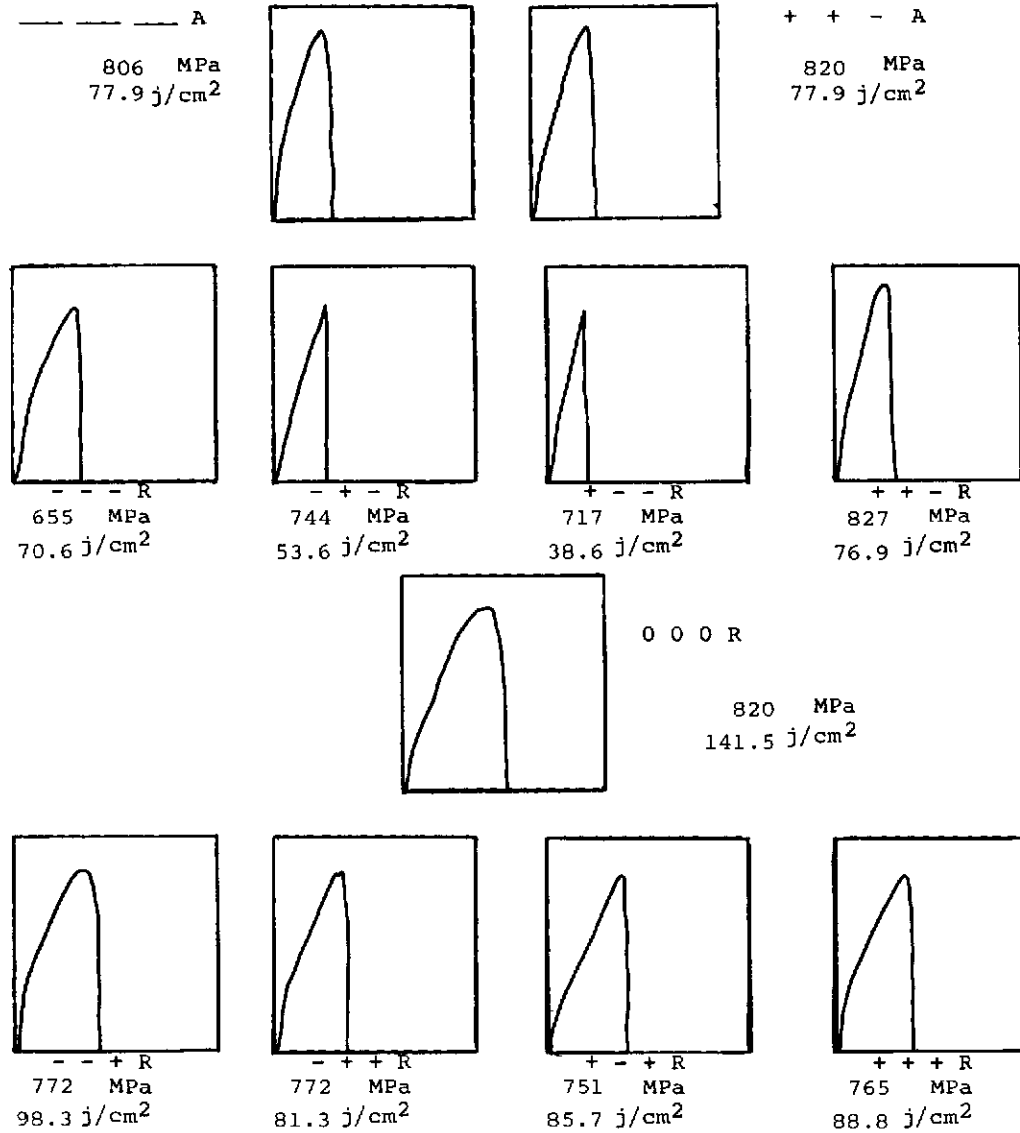
R — NO EXPOSURE
 A — RECRYSTALLIZED
 A — AS-RECEIVED
 ▽ — SMOOTH BAR



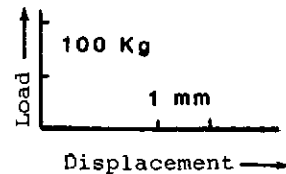
* Denotes single value.
All others are average of replicates.

Figure 22

Mechanical Properties of Notched Tensile Coupons as a Function of Exposure Conditions for T - 111



	TEMPERATURE	TIME	[O] POTENTIAL
+	800°C	130 Hrs.	100 ppm
0	550°C	70 Hrs.	50 ppm
-	300°C	10 Hrs.	2 ppm



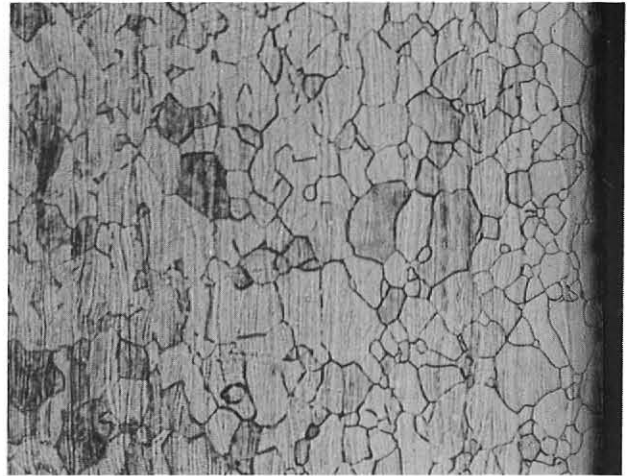
R — NO EXPOSURE
 A — RECRYSTALLIZED
 A — AS-RECEIVED
 ▽ — SMOOTH BAR

• Denotes single value.
 All others are average
 of replicates.

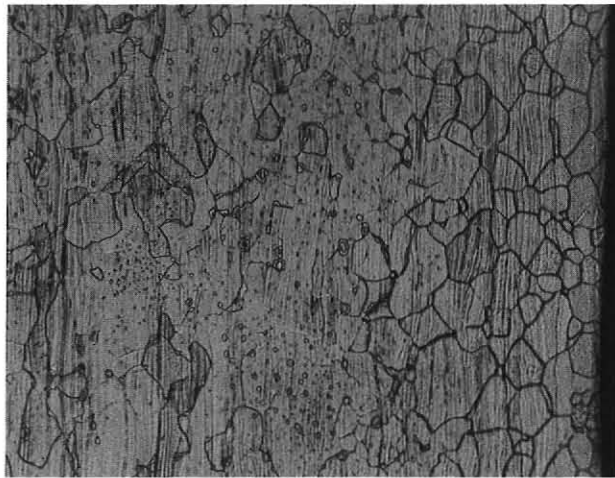
Figure 23



a. As-received



b. +++



c. ---

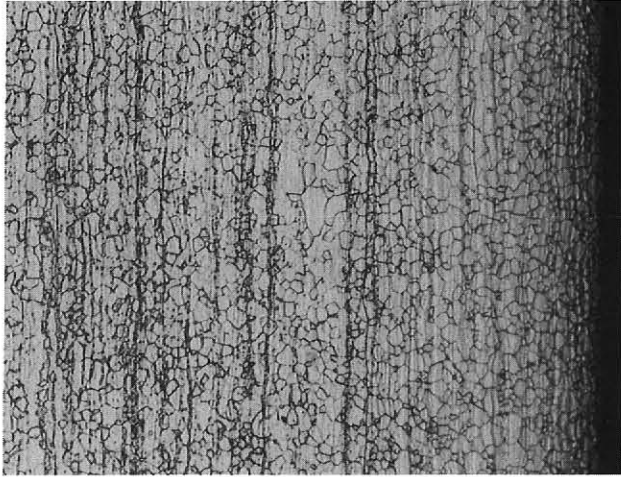
	TEMPERATURE	TIME	[O] POTENTIAL
+	800°C	130 Hrs.	100 ppm
0	550°C	70 Hrs.	50 ppm
-	300°C	10 Hrs.	2 ppm

— NO EXPOSURE
 R RECRYSTALLIZED
 A AS-RECEIVED
 ▽ SMOOTH BAR

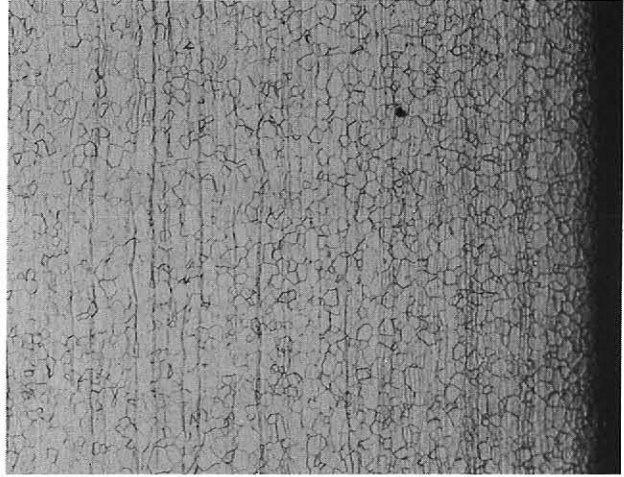
100 μM

Metallographic structure of selected Ta-10W alloy specimens.

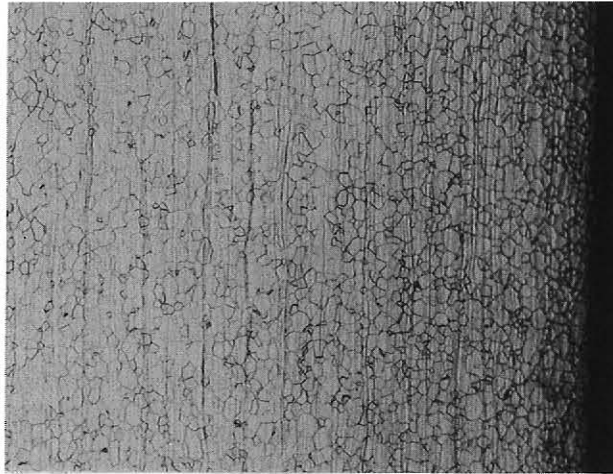
Fig. 24



a. As-received



b. +++




c. ---

	TEMPERATURE	TIME	[O] POTENTIAL
+	800°C	130 Hrs.	100 ppm
0	550°C	70 Hrs.	50 ppm
-	300°C	10 Hrs.	2 ppm

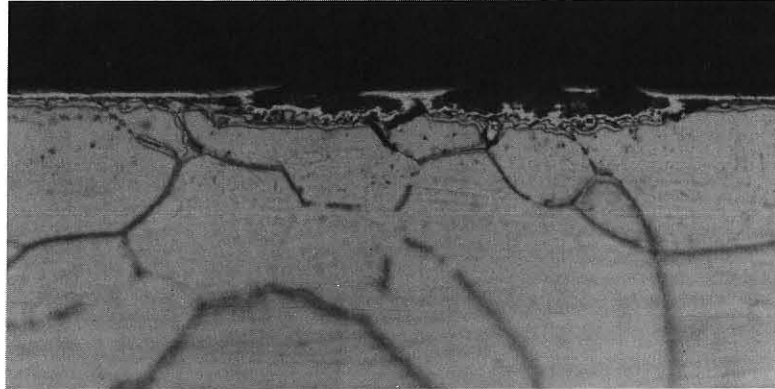
— NO EXPOSURE
 R RECRYSTALLIZED
 A AS-RECEIVED
 ▽ SMOOTH BAR

100 μM

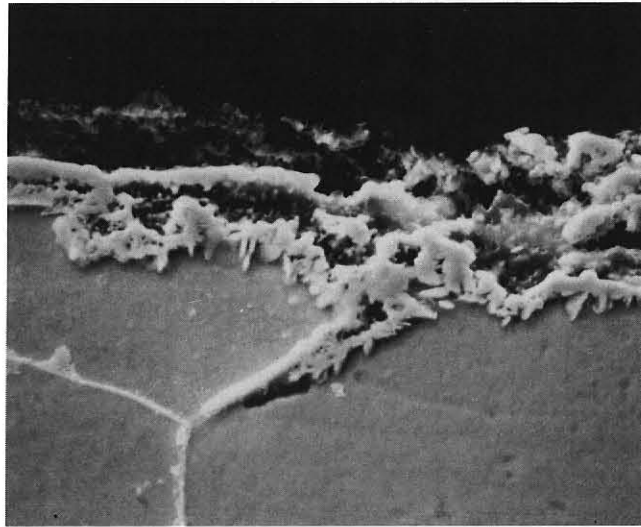


Metallographic structure of selected T-111 alloy specimens.

Fig. 25



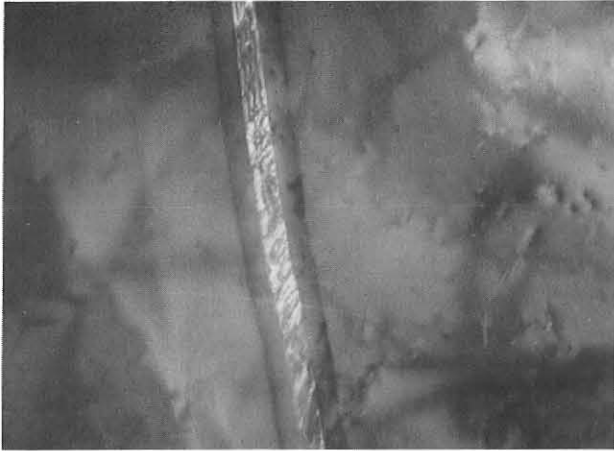
a. 500x



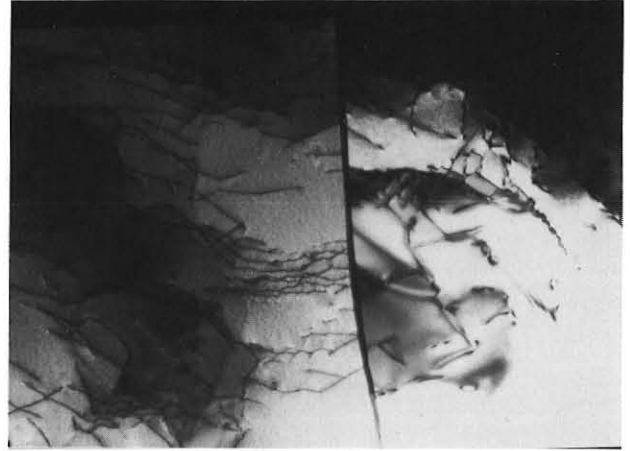
b. 2000x

Surface attack of Ta-10W exposed at 800°C for 130 hours
in Na with 100 ppm [O].

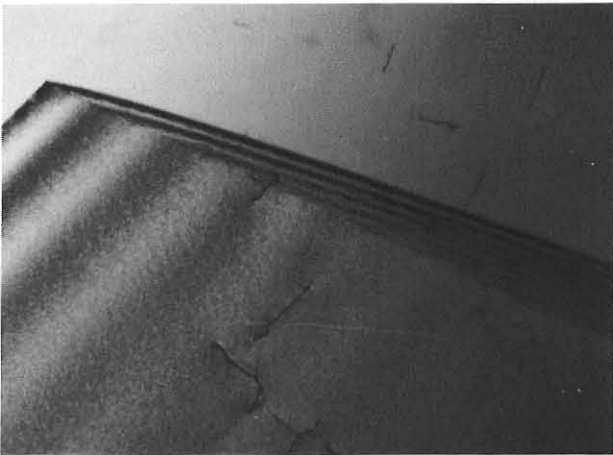
Fig. 26



A. AS-RECEIVED.



B. RECRYSTALLIZED



C. 000.

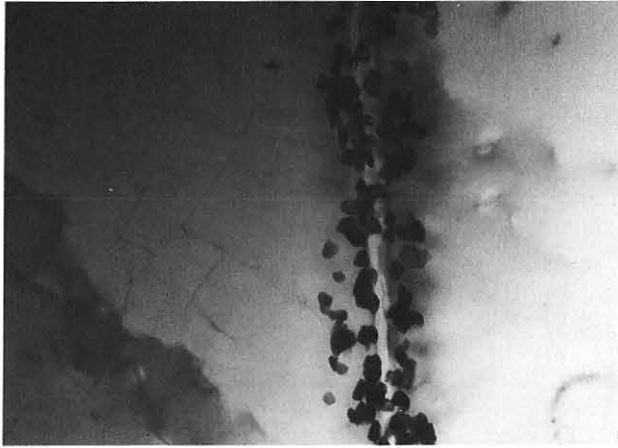
	TEMPERATURE	TIME	[O] POTENTIAL
+	800°C	130 Hrs.	100 ppm
0	550°C	70 Hrs.	50 ppm
-	300°C	10 Hrs.	2 ppm

— No EXPOSURE
 R RECRYSTALLIZED
 A AS-RECEIVED
 ▽ SMOOTH BAR



A. .5 μ M
B. .37 μ M
C. .1 μ M

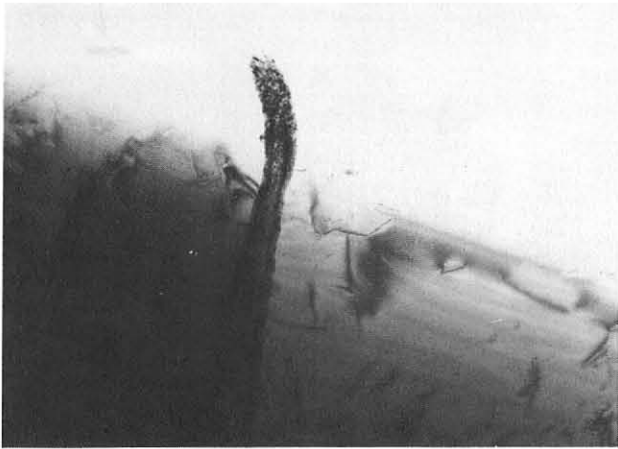
Fig. 27 TRANSMISSION ELECTRON MICROGRAPHS OF TA-10W ALLOY.



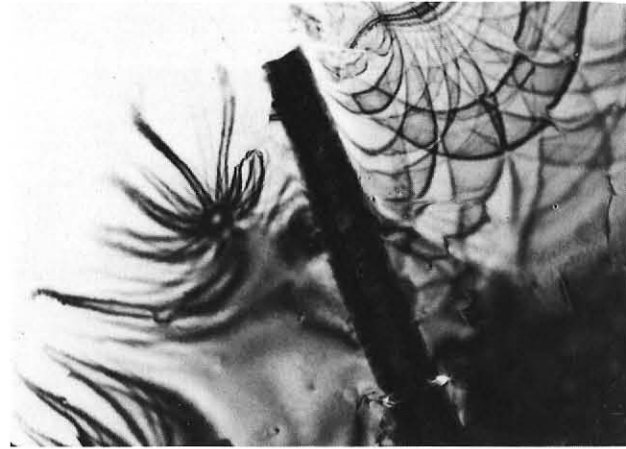
A. ---



B. -+-



C. +--



D. ++-

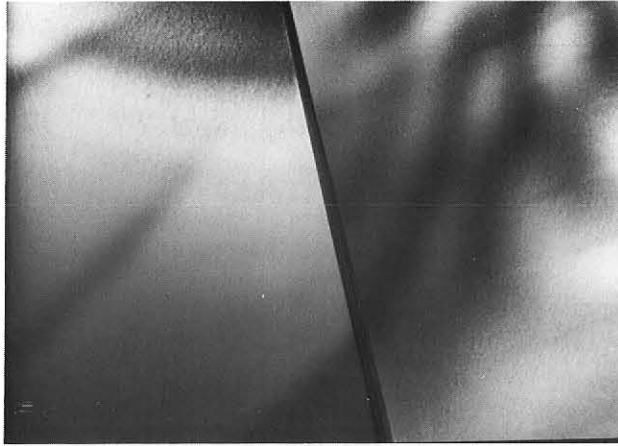
	TEMPERATURE	TIME	[O] POTENTIAL
+	800°C	130 Hrs.	100 ppm
0	550°C	70 Hrs.	50 ppm
-	300°C	10 Hrs.	2 ppm

— NO EXPOSURE
 R RECRYSTALLIZED
 A AS-RECEIVED
 ▽ SMOOTH BAR



A. .37 μM
B.C. .5 μM
D. .25 μM

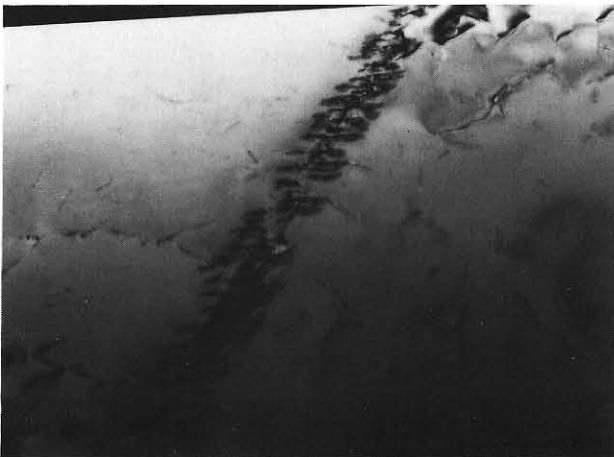
Fig. 28 TRANSMISSION ELECTRON MICROGRAPHS OF TA-10W ALLOY.



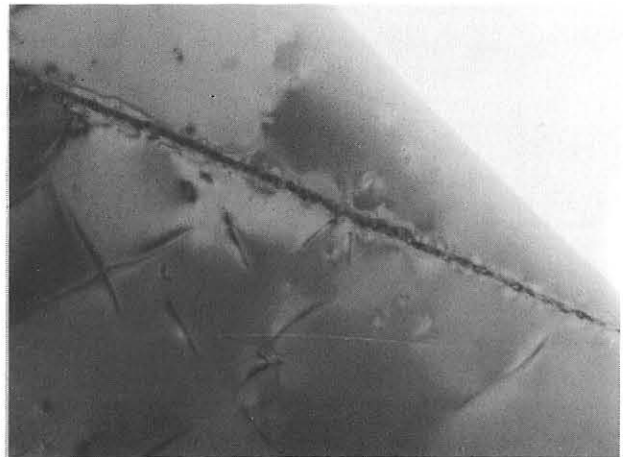
A. ---\



B. -++



C. +++



D. +++

	TEMPERATURE	TIME	[O] POTENTIAL
+	800°C	130 Hrs.	100 ppm
0	550°C	70 Hrs.	50 ppm
-	300°C	10 Hrs.	2 ppm

— NO EXPOSURE
 R RECRYSTALLIZED
 A AS-RECEIVED
 ▽ SMOOTH BAR

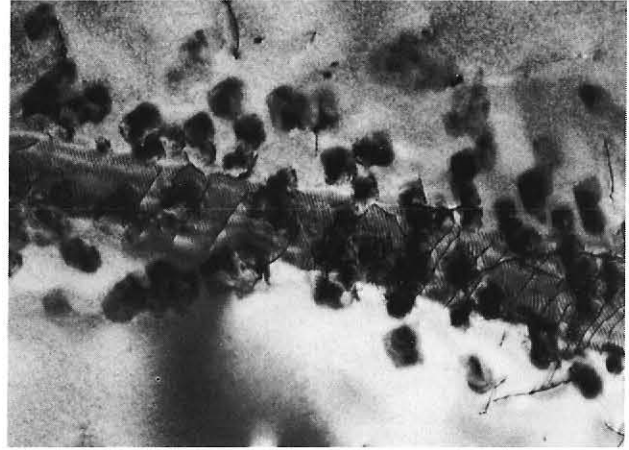


A. .7 μM
B. .25 μM
C. .1 μM
D. .5 μM

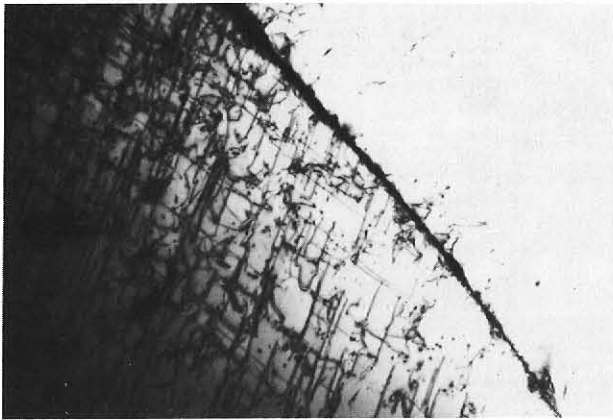
Fig. 29 TRANSMISSION ELECTRON MICROGRAPHS OF TA-10W ALLOY.



A. A/R



B. ---



C. 000



D. +++

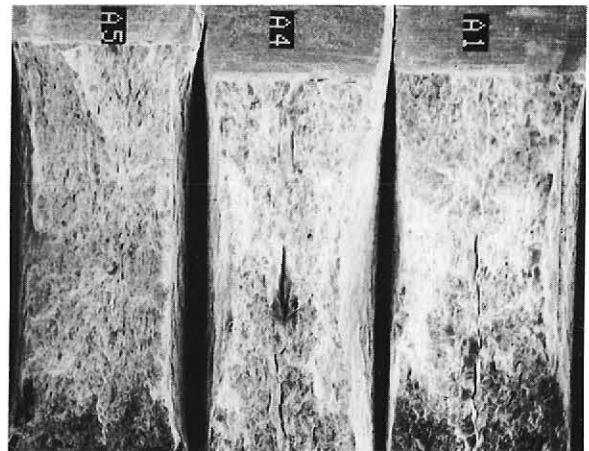
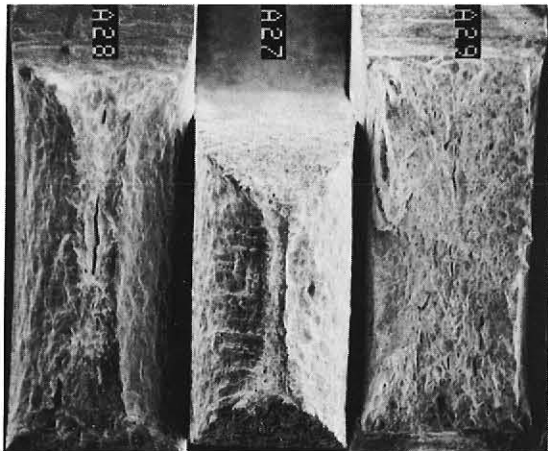
	TEMPERATURE	TIME	[O] POTENTIAL
+	800°C	130 Hrs.	100 ppm
0	550°C	70 Hrs.	50 ppm
-	300°C	10 Hrs.	2 ppm

A. .1 μ M
B. .25 μ M
C.&D. .5 μ M

— No EXPOSURE
 R RECRYSTALLIZED
 A AS-RECEIVED
 ▽ SMOOTH BAR

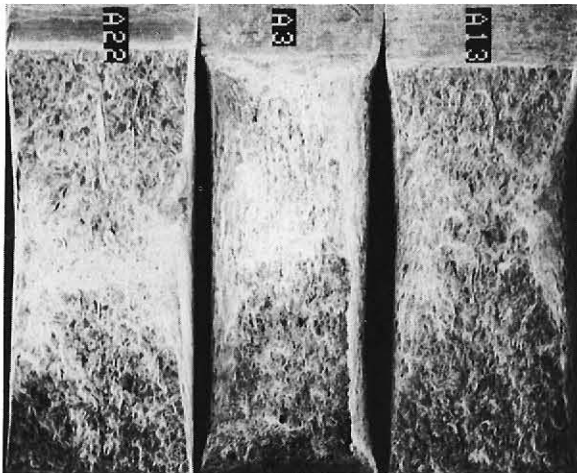


Fig. 30 TRANSMISSION ELECTRON MICROGRAPHS OF T-111 ALLOY.

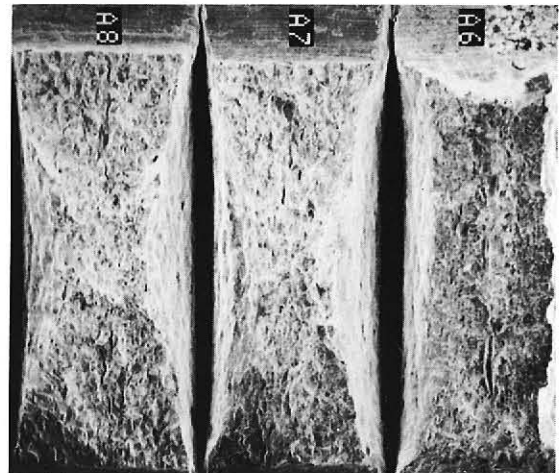


A28 — — — A
 A27 — — — A▽
 A29 + + - A

A5 + + - R
 A4 + - - R
 A1 - + - R



A22 - - - R
 A3 + + + R
 A13 + - + R



A8 - + + R
 A7 - - + R
 A6 0 0 0 R

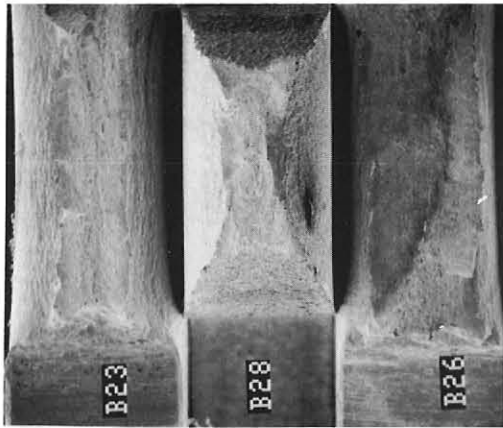
TA-10W

	TEMPERATURE	TIME	[O] POTENTIAL
+	800°C	130 HRS.	100 PPM
0	550°C	70 HRS.	50 PPM
-	300°C	10 HRS.	2 PPM

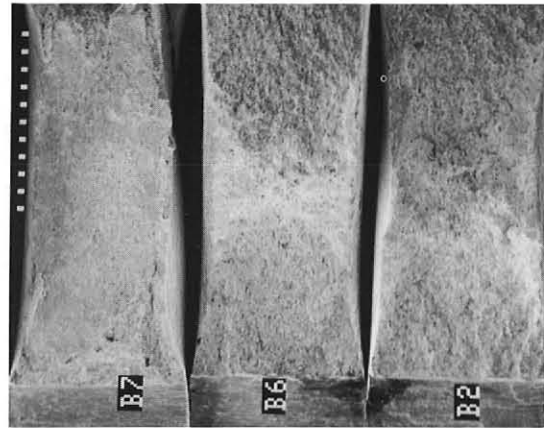
— NO EXPSOURE
 R RECRYSTALLIZED
 A AS-RECEIVED
 ▽ SMOOTH BAR

1500 μm
 ───────────┘

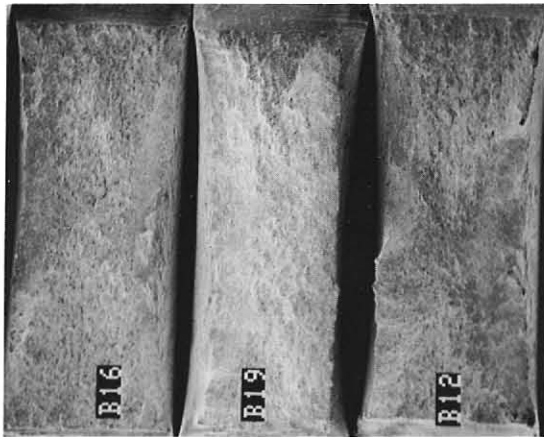
Fig. 31



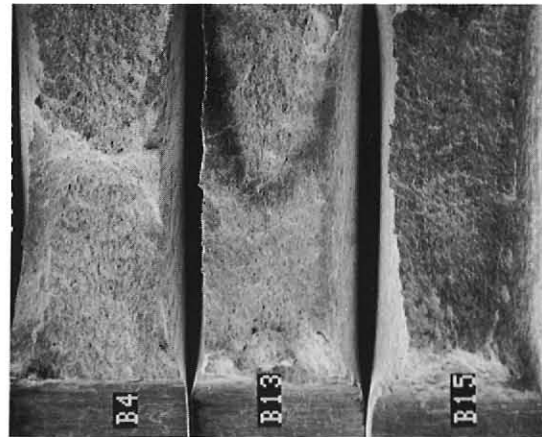
B23 — — — A
 B28 — — — A▽
 B26 + + - A



B7 + + - R
 B6 + - - R
 B2 - + - R



B16 - - - R
 B19 + + + R
 B12 + - + R



B4 - + + R
 B13 - - + R
 B15 0 0 0 R

T-111

	TEMPERATURE	TIME	[O] POTENTIAL
+	800°C	130 HRS.	100 PPM
0	550°C	70 HRS.	50 PPM
-	300°C	10 HRS.	2 PPM

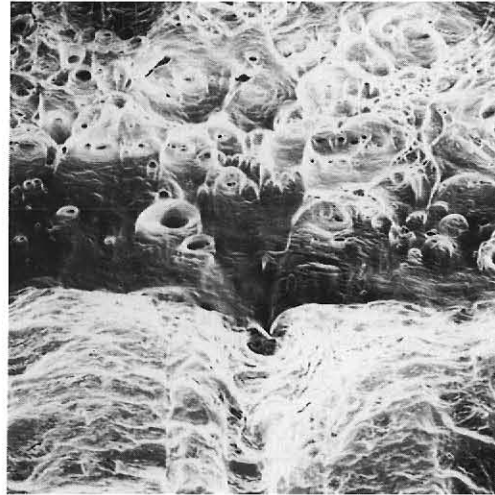
— NO EXPSOURE
 R RECRYSTALLIZED
 A AS-RECEIVED
 ▽ SMOOTH BAR

1500 μm

Fig. 32



a. As-received



b. As-received smooth



c. +- Unrecrystallized



d. +-

	TEMPERATURE	TIME	[O] POTENTIAL
+	800°C	130 Hrs.	100 ppm
0	550°C	70 Hrs.	50 ppm
-	300°C	10 Hrs.	2 ppm

— NO EXPOSURE
 R RECRYSTALLIZED
 A AS-RECEIVED
 ▽ SMOOTH BAR

50 μM

High magnification fractographs of Ta-10W alloy specimens.

Fig. 33



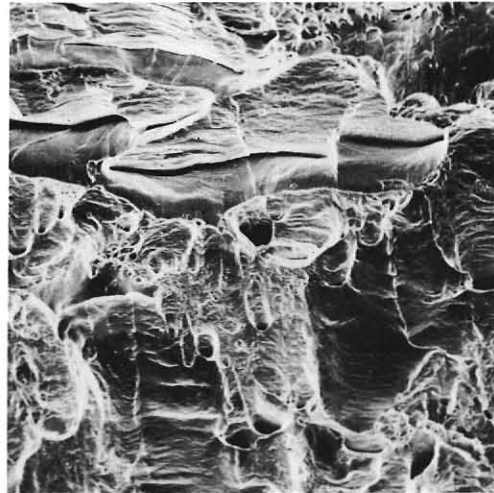
a. +--



b. --+



c. ---



d. 000

	TEMPERATURE	TIME	[O] POTENTIAL
+	800°C	130 Hrs.	100 ppm
0	550°C	70 Hrs.	50 ppm
-	300°C	10 Hrs.	2 ppm

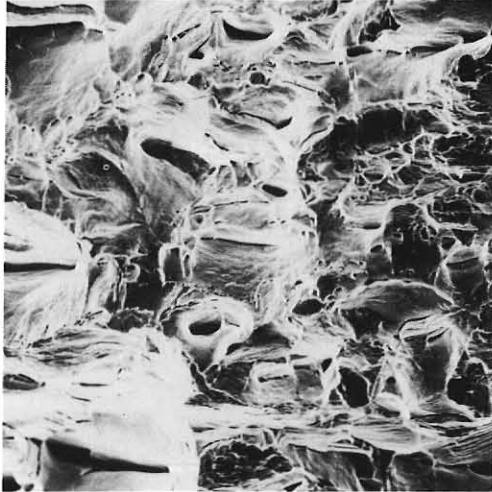
— NO EXPOSURE
 R RECRYSTALLIZED
 A AS-RECEIVED
 ▽ SMOOTH BAR

50 μM



High magnification fractographs of Ta-10W alloys specimens.

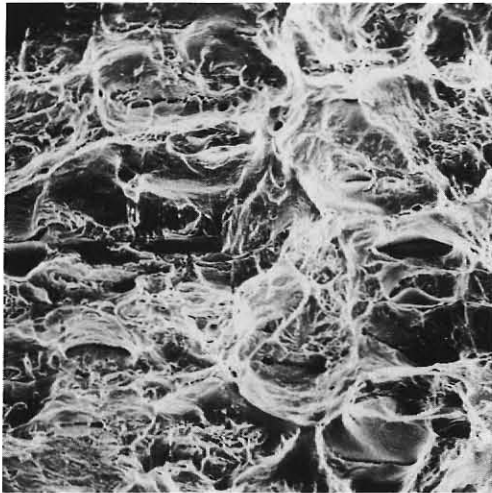
Fig. 34



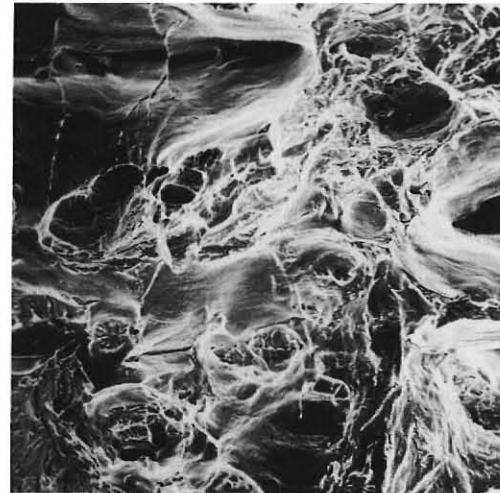
a. ++++



b. +++



c. ++



d. ++

	TEMPERATURE	TIME	[O] POTENTIAL
+	800°C	130 Hrs.	100 ppm
0	550°C	70 Hrs.	50 ppm
-	300°C	10 Hrs.	2 ppm

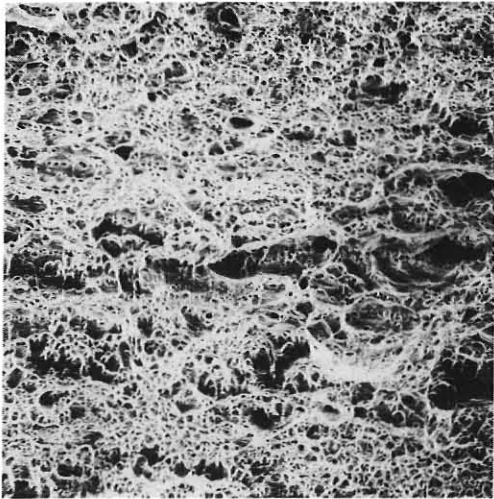
— NO EXPOSURE
 R RECRYSTALLIZED
 A AS-RECEIVED
 ▽ SMOOTH BAR

50 μM

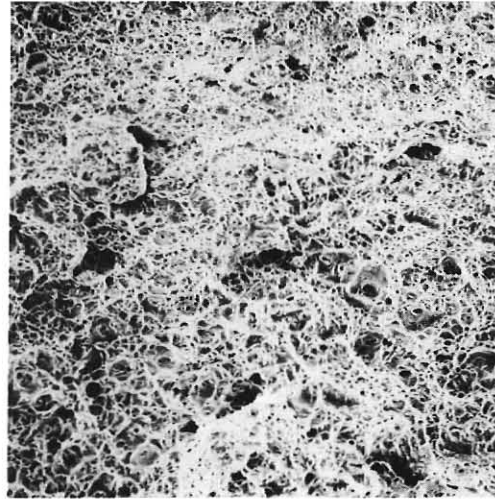


High magnification fractographs of Ta-10W alloy specimens.

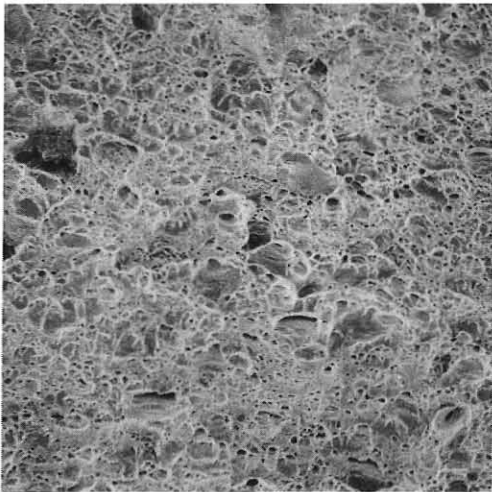
Fig. 35



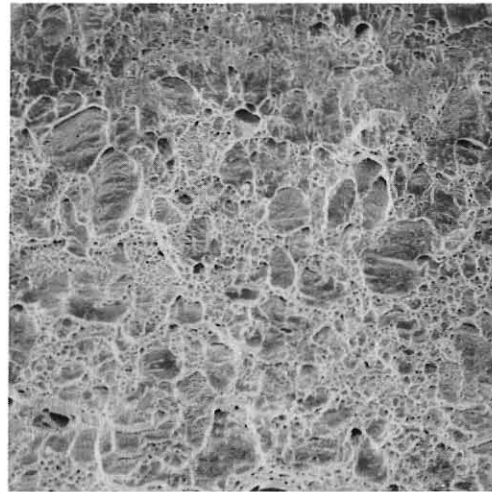
a. As-received



b. As-received smooth



c. +- Unrecrystallized



d. +-

	TEMPERATURE	TIME	[O] POTENTIAL
+	800°C	130 Hrs.	100 ppm
0	550°C	70 Hrs.	50 ppm
-	300°C	10 Hrs.	2 ppm

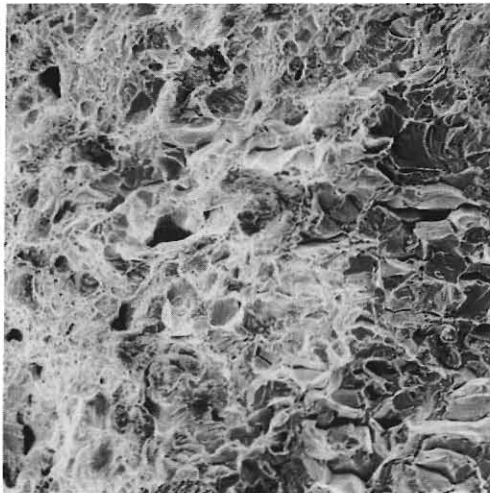
— NO EXPOSURE
 R RECRYSTALLIZED
 A AS-RECEIVED
 ▽ SMOOTH BAR

50 μM

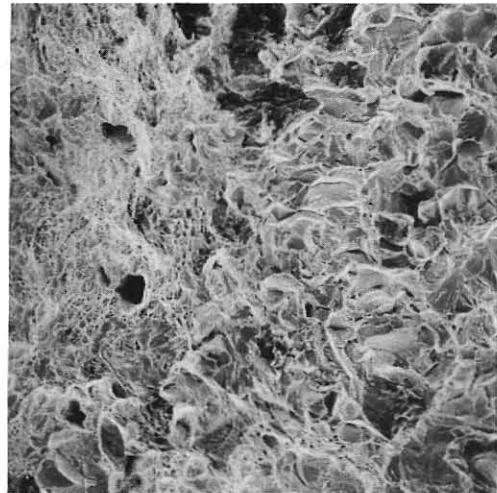


High magnification fractographs of T-111 alloys specimens.

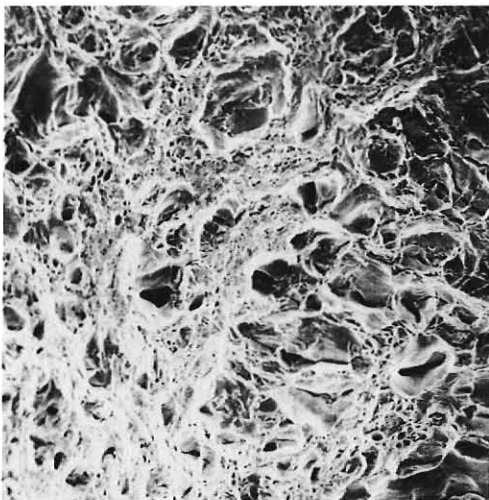
Fig. 36



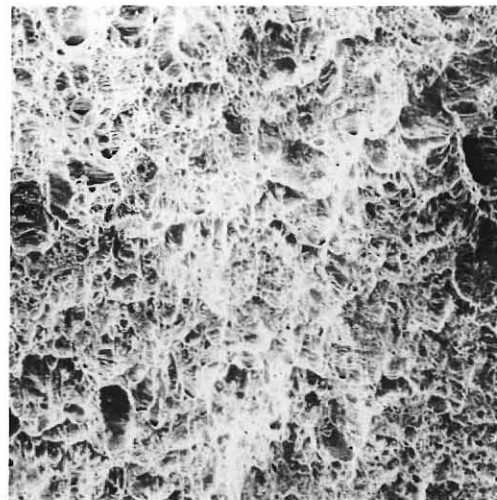
a. +--



b. --+



c. ---



d. 000

	TEMPERATURE	TIME	[O] POTENTIAL
+	800°C	130 Hrs.	100 ppm
0	550°C	70 Hrs.	50 ppm
-	300°C	10 Hrs.	2 ppm

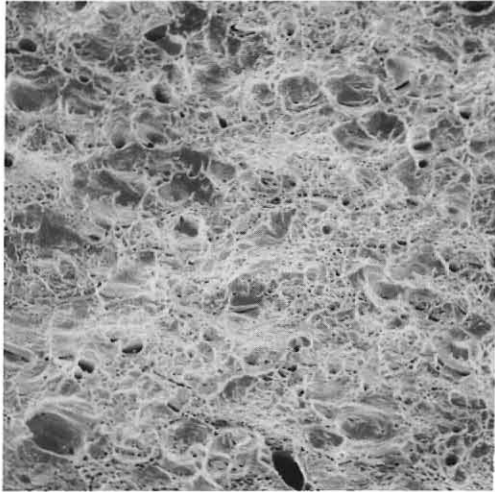
— NO EXPOSURE
 R RECRYSTALLIZED
 A AS-RECEIVED
 ▽ SMOOTH BAR

50 μM

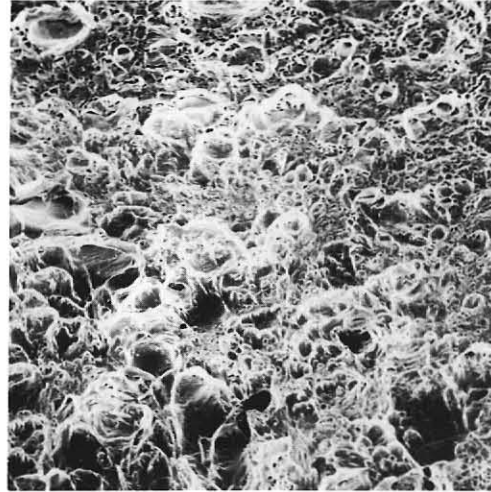


High magnification fractographs of T-111 alloy specimens.

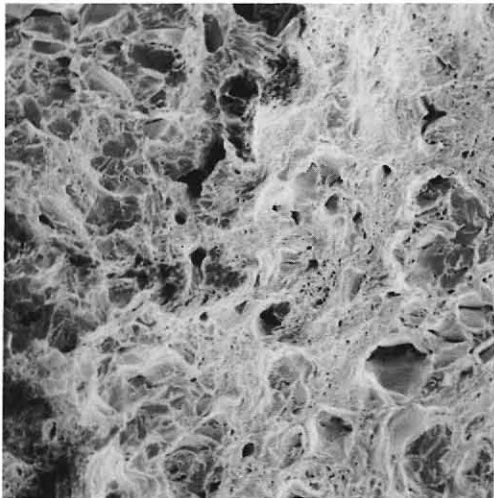
Fig. 37



a. +++



b. ++



c. -++



d. --+

	TEMPERATURE	TIME	[O] POTENTIAL
+	800°C	130 Hrs.	100 ppm
0	550°C	70 Hrs.	50 ppm
-	300°C	10 Hrs.	2 ppm

— NO EXPOSURE
 R RECRYSTALLIZED
 A AS-RECEIVED
 ▽ SMOOTH BAR

50 μM

High magnification fractographs of T-111 alloy.

Fig. 38

**TA-10W ALLOY FRACTURE ENERGY
AS A FUNCTION OF
OXYGEN CONCENTRATION AND TEMPERATURE
IN MOLTEN SODIUM (TIME = 10HRS)**

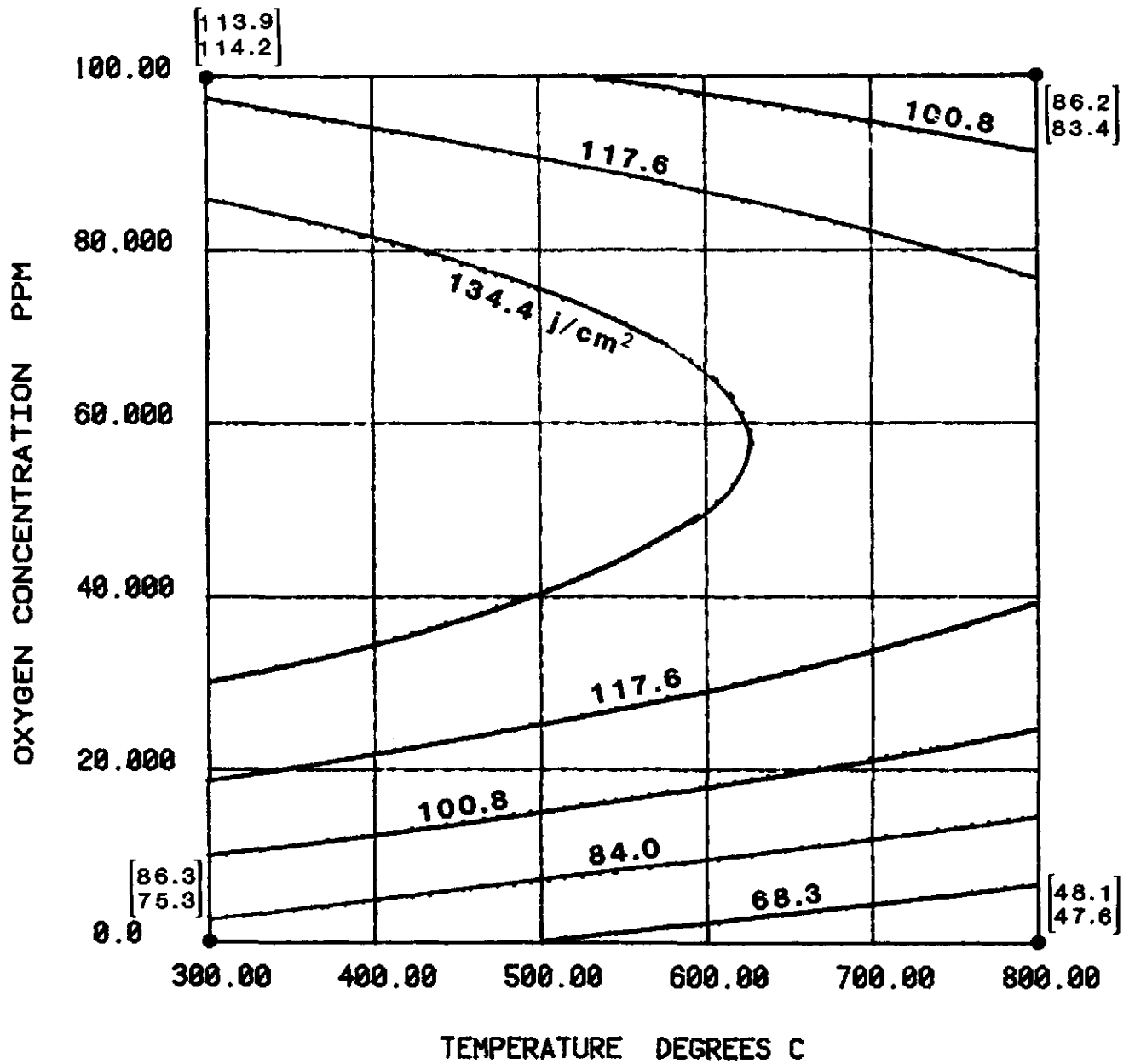


Figure 39

**TA-10W ALLOY FRACTURE ENERGY
AS A FUNCTION OF
OXYGEN CONCENTRATION AND TEMPERATURE
IN MOLTEN SODIUM (TIME = 70HRS)**

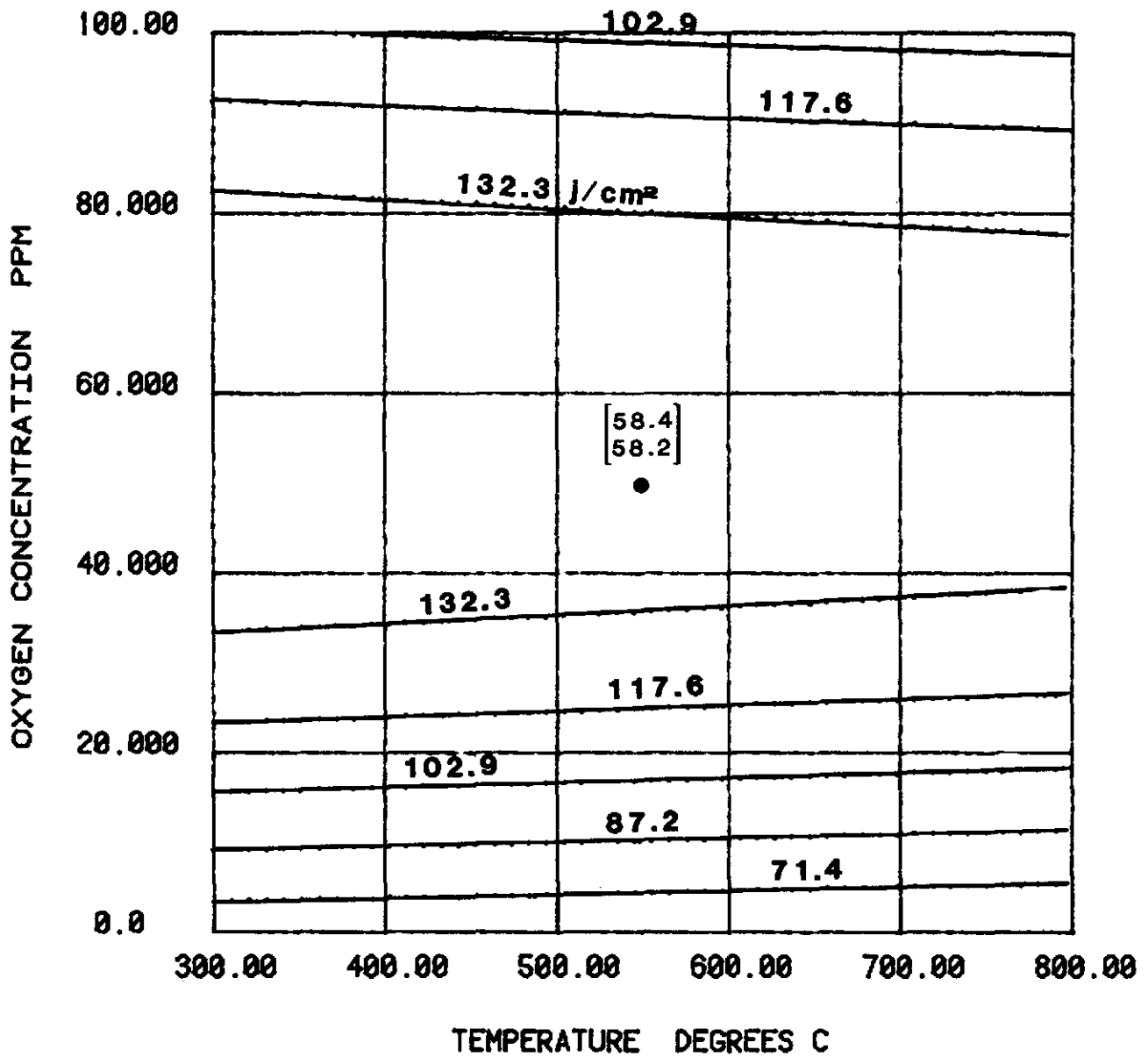


Figure 40

**TA-10W ALLOY FRACTURE ENERGY
AS A FUNCTION OF
OXYGEN CONCENTRATION AND TEMPERATURE
IN MOLTEN SODIUM (TIME=130HRS)**

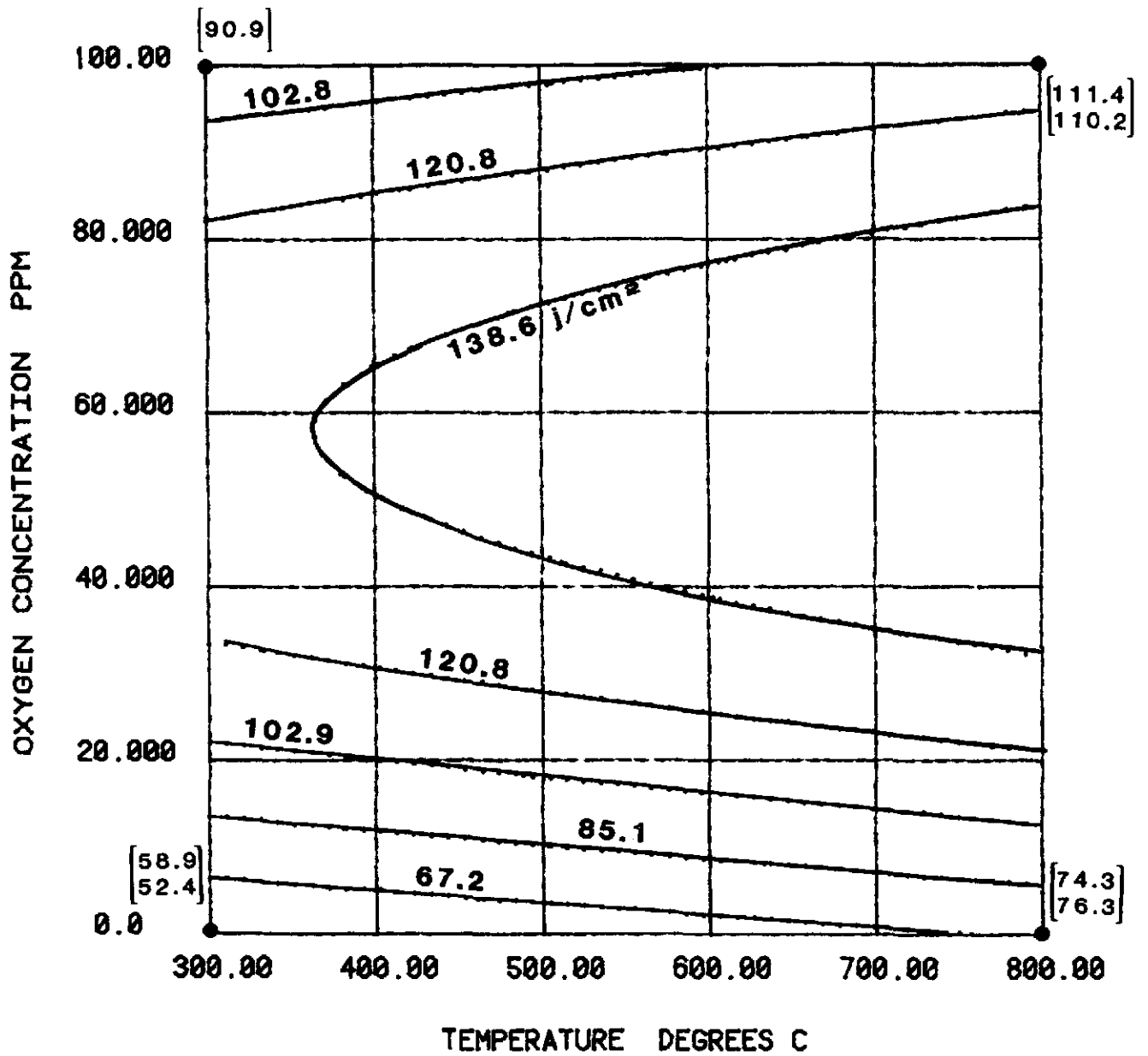


Figure 41

TA-10W ALLOY FRACTURE STRESS
AS A FUNCTION OF
OXYGEN CONCENTRATION AND TEMPERATURE
IN MOLTEN SODIUM (TIME=10 HRS)

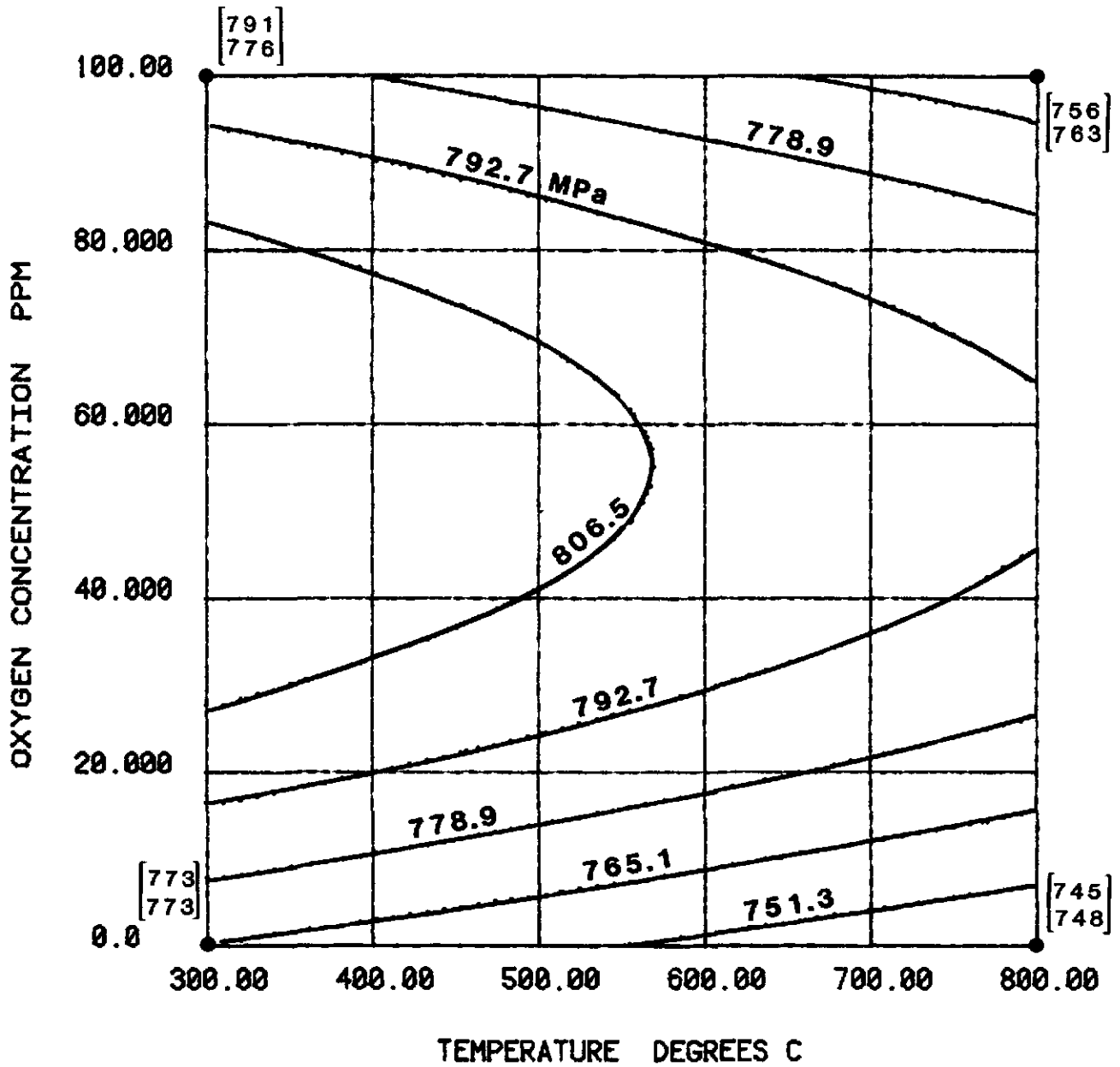


Figure 42

TA-10W ALLOY FRACTURE STRESS
AS A FUNCTION OF
OXYGEN CONCENTRATION AND TEMPERATURE
IN MOLTEN SODIUM (TIME=70 HRS)

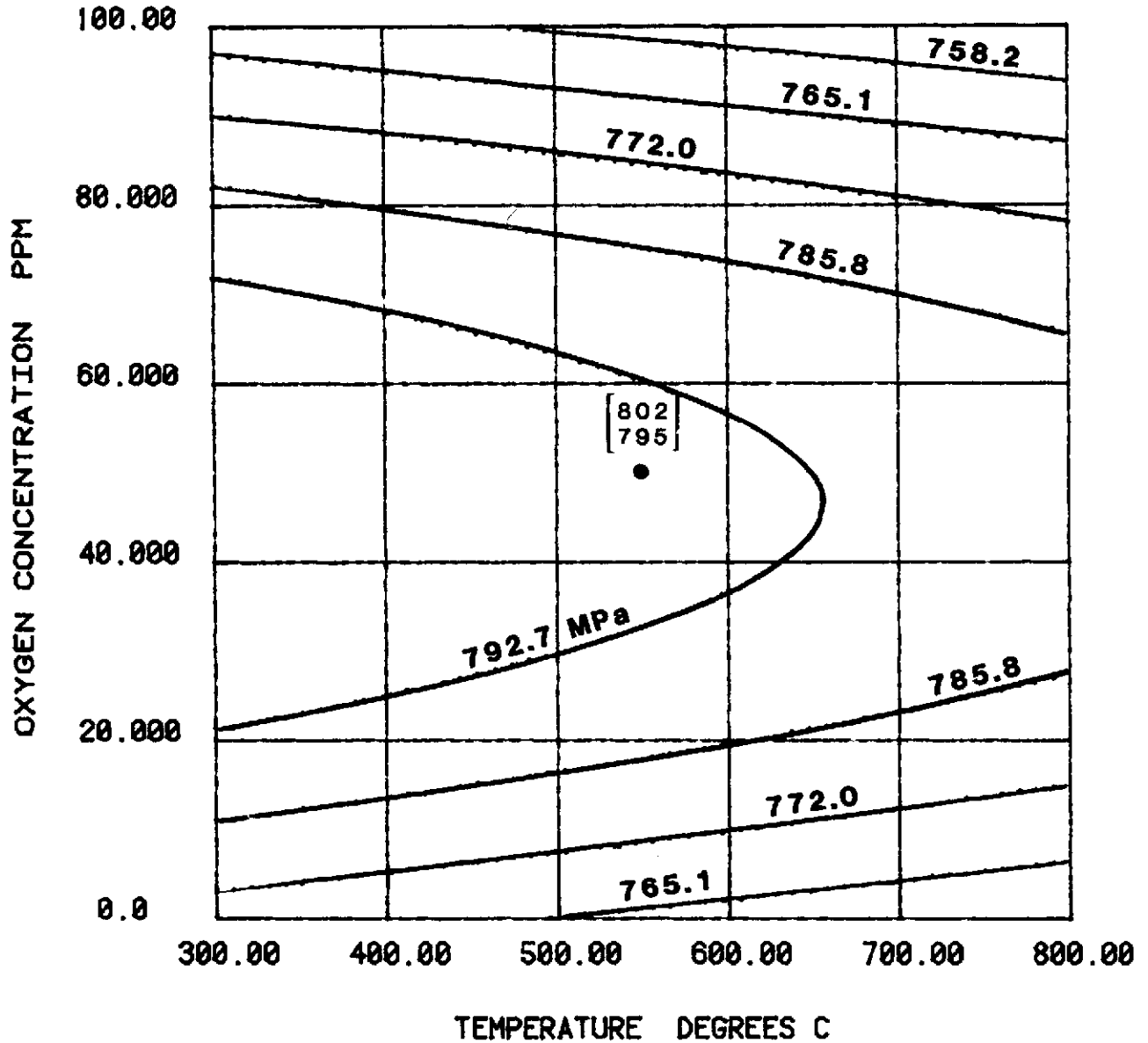


Figure 43

TA-10W ALLOY FRACTURE STRESS
AS A FUNCTION OF
OXYGEN CONCENTRATION AND TEMPERATURE
IN MOLTEN SODIUM (TIME=130 HRS)

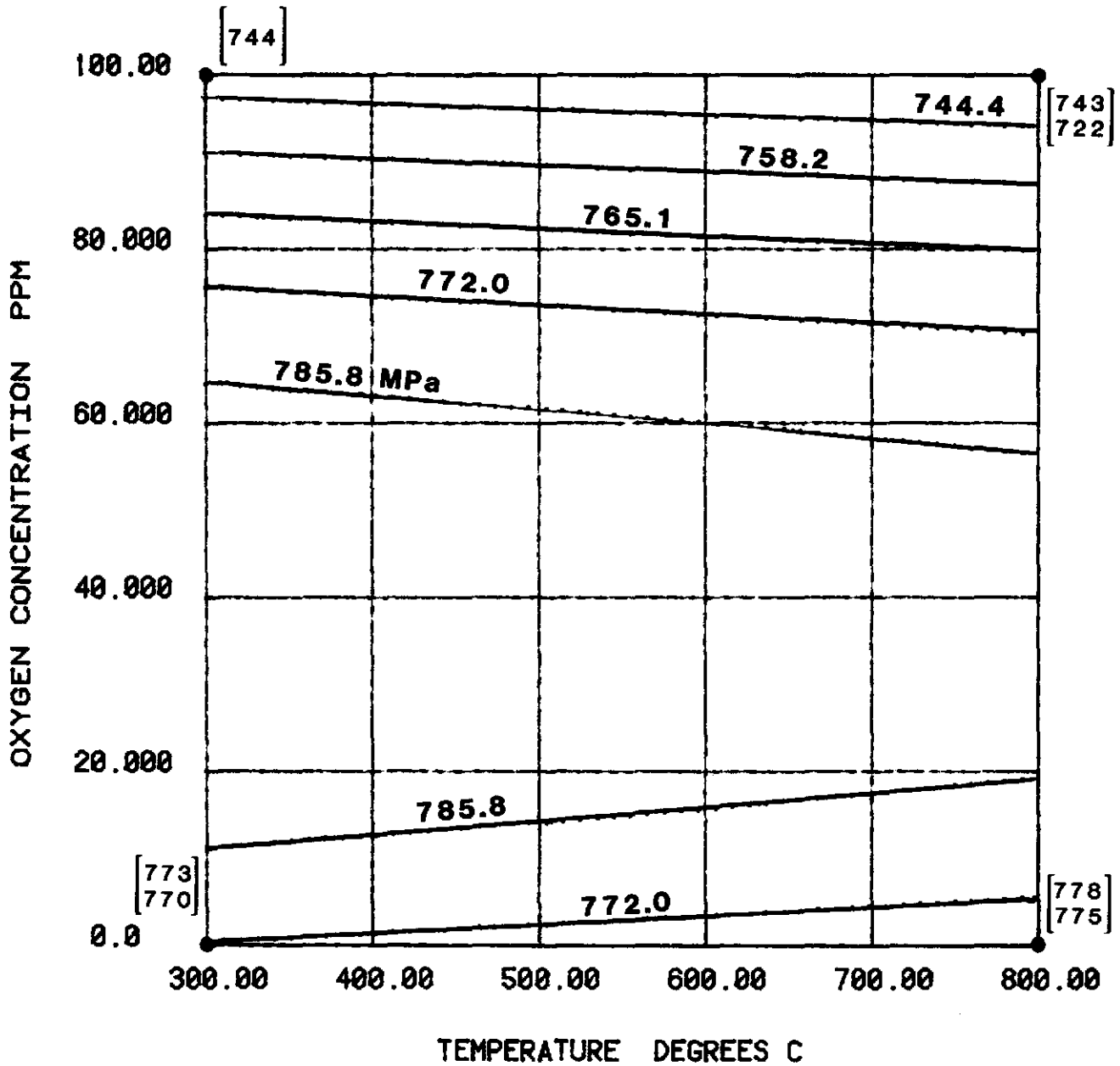


Figure 44

**T-111 ALLOY FRACTURE ENERGY
AS A FUNCTION OF
OXYGEN CONCENTRATION AND TEMPERATURE
IN MOLTEN SODIUM (TIME = 10 HRS)**

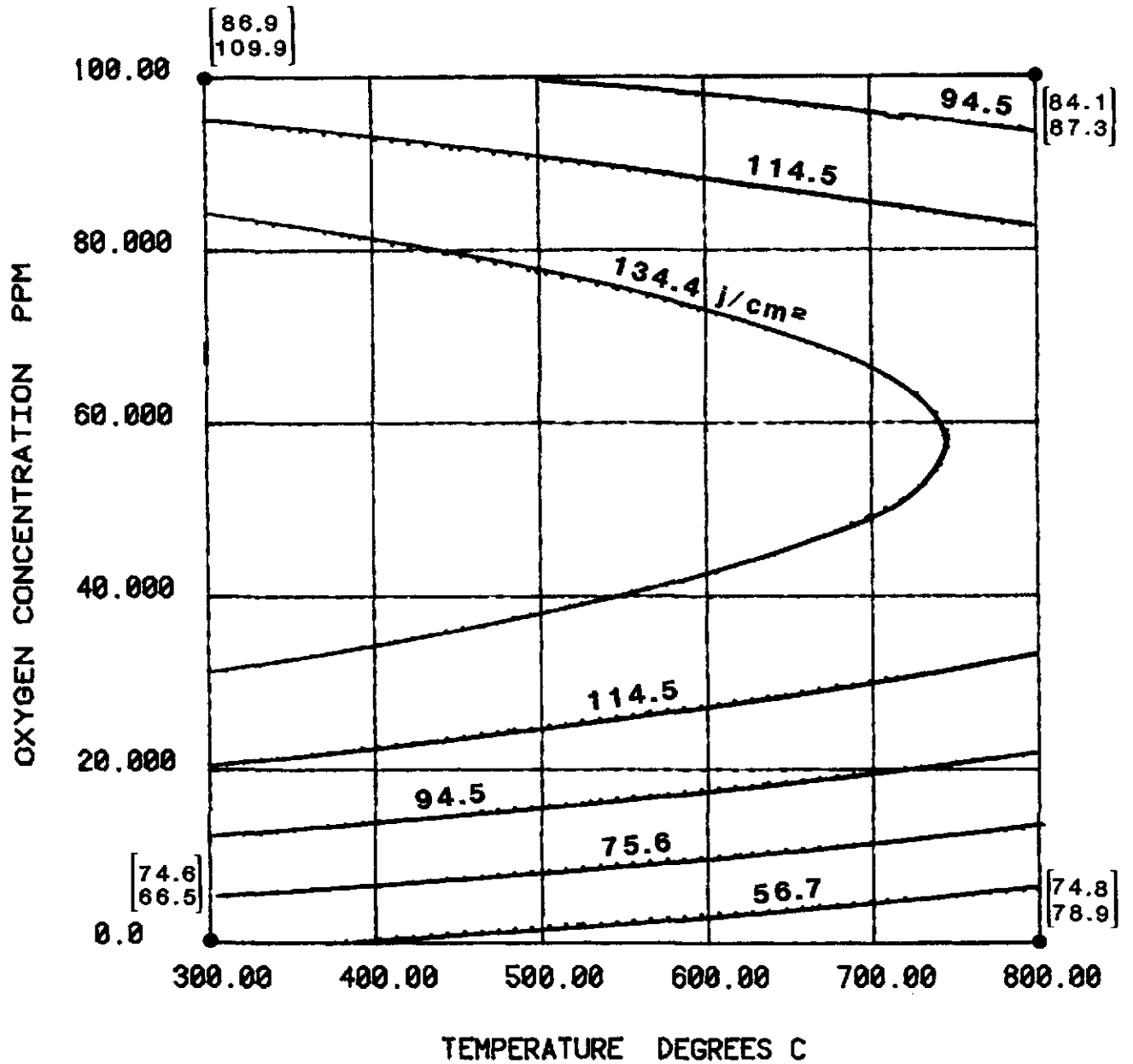


Figure 45

**T-111 ALLOY FRACTURE ENERGY
AS A FUNCTION OF
OXYGEN CONCENTRATION AND TEMPERATURE
IN MOLTEN SODIUM (TIME = 70 HRS)**

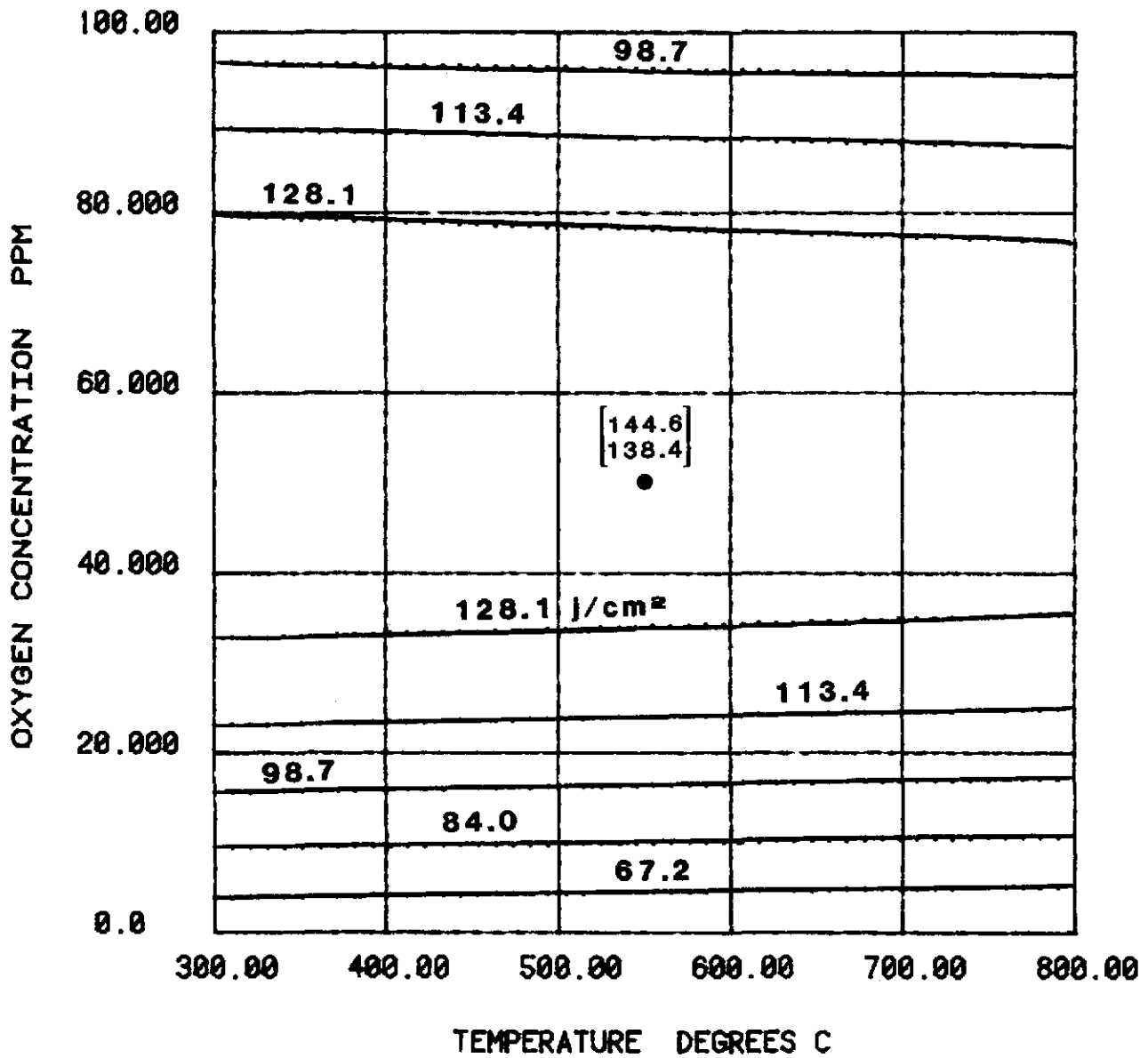


Figure 46

**T-111 ALLOY FRACTURE ENERGY
AS A FUNCTION OF
OXYGEN CONCENTRATION AND TEMPERATURE
IN MOLTEN SODIUM (TIME = 130 HRS)**

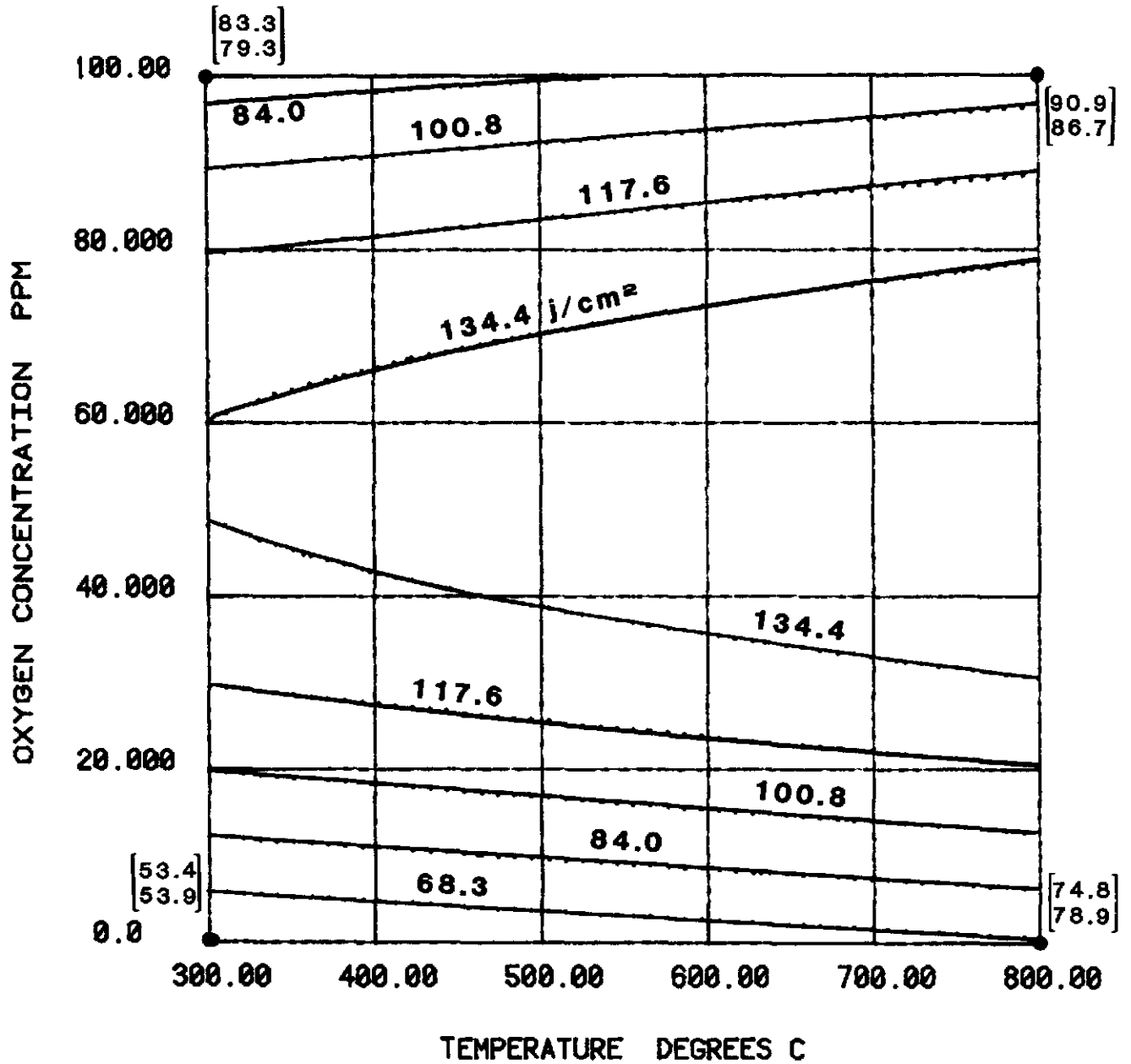


Fig. 47

T-111 ALLOY FRACTURE STRESS
AS A FUNCTION OF
OXYGEN CONCENTRATION AND TEMPERATURE
IN MOLTEN SODIUM (TIME=10 HRS)

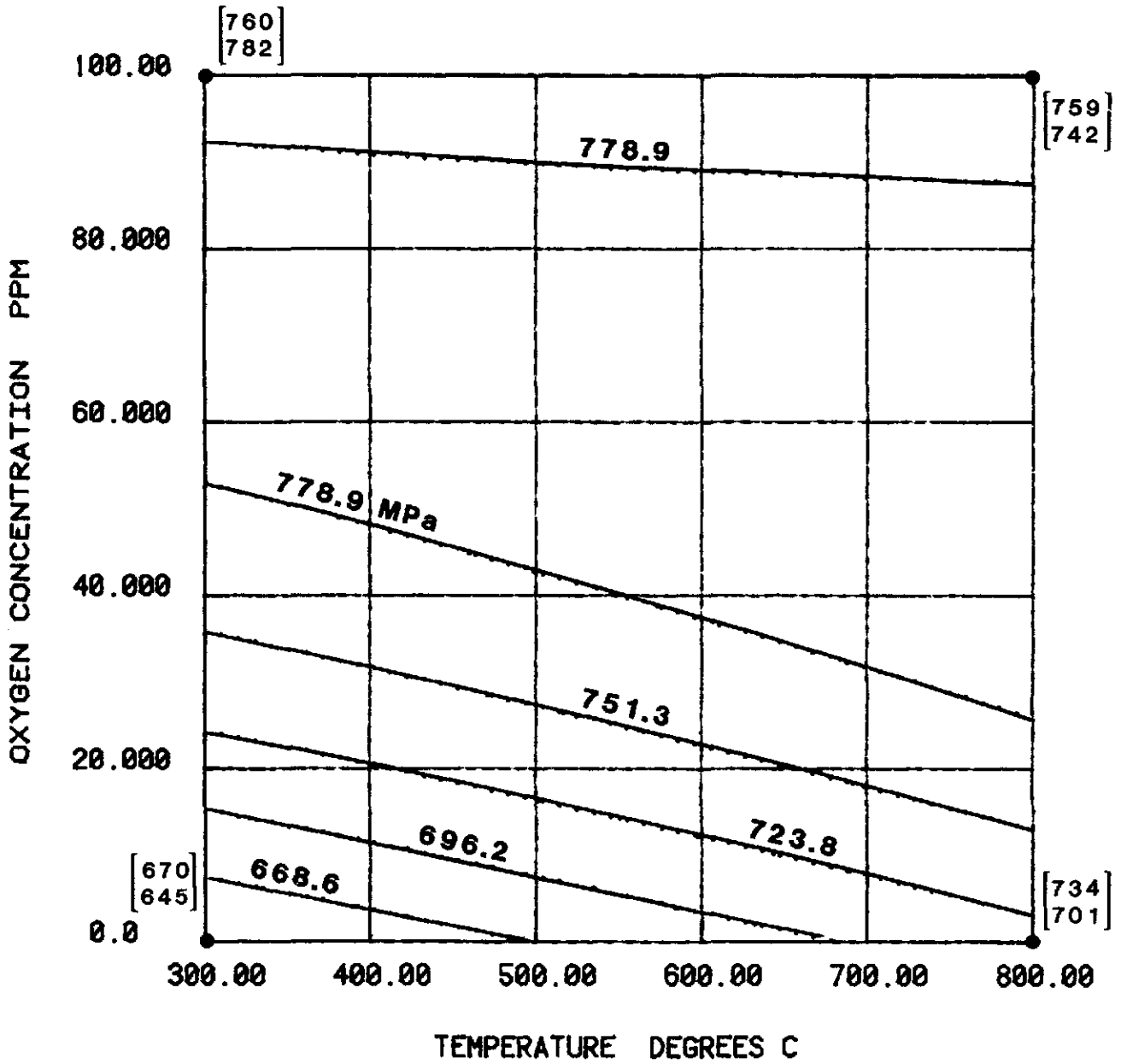


Fig. 48

T-111 ALLOY FRACTURE STRESS
 AS A FUNCTION OF
 OXYGEN CONCENTRATION AND TEMPERATURE
 IN MOLTEN SODIUM (TIME=70 HRS)

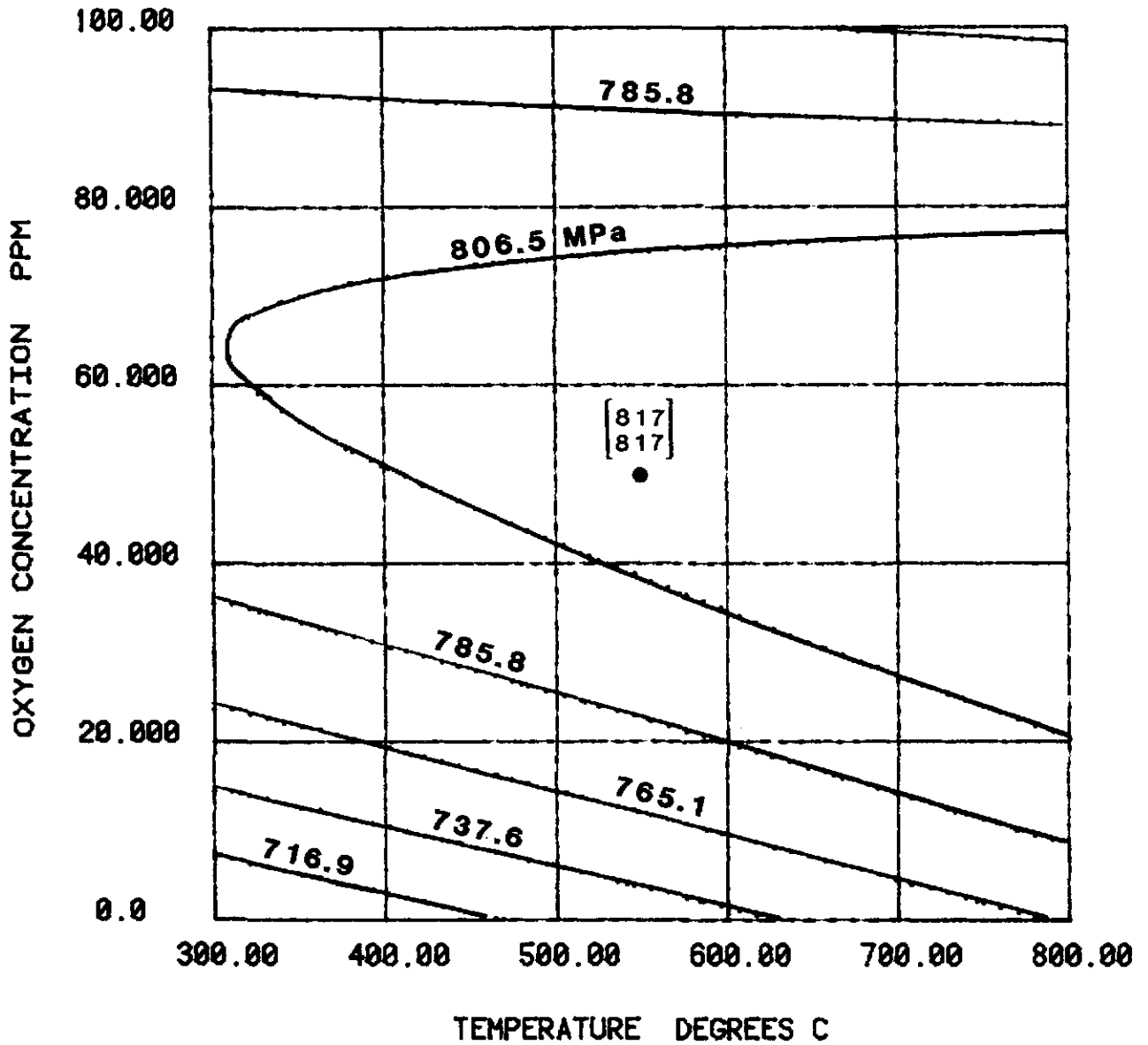


Fig. 49

T-111 ALLOY FRACTURE STRESS
AS A FUNCTION OF
OXYGEN CONCENTRATION AND TEMPERATURE
IN MOLTEN SODIUM (TIME=130 HRS)

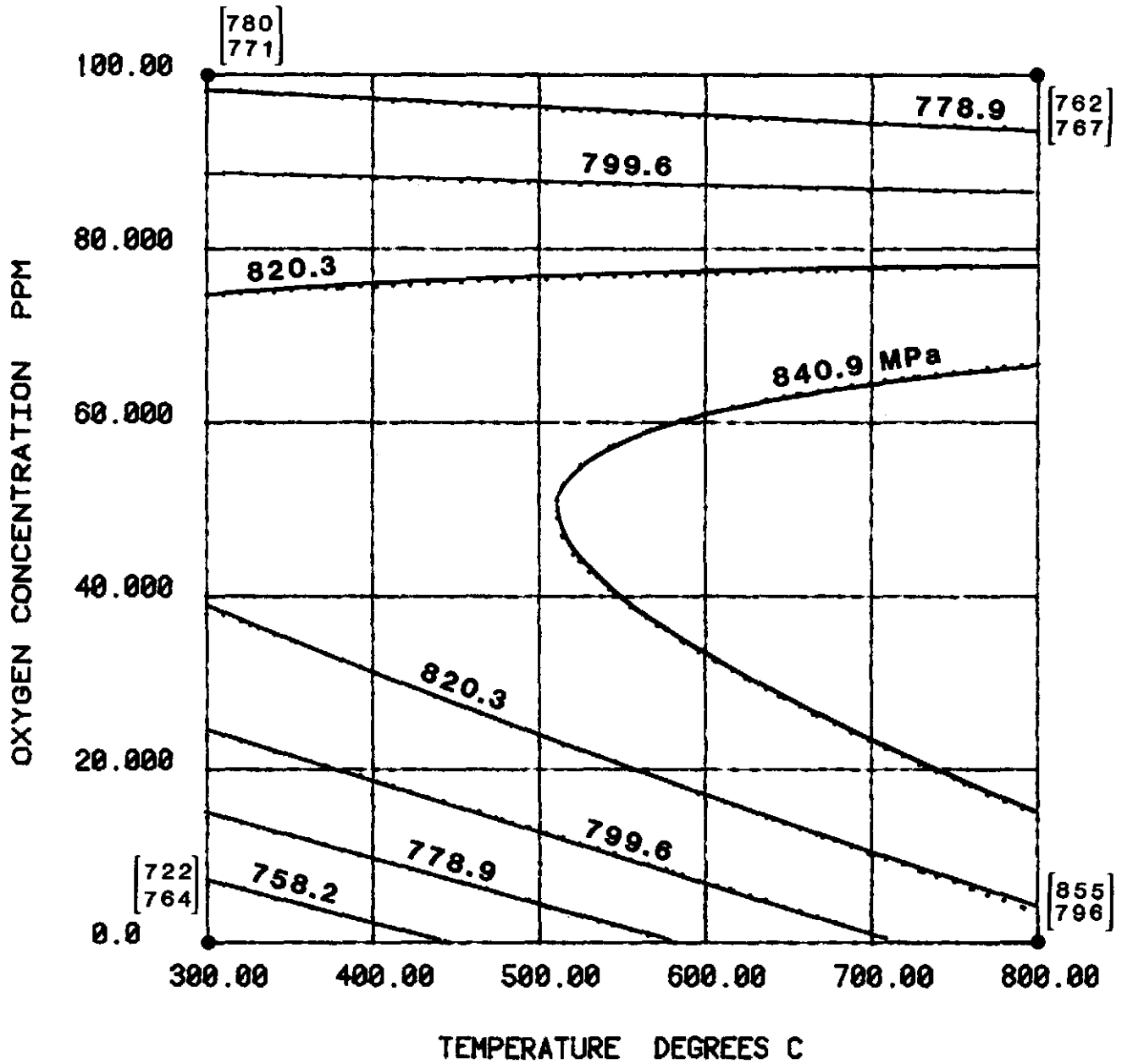
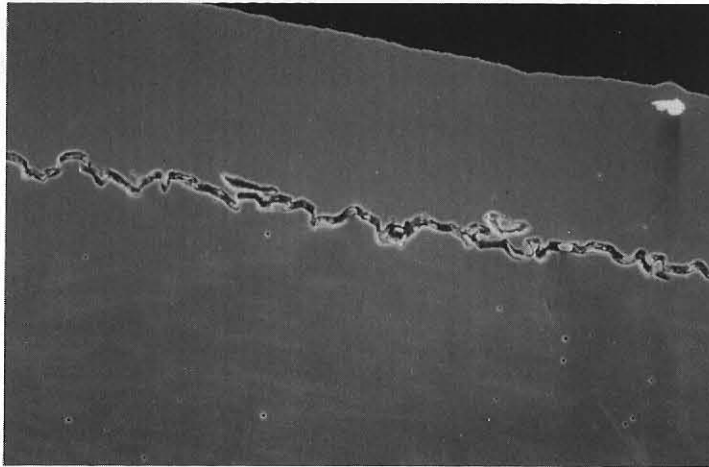
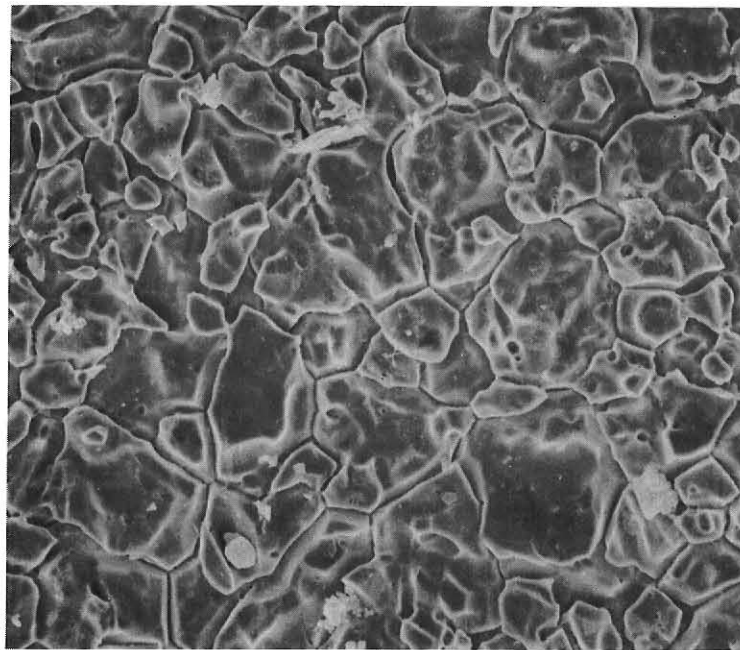


Fig. 50



a. SEM photomicrograph of inside surface.

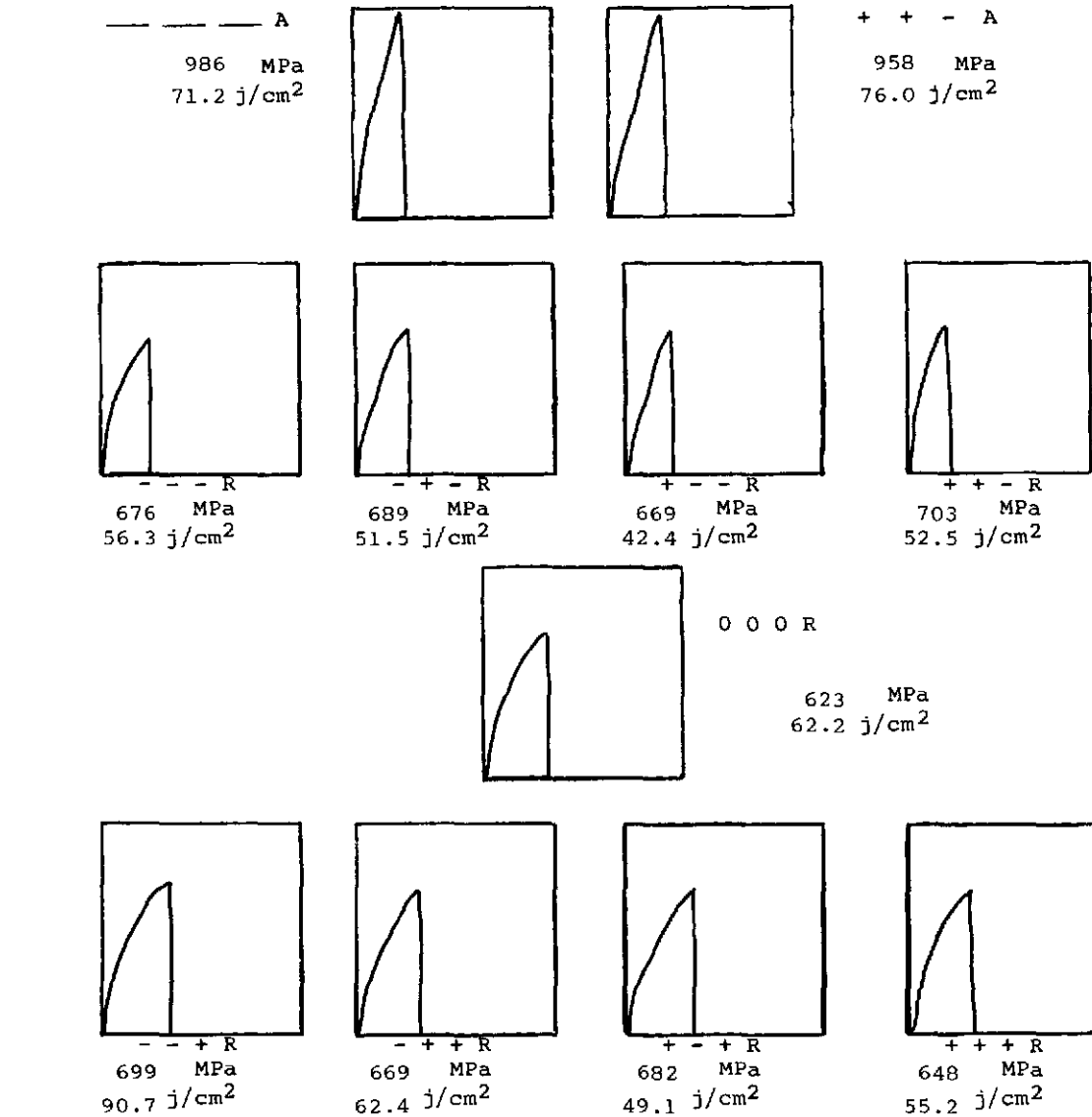


b. Photomicrograph of cross-section.

Inside surface and cross-section of a 316 stainless steel crucible after exposure to sodium.

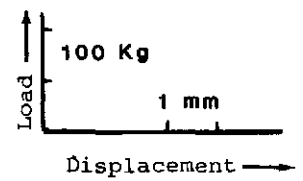
Fig. 51

Mechanical Properties of Notched Tensile Coupons as a Function of Exposure Conditions for Mo (source 1)



	TEMPERATURE	TIME	[O] POTENTIAL
+	800°C	130 Hrs.	100 ppm
0	550°C	70 Hrs.	50 ppm
-	300°C	10 Hrs.	2 ppm

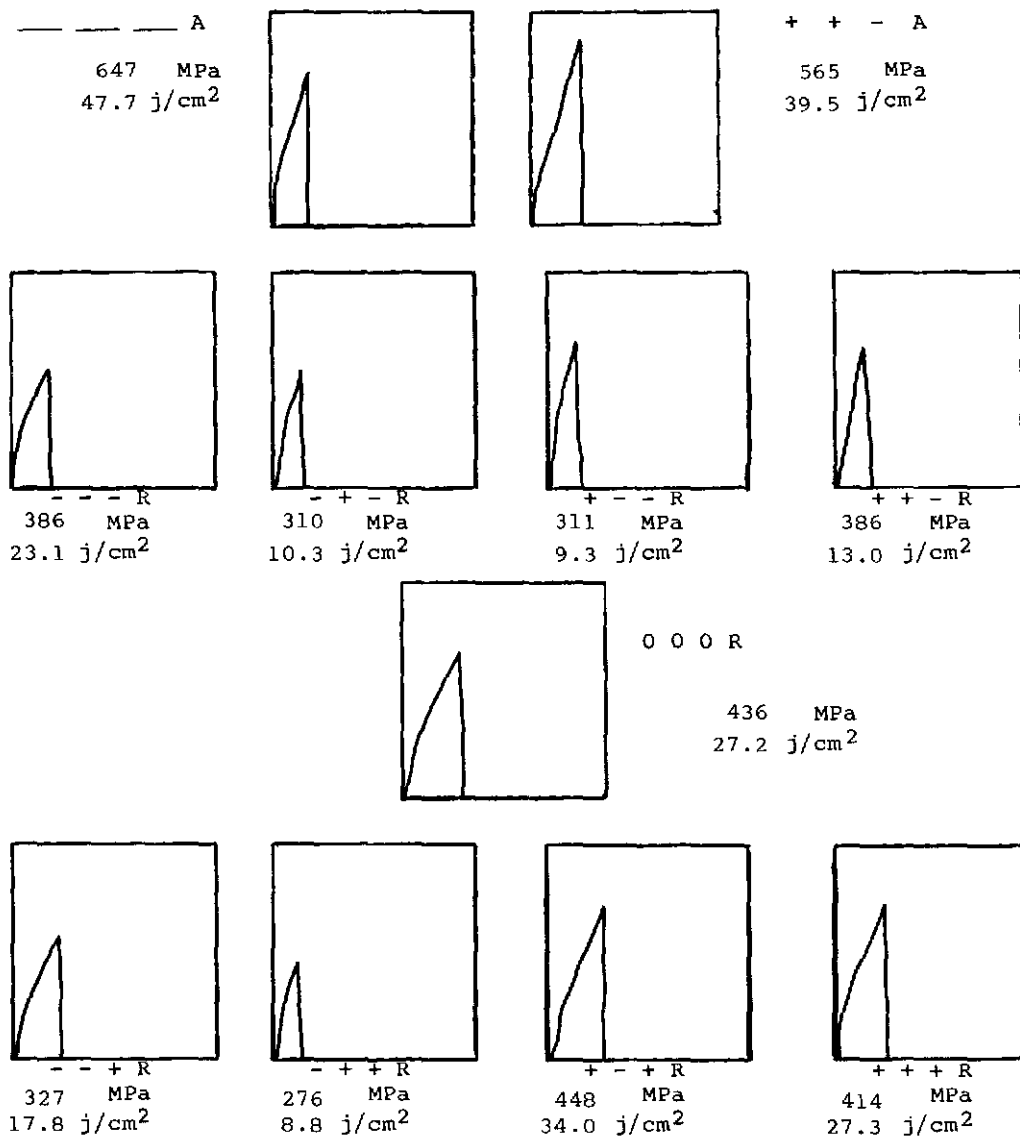
--- NO EXPOSURE
R RECRYSTALLIZED
A AS-RECEIVED
▽ SMOOTH BAR



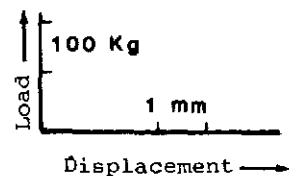
* Denotes single value.
All others are average of replicates.

Figure 52

Mechanical Properties of Notched Tensile Coupons as a Function of Exposure Conditions for Mo (source 2)



	TEMPERATURE	TIME	[O] POTENTIAL
+	800°C	130 Hrs.	100 ppm
0	550°C	70 Hrs.	50 ppm
-	300°C	10 Hrs.	2 ppm

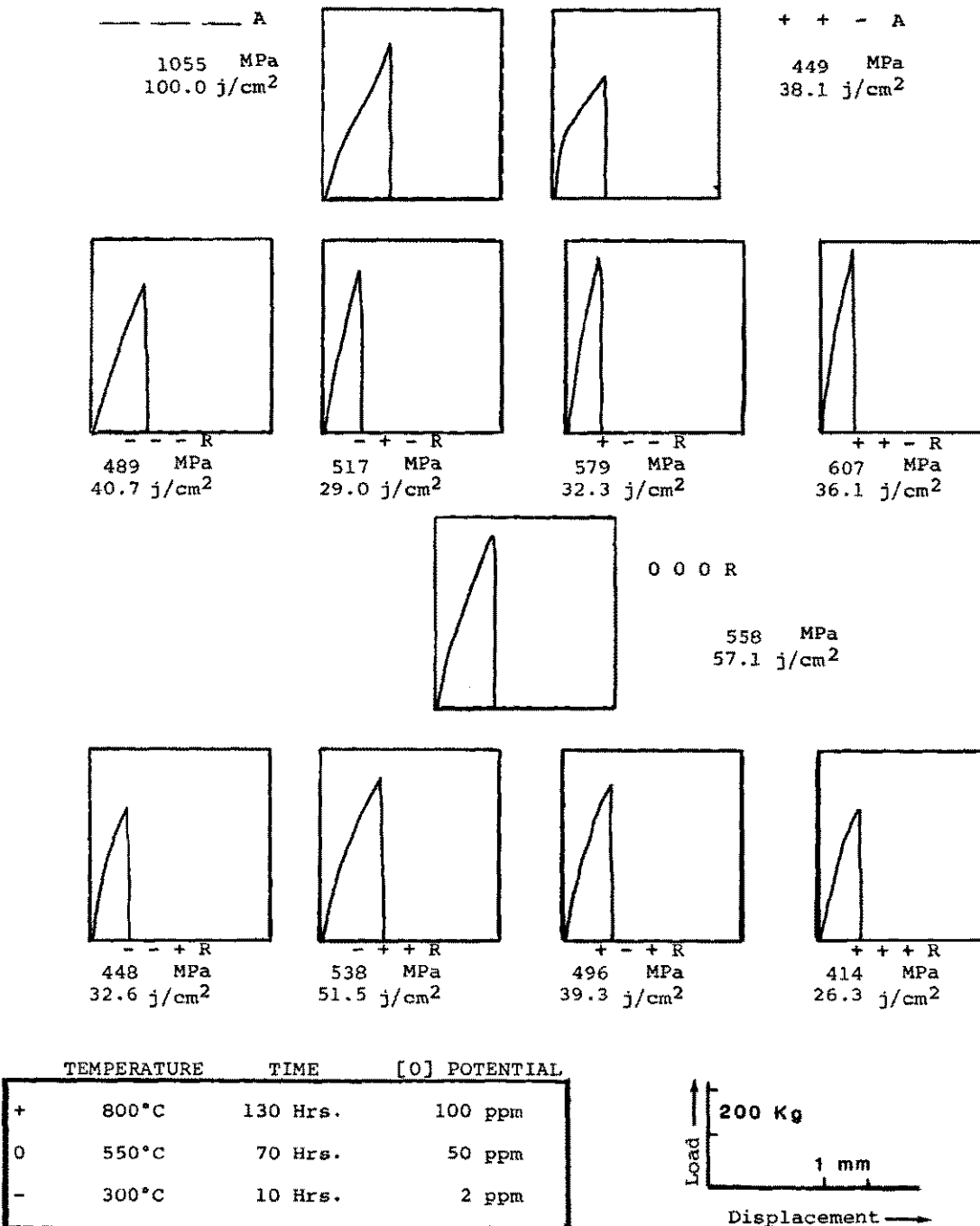


— NO EXPOSURE
 R RECRYSTALLIZED
 A AS-RECEIVED
 ∇ SMOOTH BAR

• Denotes single value.
 All others are average of replicates.

Figure 53

Mechanical Properties of Notched Tensile Coupons as a Function of Exposure Conditions for TZM (source 1)

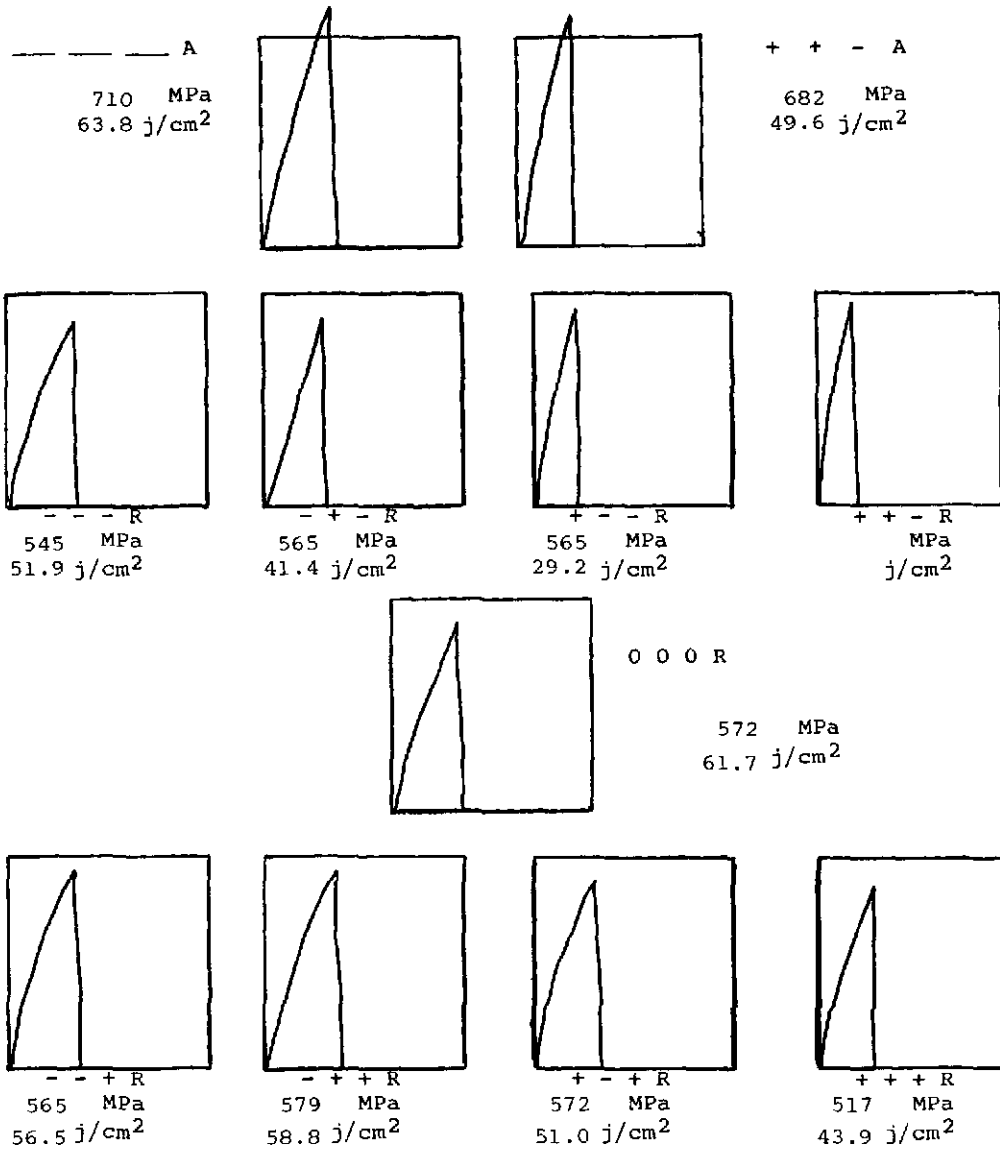


— NO EXPOSURE
 R RECRYSTALLIZED
 A AS-RECEIVED
 - SMOOTH BAR

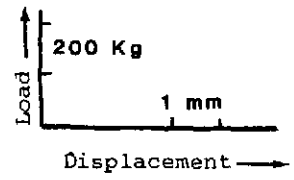
* Denotes single value.
 All others are average of replicates.

Figure 54

Mechanical Properties of Notched Tensile Coupons as a Function of Exposure Conditions for TZM (source 2)



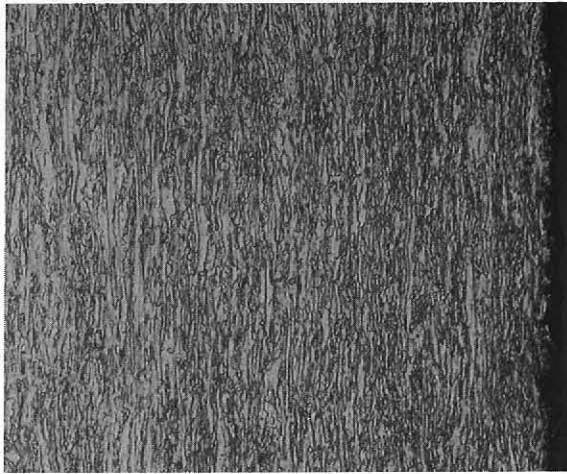
	TEMPERATURE	TIME	[O] POTENTIAL
+	800°C	130 Hrs.	100 ppm
O	550°C	70 Hrs.	50 ppm
-	300°C	10 Hrs.	2 ppm



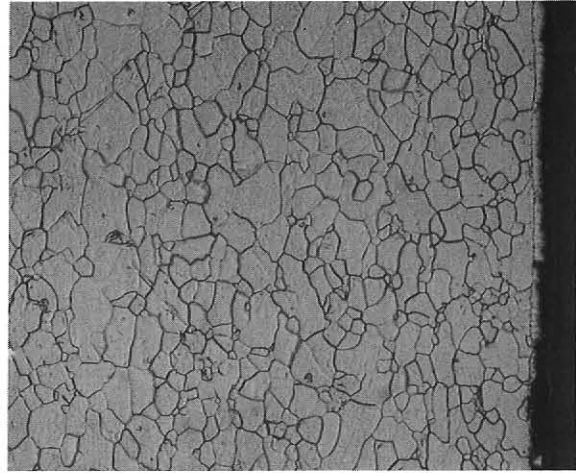
--- NO EXPOSURE
R RECRYSTALLIZED
A AS-RECEIVED
∇ SMOOTH BAR

* Denotes single value.
All others are average of replicates.

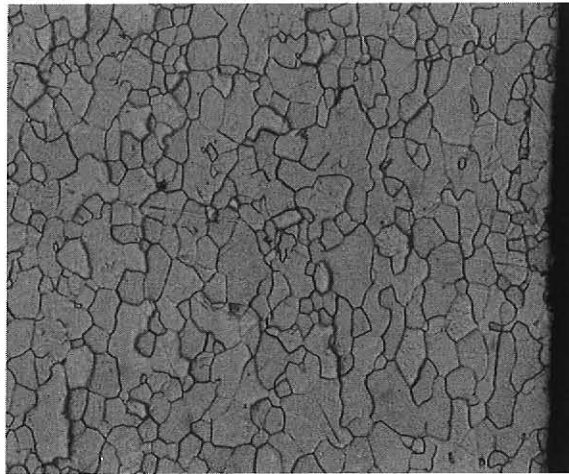
Figure 55



a. As-received




b. +++



c. ---

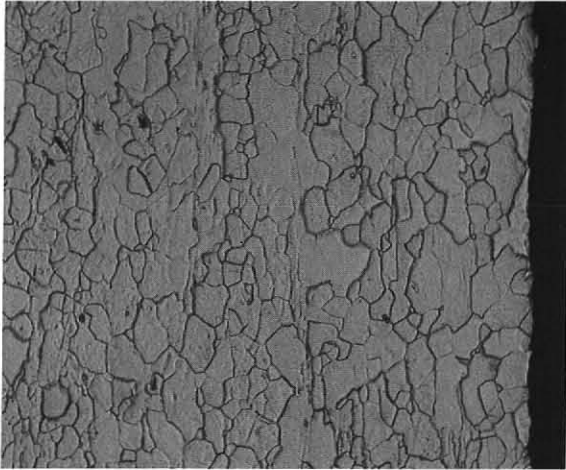
	TEMPERATURE	TIME	[O] POTENTIAL
+	800°C	130 Hrs.	100 ppm
0	550°C	70 Hrs.	50 ppm
-	300°C	10 Hrs.	2 ppm

— No EXPOSURE
 R RECRYSTALLIZED
 A AS-RECEIVED
 ▽ SMOOTH BAR

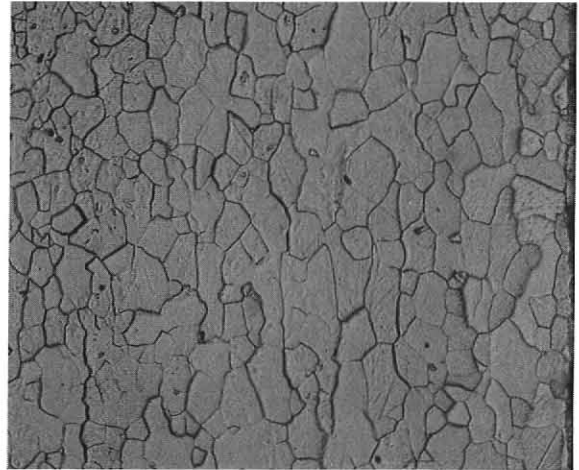
50 μM


METALLOGRAPHIC STRUCTURE OF SELECTED Mo (SOURCE 1) SPECIMENS.

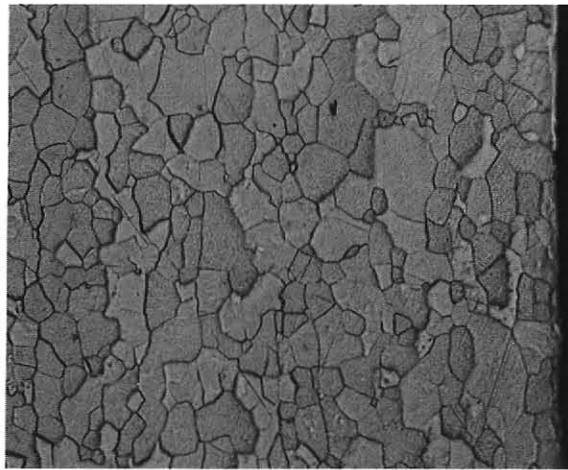
Fig. 56



a. As-received




b. +++



c. ---

	TEMPERATURE	TIME	[O] POTENTIAL
+	800°C	130 Hrs.	100 ppm
0	550°C	70 Hrs.	50 ppm
-	300°C	10 Hrs.	2 ppm

— NO EXPOSURE
 R RECRYSTALLIZED
 A AS-RECEIVED
 ▽ SMOOTH BAR

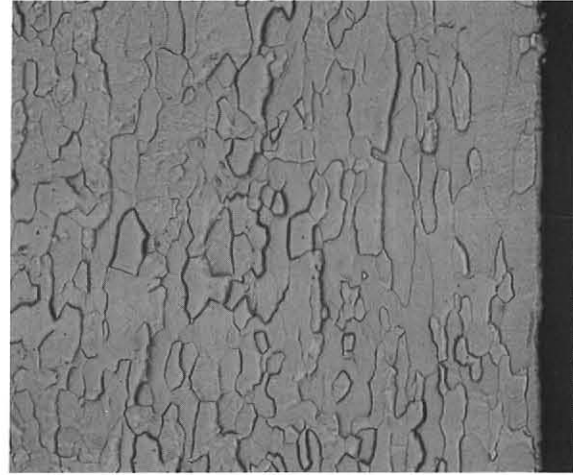
50 μM


Metallographic structure of selected Mo (Source 2) specimens.

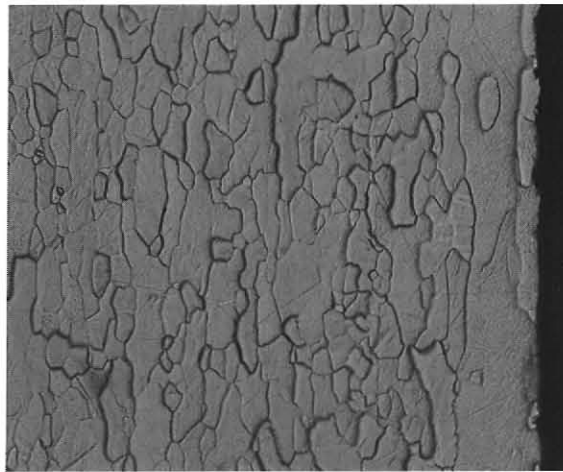
Fig. 57



a. As-received



b. +++

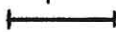


c. ---

	TEMPERATURE	TIME	[O] POTENTIAL
+	800°C	130 Hrs.	100 ppm
0	550°C	70 Hrs.	50 ppm
-	300°C	10 Hrs.	2 ppm

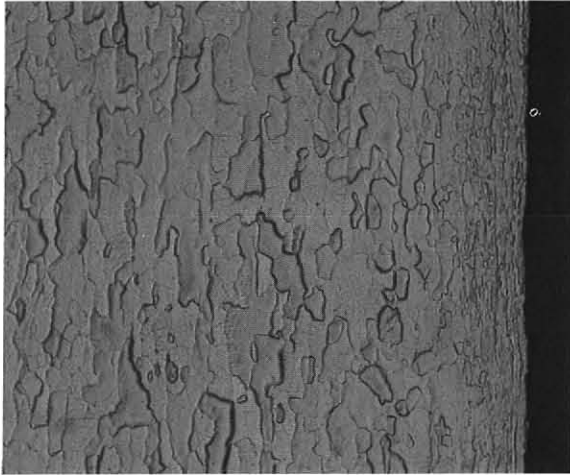
— NO EXPOSURE
 R RECRYSTALLIZED
 A AS-RECEIVED
 ▽ SMOOTH BAR

50 μM

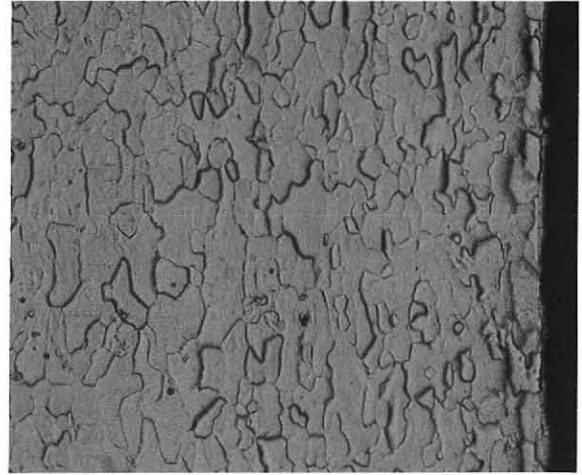


Metallographic structure of selected TZM (Source 1) specimens.

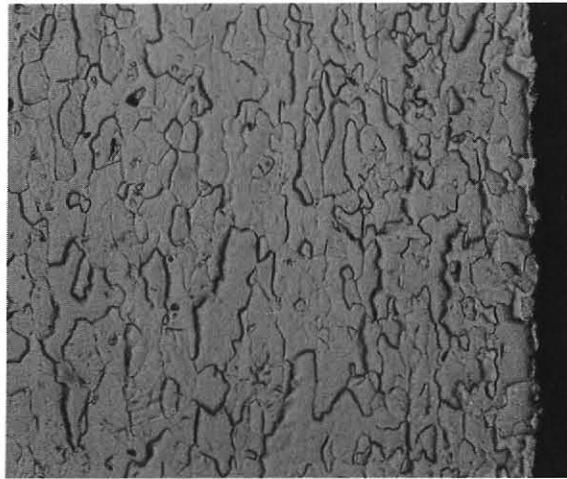
Fig. 58



a. As-received



b. +++



c. ---

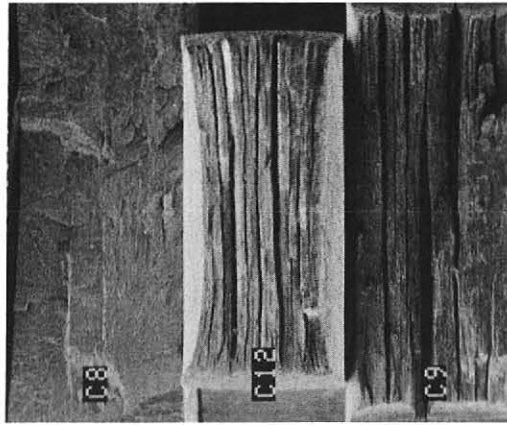
	TEMPERATURE	TIME	[O] POTENTIAL
+	800°C	130 Hrs.	100 ppm
0	550°C	70 Hrs.	50 ppm
-	300°C	10 Hrs.	2 ppm

— NO EXPOSURE
 R RECRYSTALLIZED
 A AS-RECEIVED
 ▽ SMOOTH BAR

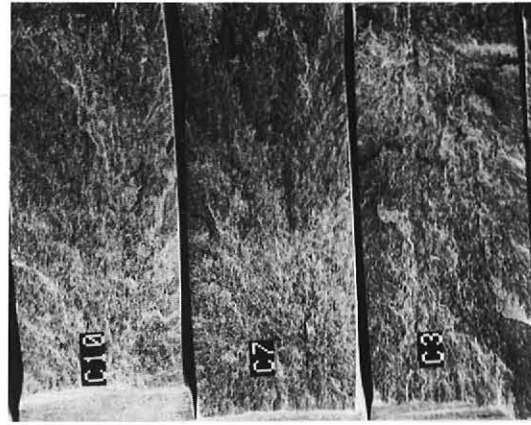
50 μM

Metallographic structure of TZM (Source 2) specimens.

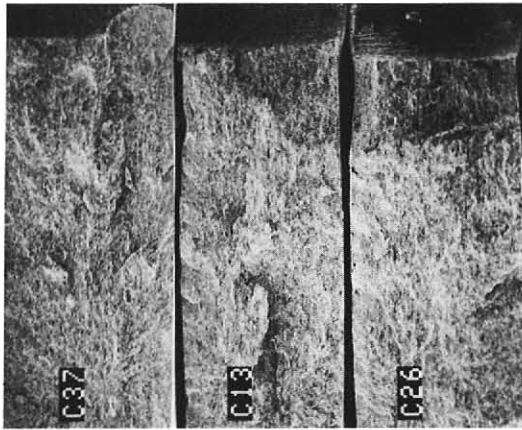
Fig. 59



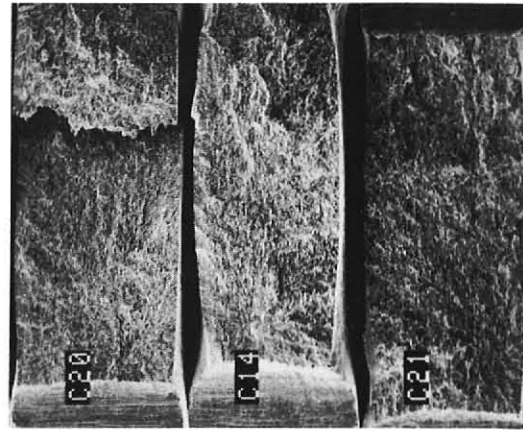
C8	—	—	—	A
C12	—	—	—	A▽
C9	+	+	-	A



C10	+	+	-	R
C7	+	-	-	R
C3	-	+	-	R



C37	-	-	-	R
C13	+	+	+	R
C26	+	-	+	R



C20	-	+	+	R
C14	-	-	+	R
C21	0	0	0	R

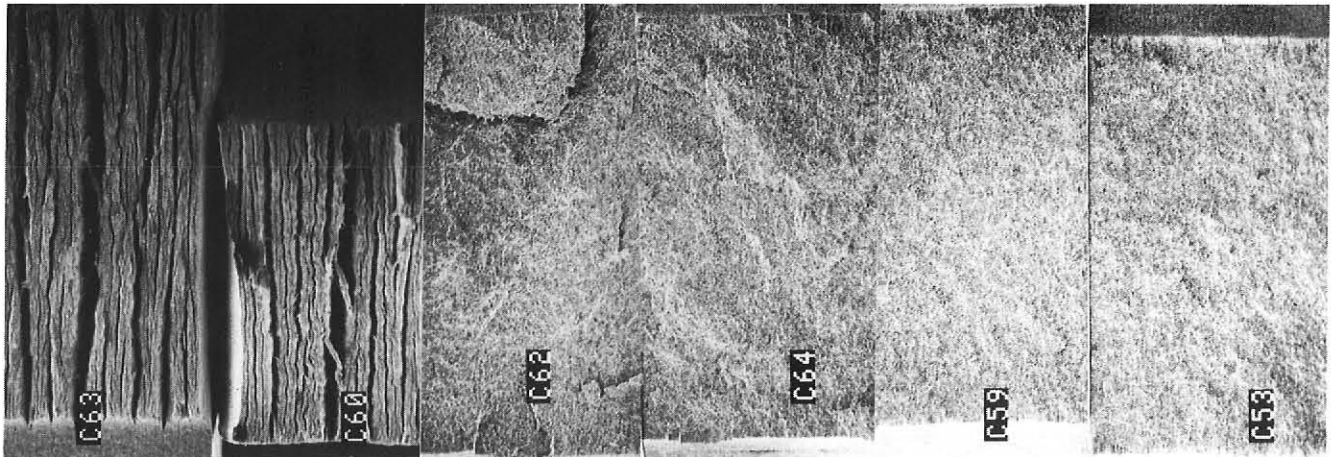
Mo (SOURCE 1)

	TEMPERATURE	TIME	[O] POTENTIAL
+	800°C	130 Hrs.	100 PPM
0	550°C	70 Hrs.	50 PPM
-	300°C	10 Hrs.	2 PPM

— NO EXPOSURE
 R RECRYSTALLIZED
 A AS-RECEIVED
 ▽ SMOOTH BAR

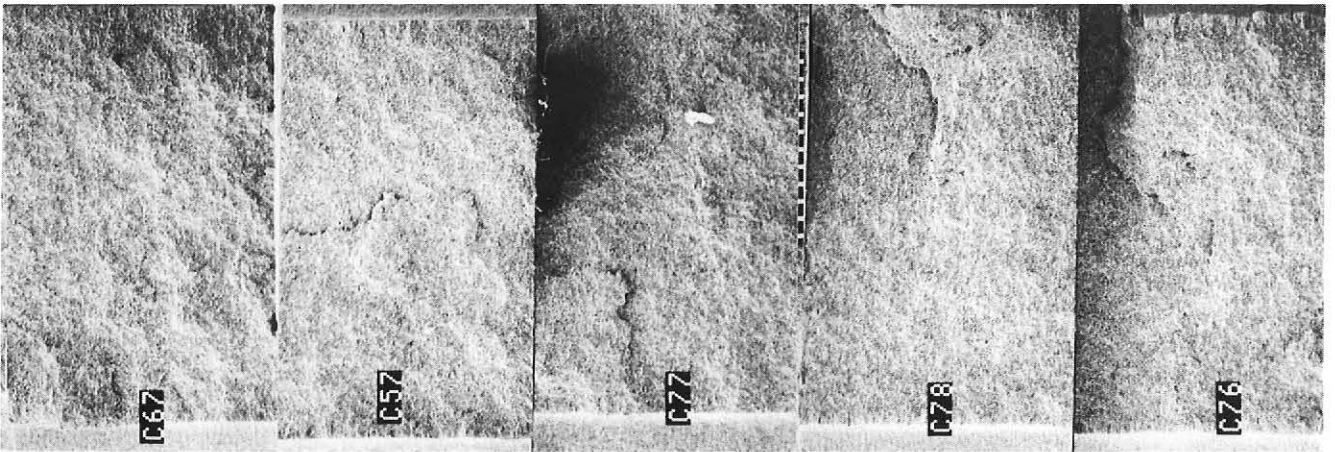
1500 μm

Fig. 60



C63 — — — A
 C60 — — — A▽
 C62 + + - A

C64 + + - R
 C59 + - - R
 C53 - + - R



C67 - - - R
 C57 + + + R
 C77 + - + R

C78 - + + R
 C76 - - + R

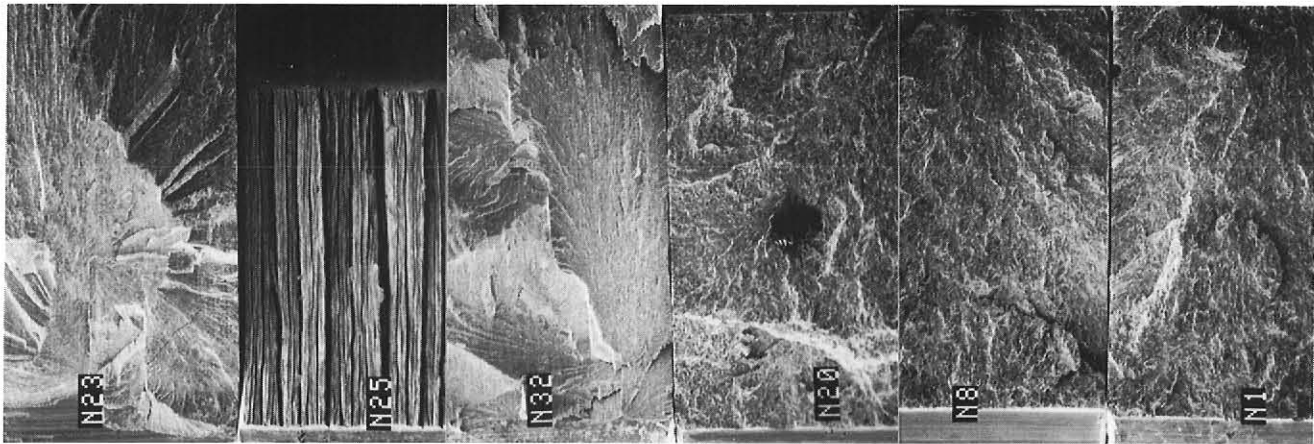
Mo (SOURCE 2)

	TEMPERATURE	TIME	[O] POTENTIAL
+	800°C	130 Hrs.	100 PPM
0	550°C	70 Hrs.	50 PPM
-	300°C	10 Hrs.	2 PPM

— NO EXPOSURE
 R RECRYSTALLIZED
 A AS-RECEIVED
 ▽ SMOOTH BAR

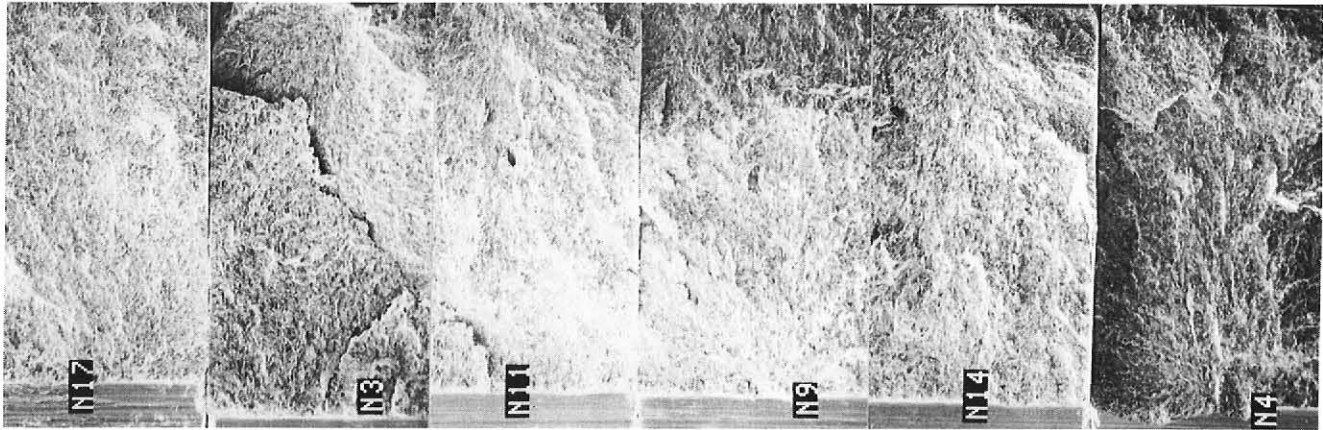
1500 μm

Fig. 61



N23 — — — A
 N25 — — — A▽
 N32 + + - A

N20 + + - A
 N8 + - - R
 N1 - + - R



N17 - - - R
 N3 + + + R
 N11 + - + R

N9 - + + R
 N14 - - + R
 N4 0 0 0 R

TZM (SOURCE 1)

	TEMPERATURE	TIME	[O] POTENTIAL
+	800°C	130 Hrs.	100 PPM
0	550°C	70 Hrs.	50 PPM
-	300°C	10 Hrs.	2 PPM

— NO EXPOSURE
 R RECRYSTALLIZED
 A AS-RECEIVED
 ▽ SMOOTH BAR

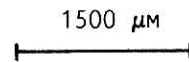
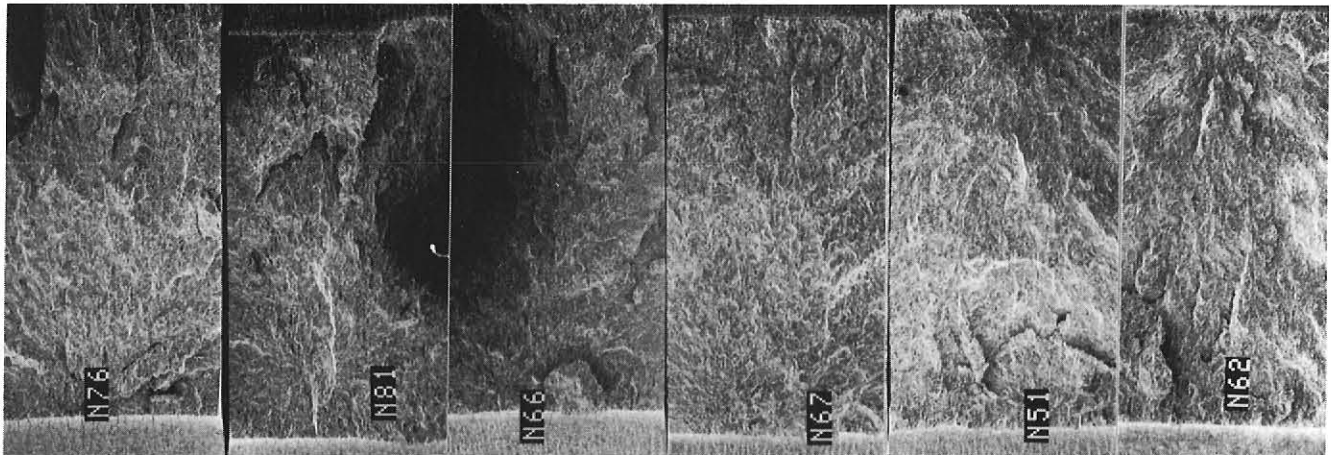
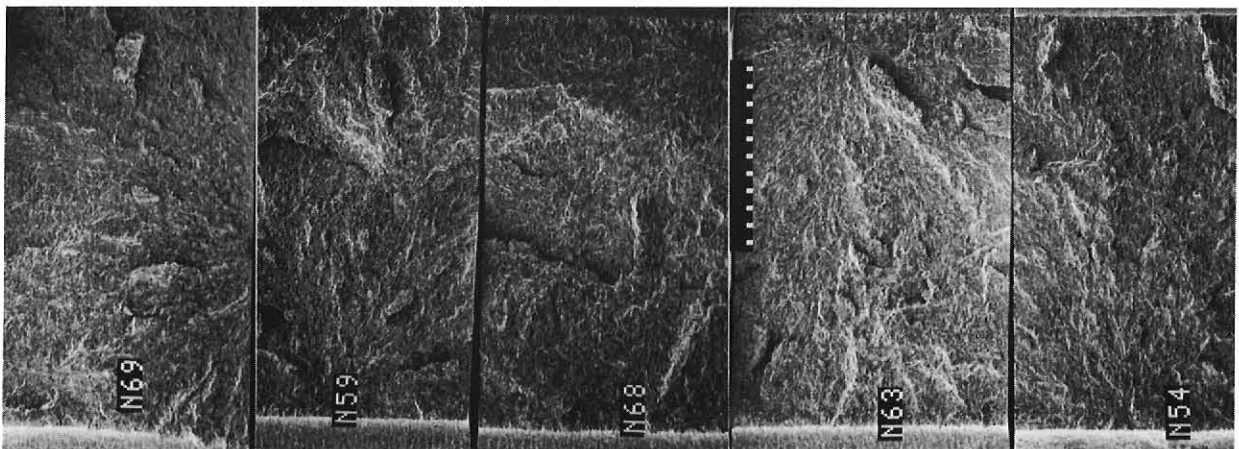


Fig. 62



N76	—	—	—	A	N67	+	-	-	R
N81	+	+	-	A	N51	-	+	-	R
N66	+	+	-	R	N62	-	-	-	R



N69	+	+	+	R	N63	-	-	+	R
N59	+	-	+	R	N54	0	0	0	R
N68	-	+	+	R					

TZM (SOURCE 2)

	TEMPERATURE	TIME	[O] POTENTIAL
+	800°C	130 Hrs.	100 PPM
0	550°C	70 Hrs.	50 PPM
-	300°C	10 Hrs.	2 PPM

— No EXPSOURE
 R RECRYSTALLIZED
 A AS-RECEIVED
 ▽ SMOOTH BAR

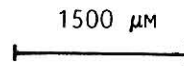
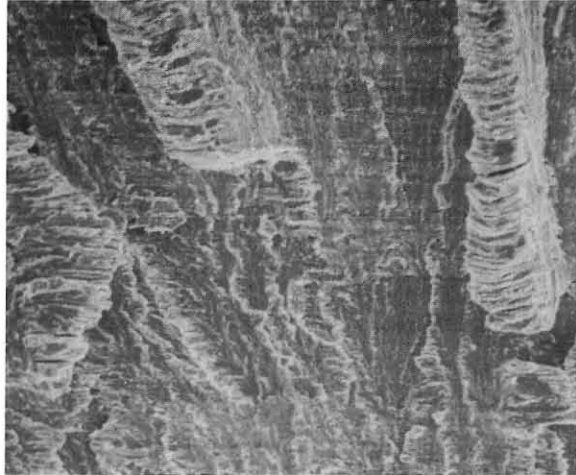


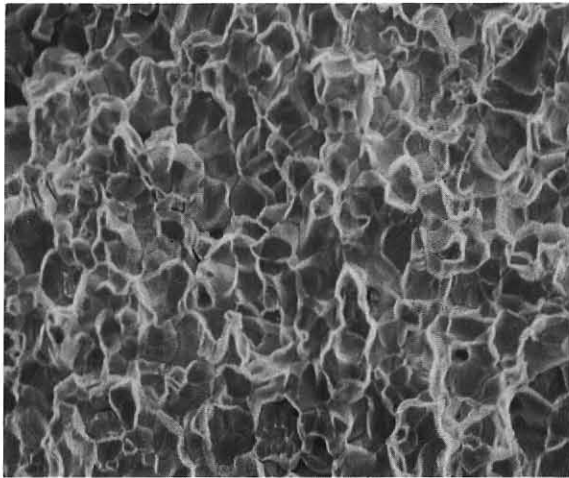
Fig. 63



a. Lammelar mode.



b. Quaisi cleavage.



c. Intergranular.

	TEMPERATURE	TIME	[O] POTENTIAL
+	800°C	130 Hrs.	100 ppm
0	550°C	70 Hrs.	50 ppm
-	300°C	10 Hrs.	2 ppm

— NO EXPOSURE
 R RECRYSTALLIZED
 A AS-RECEIVED
 ∇ SMOOTH BAR

50 μM

Typical high magnification fractograph for Mo and TZM alloy.

Fig. 64

WEIGHT CHANGE OF MO (Source 2)
 AS A FUNCTION OF
 OXYGEN CONCENTRATION AND TEMPERATURE
 IN MOLTEN SODIUM (TIME=10 HRS)

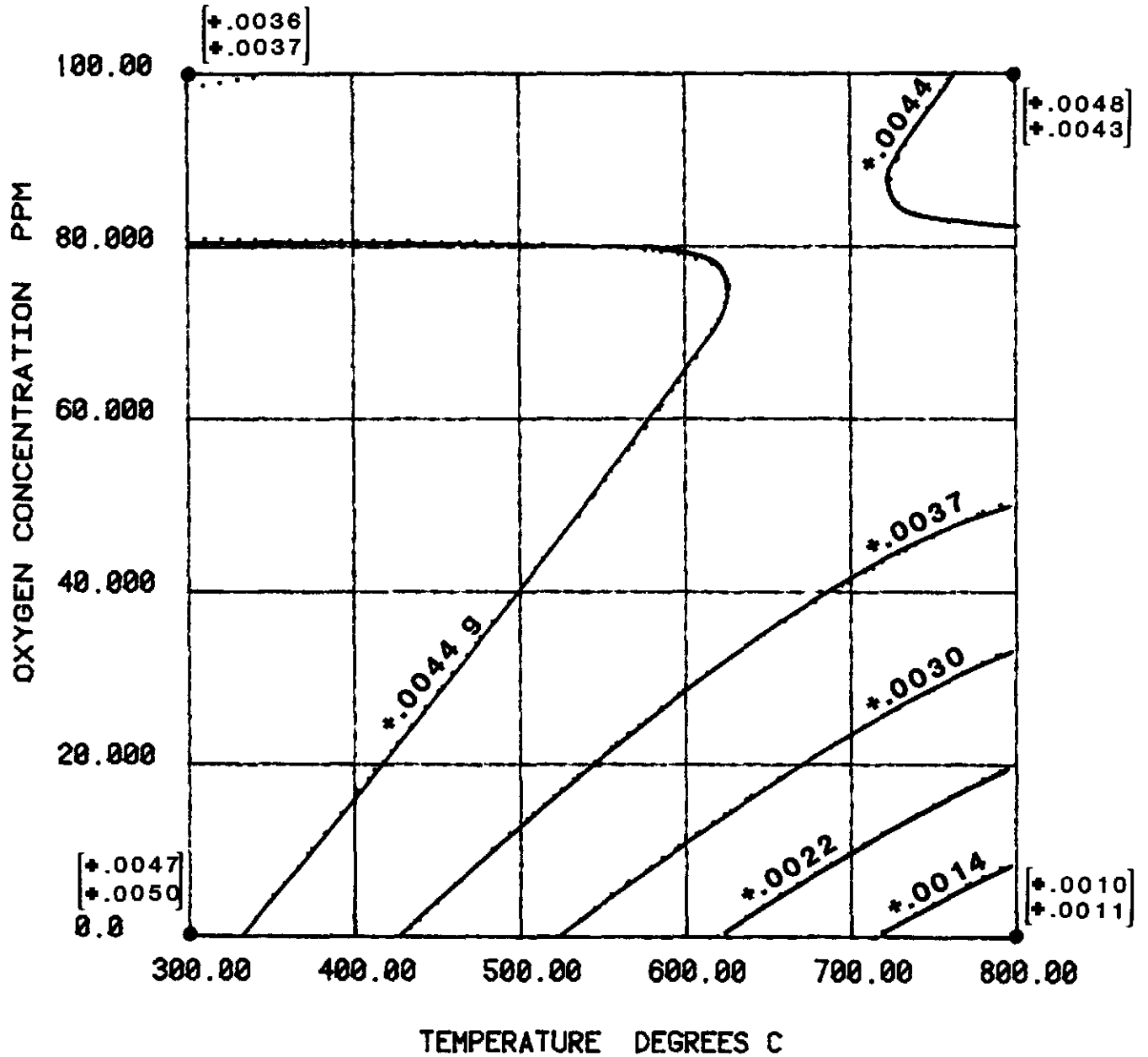


Fig. 65

WEIGHT CHANGE OF MO (Source 2)
 AS A FUNCTION OF
 OXYGEN CONCENTRATION AND TEMPERATURE
 IN MOLTEN SODIUM (TIME=70 HRS)

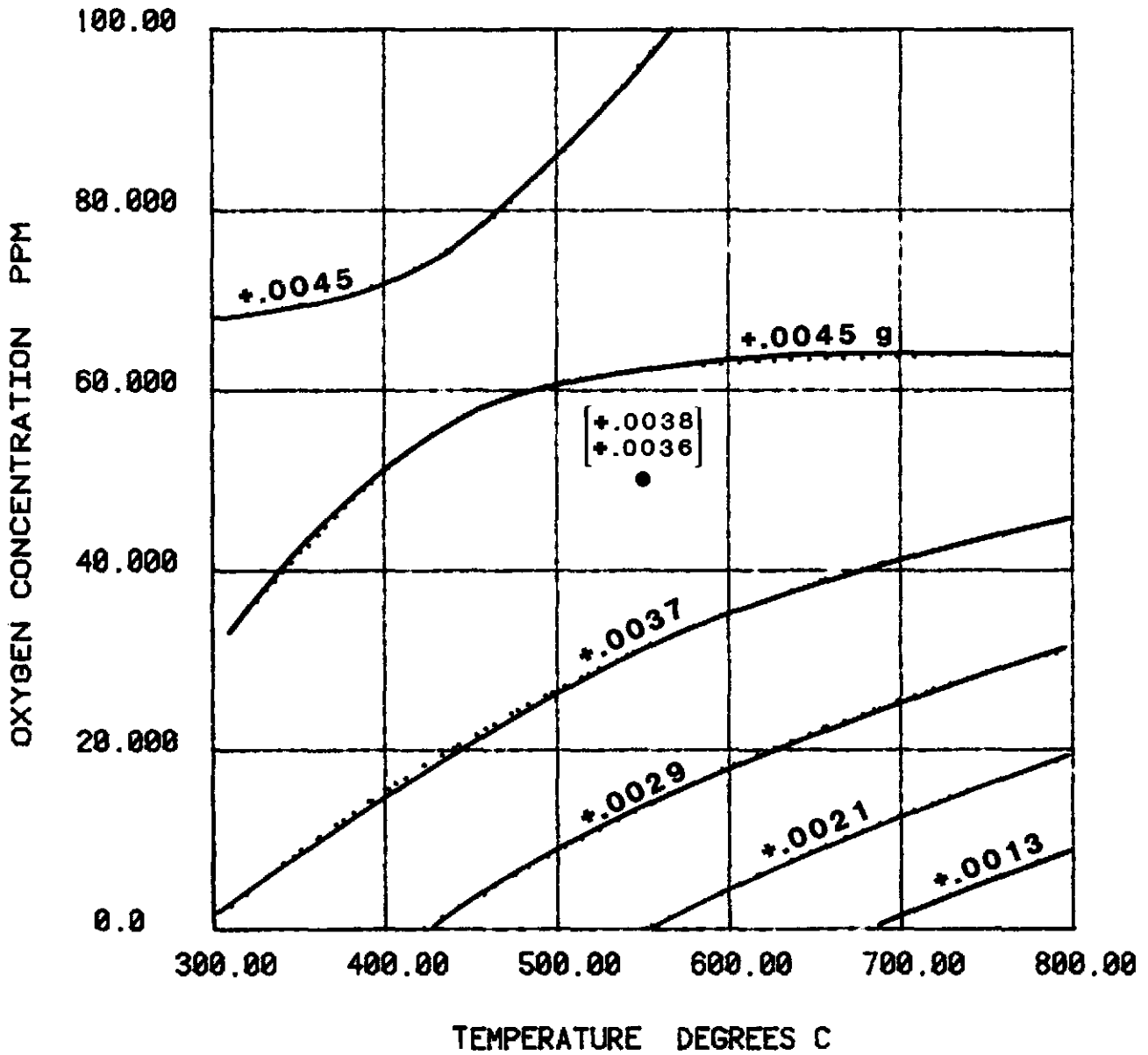


Fig. 66

WEIGHT CHANGE OF MO (Source 2)
 AS A FUNCTION OF
 OXYGEN CONCENTRATION AND TEMPERATURE
 IN MOLTEN SODIUM (TIME=130 HRS)

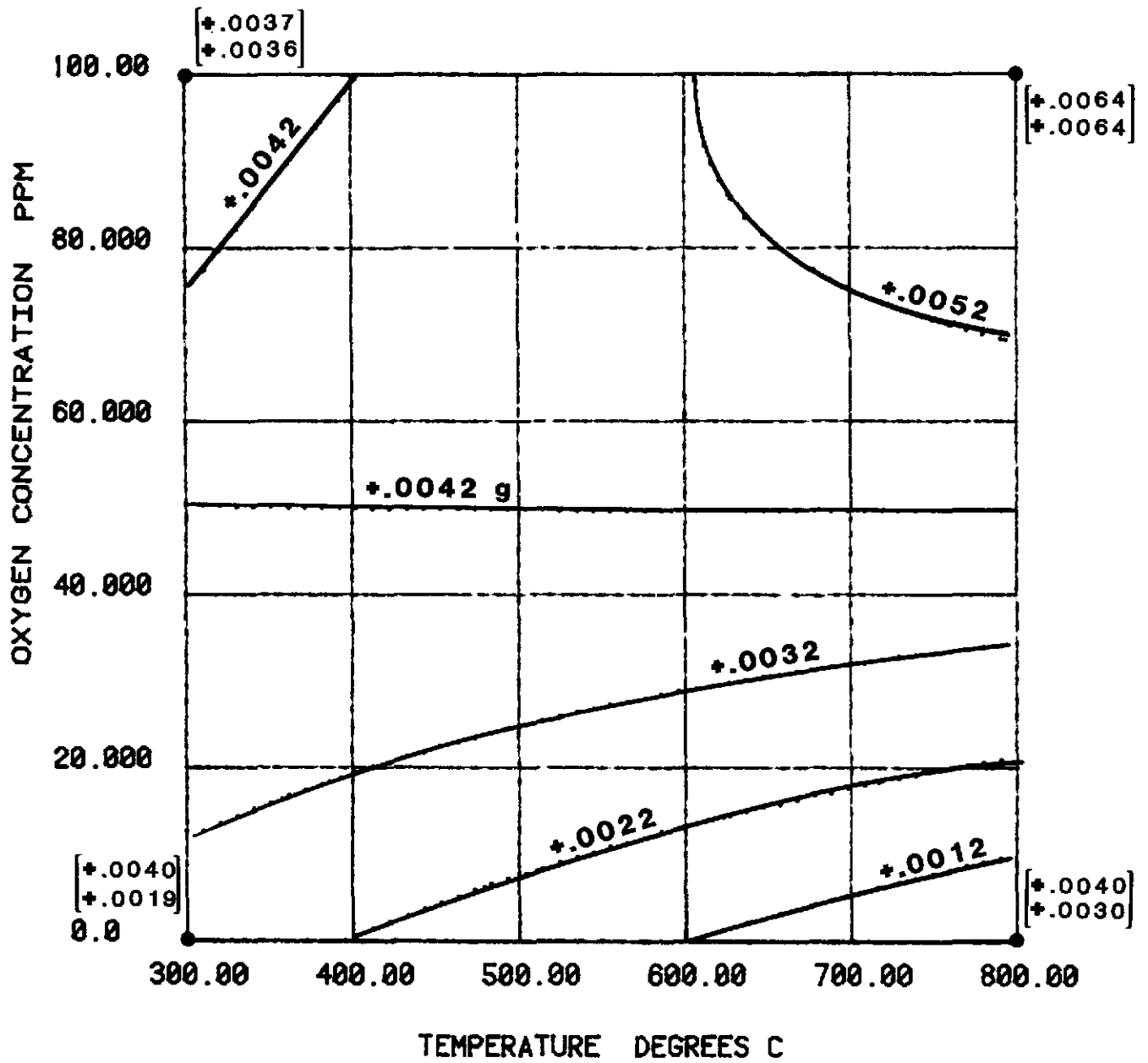


Fig. 67

WEIGHT CHANGE OF TZM ALLOY (Source 2)
 AS A FUNCTION OF
 OXYGEN CONCENTRATION AND TEMPERATURE
 IN MOLTEN SODIUM (TIME=10 HRS)

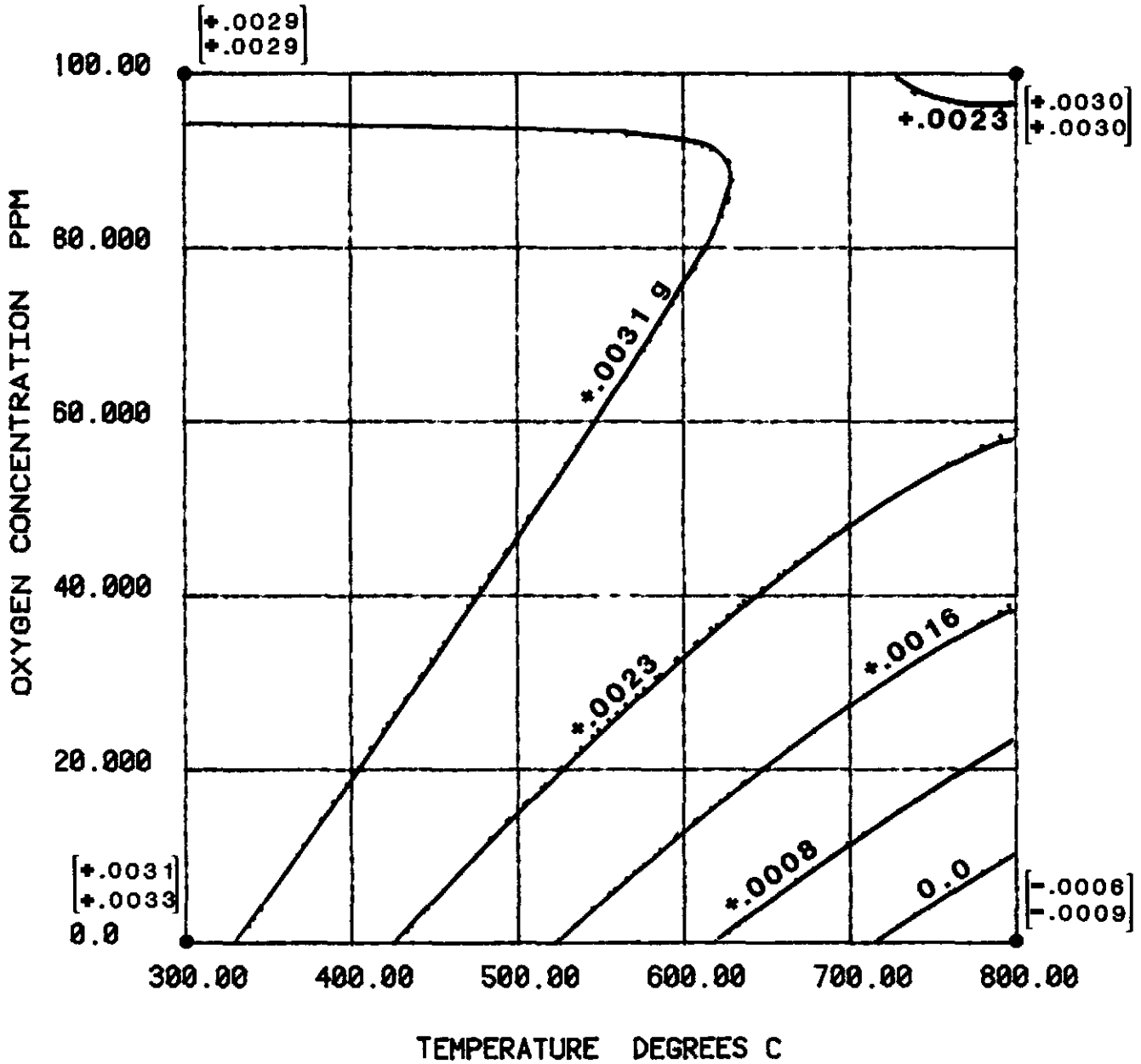


Fig. 68

WEIGHT CHANGE OF TZM ALLOY (Source 2)
 AS A FUNCTION OF
 OXYGEN CONCENTRATION AND TEMPERATURE
 IN MOLTEN SODIUM (TIME=70 HRS)

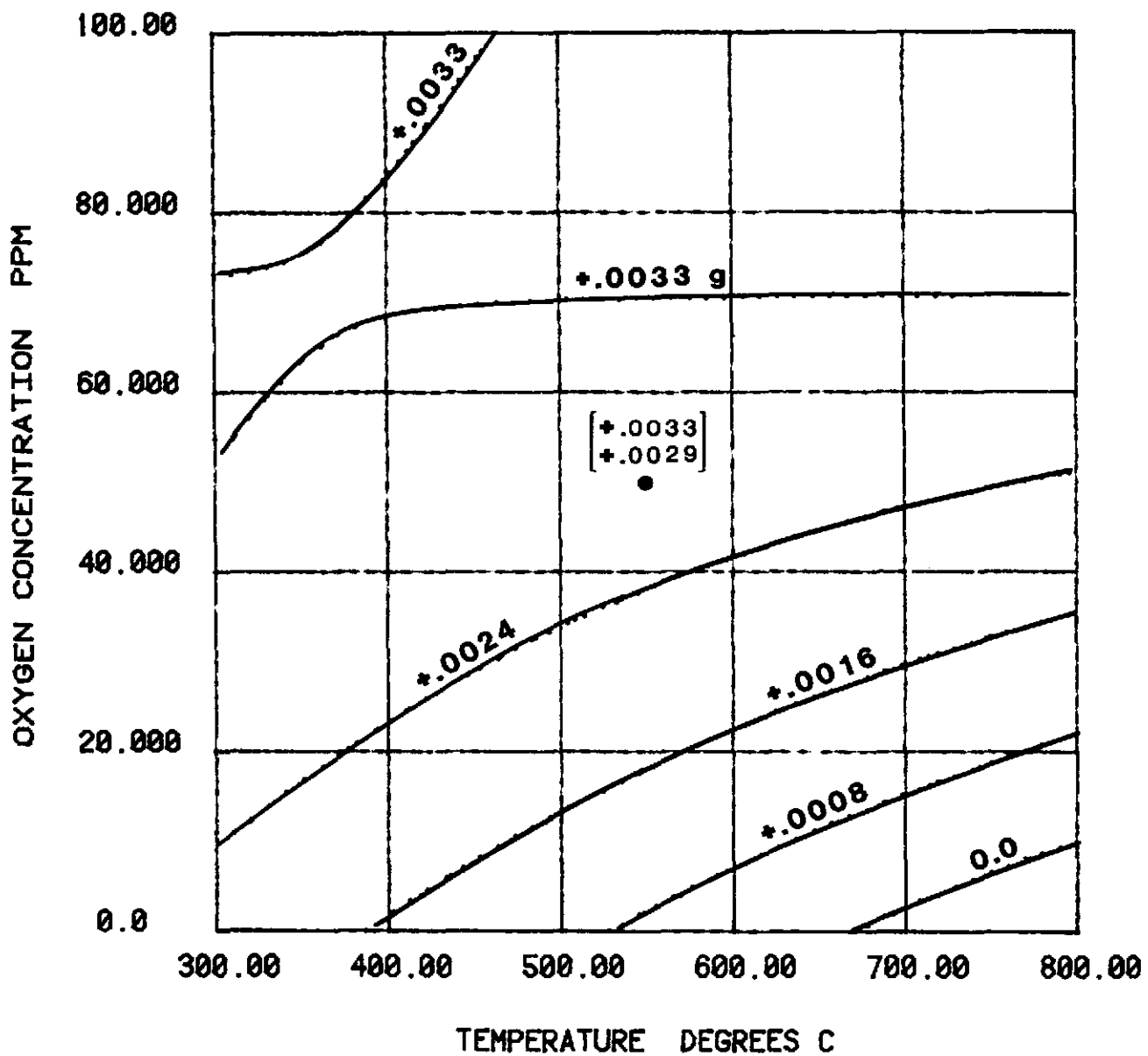


Fig. 69

WEIGHT CHANGE OF TZM ALLOY (Source 2)
 AS A FUNCTION OF
 OXYGEN CONCENTRATION AND TEMPERATURE
 IN MOLTEN SODIUM (TIME=130 HRS)

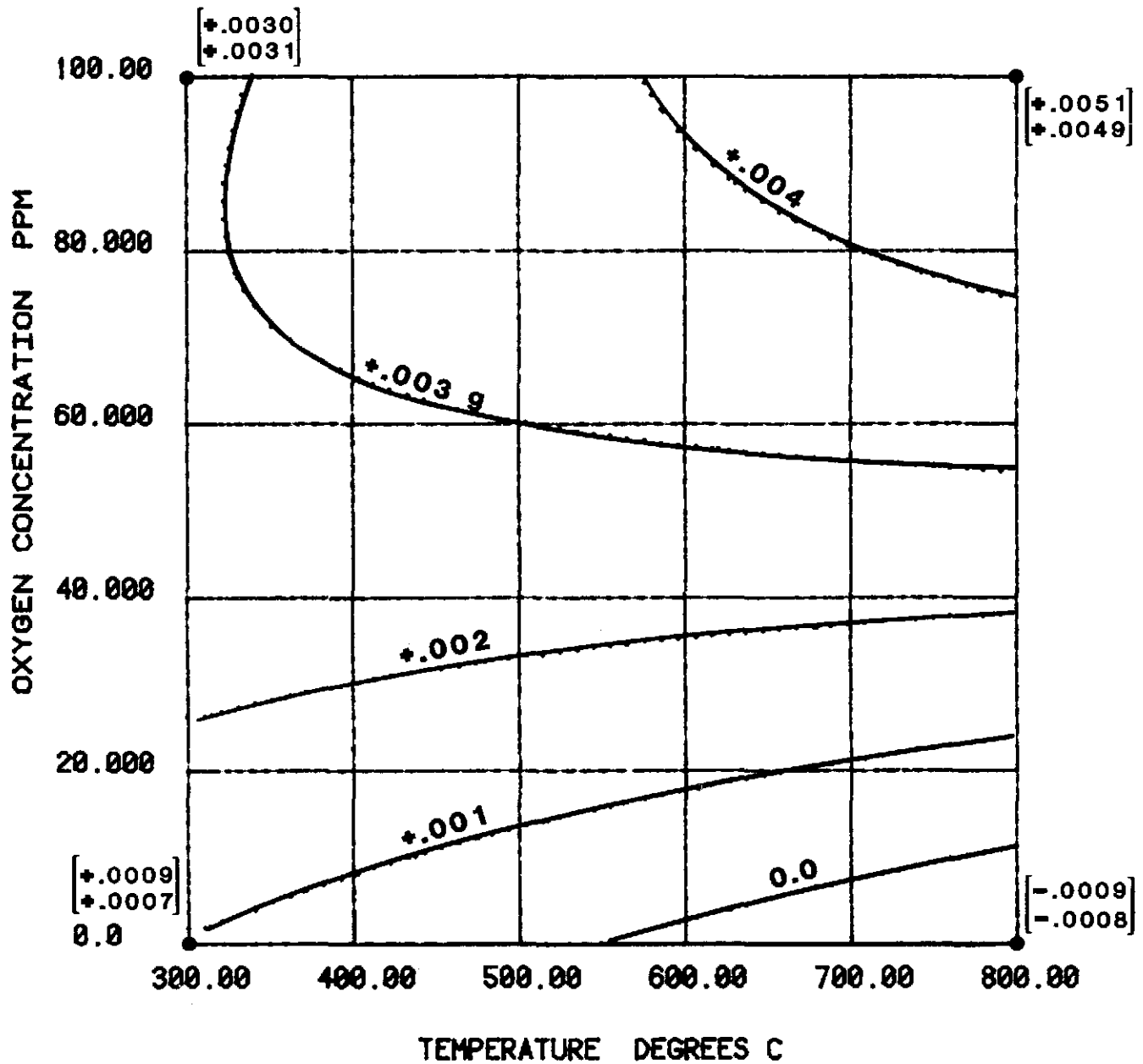
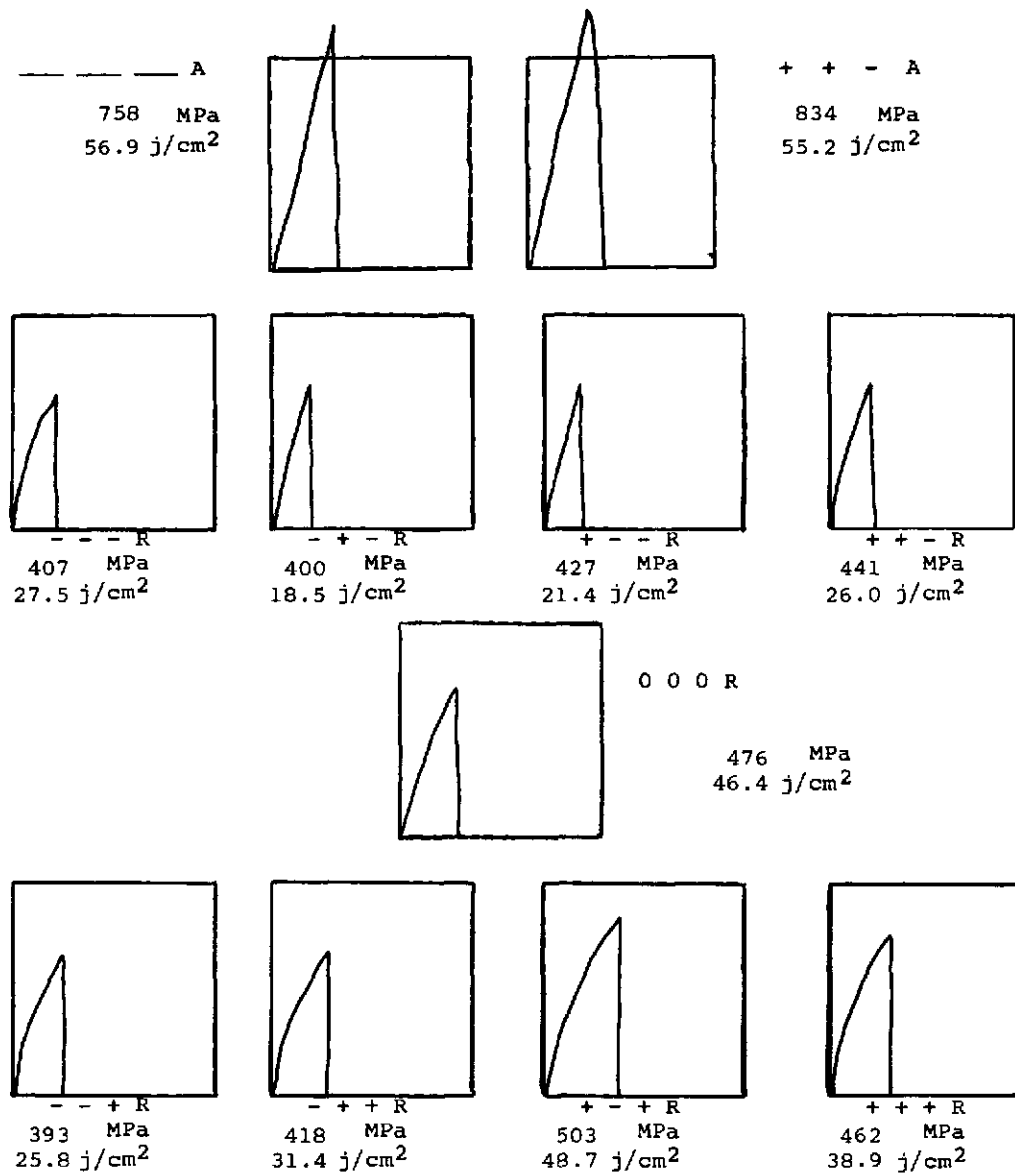
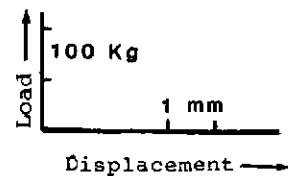


Fig. 70

Mechanical Properties of Notched Tensile Coupons as a Function of Exposure Conditions for Mo - 13 Re



	TEMPERATURE	TIME	[O] POTENTIAL
+	800°C	130 Hrs.	100 ppm
0	550°C	70 Hrs.	50 ppm
-	300°C	10 Hrs.	2 ppm



• Denotes single value.
All others are average of replicates.

--- NO EXPOSURE
R RECRYSTALLIZED
A AS-RECEIVED
▽ SMOOTH BAR

Figure 71

Mechanical Properties of Notched Tensile Coupons as a Function of Exposure Conditions for Mo - 26 Re (source 1)

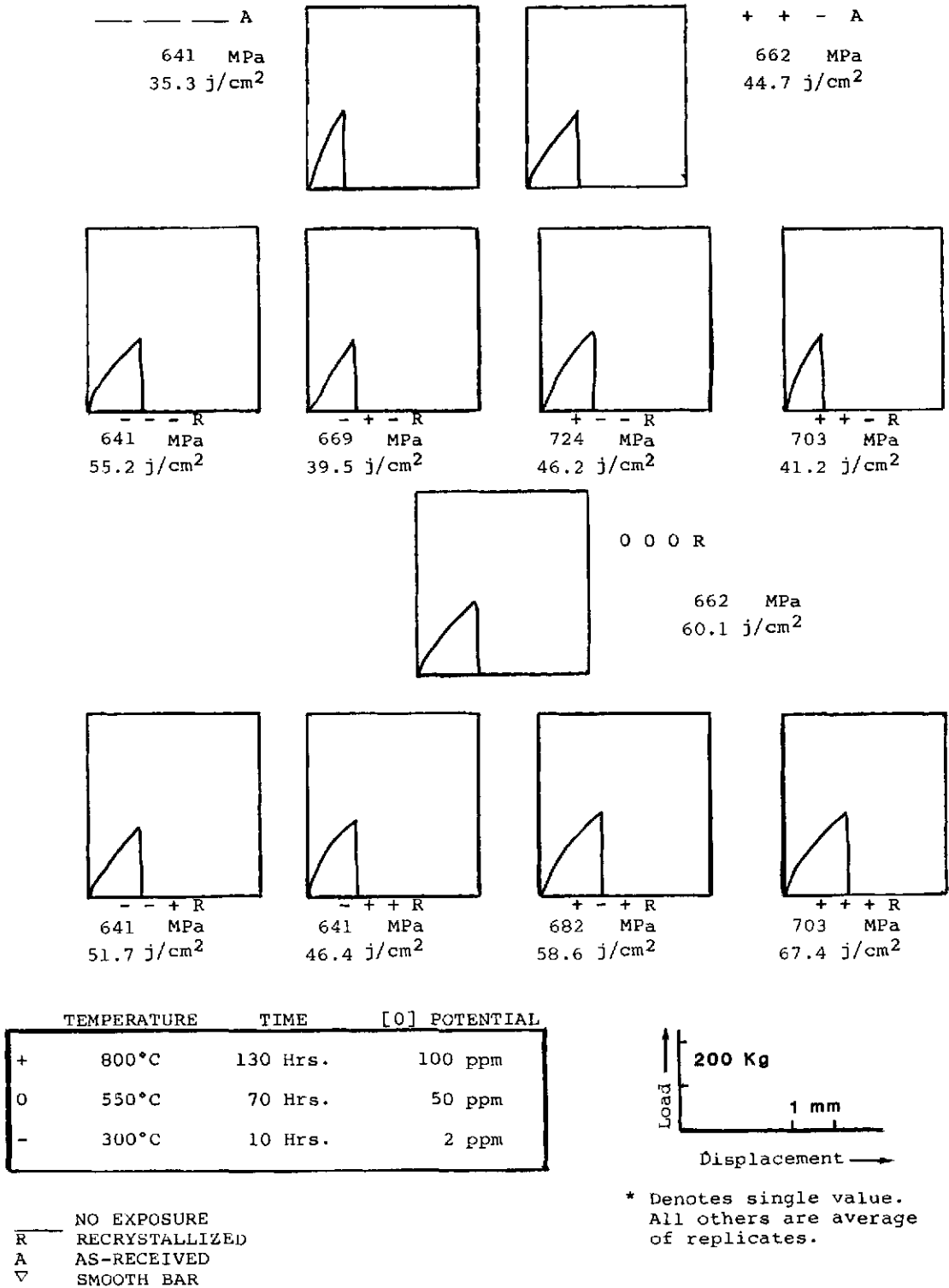
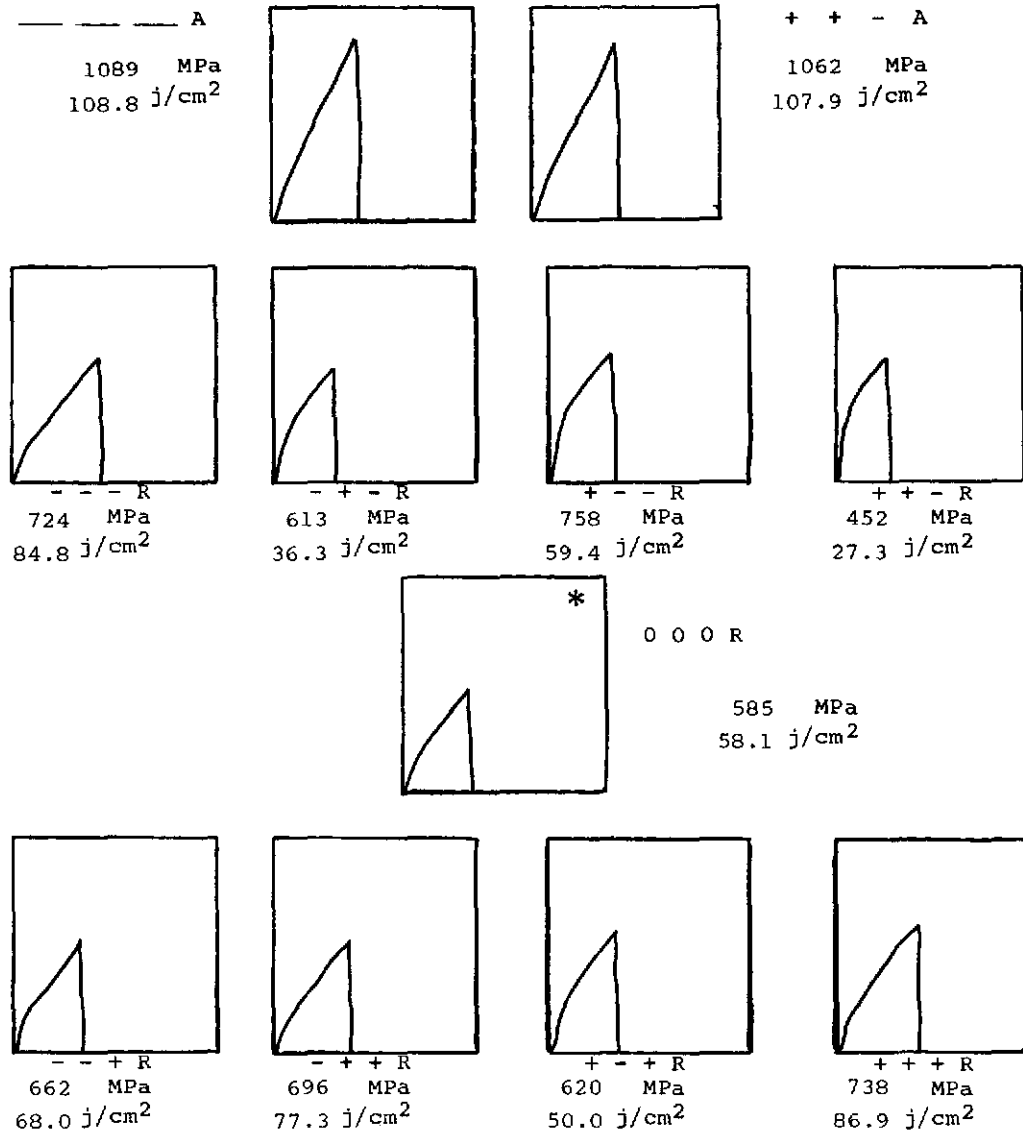
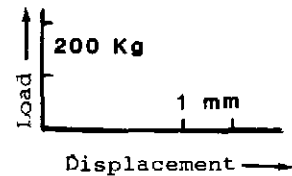


Figure 72

Mechanical Properties of Notched Tensile Coupons as a Function of Exposure Conditions for Mo - 26 Re (source 2)



	TEMPERATURE	TIME	[O] POTENTIAL
+	800°C	130 Hrs.	100 ppm
0	550°C	70 Hrs.	50 ppm
-	300°C	10 Hrs.	2 ppm

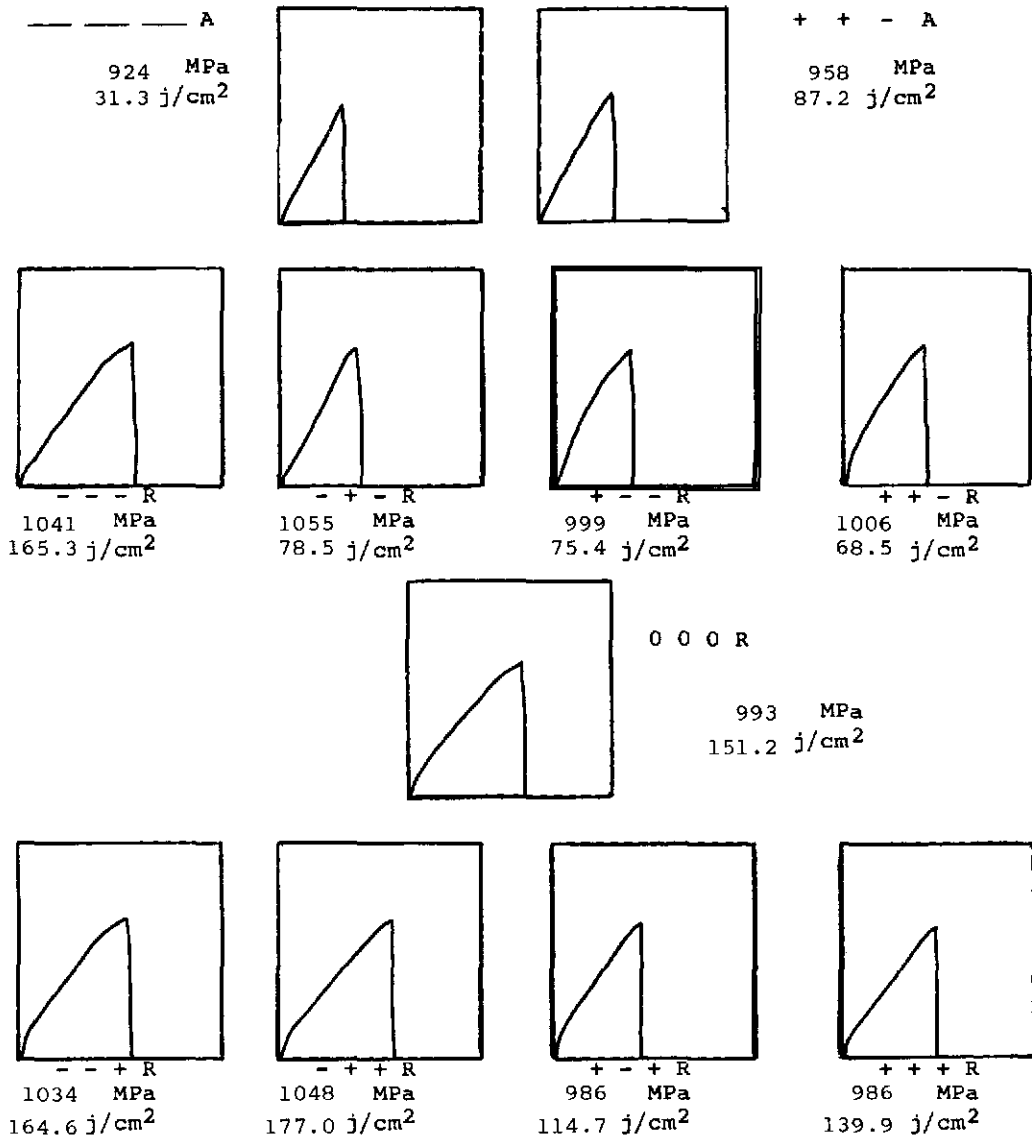


— NO EXPOSURE
 R RECRYSTALLIZED
 A AS-RECEIVED
 ∇ SMOOTH BAR

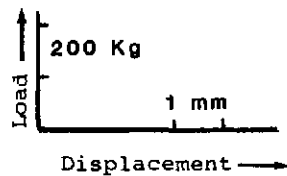
* Denotes single value.
 All others are average
 of replicates.

Figure 73

Mechanical Properties of Notched Tensile Coupons as a Function of Exposure Conditions for Mo - 41 Re (source 1)



	TEMPERATURE	TIME	[O] POTENTIAL
+	800°C	130 Hrs.	100 ppm
0	550°C	70 Hrs.	50 ppm
-	300°C	10 Hrs.	2 ppm

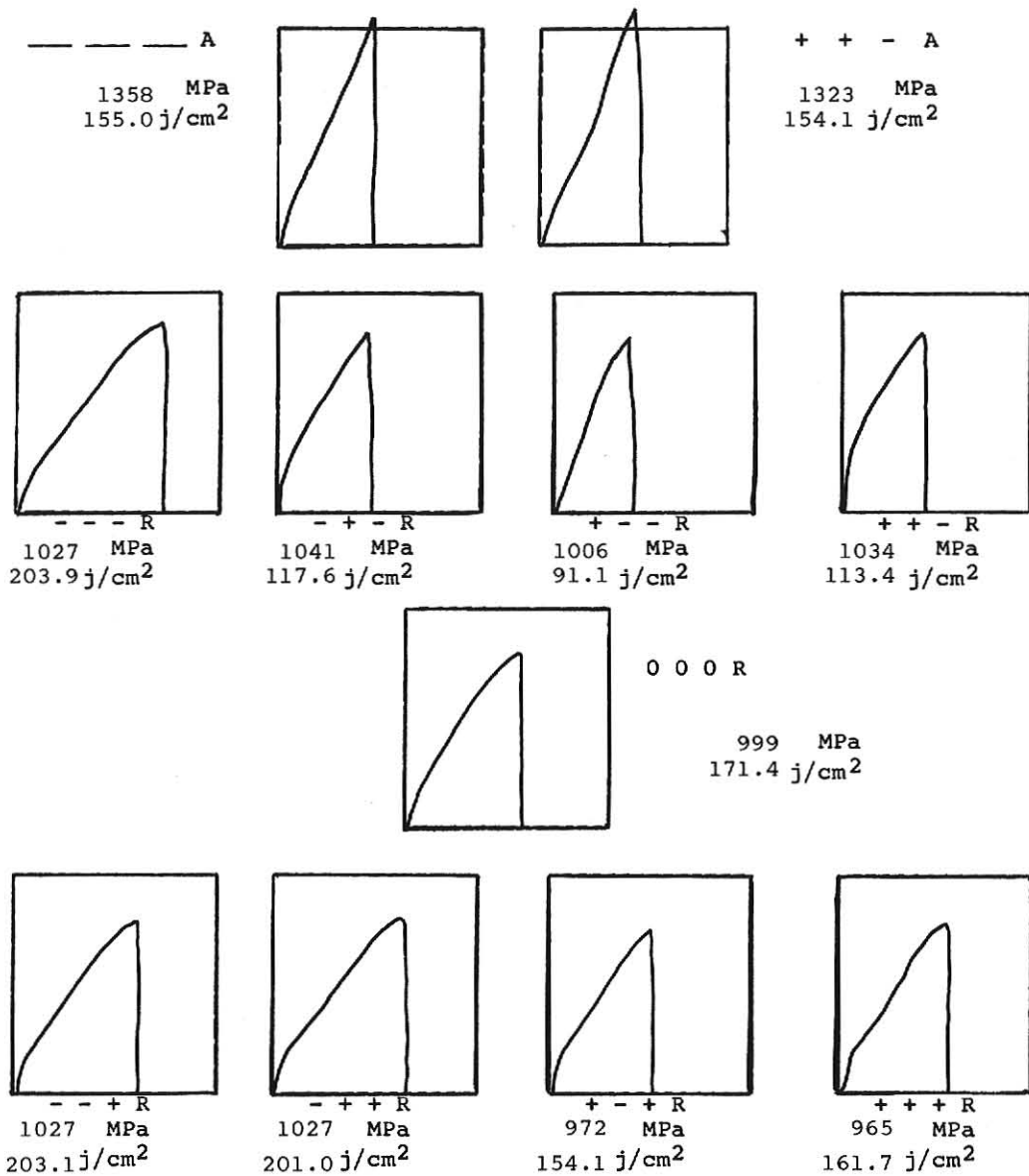


— NO EXPOSURE
R RECRYSTALLIZED
A AS-RECEIVED
▽ SMOOTH BAR

• Denotes single value.
All others are average
of replicates.

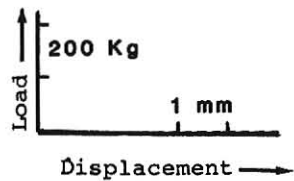
Figure 74

Mechanical Properties of Notched Tensile Coupons as a Function of Exposure Conditions for Mo - 41 Re (source 2)



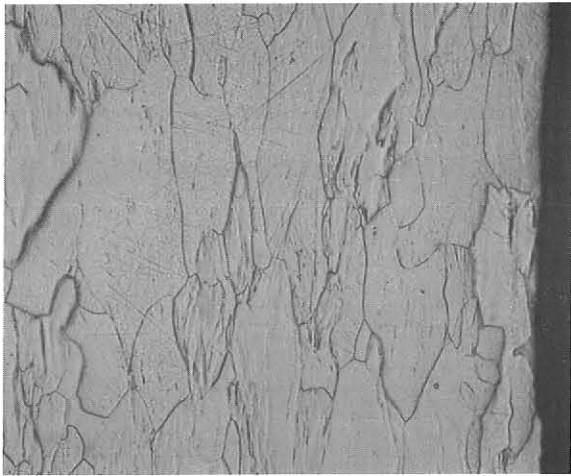
	TEMPERATURE	TIME	[O] POTENTIAL
+	800°C	130 Hrs.	100 ppm
0	550°C	70 Hrs.	50 ppm
-	300°C	10 Hrs.	2 ppm

— NO EXPOSURE
R RECRYSTALLIZED
A AS-RECEIVED
▽ SMOOTH BAR

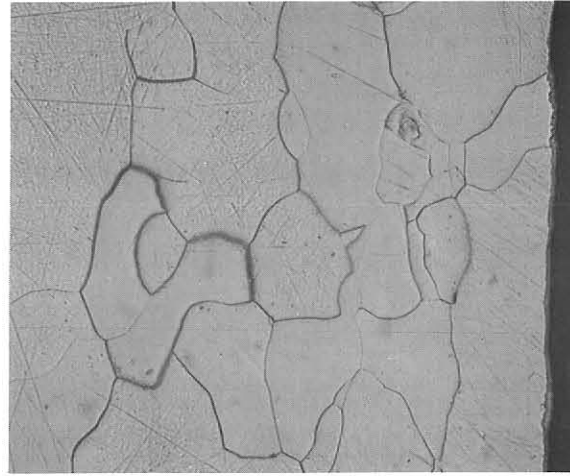


* Denotes single value.
All others are average of replicates.

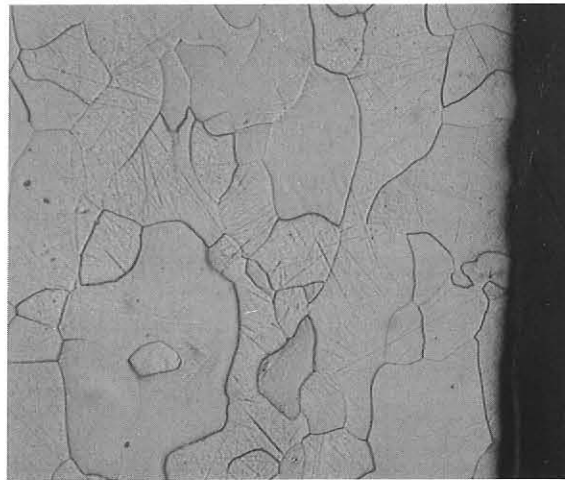
Figure 75



a. As-received



b. +++



c. ---

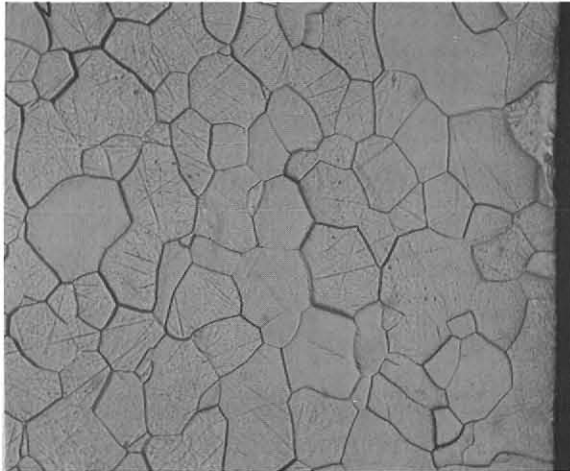
	TEMPERATURE	TIME	[O] POTENTIAL
+	800°C	130 Hrs.	100 ppm
0	550°C	70 Hrs.	50 ppm
-	300°C	10 Hrs.	2 ppm

— NO EXPOSURE
 R RECRYSTALLIZED
 A AS-RECEIVED
 ▽ SMOOTH BAR

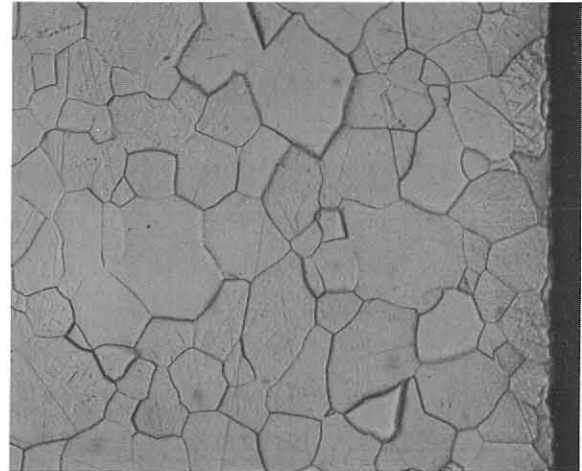
50 μM

Metallographic structure of selected Mo-13Re specimens.

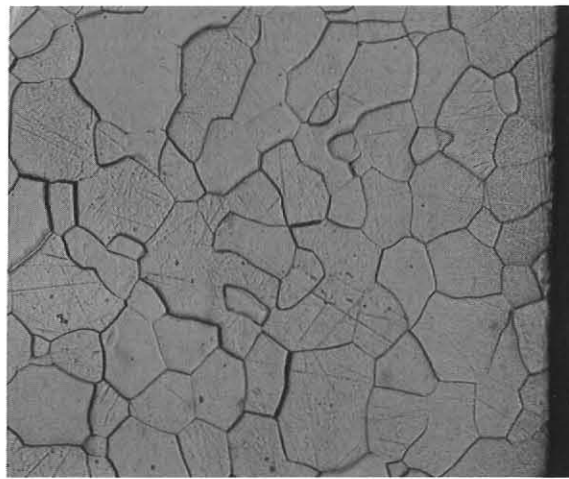
Fig. 76



a. As-received




b. + + +



c. ---

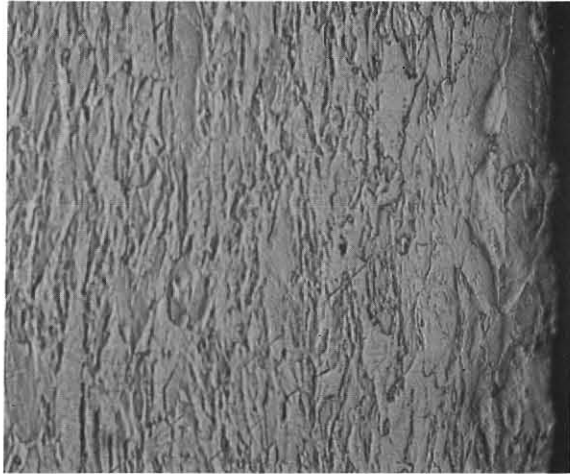
	TEMPERATURE	TIME	[O] POTENTIAL
+	800°C	130 Hrs.	100 ppm
0	550°C	70 Hrs.	50 ppm
-	300°C	10 Hrs.	2 ppm

— NO EXPOSURE
 R RECRYSTALLIZED
 A AS-RECEIVED
 ▽ SMOOTH BAR

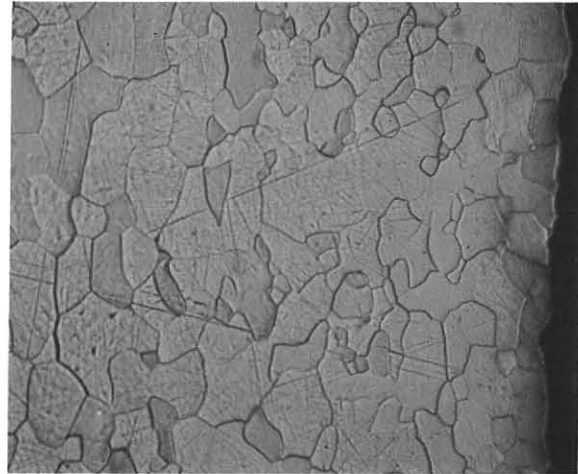
50 μM


METALLOGRAPHIC STRUCTURE OF SELECTED Mo-26Re (SOURCE 1) SPECIMENS.

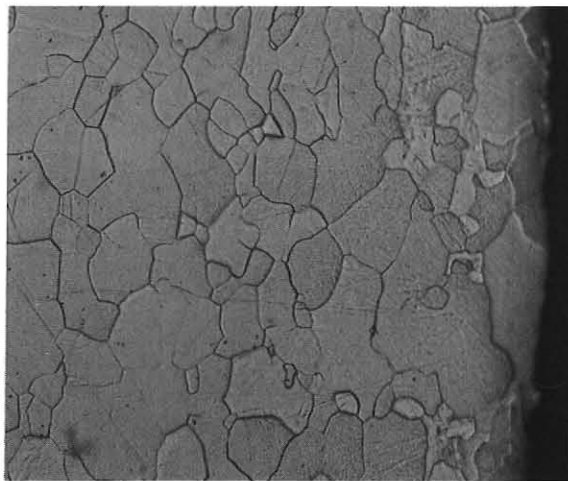
Fig. 77



a. As-received



b. +++



c. ---

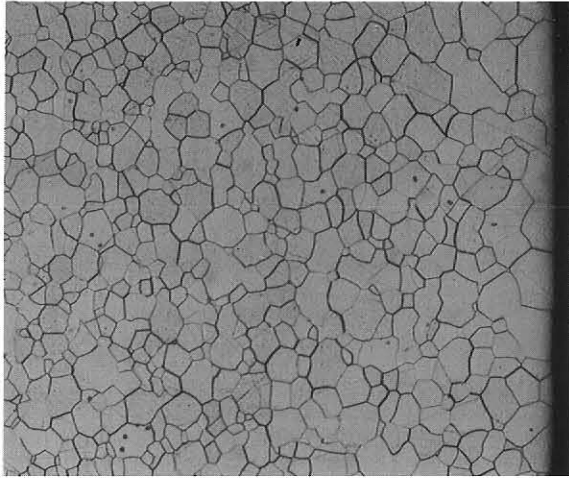
	TEMPERATURE	TIME	[O] POTENTIAL
+	800°C	130 Hrs.	100 ppm
0	550°C	70 Hrs.	50 ppm
-	300°C	10 Hrs.	2 ppm

— NO EXPOSURE
 R RECRYSTALLIZED
 A AS-RECEIVED
 ▽ SMOOTH BAR

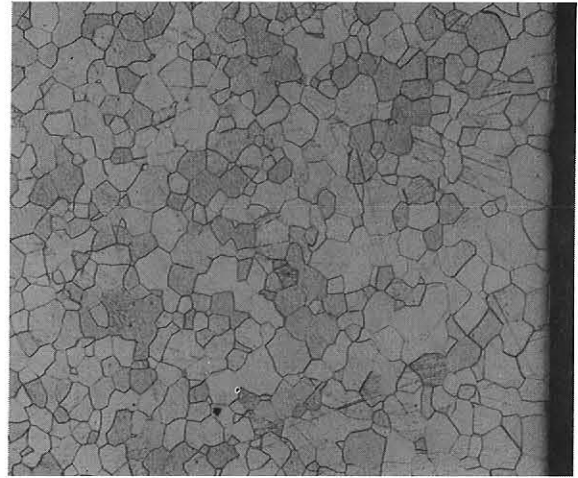
50 μM

METALLOGRAPHIC STRUCTURE OF SELECTED Mo-41Re (SOURCE 2) SPECIMENS.

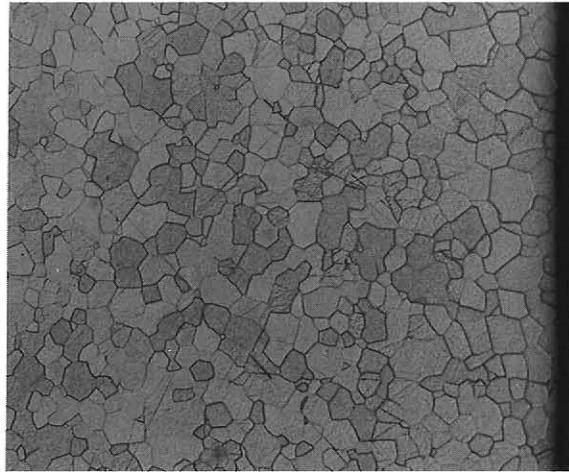
Fig. 78



a. As-received



b. +++




c. ---

	TEMPERATURE	TIME	[O] POTENTIAL
+	800°C	130 Hrs.	100 ppm
0	550°C	70 Hrs.	50 ppm
-	300°C	10 Hrs.	2 ppm

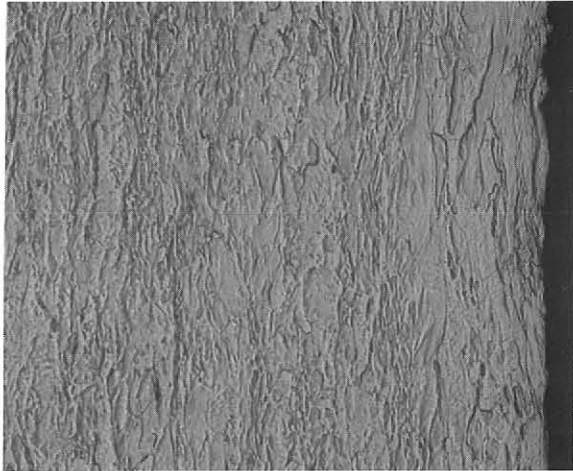
— NO EXPOSURE
 R RECRYSTALLIZED
 A AS-RECEIVED
 ▽ SMOOTH BAR

100 μM

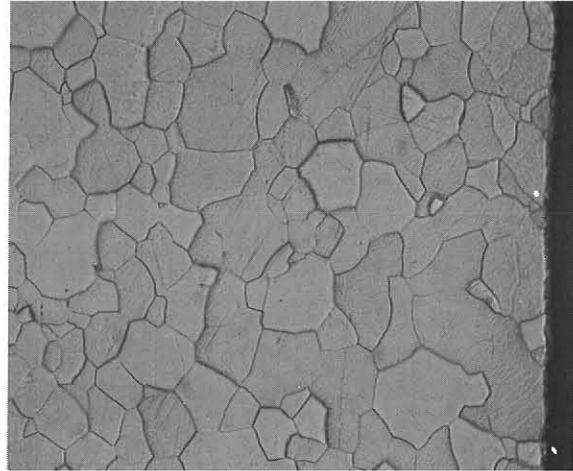


Metallographic structure of selected Mo-41Re (Source 1) specimens.

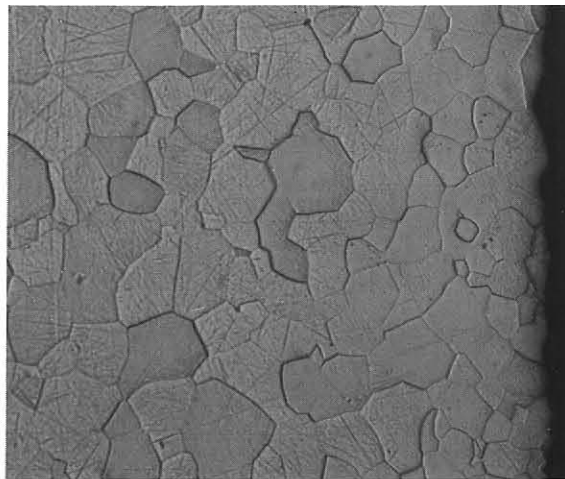
Fig. 79



a. AR



b. +++



c. +-

	TEMPERATURE	TIME	[O] POTENTIAL
+	800°C	130 Hrs.	100 ppm
0	550°C	70 Hrs.	50 ppm
-	300°C	10 Hrs.	2 ppm

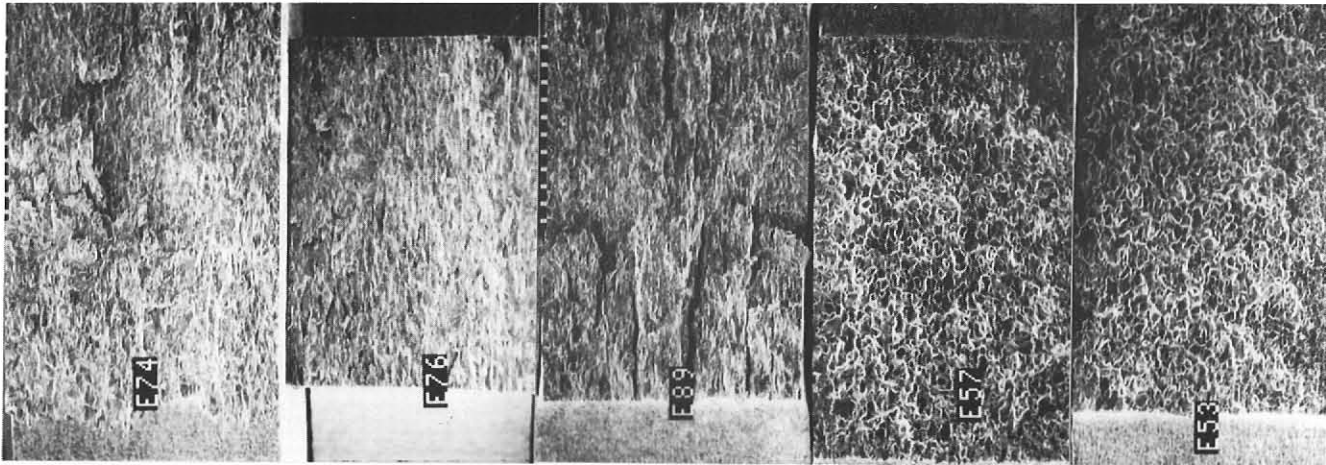
— NO EXPOSURE
 R RECRYSTALLIZED
 A AS-RECEIVED
 ▽ SMOOTH BAR

50 μM

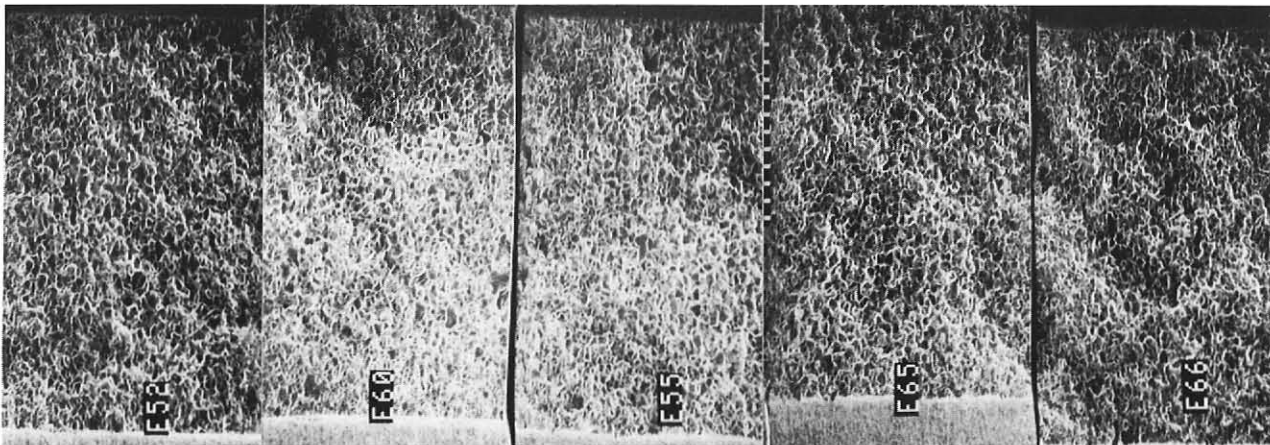


Metallographic structure of selected Mo-41Re (Source 2) specimens.

Fig. 80



E74	—	—	—	A
E76	—	—	—	A▽
E89	+	+	-	A
E57	+	+	-	R
E53	+	-	-	R



E52	-	+	-	R
E60	+	-	+	R
E55	-	+	+	R
E65	-	-	+	R
E66	0	0	0	R

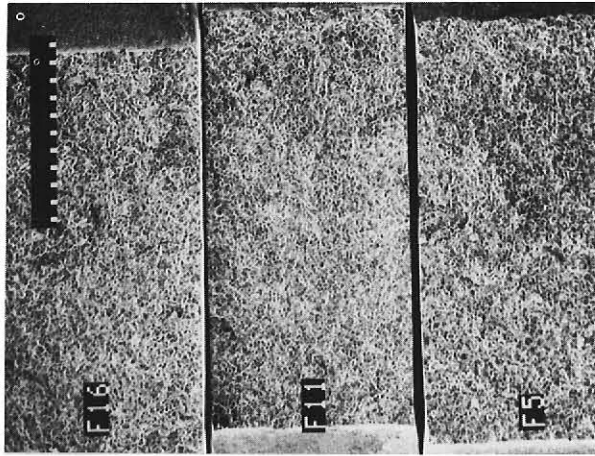
Mo-13Re (SOURCE 2)

	TEMPERATURE	TIME	[O] POTENTIAL
+	800°C	130 HRS.	100 PPM
0	550°C	70 HRS.	50 PPM
-	300°C	10 HRS.	2 PPM

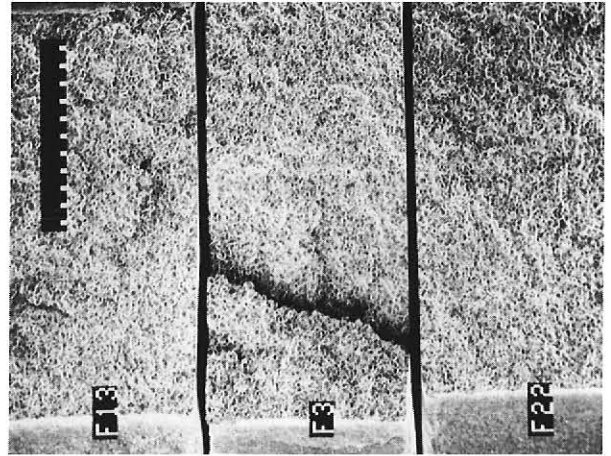
— NO EXPSOURE
 R RECRYSTALLIZED
 A AS-RECEIVED
 ▽ SMOOTH BAR

1500 μm

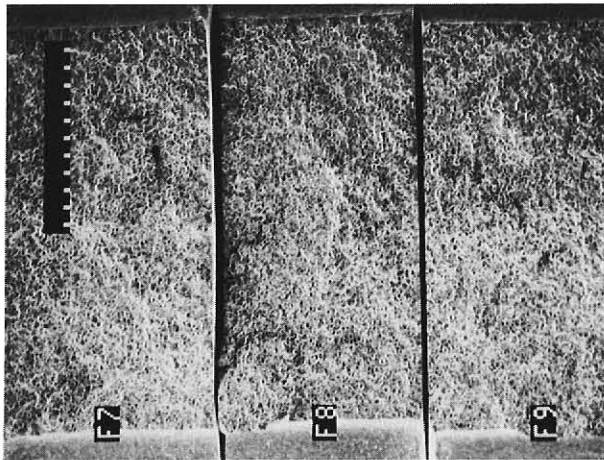
Fig. 81



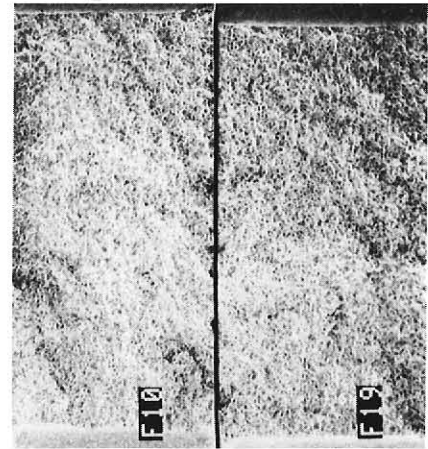
F16	—	—	—	A
F11	+	+	-	A
F5	+	+	-	R



F13	+	-	-	R
F3	-	+	-	R
F22	-	-	-	R



F7	+	+	+	R
F8	+	-	+	R
F9	-	+	+	R



F10	-	-	+	R
F19	0	0	0	R

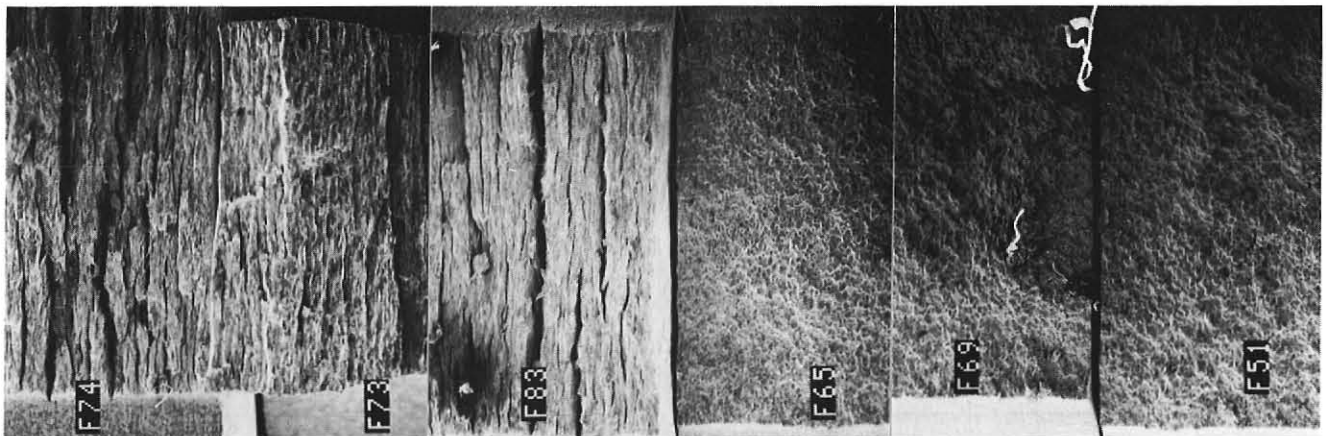
Mo-26Re (SOURCE 1)

	TEMPERATURE	TIME	[O] POTENTIAL
+	800°C	130 HRS.	100 PPM
0	550°C	70 HRS.	50 PPM
-	300°C	10 HRS.	2 PPM

— NO EXPOSURE
 R RECRYSTALLIZED
 A AS-RECEIVED
 ▽ SMOOTH BAR

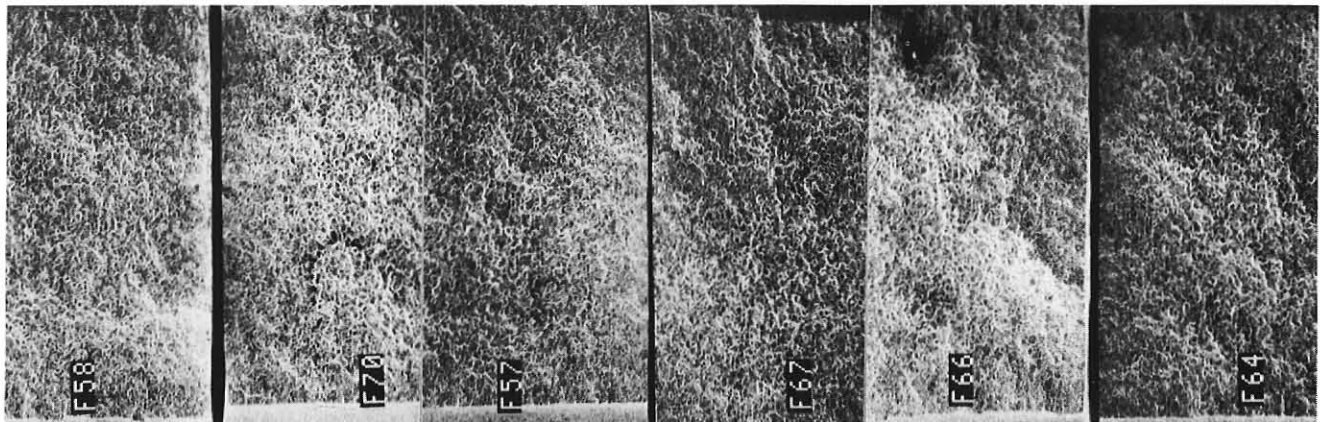
1500 μm

Fig. 82



F74 — — — A
 F73 — — — A▽
 F83 + + - A

F65 + + - R
 F69 + - - R
 F51 - + - R



F58 - - - R
 F70 + + + R
 F57 + - + R

F67 - - + R
 F66 - - - R
 F64 0 0 0 R

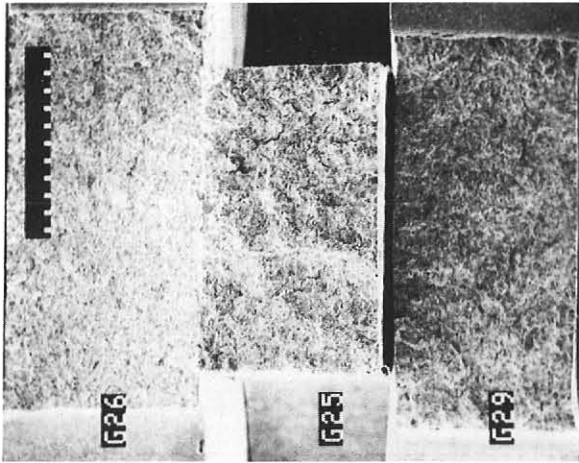
Mo-26Re (SOURCE 2)

	TEMPERATURE	TIME	[O] POTENTIAL
+	800°C	130 Hrs.	100 PPM
0	550°C	70 Hrs.	50 PPM
-	300°C	10 Hrs.	2 PPM

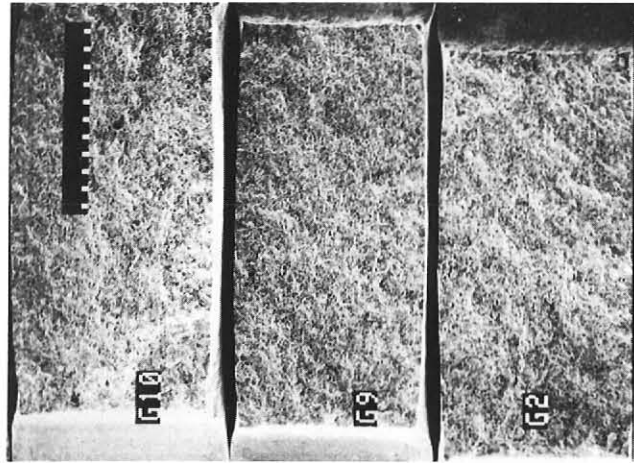
— NO EXPOSURE
 R RECRYSTALLIZED
 A AS-RECEIVED
 ▽ SMOOTH BAR

1500 μm

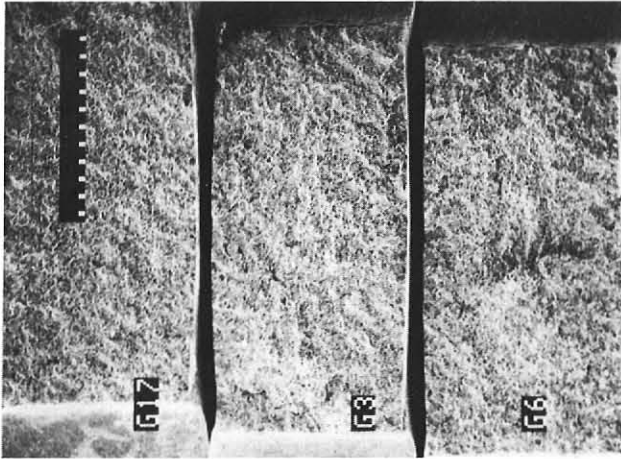
Fig. 83



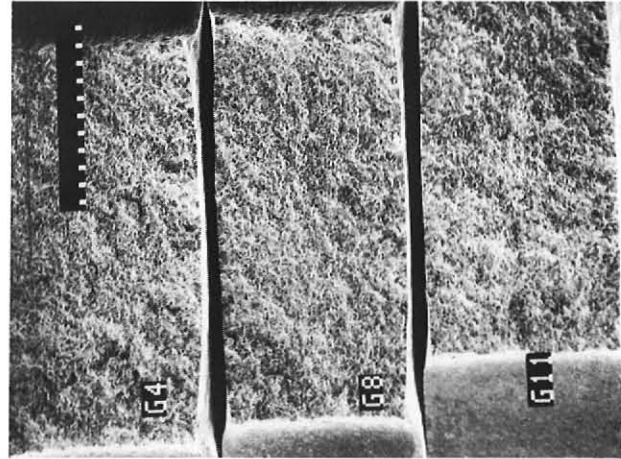
G26 — — — A
 G25 — — — A∇
 G29 + + - A



G10 + + - R
 G9 + - - RR
 G2 - + - R



G17 - - - R
 G3 + + + RR
 G6 + - - R



G4 - + + RR
 G8 + - + RR
 G11 0 0 0 R

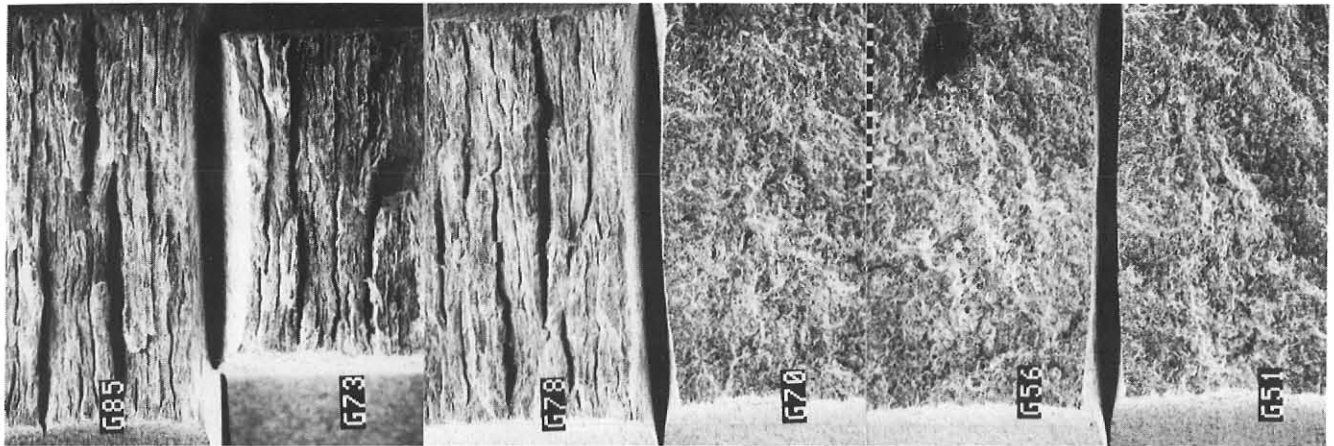
Mo-41Re (SOURCE 1)

	TEMPERATURE	TIME	[O] POTENTIAL
+	800°C	130 HRS.	100 PPM
0	550°C	70 HRS.	50 PPM
-	300°C	10 HRS.	2 PPM

— NO EXPSOURE
 R RECRYSTALLIZED
 A AS-RECEIVED
 ∇ SMOOTH BAR

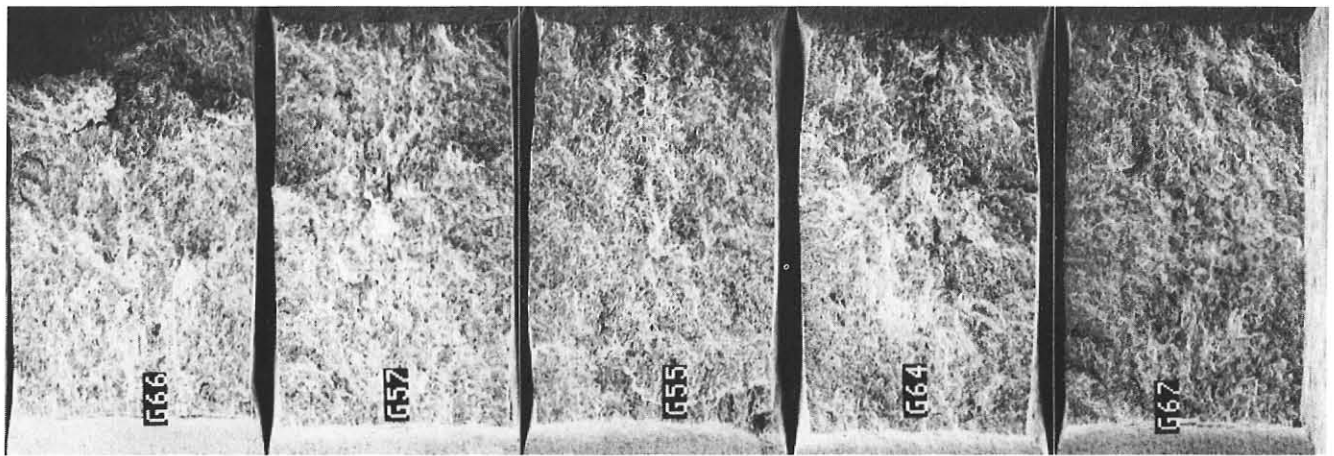
1500 μM

Fig. 84



G85	—	—	—	A
G73	—	—	—	A▽
G78	+	+	-	A

G70	+	+	-	R
G56	-	-	-	R
G51	-	+	-	R



G66	+	+	+	R
G57	+	-	+	R
G55	-	+	+	R

G64	-	-	±	R
G67	0	0	0	R

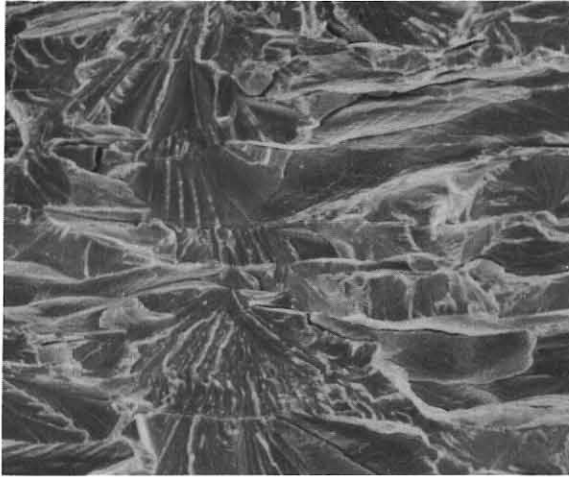
Mo-41Re (SOURCE 2)

	TEMPERATURE	TIME	[O] POTENTIAL
+	800°C	130 HRS.	100 PPM
0	550°C	70 HRS.	50 PPM
-	300°C	10 HRS.	2 PPM

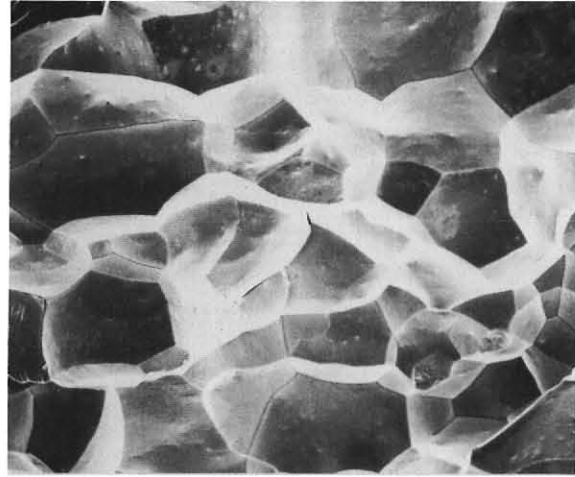
— NO EXPSOURE
 R RECRYSTALLIZED
 A AS-RECEIVED
 ▽ SMOOTH BAR

1500 μm

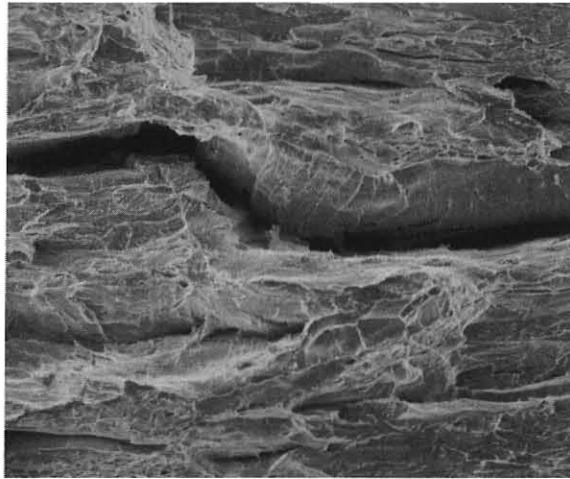
Fig. 85



a. Cleavage



b. Intergranular



c. Lammelar

50 μM

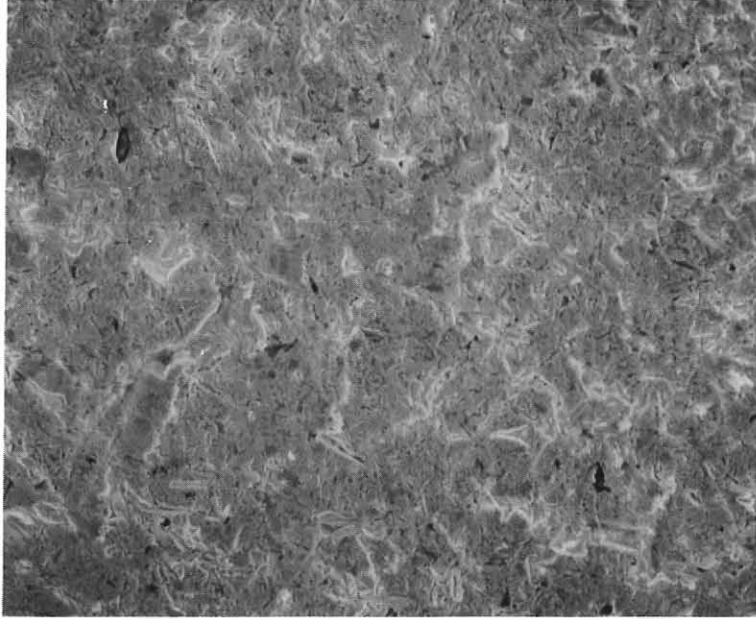
	TEMPERATURE	TIME	[O] POTENTIAL
+	800°C	130 Hrs.	100 ppm
0	550°C	70 Hrs.	50 ppm
-	300°C	10 Hrs.	2 ppm

— NO EXPOSURE
 R RECRYSTALLIZED
 A AS-RECEIVED
 ▽ SMOOTH BAR

a. b.
 50 μM

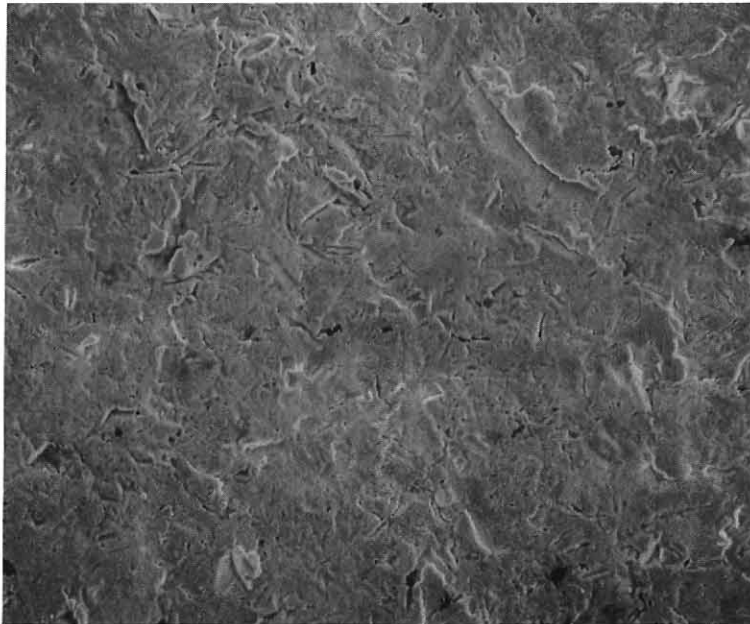
Typical high magnification fractograph for Mo-26 Re alloy.

Fig. 86



50 μM

a. As-received

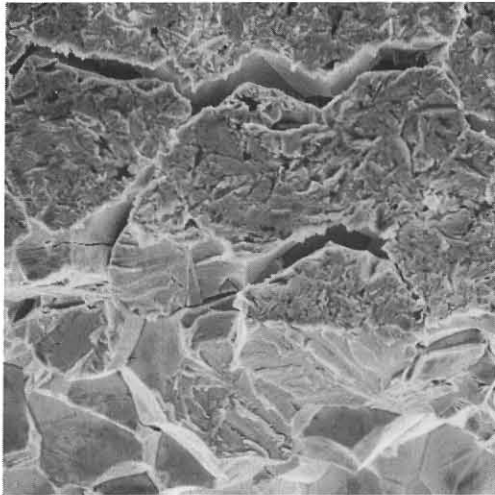


50 μM

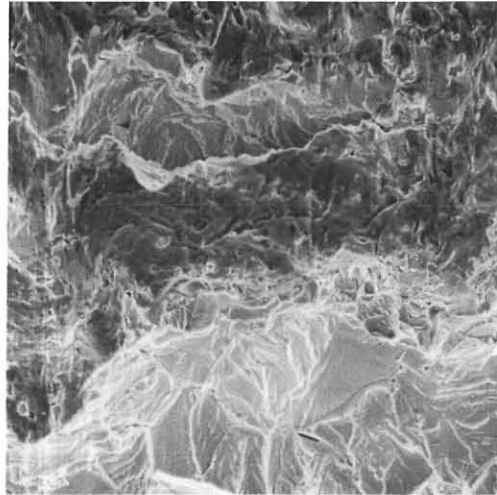
b. Na exposed

Specimen surface appearance as a function of Na exposure for the Mo-41 Re alloy (Source 1).

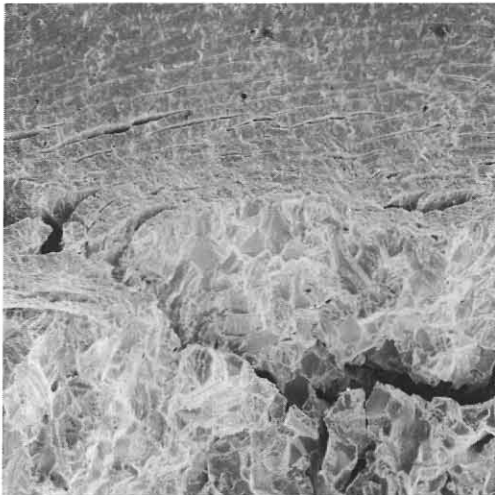
Fig. 87



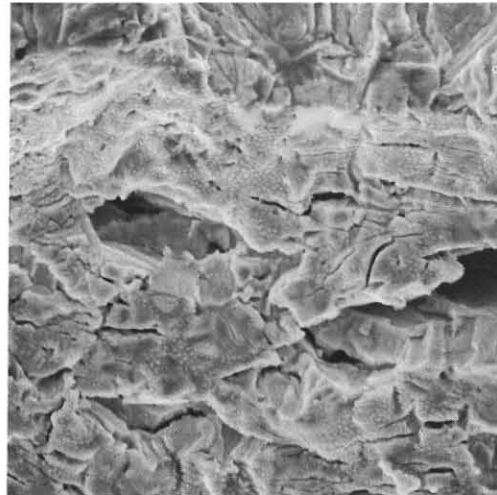
a. As-received



b. +---



c. +++



d. 000

	TEMPERATURE	TIME	[O] POTENTIAL
+	800°C	130 Hrs.	100 ppm
0	550°C	70 Hrs.	50 ppm
-	300°C	10 Hrs.	2 ppm

— NO EXPOSURE
 R RECRYSTALLIZED
 A AS-RECEIVED
 ▽ SMOOTH BAR



a. & b. 60 μM
c. 200 μM
d. 25 μM

Fracture initiation for selected exposure for the Mo-41Re alloy (Source 1).

Fig. 88

WEIGHT CHANGE OF MO-13RE ALLOY
 AS A FUNCTION OF
 OXYGEN CONCENTRATION AND TEMPERATURE
 IN MOLTEN SODIUM (TIME=10 HRS)

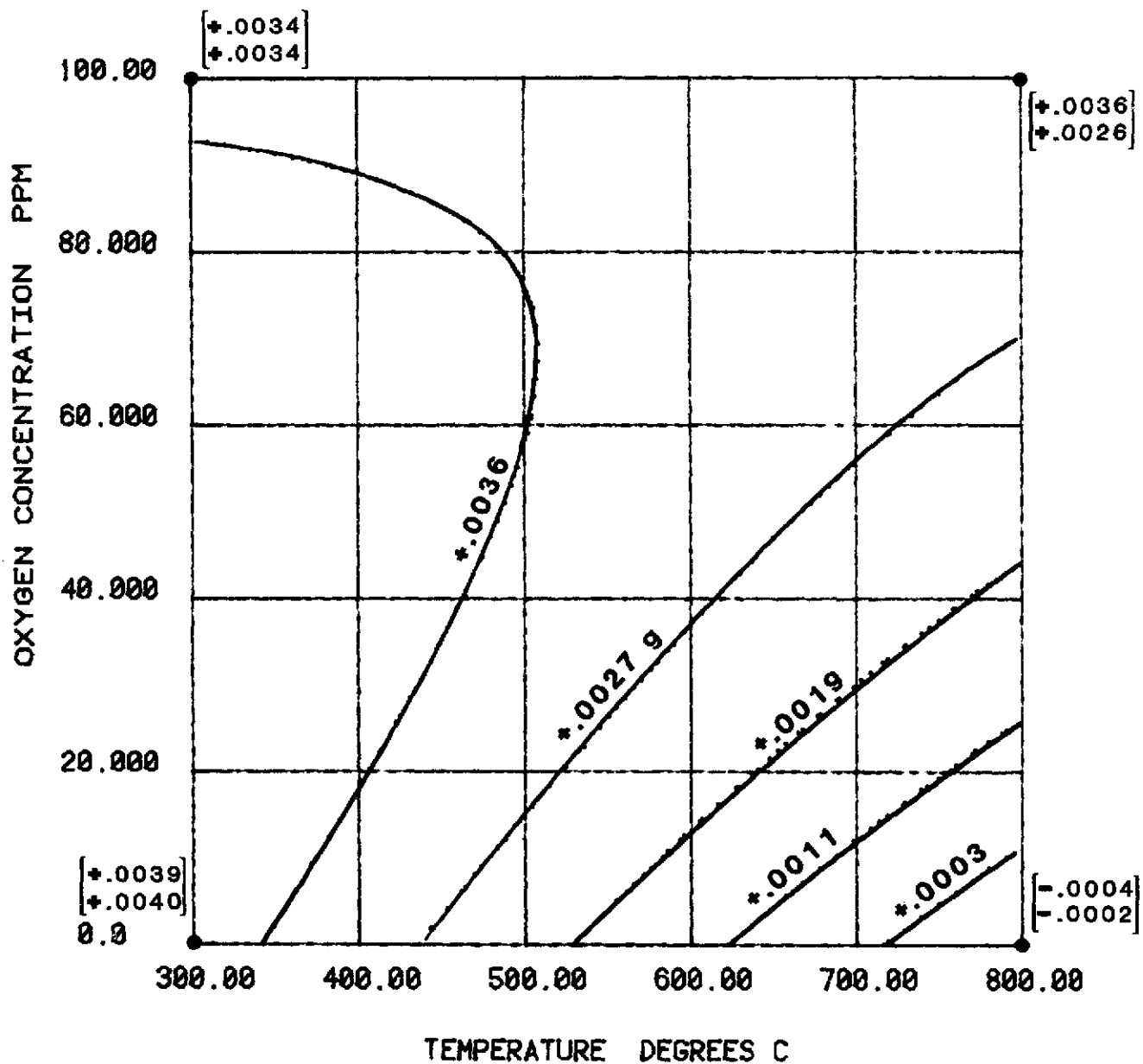


Fig. 89

WEIGHT CHANGE OF MO-13RE ALLOY
 AS A FUNCTION OF
 OXYGEN CONCENTRATION AND TEMPERATURE
 IN MOLTEN SODIUM (TIME=70 HRS)

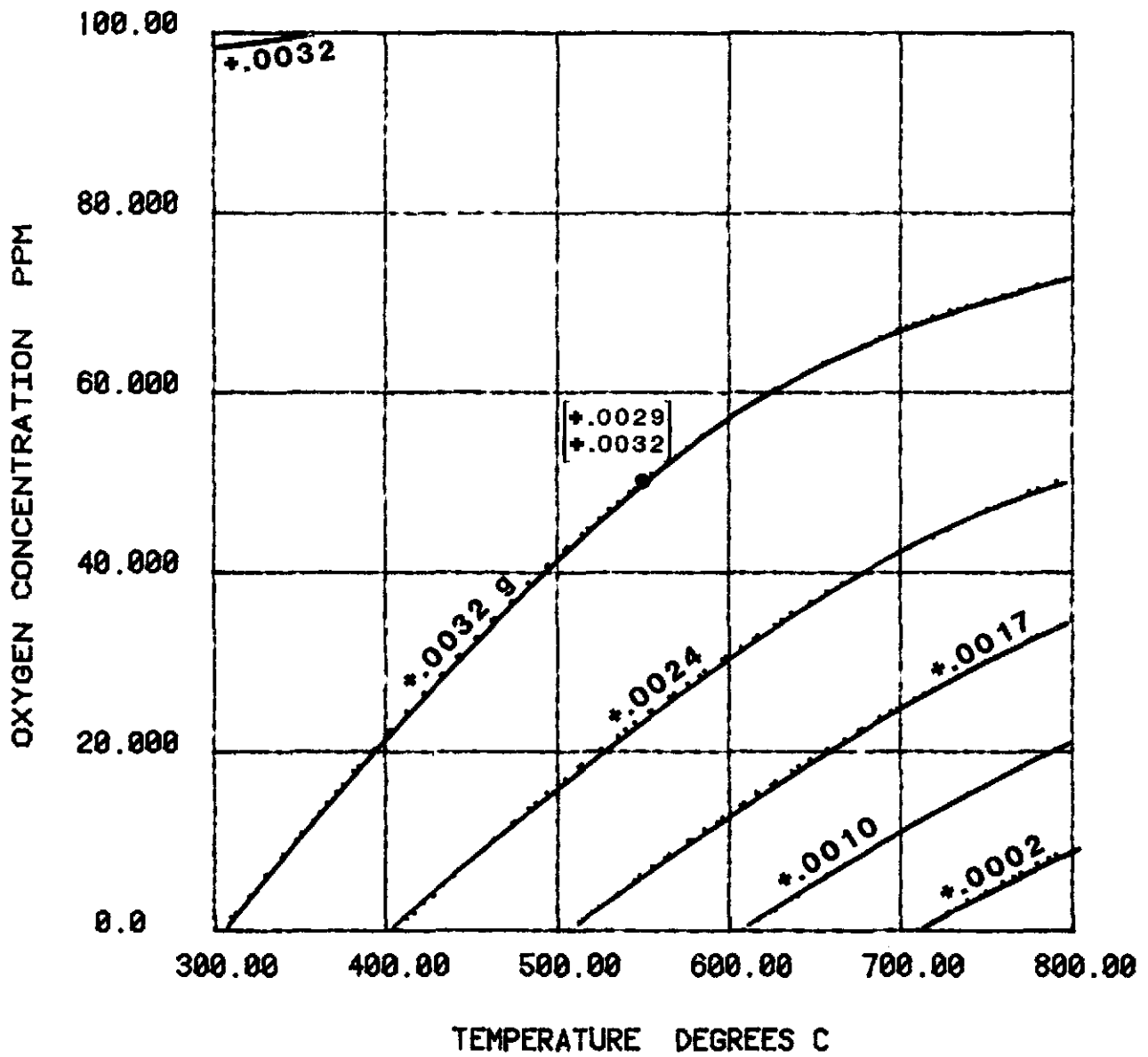


Fig. 90

WEIGHT CHANGE OF MO-13RE ALLOY
 AS A FUNCTION OF
 OXYGEN CONCENTRATION AND TEMPERATURE
 IN MOLTEN SODIUM (TIME=130 HRS)

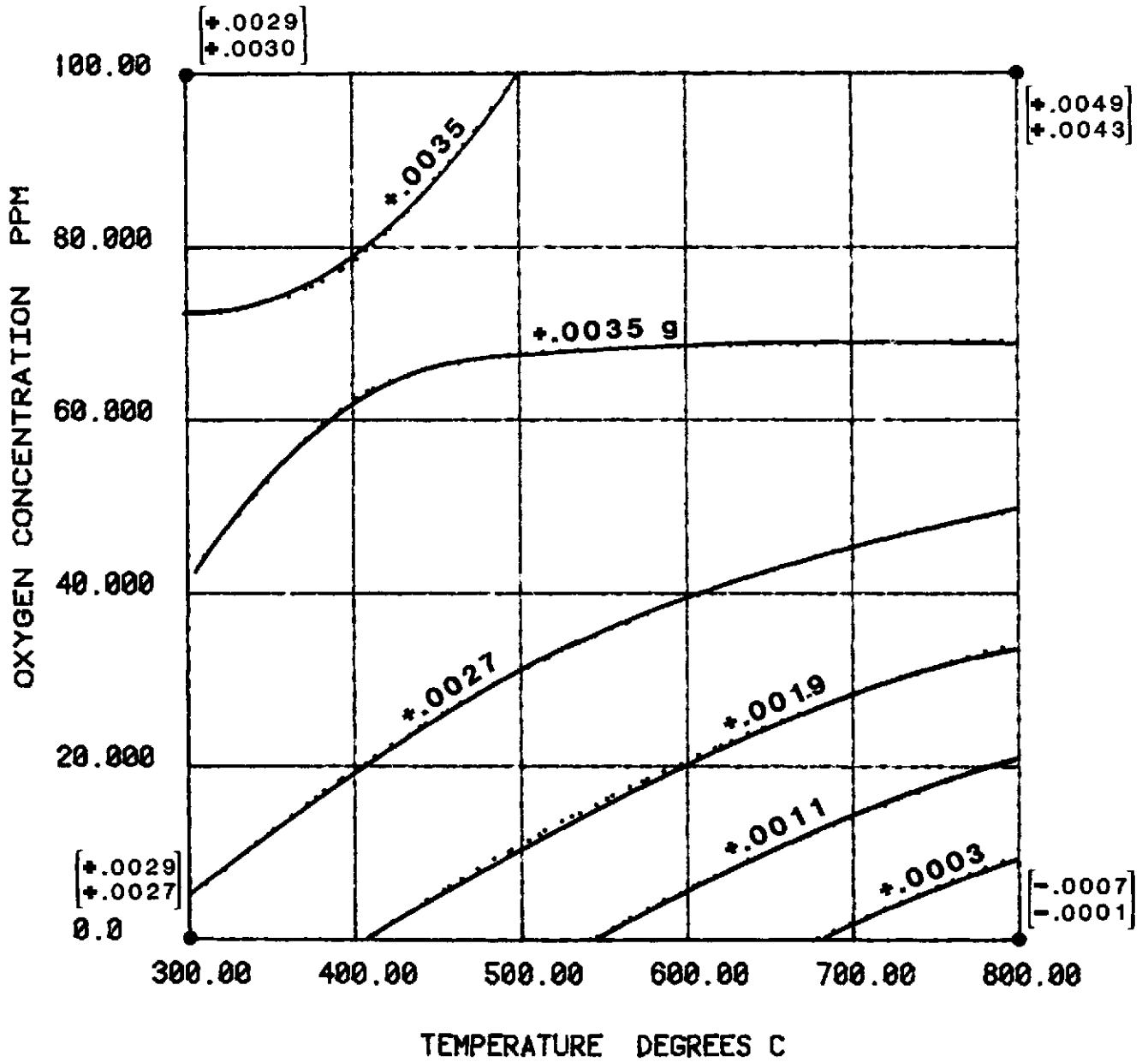


Fig. 91

WEIGHT CHANGE OF MO-41RE ALLOY (Source 1)
AS A FUNCTION OF
OXYGEN CONCENTRATION AND TEMPERATURE
IN MOLTEN SODIUM (TIME=10 HRS)

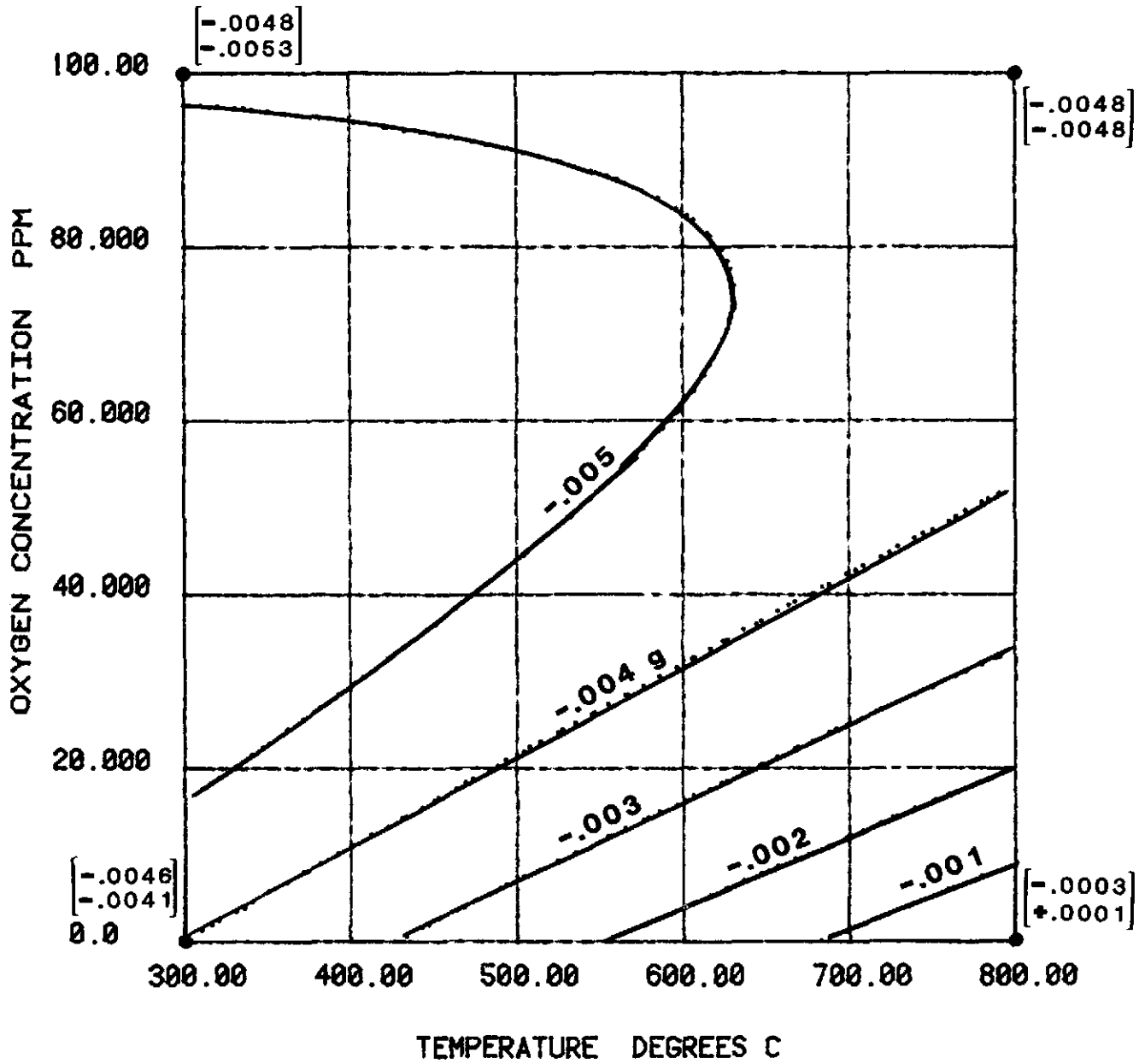


Fig. 92

WEIGHT CHANGE OF MO-41RE ALLOY (Source 1)
 AS A FUNCTION OF
 OXYGEN CONCENTRATION AND TEMPERATURE
 IN MOLTEN SODIUM (TIME=70 HRS)

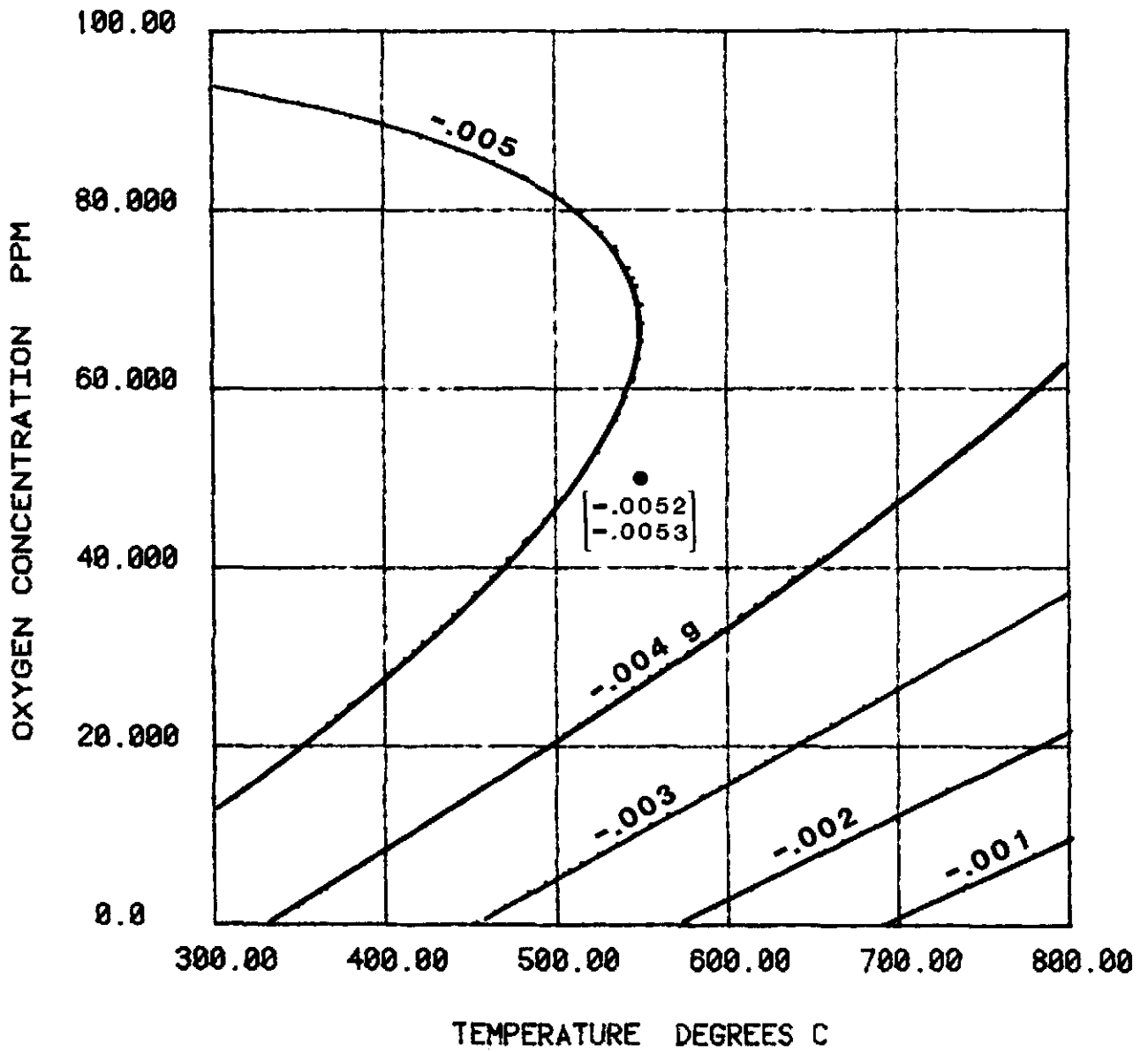


Fig. 93

WEIGHT CHANGE OF MO-41RE ALLOY (Source 1)
 AS A FUNCTION OF
 OXYGEN CONCENTRATION AND TEMPERATURE
 IN MOLTEN SODIUM (TIME=130 HRS)

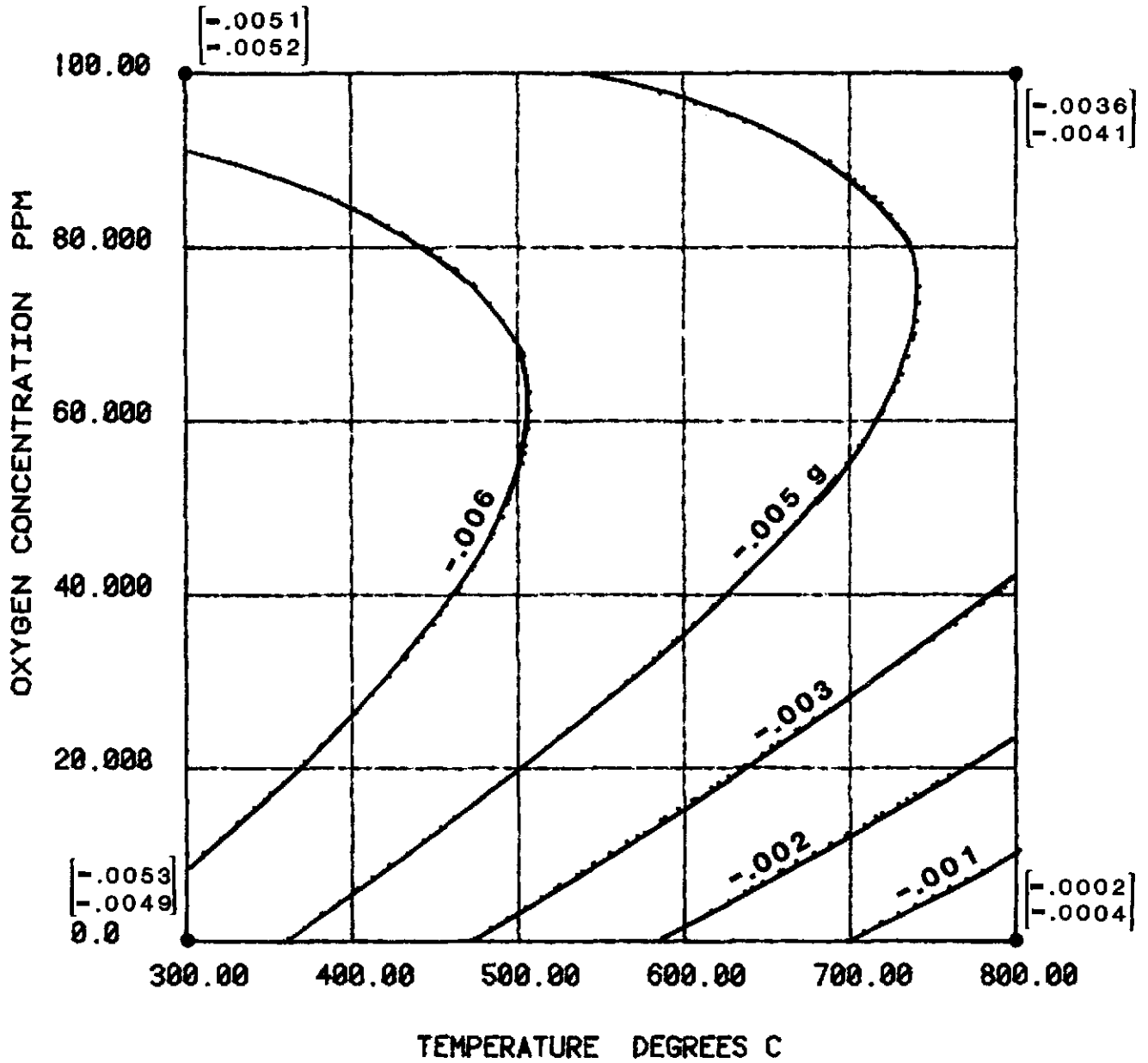
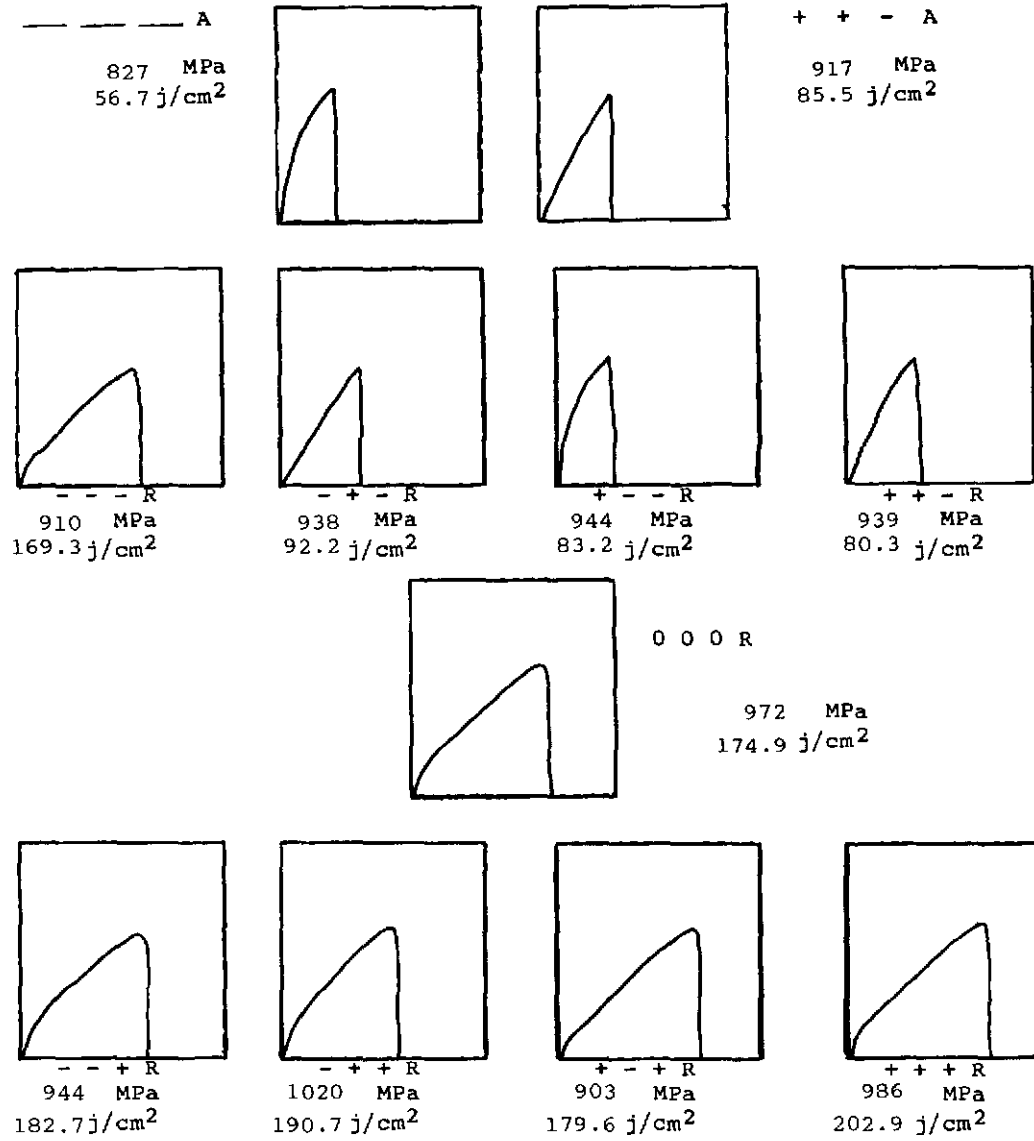
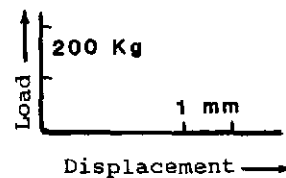


Fig. 94

Mechanical Properties of Notched Tensile Coupons as a Function of Exposure Conditions for Re (Wrought)



	TEMPERATURE	TIME	[O] POTENTIAL
+	800°C	130 Hrs.	100 ppm
0	550°C	70 Hrs.	50 ppm
-	300°C	10 Hrs.	2 ppm

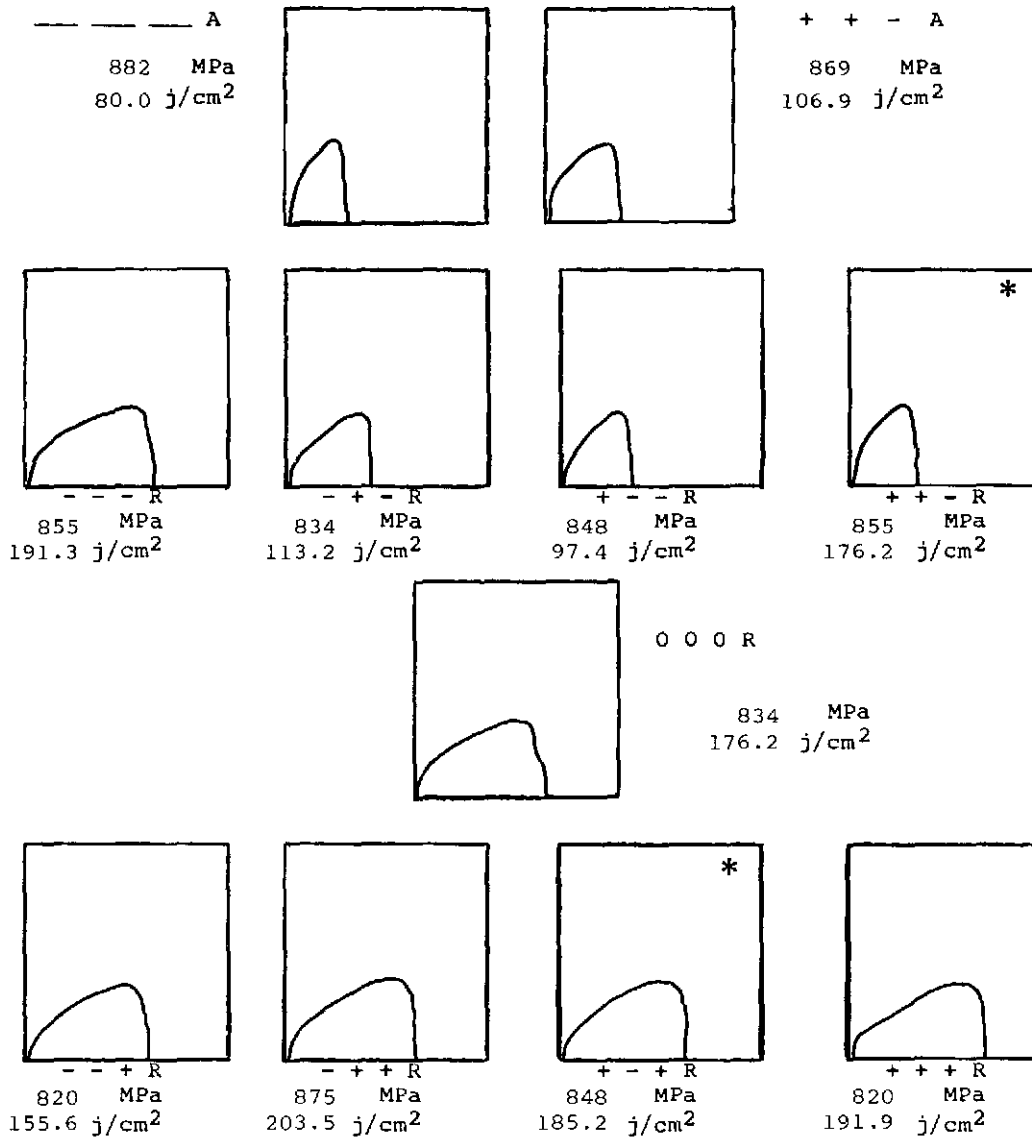


— NO EXPOSURE
R RECRYSTALLIZED
A AS-RECEIVED
▽ SMOOTH BAR

* Denotes single value.
All others are average
of replicates.

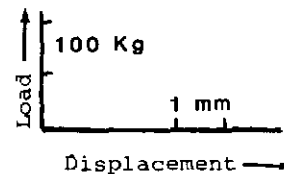
Figure 95

Mechanical Properties of Notched Tensile Coupons as a Function of Exposure Conditions for Re (CVD)



	TEMPERATURE	TIME	[O] POTENTIAL
+	800°C	130 Hrs.	100 ppm
0	550°C	70 Hrs.	50 ppm
-	300°C	10 Hrs.	2 ppm

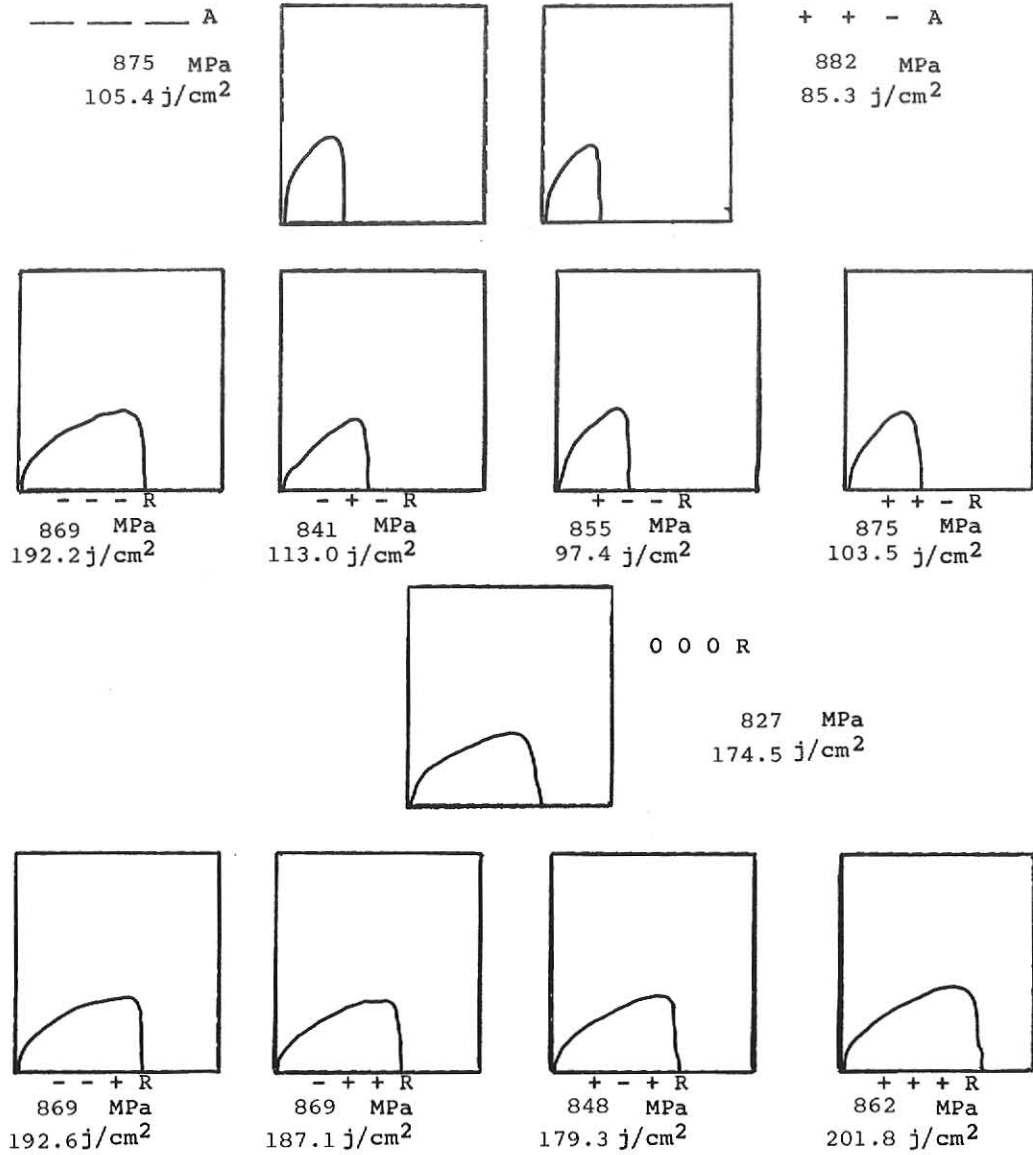
— NO EXPOSURE
R RECRYSTALLIZED
A AS-RECEIVED
▽ SMOOTH BAR



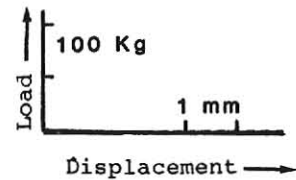
* Denotes single value.
All others are average
of replicates.

Figure 96

Mechanical Properties of Notched Tensile Coupons as a Function of Exposure Conditions for Re - 5W (CVD)



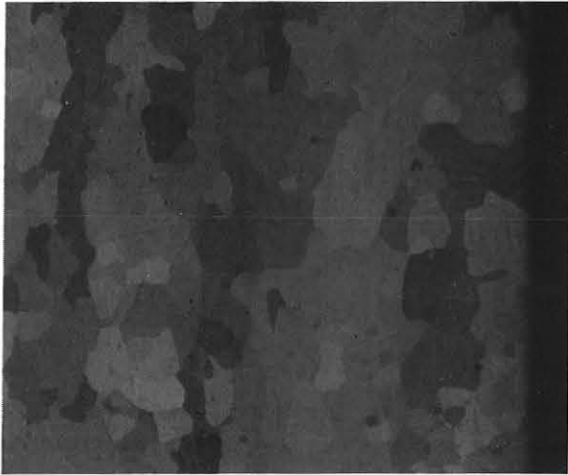
	TEMPERATURE	TIME	[O] POTENTIAL
+	800°C	130 Hrs.	100 ppm
0	550°C	70 Hrs.	50 ppm
-	300°C	10 Hrs.	2 ppm



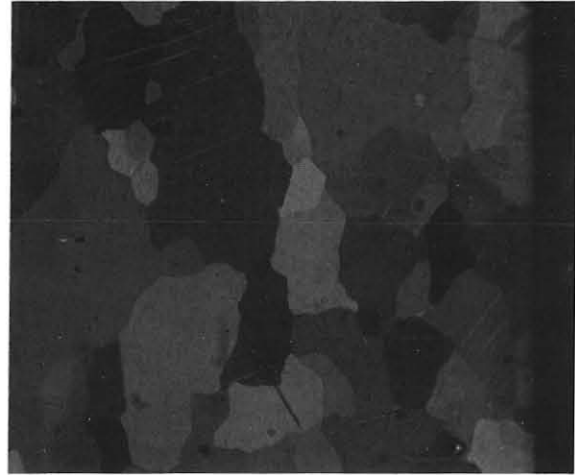
--- NO EXPOSURE
R RECRYSTALLIZED
A AS-RECEIVED
▽ SMOOTH BAR

* Denotes single value.
All others are average
of replicates.

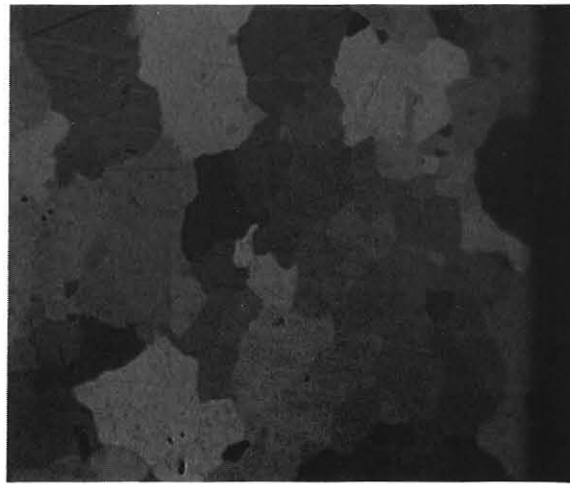
Figure 97



a. As-received



b. +++



c. ---

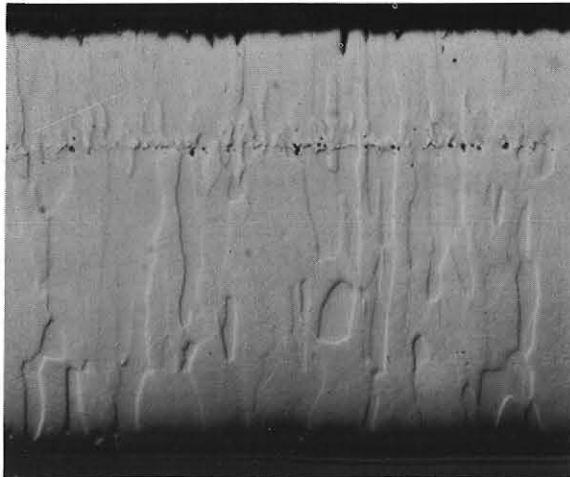
	TEMPERATURE	TIME	[O] POTENTIAL
+	800°C	130 Hrs.	100 ppm
0	550°C	70 Hrs.	50 ppm
-	300°C	10 Hrs.	2 ppm

— NO EXPOSURE
 R RECRYSTALLIZED
 A AS-RECEIVED
 ▽ SMOOTH BAR

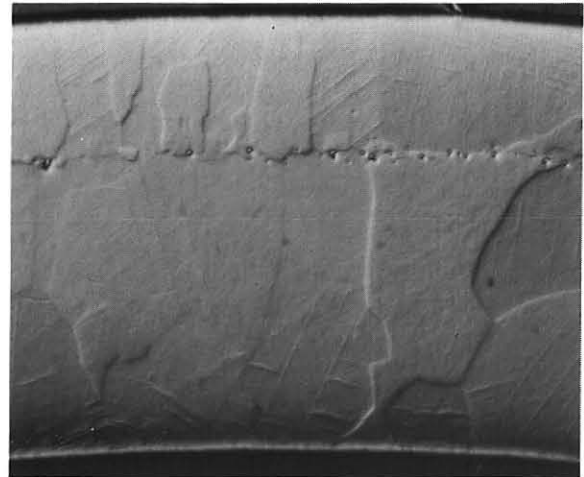
50 μm

Metallographic structure of selected wrought Re specimens.

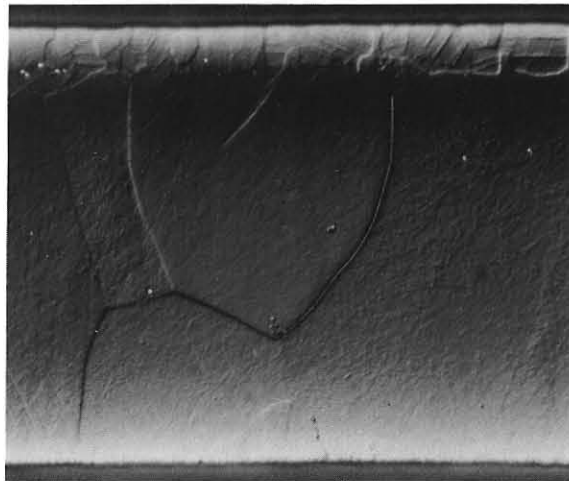
Fig. 98



a. As-received




b. +++



c. ---

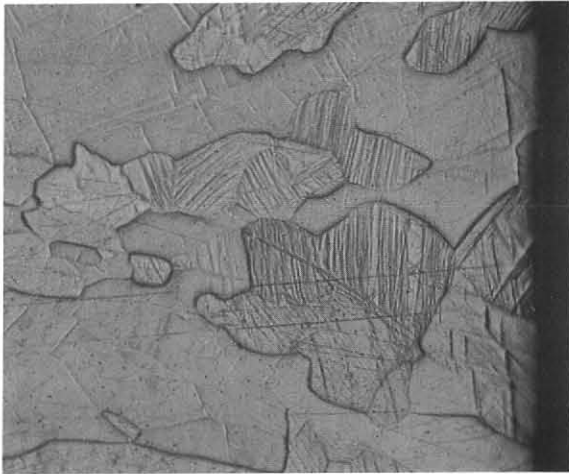
	TEMPERATURE	TIME	[O] POTENTIAL
+	800°C	130 Hrs.	100 ppm
0	550°C	70 Hrs.	50 ppm
-	300°C	10 Hrs.	2 ppm

— NO EXPOSURE
 R RECRYSTALLIZED
 A AS-RECEIVED
 ▽ SMOOTH BAR

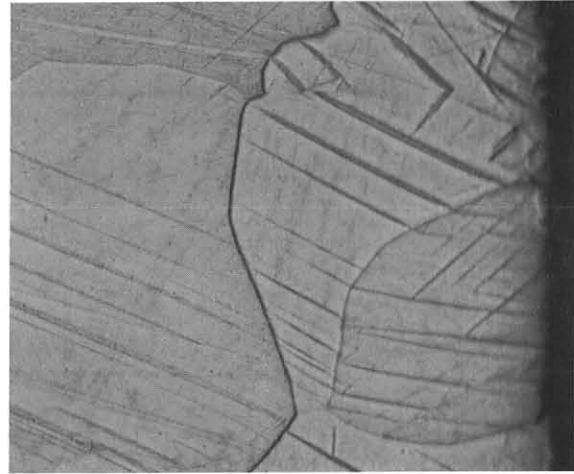
100 μM


Metallographic structure of selected CVD Re specimens.

Fig. 99



a. As-received



b. +++



c. ---

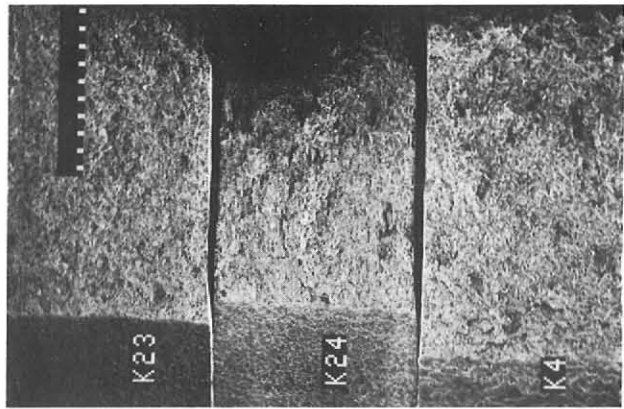
	TEMPERATURE	TIME	[O] POTENTIAL
+	800°C	130 Hrs.	100 ppm
0	550°C	70 Hrs.	50 ppm
-	300°C	10 Hrs.	2 ppm

— NO EXPOSURE
 R RECRYSTALLIZED
 A AS-RECEIVED
 ▽ SMOOTH BAR

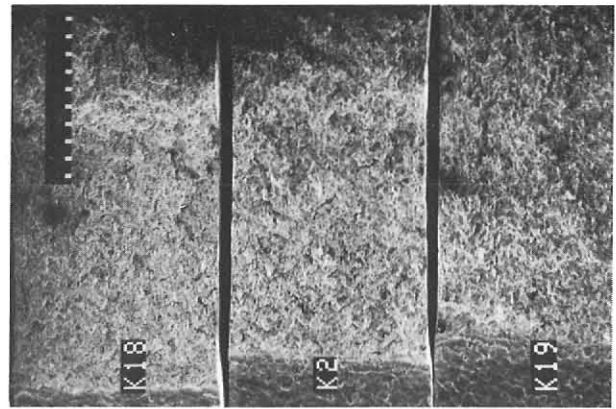
50 μM

Metallographic structure of selected CVD Re-5W alloy specimens.

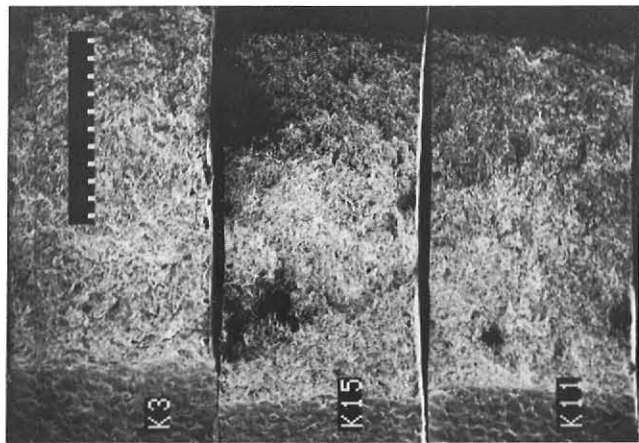
Fig. 100



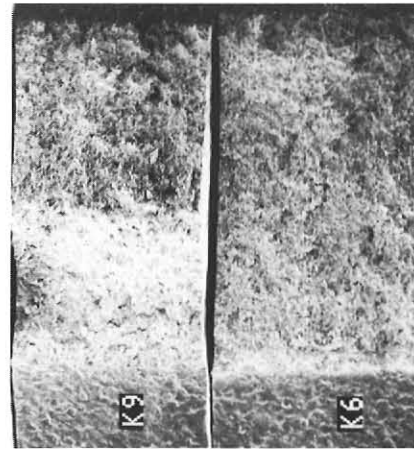
K23	—	—	—	A
K24	+	+	-	A
K4	+	+	-	R



K18	+	-	-	R
K2	-	+	-	R
K19	-	-	-	R



K3	+	+	+	R
K15	+	-	+	R
K11	-	+	+	R



K9	-	-	+	R
K6	0	0	0	R

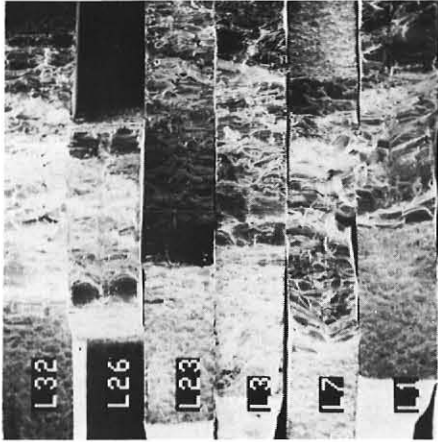
RE (WROUGHT)

	TEMPERATURE	TIME	[O] POTENTIAL
+	800°C	130 HRS.	100 PPM
0	550°C	70 HRS.	50 PPM
-	300°C	10 HRS.	2 PPM

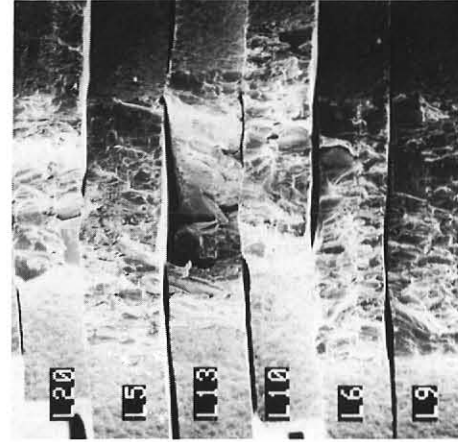
— NO EXPOSURE
 R RECRYSTALLIZED
 A AS-RECEIVED
 ▽ SMOOTH BAR

1500 μm

Fig. 101

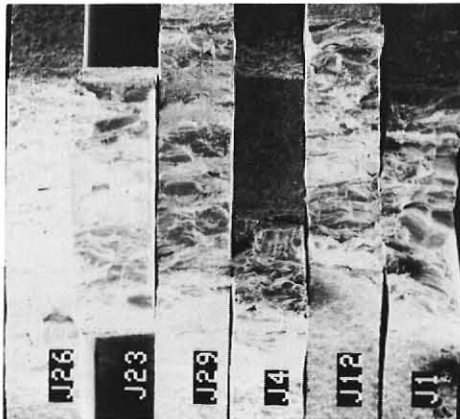


L32	---	---	---	A▽
L26	---	---	---	A
L23	+	+	-	A
L3	+	+	-	R
L7	+	-	-	R
L1	-	+	-	R



L20	-	-	-	R
L5	+	+	+	R
L13	+	+	+	R
L10	-	+	+	R
L6	-	-	+	R
L9	0	0	0	R

RE-5W (CVD)



J26	---	---	---	A
J23	---	---	---	A▽
J29	+	+	-	A
J4	+	+	-	R
J12	+	-	-	R
J11	-	+	+	R



J19	-	-	-	R
J3	+	+	+	R
J14	+	-	+	R
J9	-	+	+	R
J17	-	-	+	R
J13	0	0	0	R

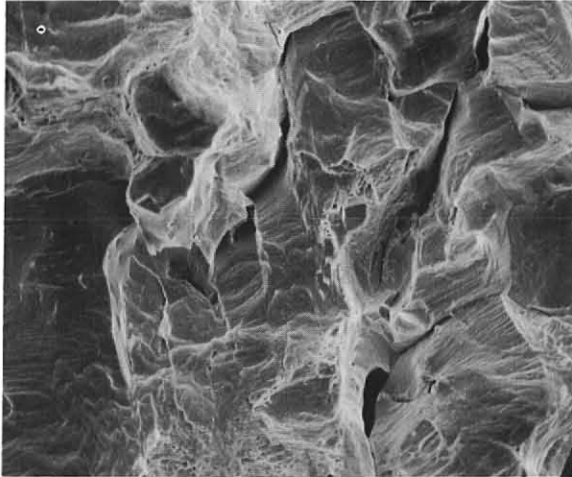
RE (CVD)

	TEMPERATURE	TIME	[O] POTENTIAL
+	800°C	130 Hrs.	100 PPM
0	550°C	70 Hrs.	50 PPM
-	300°C	10 Hrs.	2 PPM

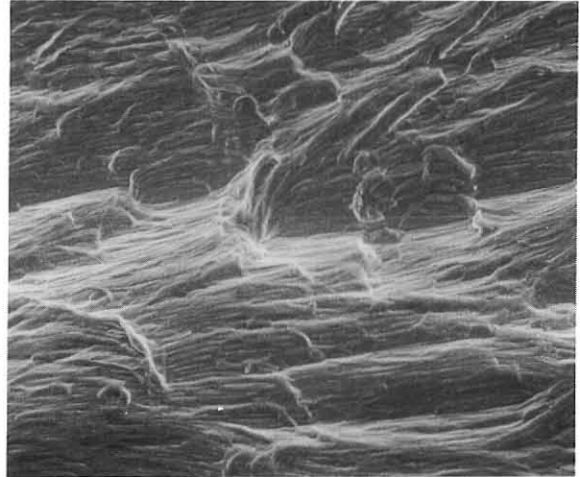
--- NO EXPOSURE
 R RECRYSTALLIZED
 A AS-RECEIVED
 ▽ SMOOTH BAR

1500 μm

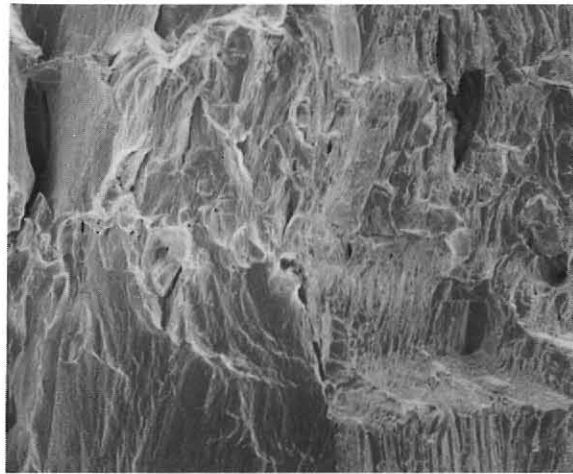
Fig. 102



a. Wrought Re



b. CVD Re



c. CVD Re-5W

50 μ M

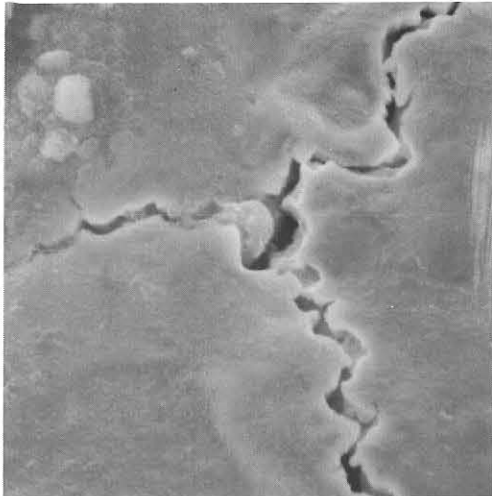
	TEMPERATURE	TIME	[O] POTENTIAL
+	800°C	130 Hrs.	100 ppm
0	550°C	70 Hrs.	50 ppm
-	300°C	10 Hrs.	2 ppm

— NO EXPOSURE
 R RECRYSTALLIZED
 A AS-RECEIVED
 ▽ SMOOTH BAR

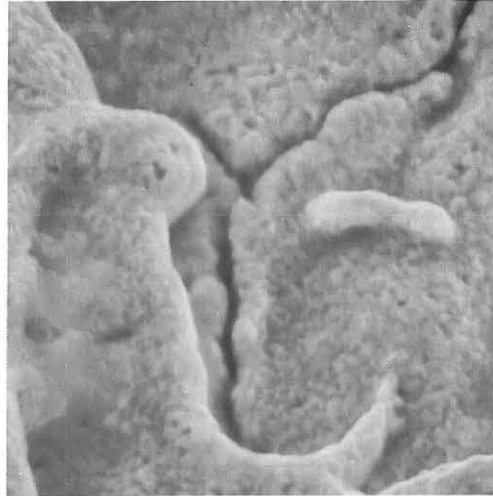
a. b.
 15 μ M

Typical high magnification fractographs for wrought Re, CVD Re and CVD Re-5W specimens.

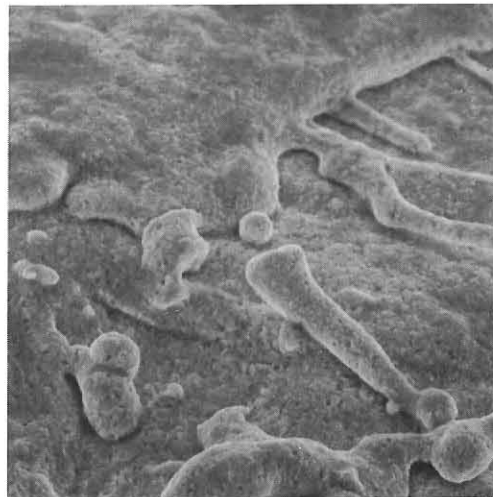
Fig. 103



a. As-received



b. +++



c. +++

	TEMPERATURE	TIME	[O] POTENTIAL
+	800°C	130 Hrs.	100 ppm
0	550°C	70 Hrs.	50 ppm
-	300°C	10 Hrs.	2 ppm

— NO EXPOSURE
 R RECRYSTALLIZED
 A AS-RECEIVED
 ▽ SMOOTH BAR

a. & b. 6 μM
 c. 15 μM

Surface characterization of selected CVD Re specimens as a function of Na exposure.

Fig. 104

**RE-5W ALLOY FRACTURE ENERGY
AS A FUNCTION OF
OXYGEN CONCENTRATION AND TEMPERATURE
IN MOLTEN SODIUM (TIME= 10 HRS)**

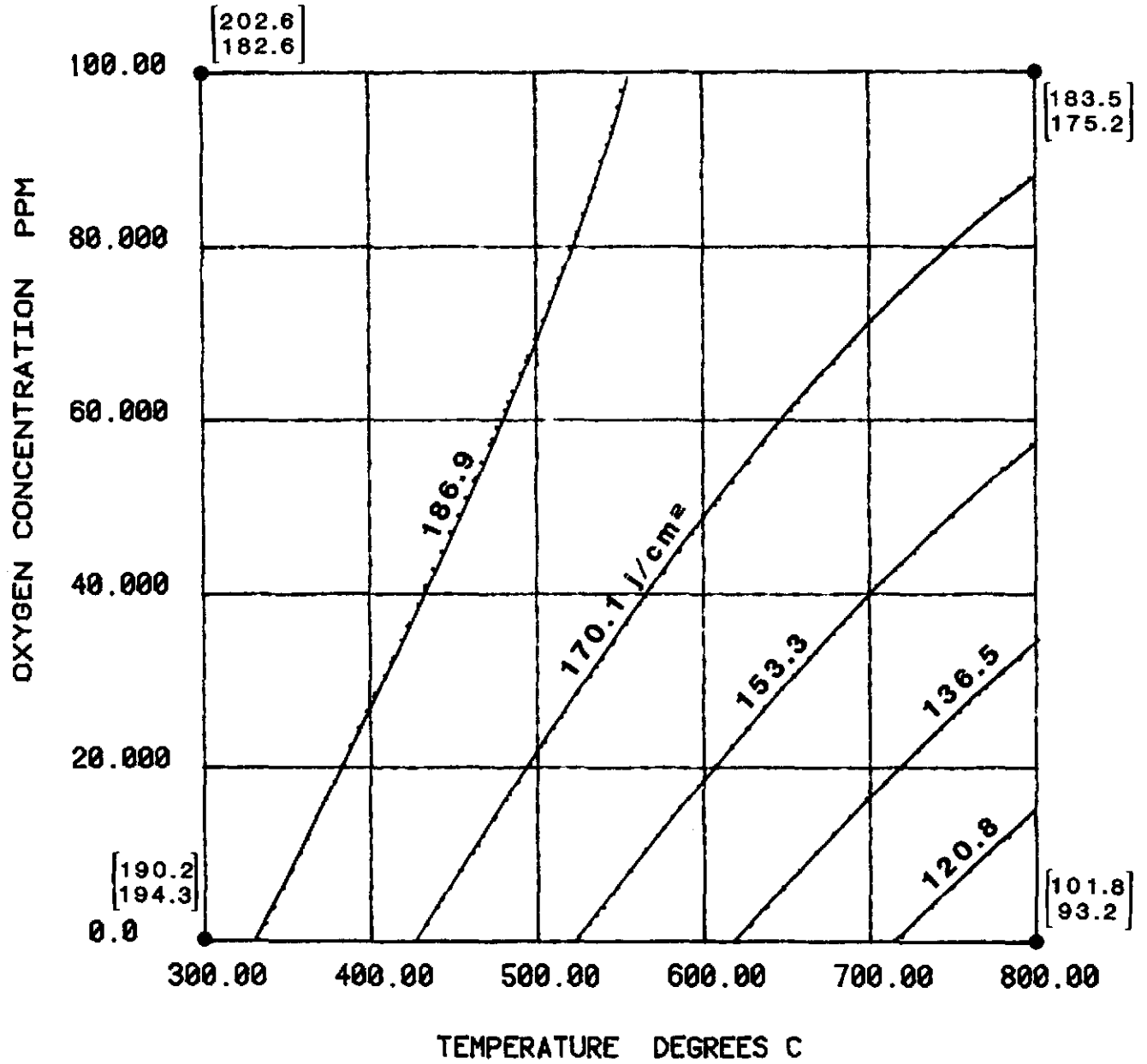


Fig. 105

**RE-5W ALLOY FRACTURE ENERGY
AS A FUNCTION OF
OXYGEN CONCENTRATION AND TEMPERATURE
IN MOLTEN SODIUM (TIME = 70 HRS)**

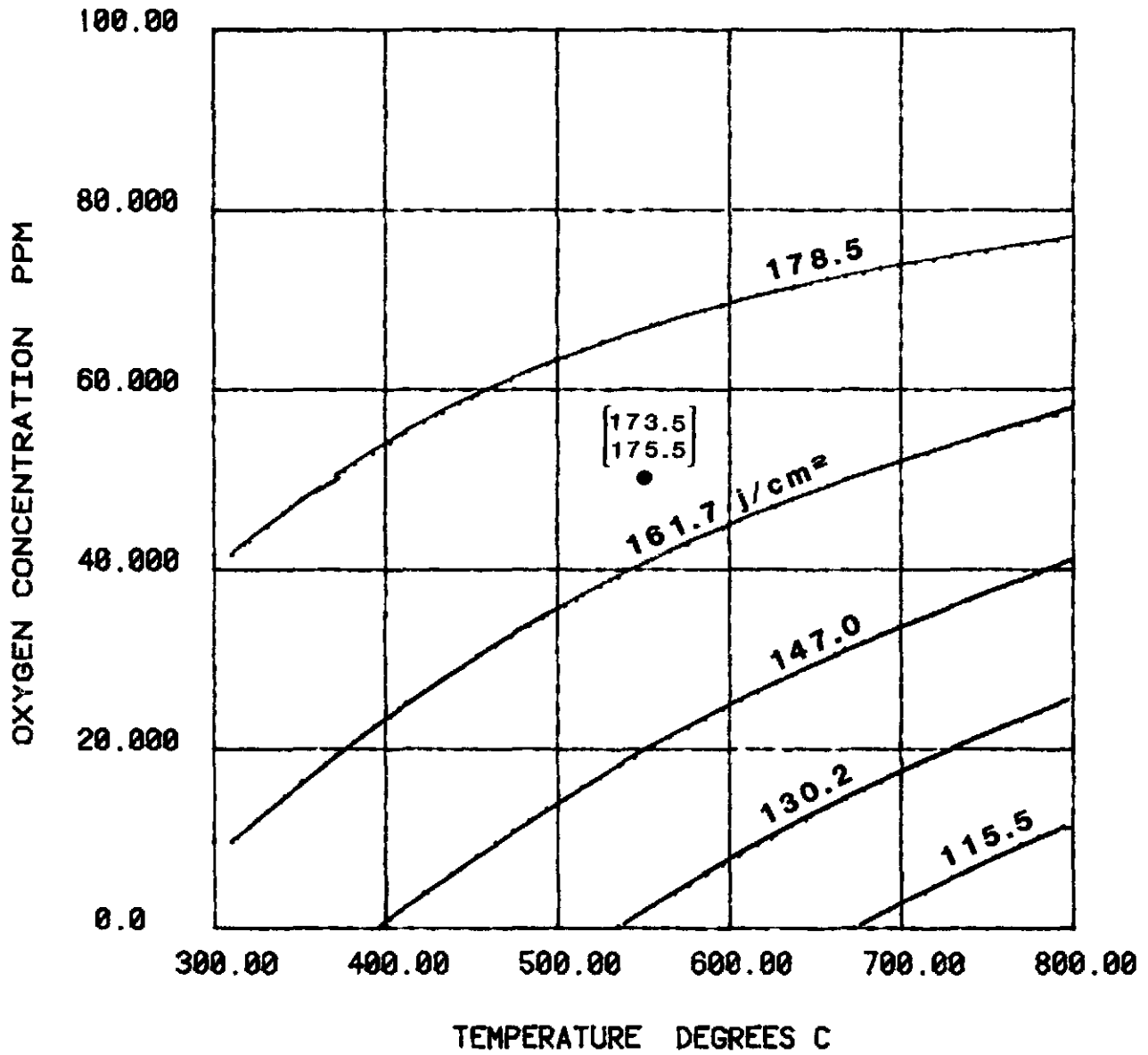


Fig. 106

**RE-5W ALLOY FRACTURE ENERGY
AS A FUNCTION OF
OXYGEN CONCENTRATION AND TEMPERATURE
IN MOLTEN SODIUM (TIME = 130 HRS)**

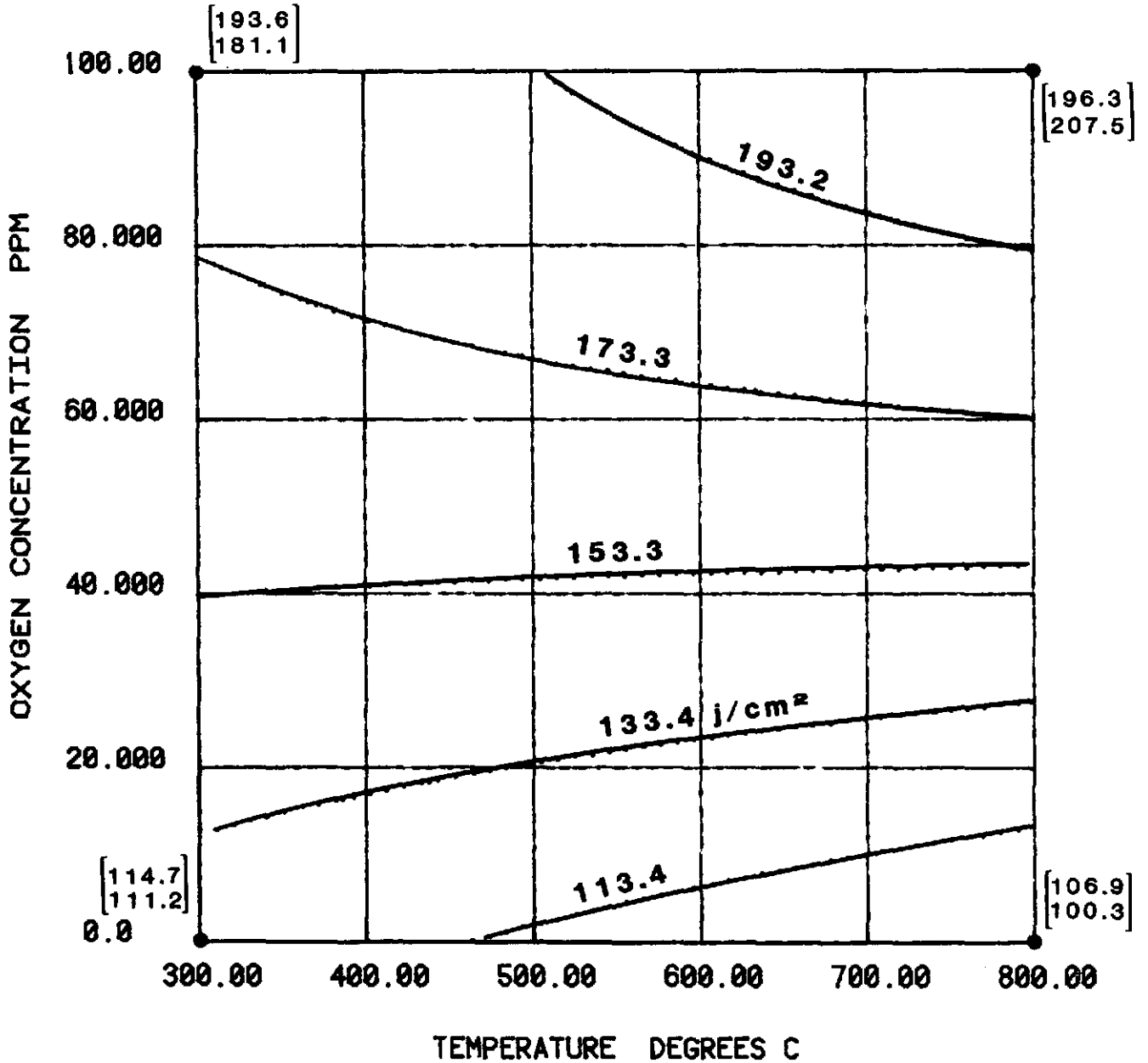


Fig. 107

WEIGHT CHANGE OF WROUGHT RE
AS A FUNCTION OF
OXYGEN CONCENTRATION AND TEMPERATURE
IN MOLTEN SODIUM (TIME=10 HRS)

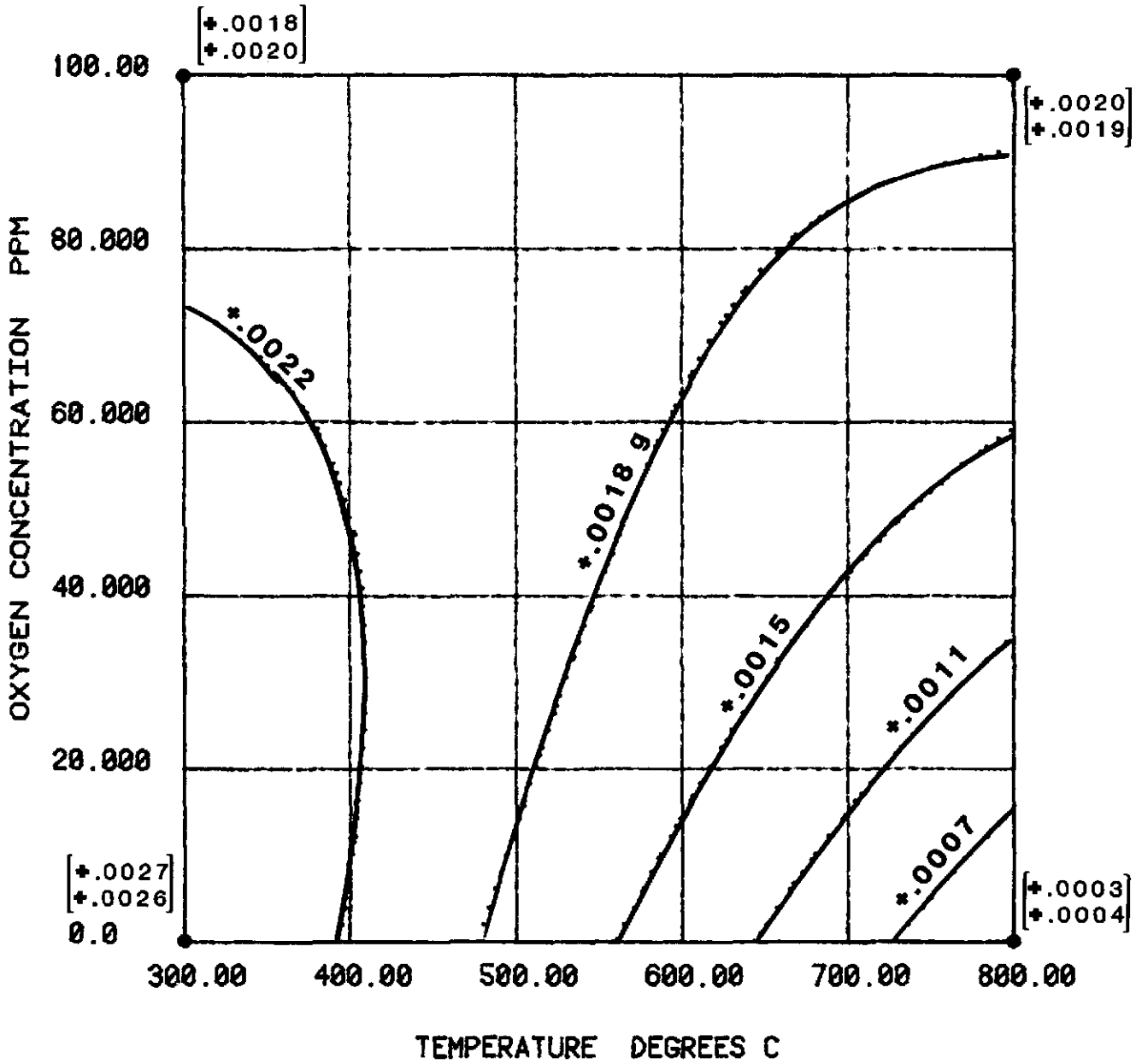


Fig. 108

WEIGHT CHANGE OF WROUGHT RE
 AS A FUNCTION OF
 OXYGEN CONCENTRATION AND TEMPERATURE
 IN MOLTEN SODIUM (TIME=70 HRS)

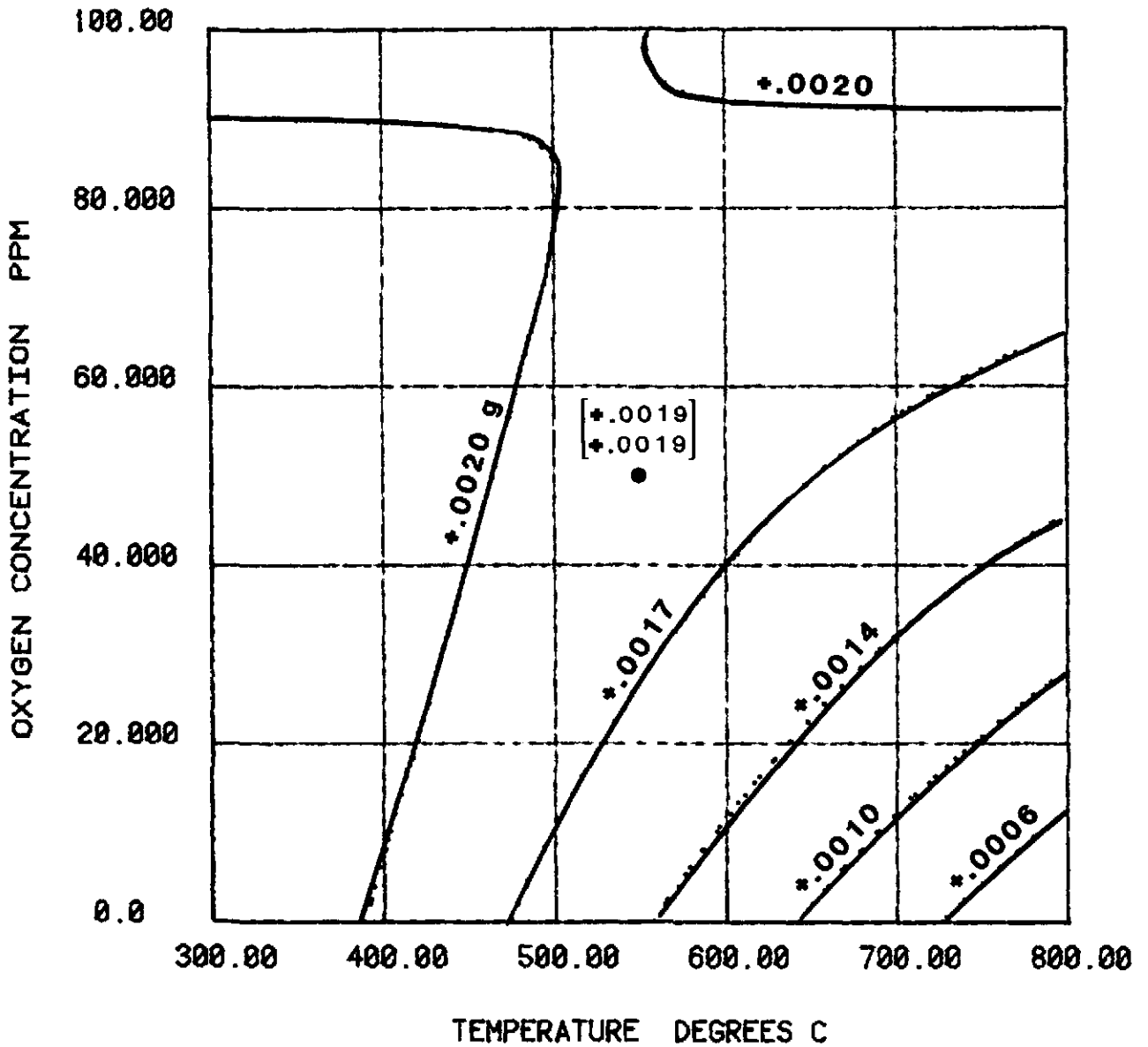


Fig. 109

WEIGHT CHANGE OF WROUGHT RE
AS A FUNCTION OF
OXYGEN CONCENTRATION AND TEMPERATURE
IN MOLTEN SODIUM (TIME=130 HRS)

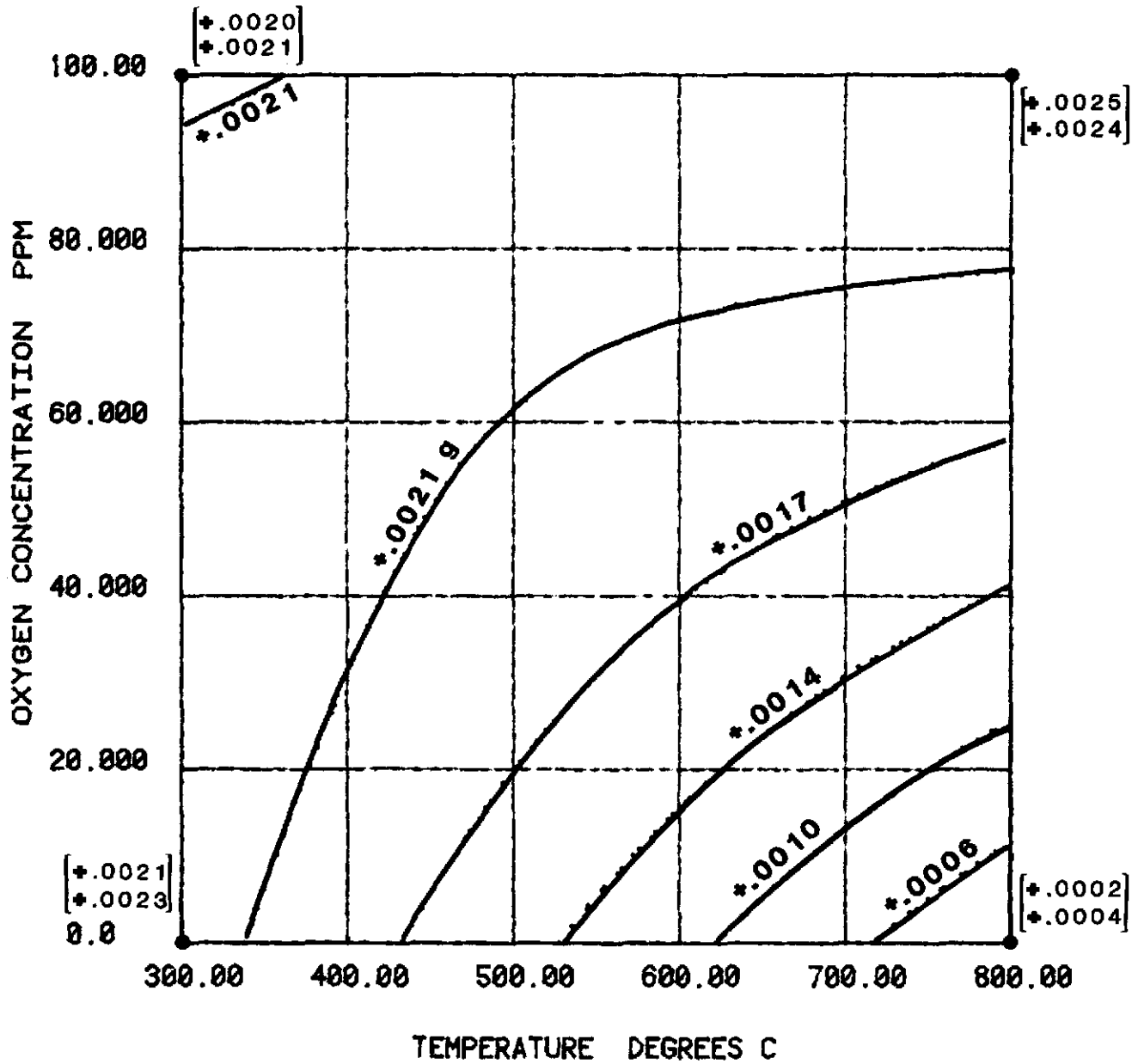


Fig. 110

WEIGHT CHANGE OF CVD RE
 AS A FUNCTION OF
 OXYGEN CONCENTRATION AND TEMPERATURE
 IN MOLTEN SODIUM (TIME=10 HRS)

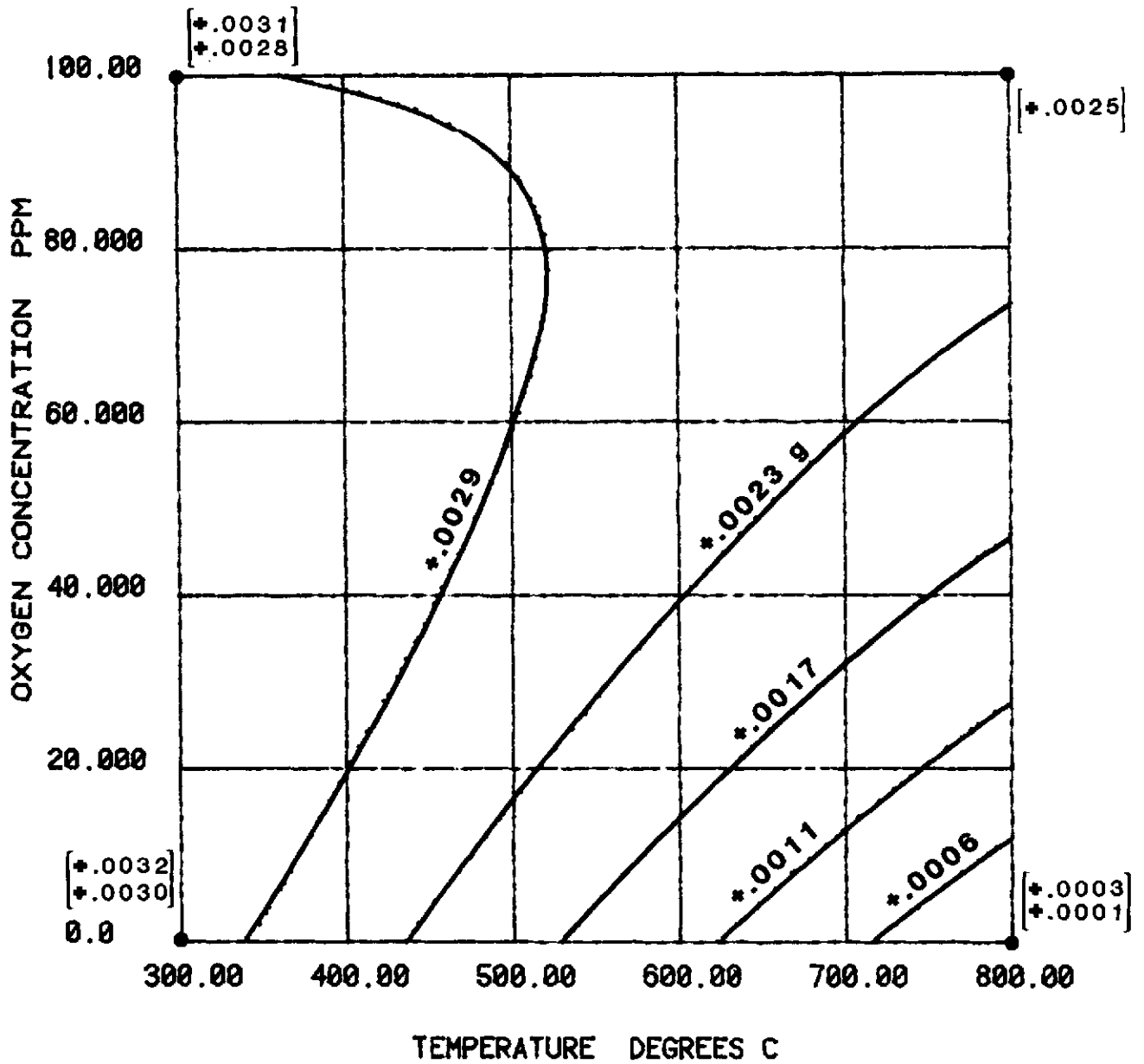


Fig. 111

WEIGHT CHANGE OF CVD RE
 AS A FUNCTION OF
 OXYGEN CONCENTRATION AND TEMPERATURE
 IN MOLTEN SODIUM (TIME=70 HRS)

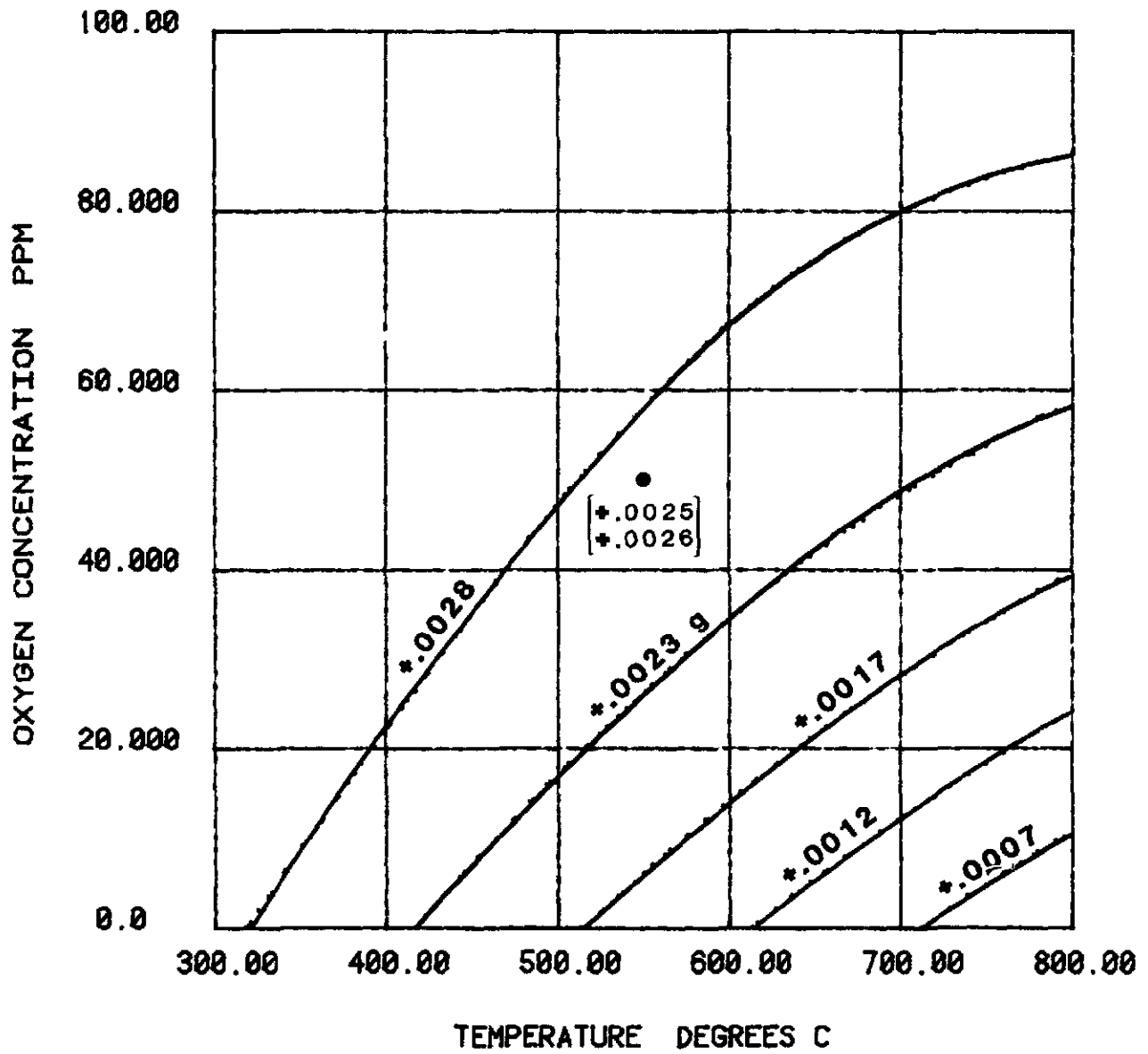


Fig. 112

WEIGHT CHANGE OF CVD RE
 AS A FUNCTION OF
 OXYGEN CONCENTRATION AND TEMPERATURE
 IN MOLTEN SODIUM (TIME=130 HRS)

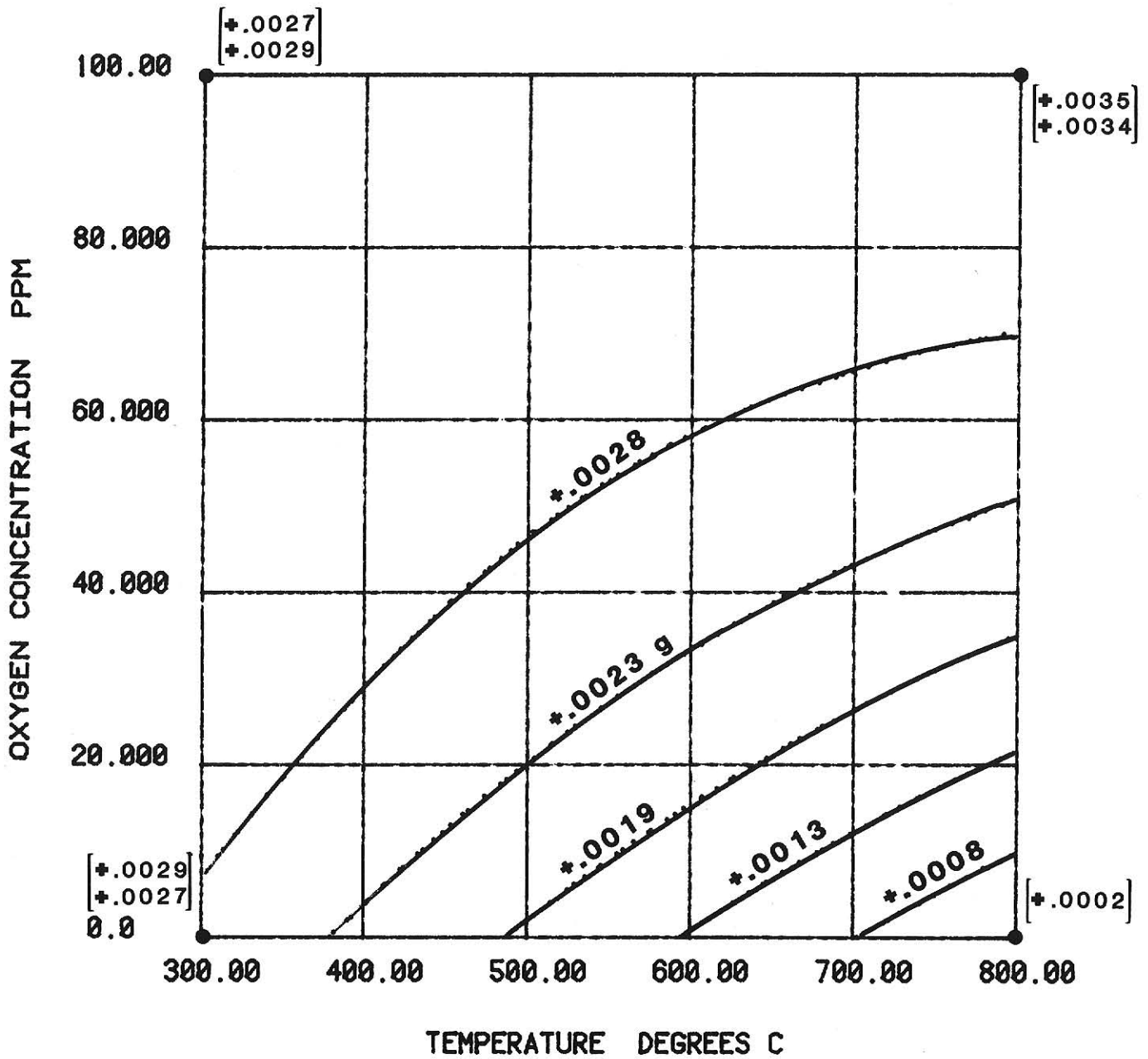
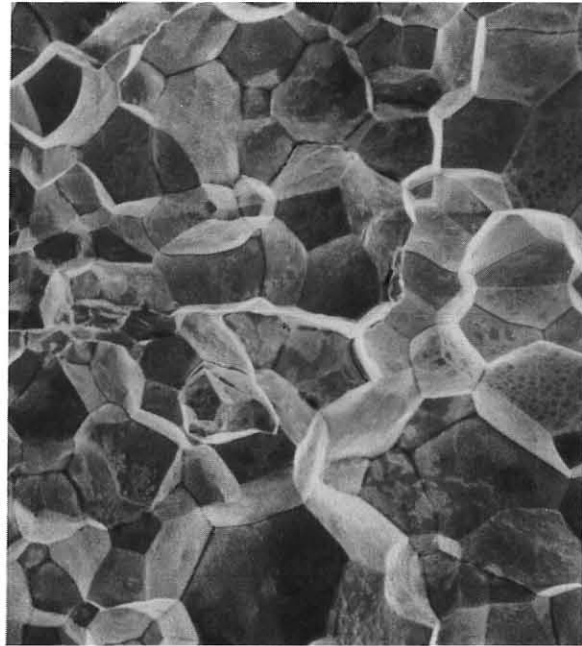


Fig. 113



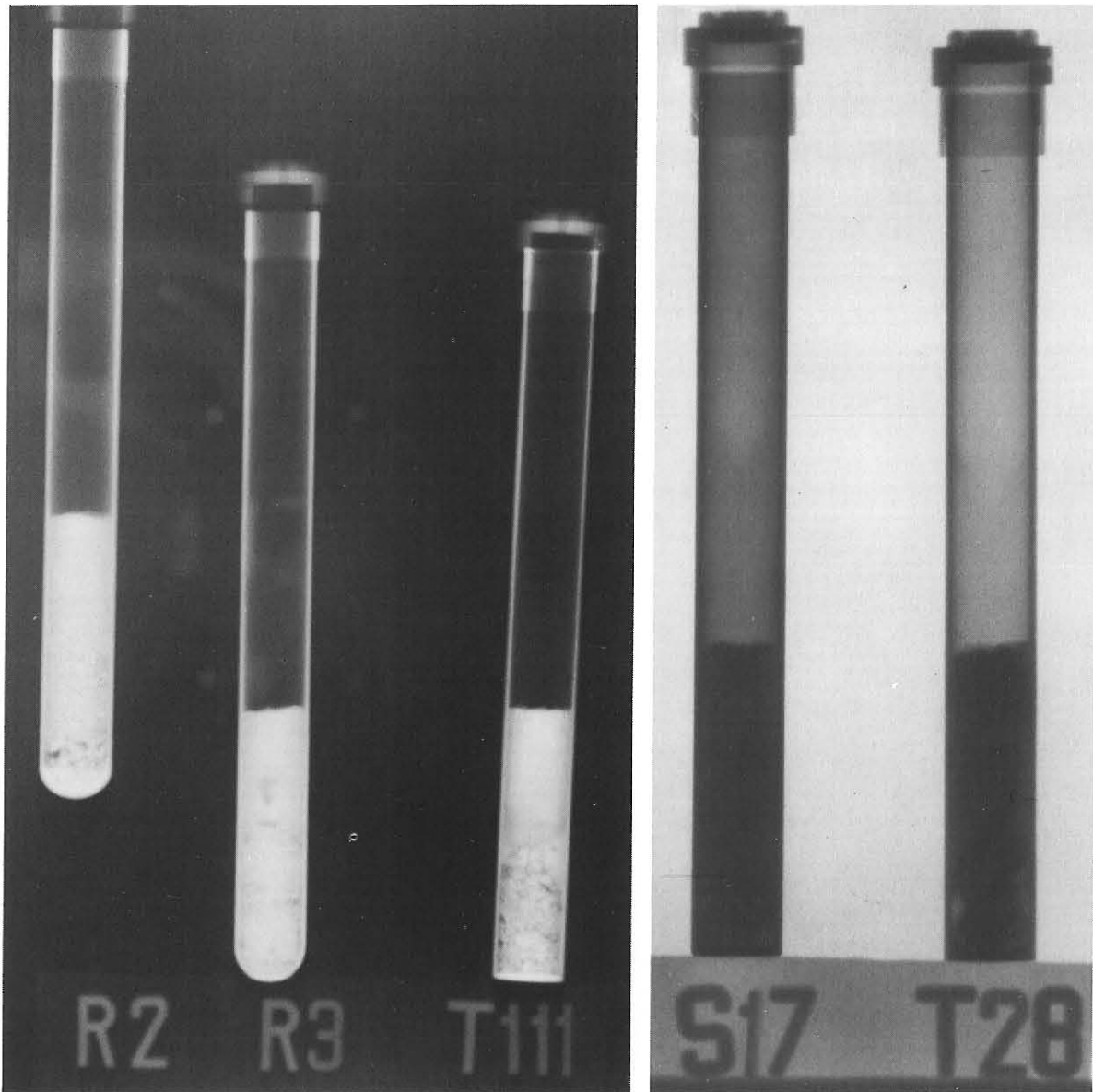
a. Quasi-cleavage.



b. Intergranular.

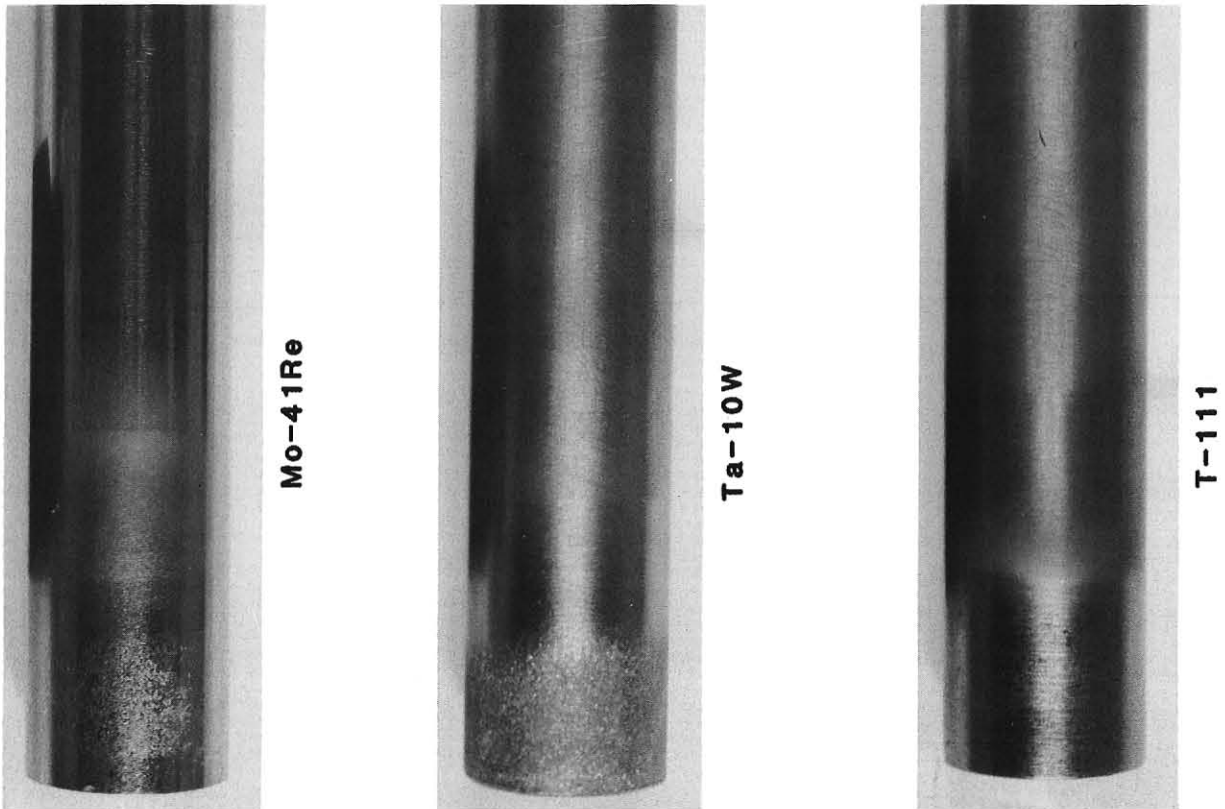
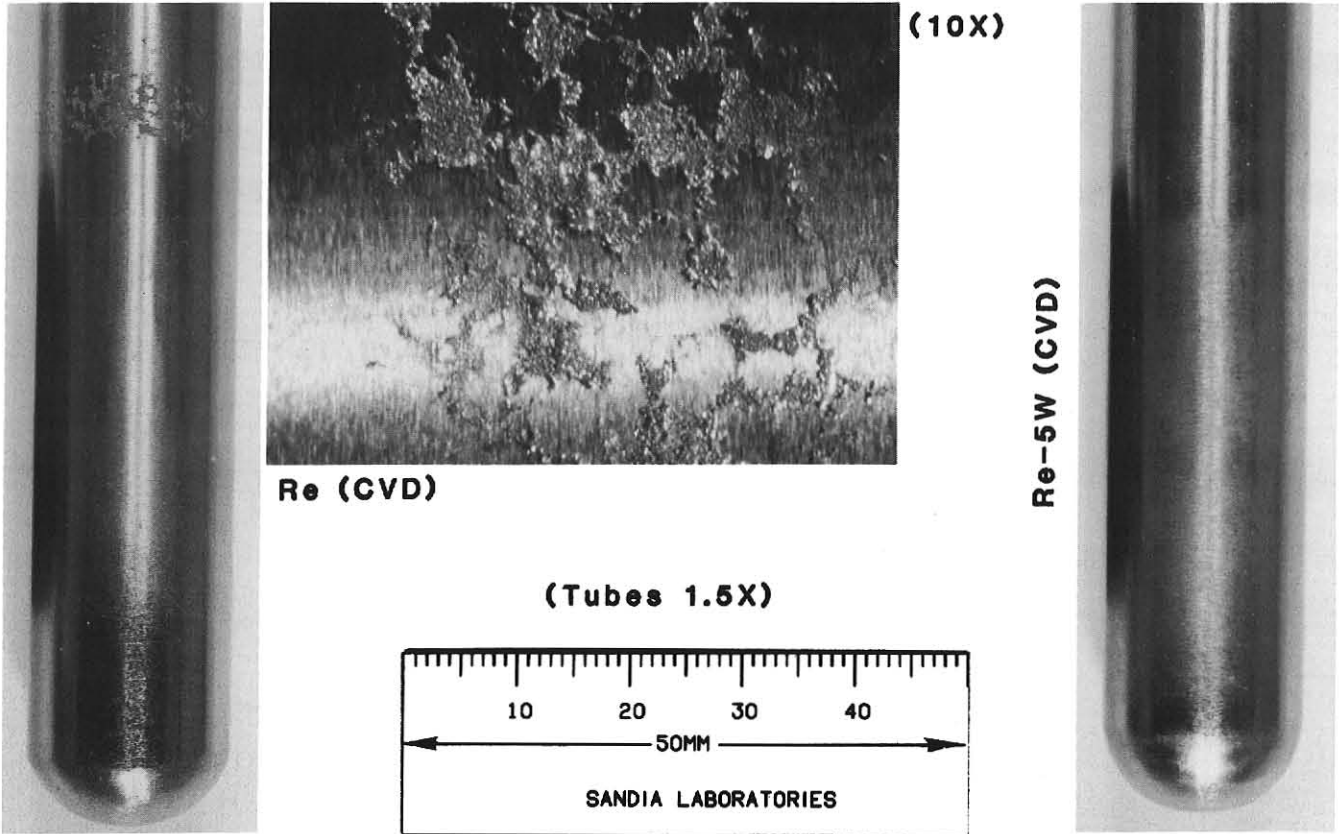
Typical W fractography.

Fig. 114



CONTACT RADIOGRAPHS OF LOAD TUBES AFTER TESTING.

Fig. 115



Outside Surface Appearance of Tubes After Testing

Fig. 116

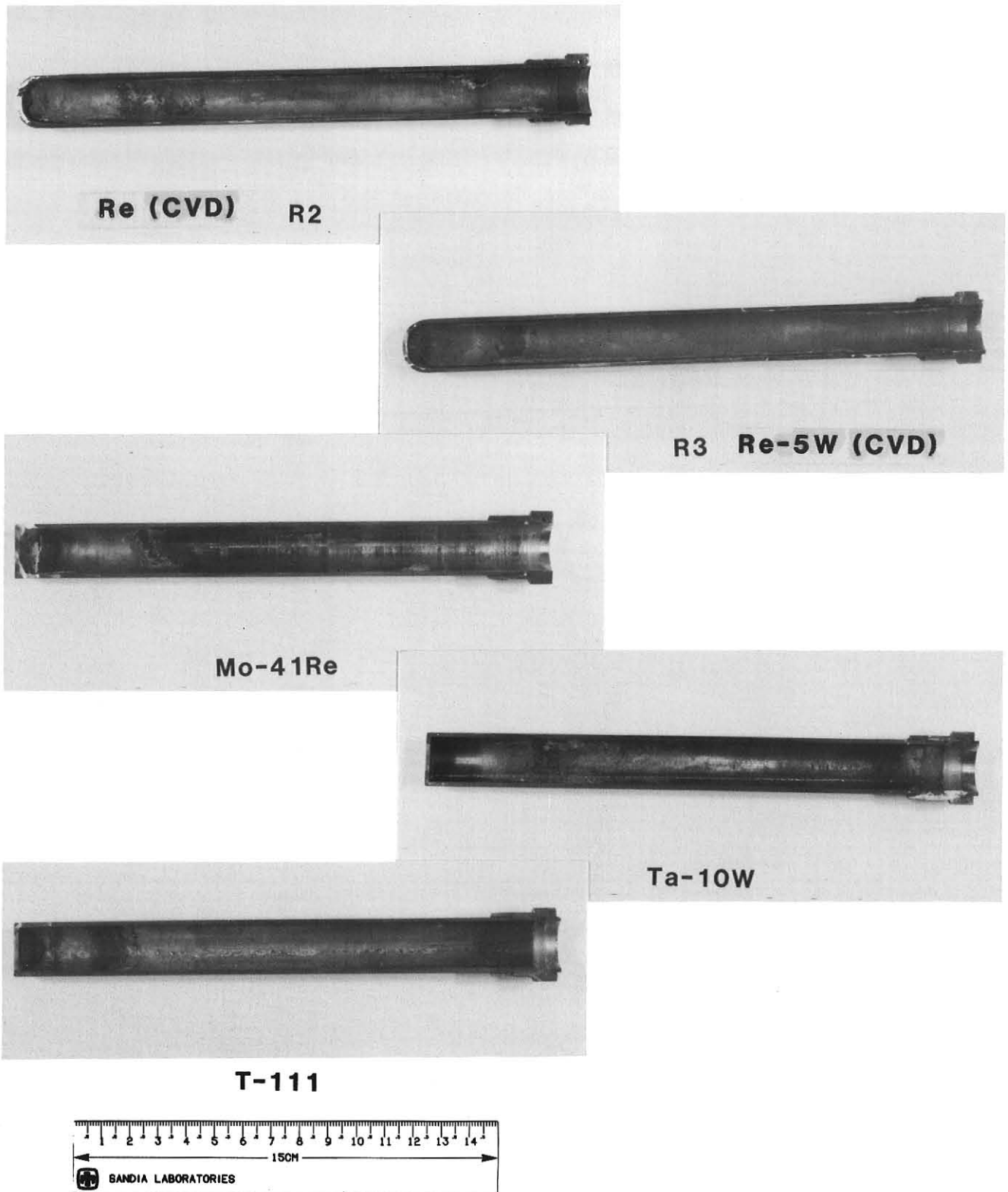


Fig. 117 Inside Surface Appearance of Tubes After Testing

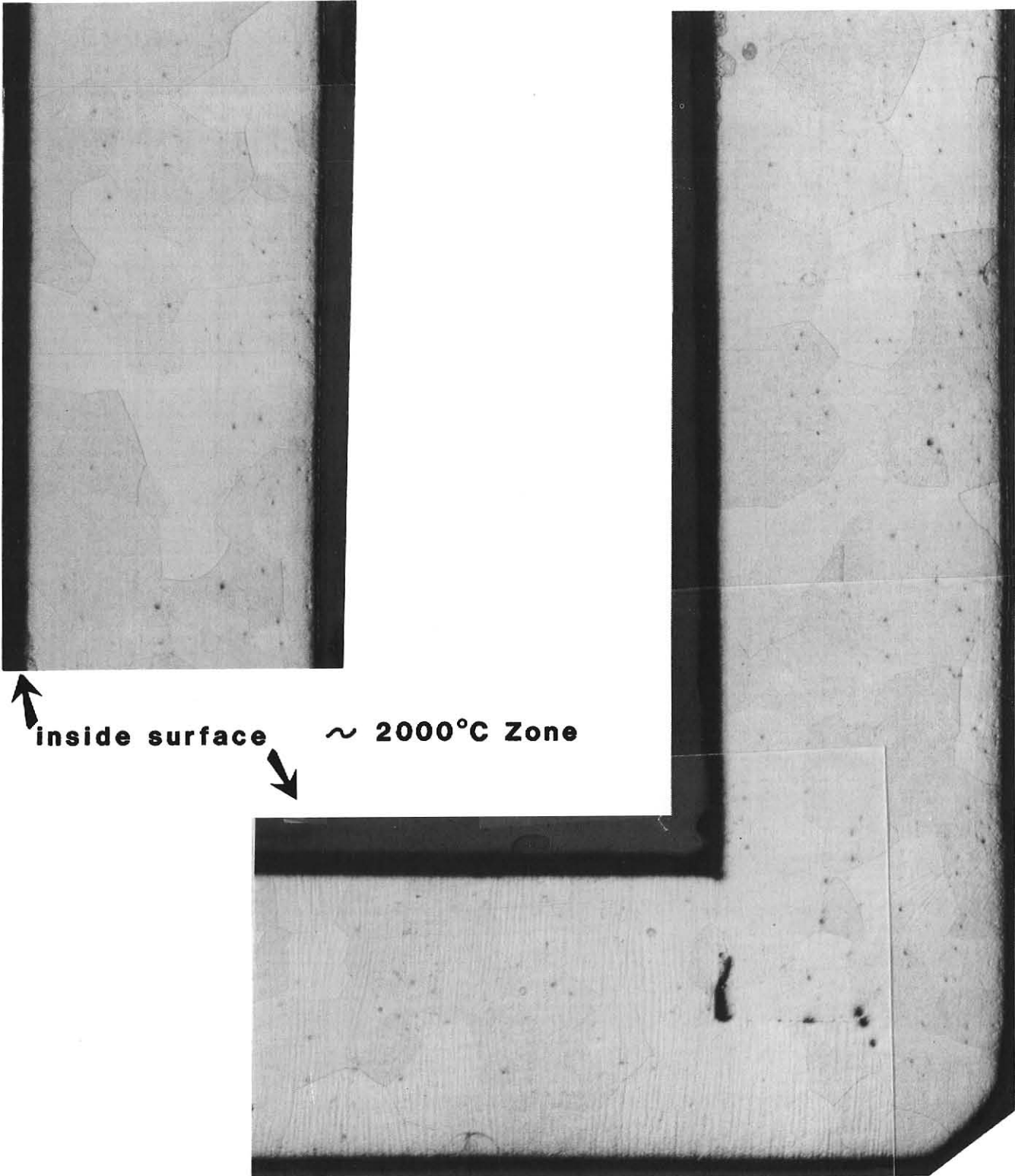


Fig. 118 TA-10W ALLOY TUBE METALLOGRAPHIC SECTIONS.

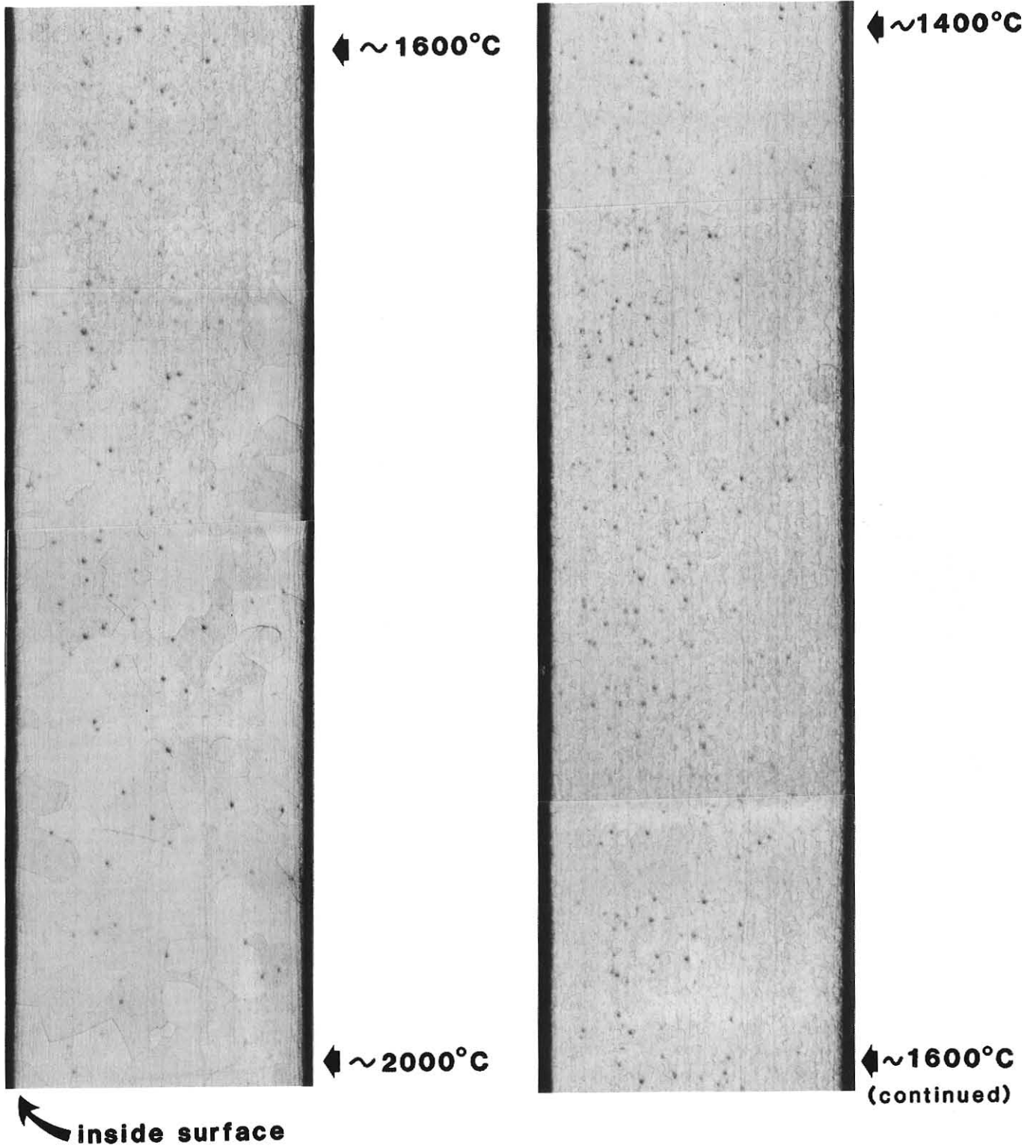
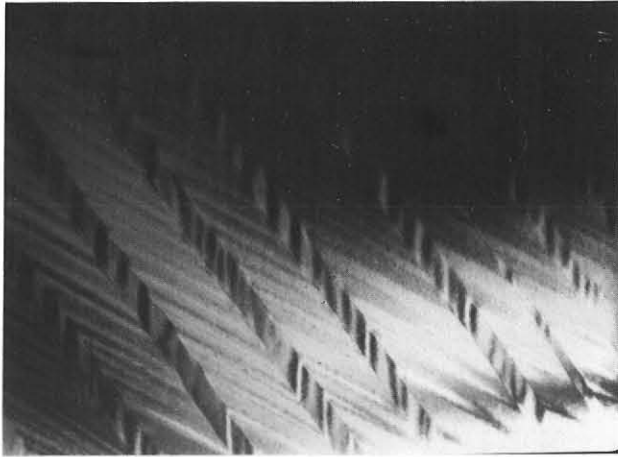
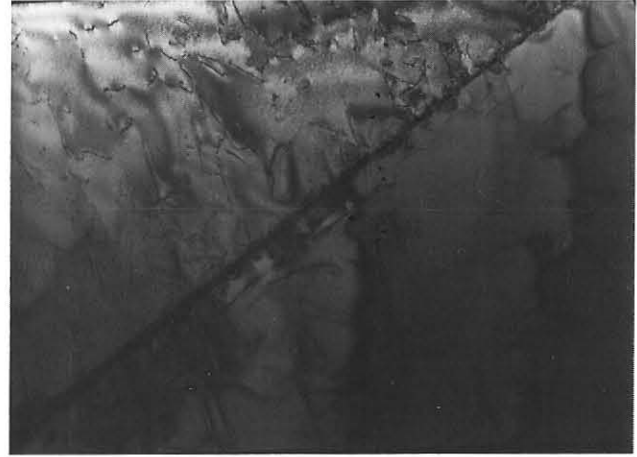


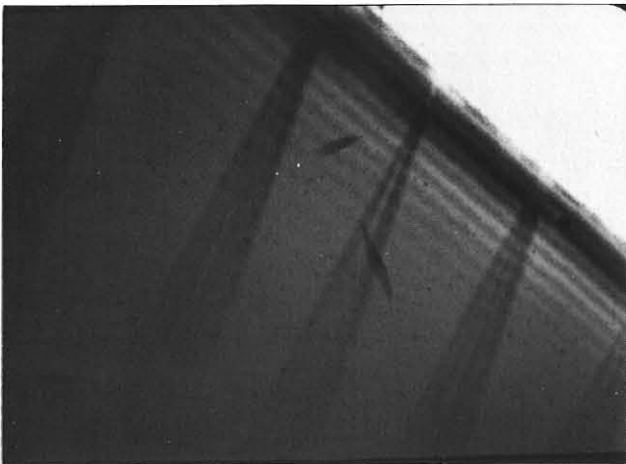
Fig. 119 TA-10W ALLOY TUBE METALLOGRAPHIC SECTIONS.



(A)



(B)



(C)

	TEMPERATURE	TIME	[0] POTENTIAL
+	800°C	130 Hrs.	100 ppm
0	550°C	70 Hrs.	50 ppm
-	300°C	10 Hrs.	2 ppm

— NO EXPOSURE
 R RECRYSTALLIZED
 A AS-RECEIVED
 ▽ SMOOTH BAR

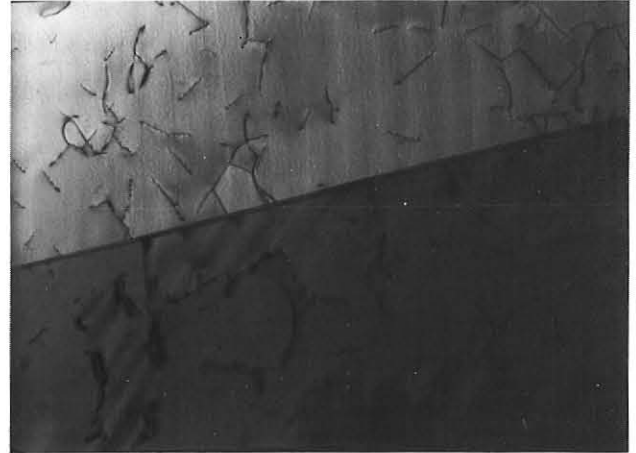


A. .7 μM
B. .25 μM
C. .5 μM

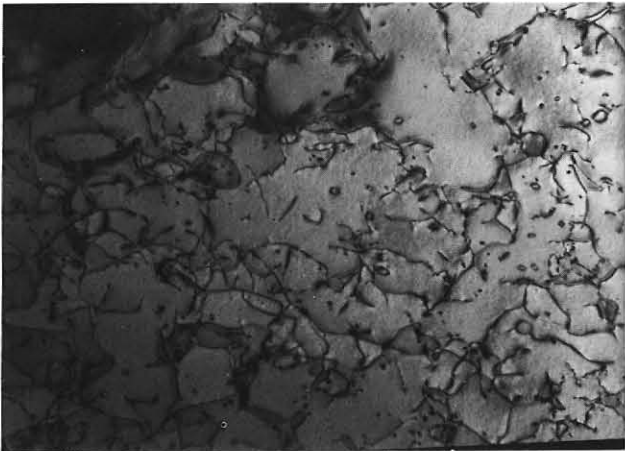
Fig. 120 TA-10W ALLOY TUBE TEM MICROSTRUCTURES.



(A)



(B)



(C)

	TEMPERATURE	TIME	[O] POTENTIAL
+	800°C	130 Hrs.	100 ppm
0	550°C	70 Hrs.	50 ppm
-	300°C	10 Hrs.	2 ppm

— NO EXPOSURE
 R RECRYSTALLIZED
 A AS-RECEIVED
 ▽ SMOOTH BAR



A. 1 μM
B. .5 μM
C. .25 μM

Fig. 121 TA-10W ALLOY TUBE TEM MICROSTRUCTURES.

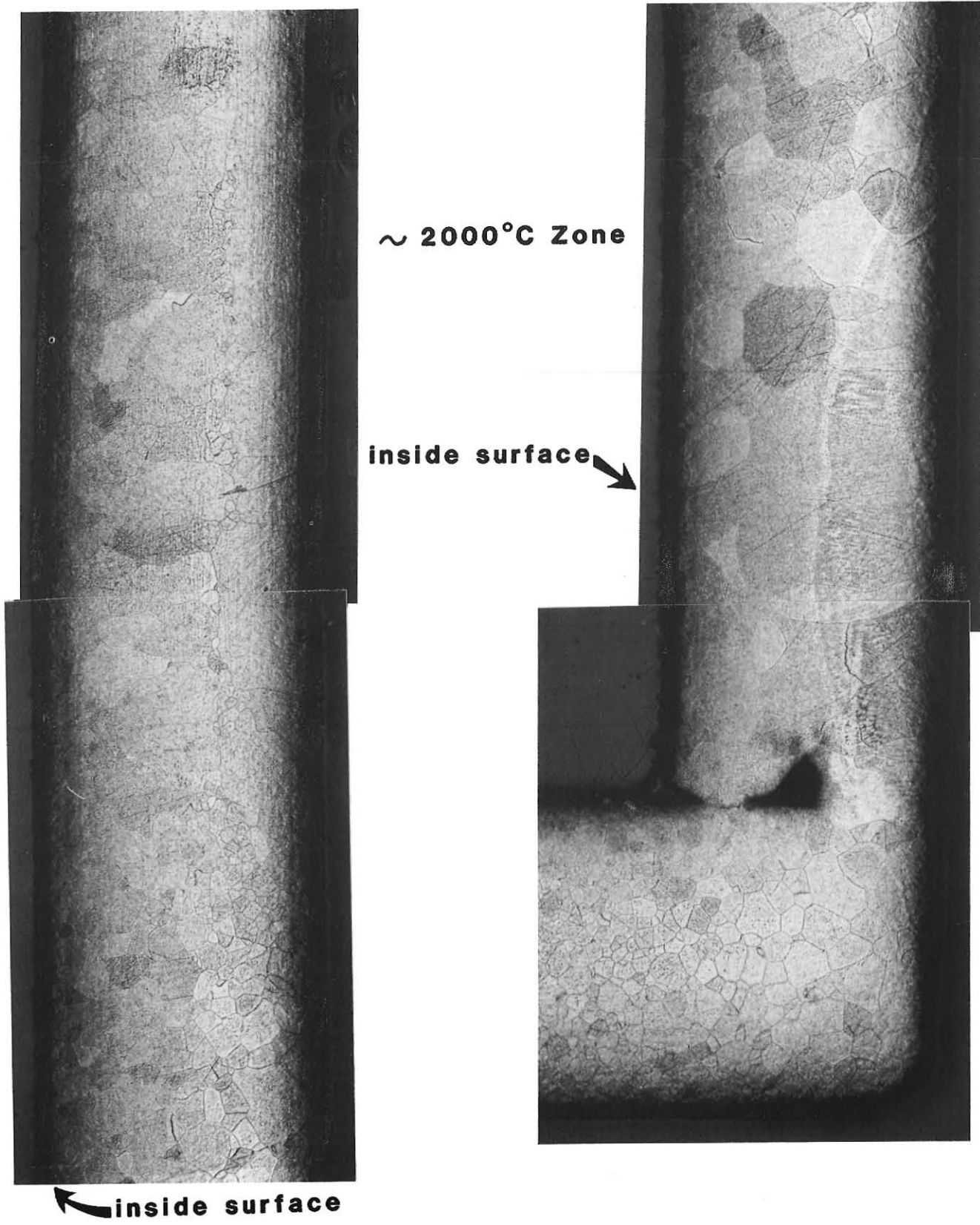


Fig. 122 T-111 ALLOY TUBE METALLOGRAPHIC SECTIONS.

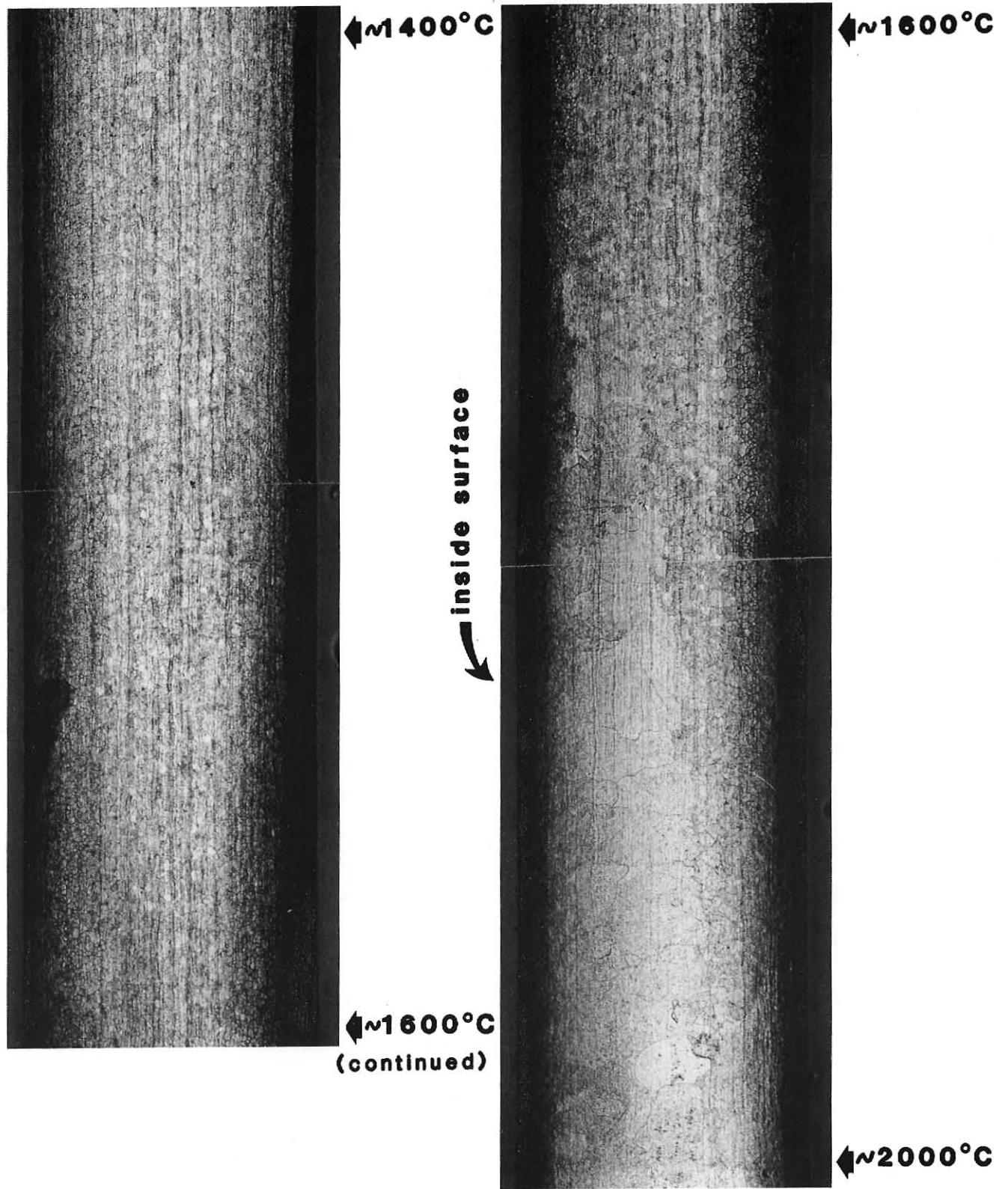


Fig. 123 T-111 ALLOY TUBE METALLOGRAPHIC SECTIONS.

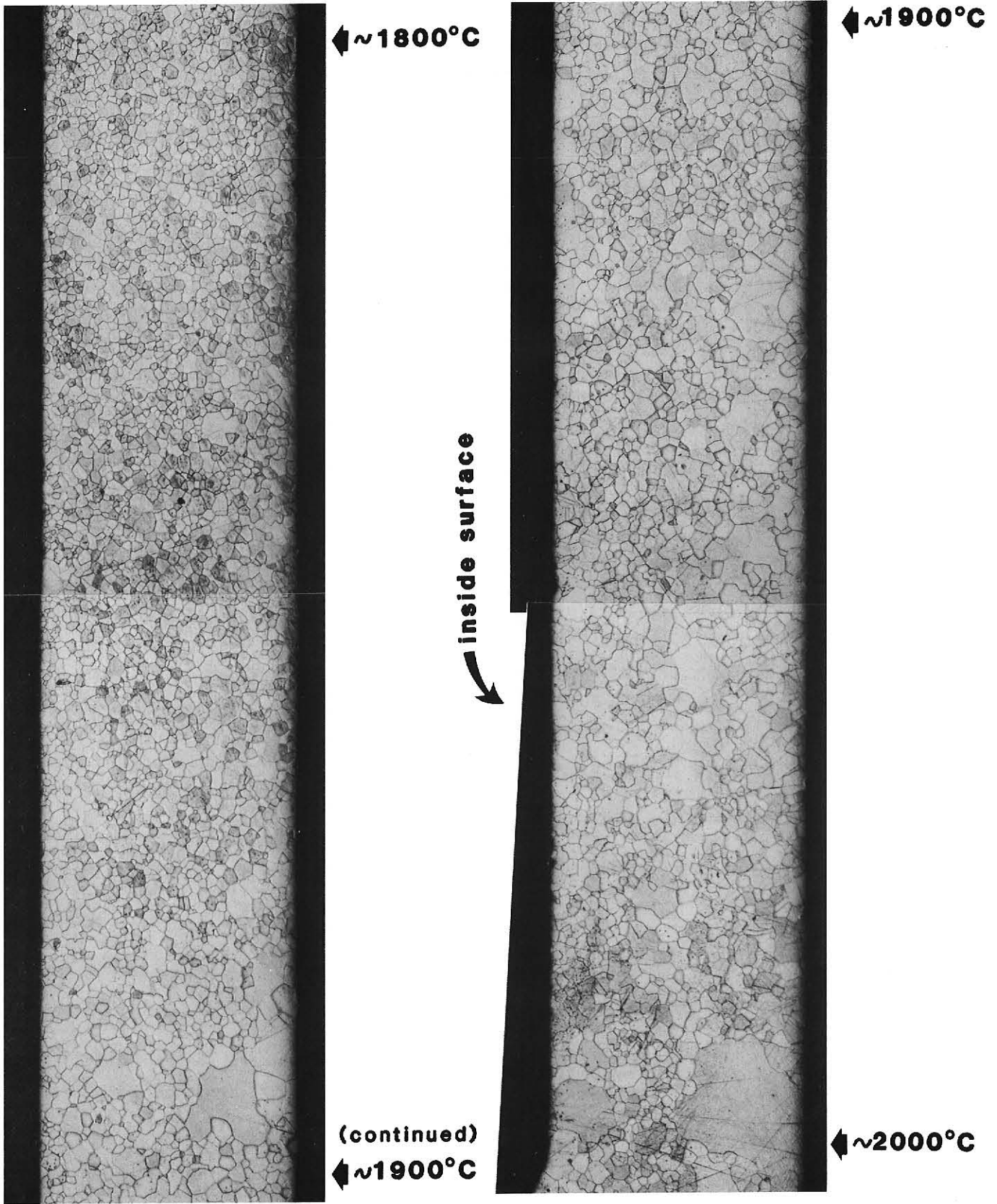
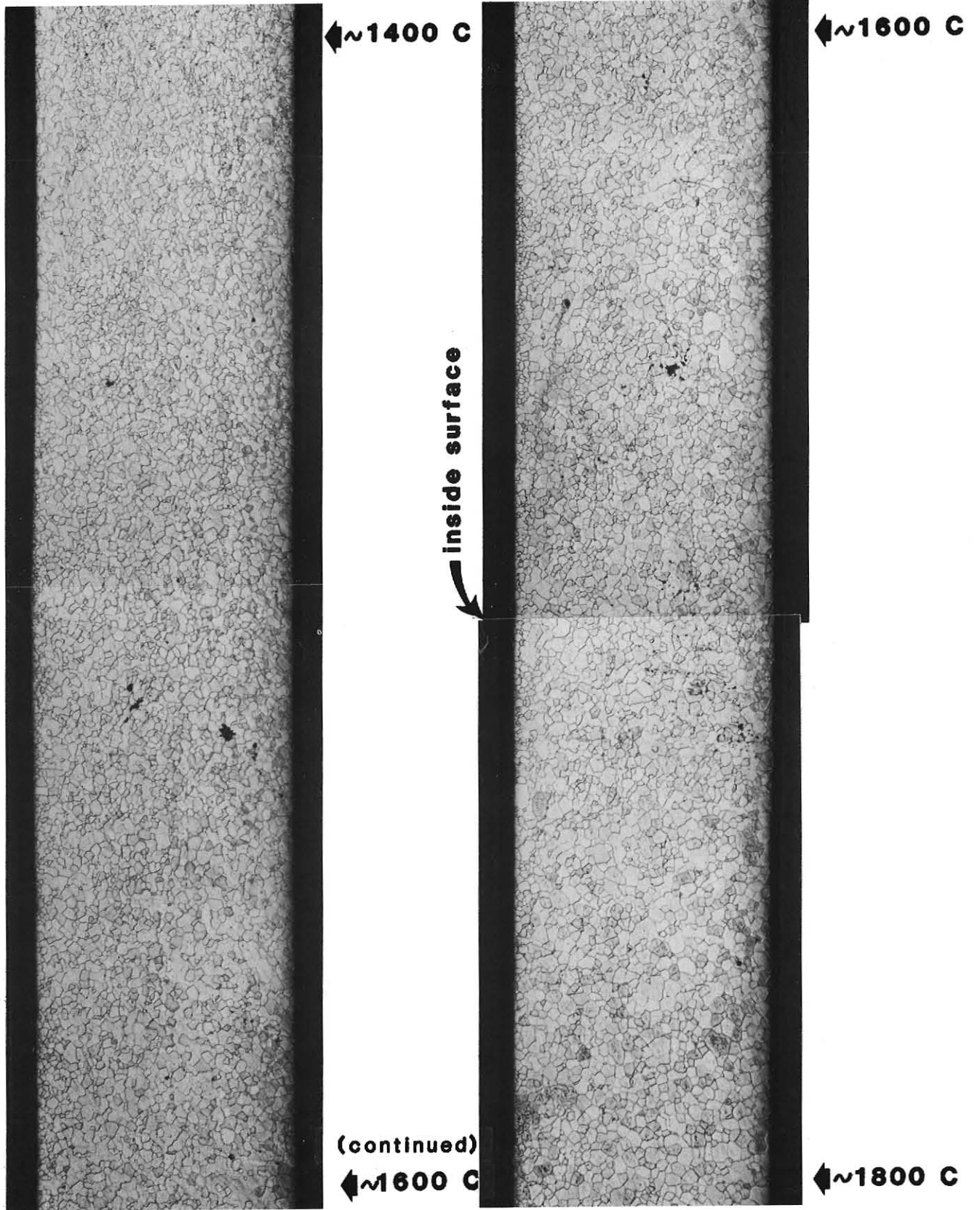


Fig. 124 Mo-41Re ALLOY TUBE METALLOGRAPHIC SECTIONS.



Mo-41Re Alloy Tube Metallographic Sections

Fig. 125

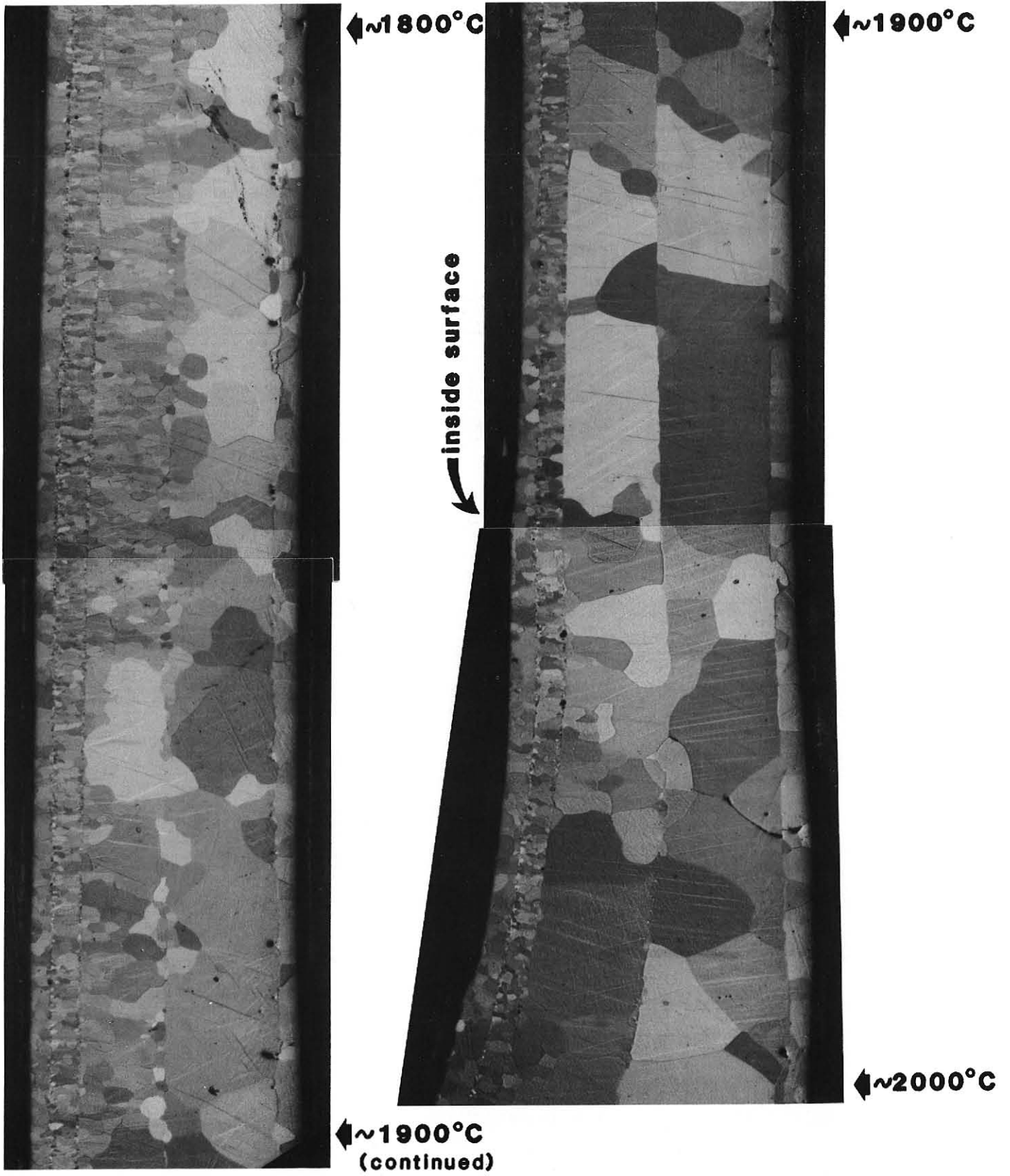


Fig. 126 CVD RE TUBE METALLOGRAPHIC SECTIONS.



Fig. 127 CVD RE TUBE METALLOGRAPHIC SECTIONS.

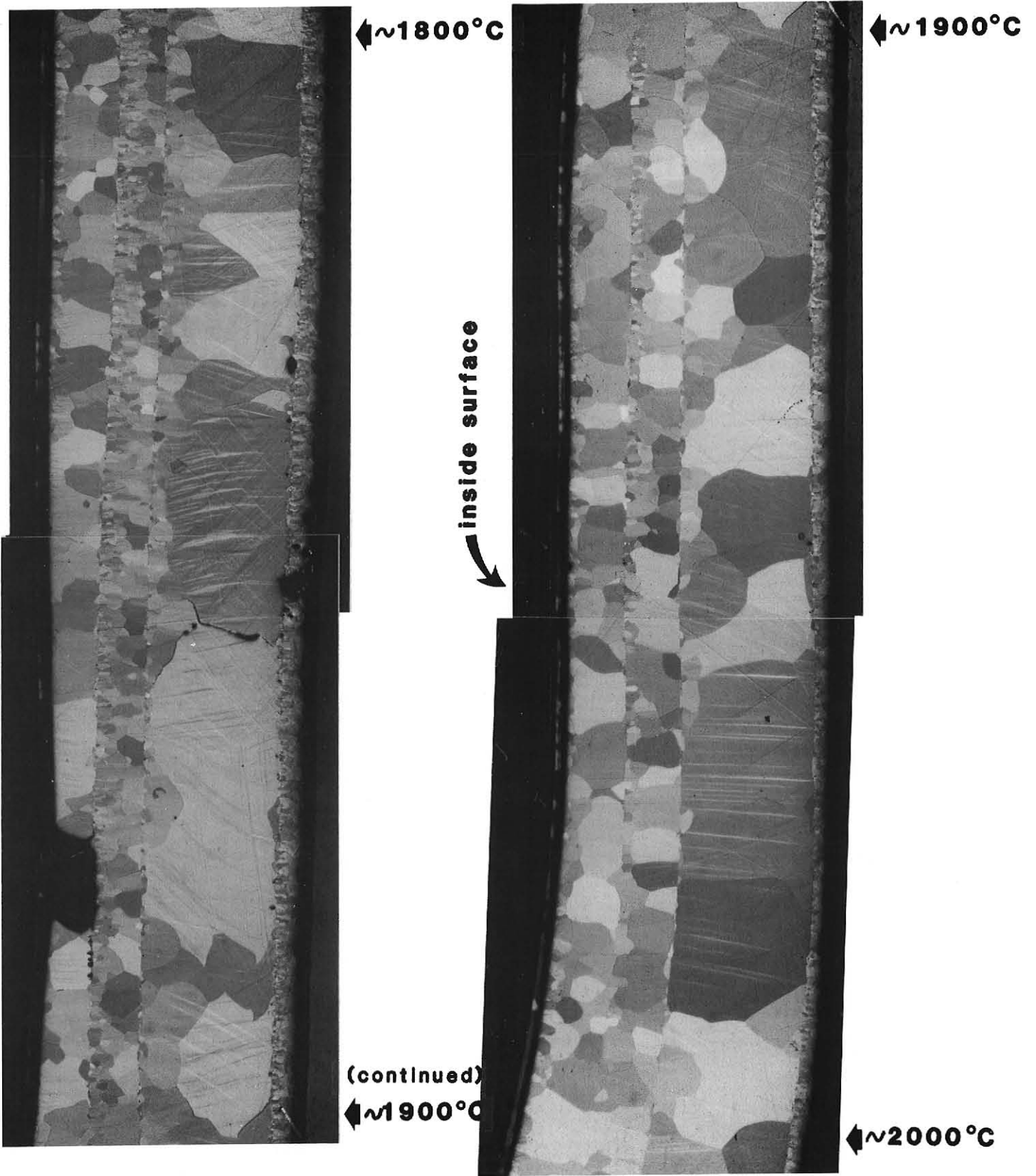


Fig. 128 CVD RE-5W ALLOY TUBE METALLOGRAPHIC SECTIONS.

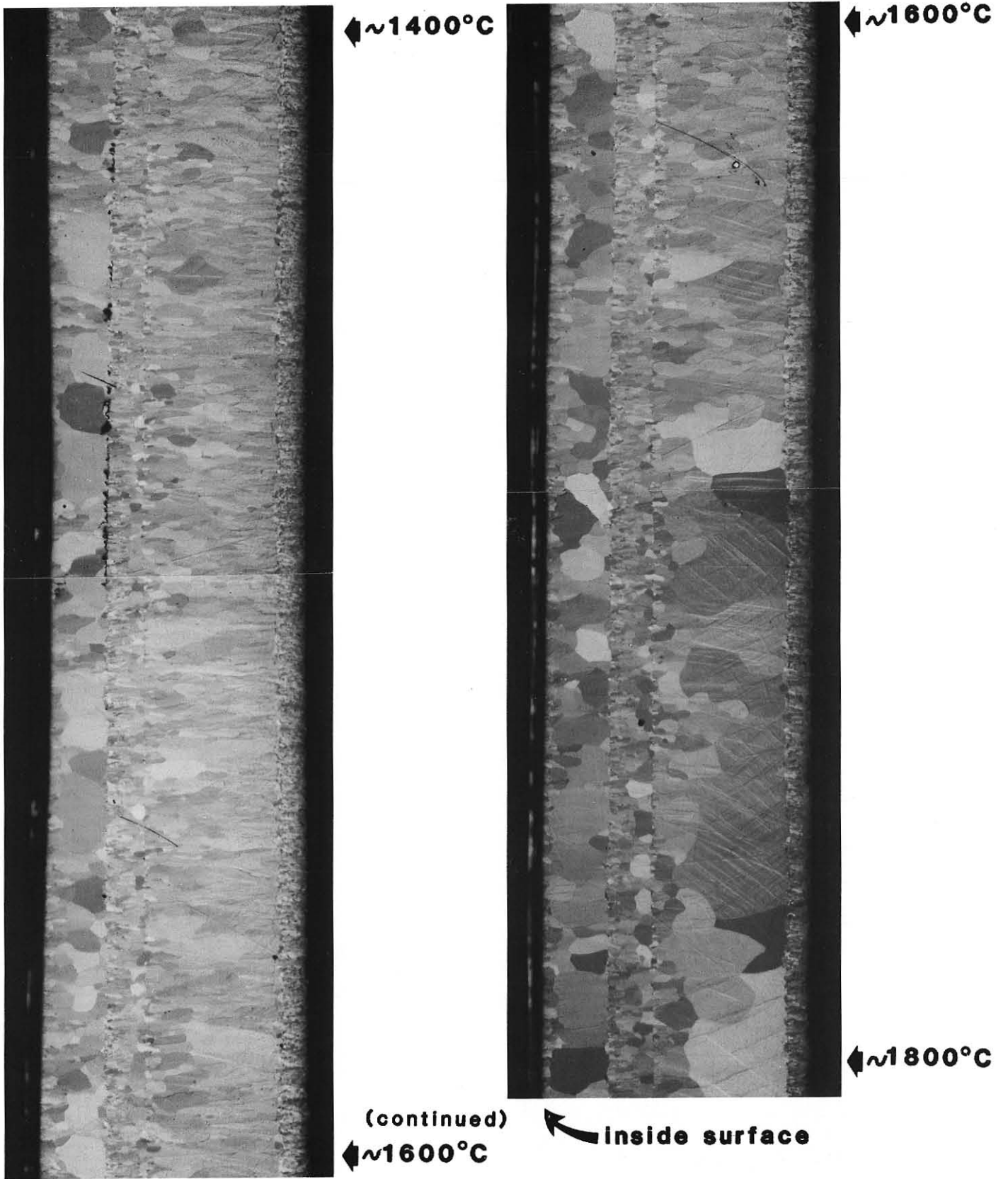


Fig. 129 CVD RE-5W ALLOY TUBE METALLOGRAPHIC SECTIONS.

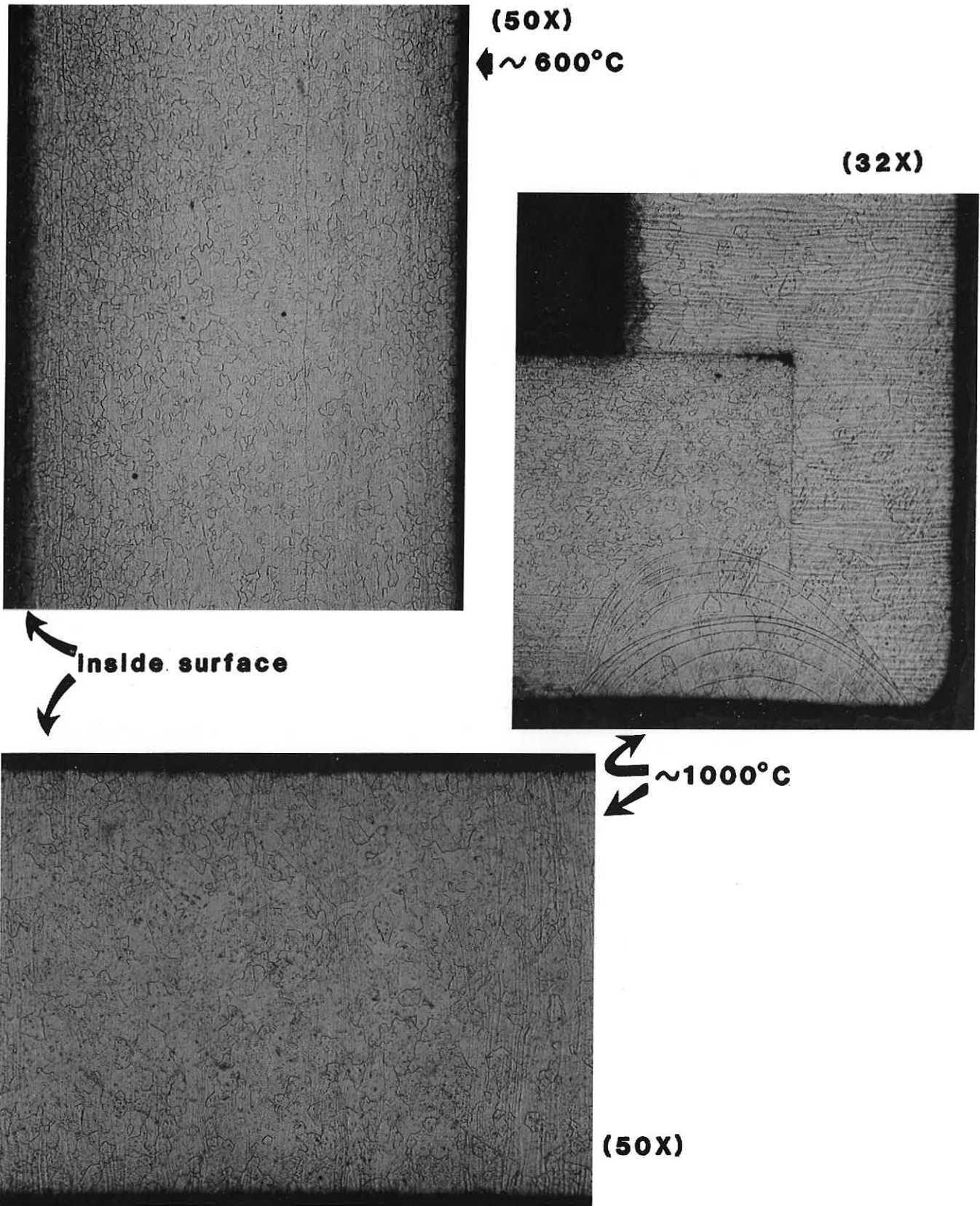


Fig. 130 TYPICAL METALLOGRAPHIC SECTIONS FOR SECOND TA-10W ALLOY TUBE.

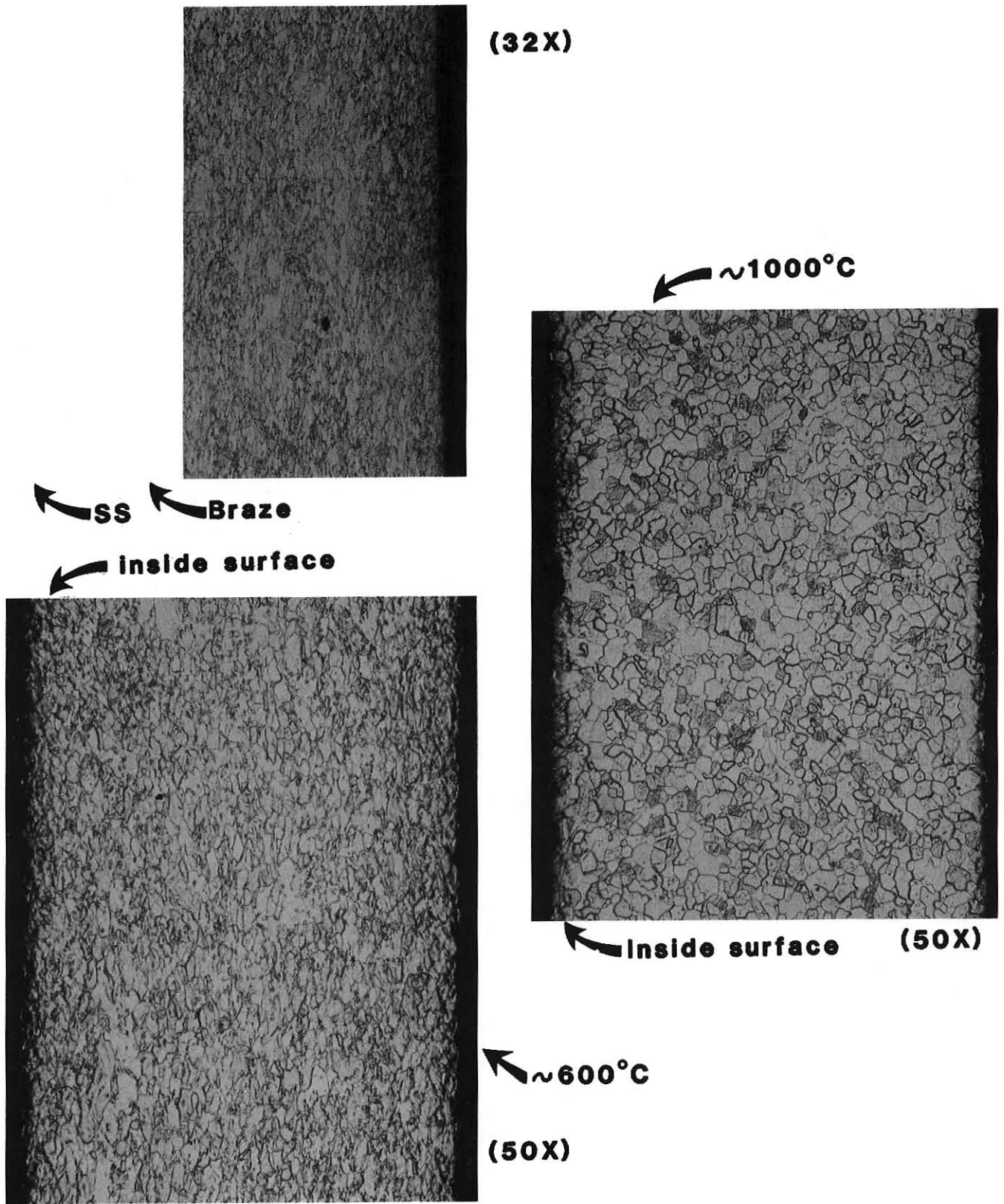
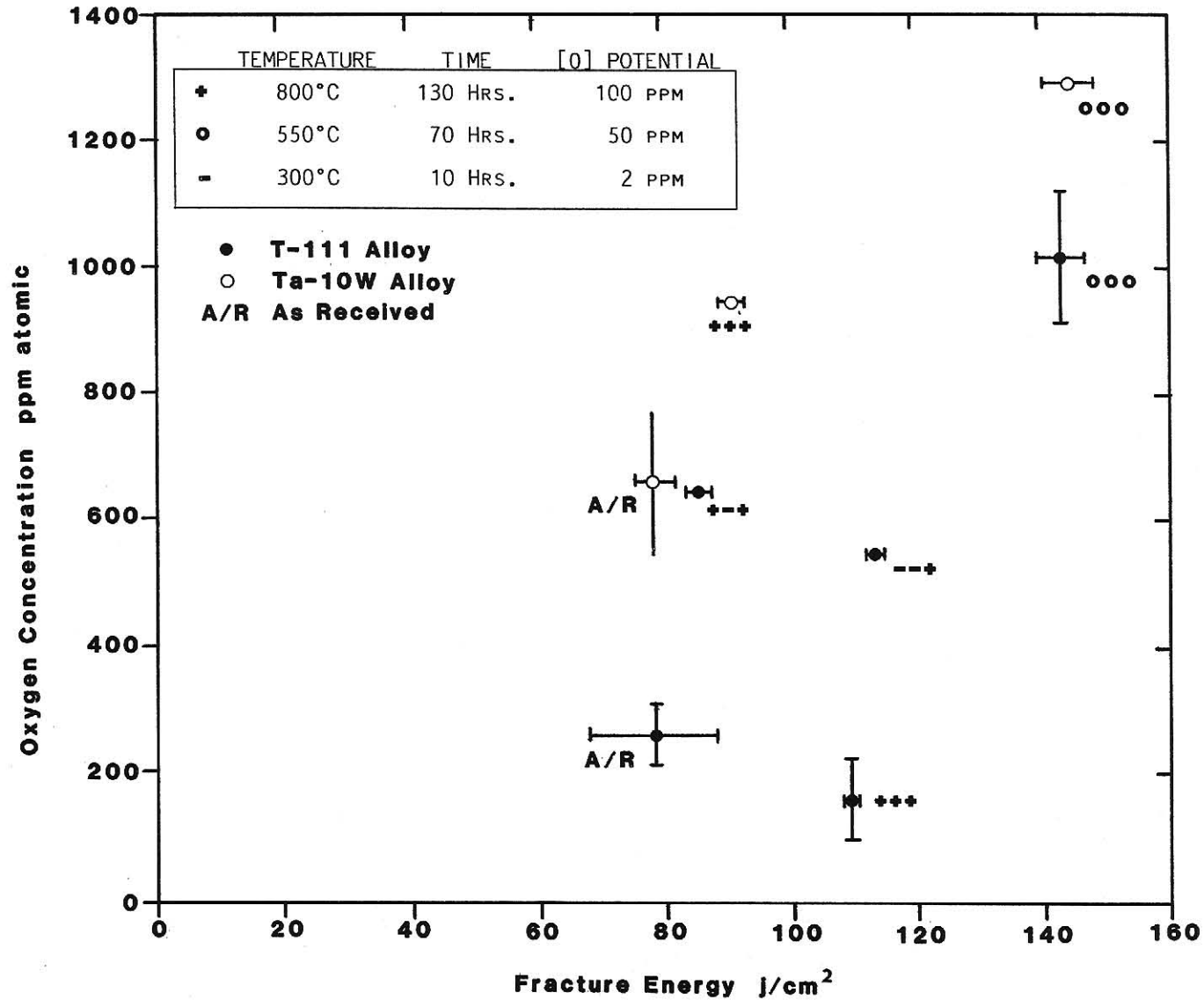
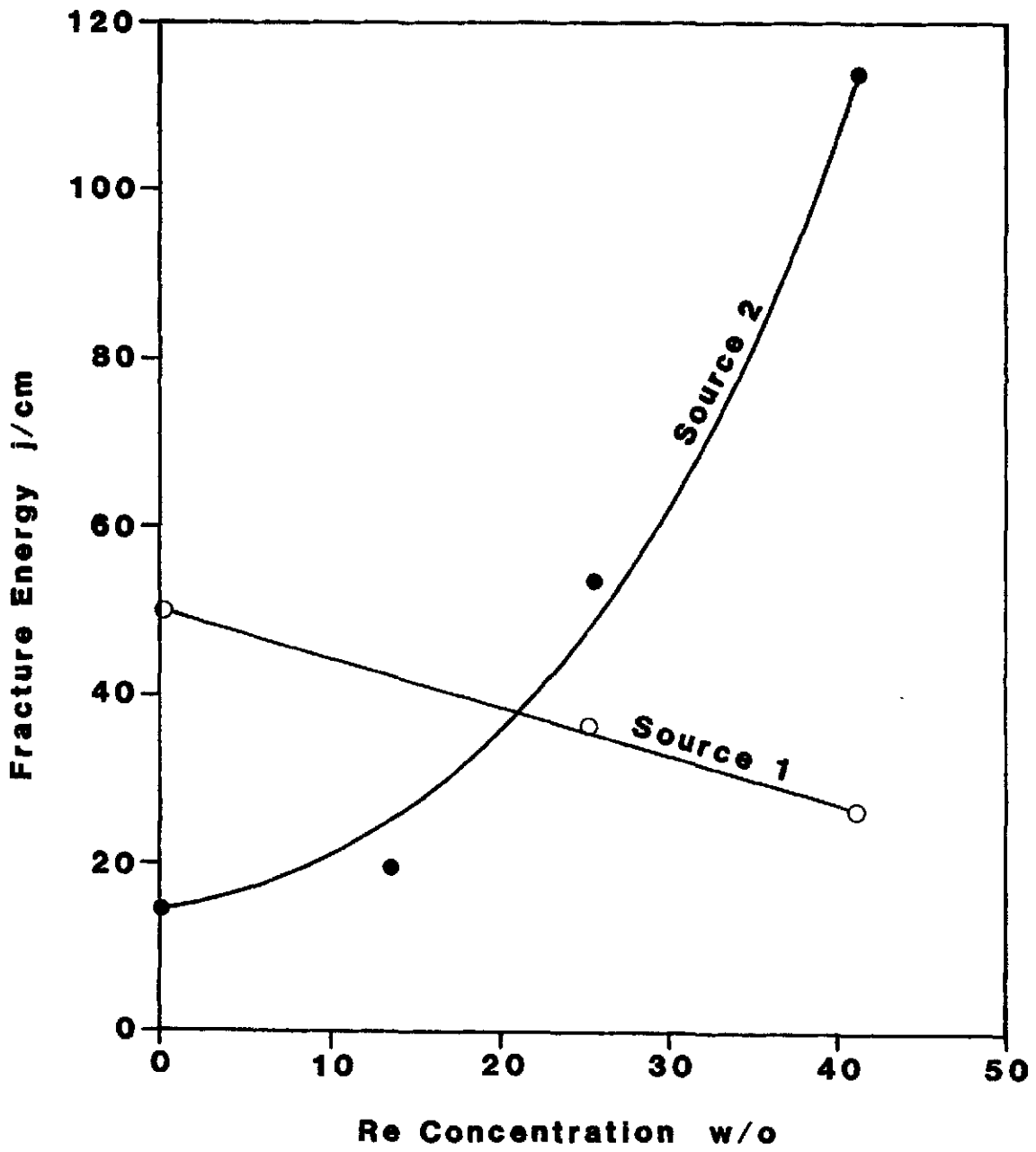


Fig. 131 TYPICAL METALLOGRAPH SECTIONS FOR SECOND Mo-41Re ALLOY TUBE.



Average Oxygen Concentration of Selected Ta-10W and T-111 Alloy Specimens as a Function of Fracture Energy

Fig. 132



EFFECT OF RE ADDITIONS ON THE FRACTURE ENERGY OF Mo.

Fig. 133

Table 1
Material Chemisty Analysis

	Typical Analysis Mo Source 1 wt. %	Typical Analysis W Source 1 wt. %	Typical Analysis Re (Wrought) wt. %	T-111 wt. %	Mo Source 2 wt. %	W Source 2 wt. %	Mo-13Re wt. %	W-26Re wt. %	TZM wt. %
Al	0.001	0.002	0.0005		0.002	0.001	0.002	0.001	0.0005
B			0.0001						
Ca	0.003	0.003	0.0001		0.002	0.003	0.002	0.003	0.002
Cb				0.065					
Cr	0.005	0.002	0.0003	<0.001		0.001		0.001	
Co			0.0003	<0.0005					
Cu	0.001	0.002	0.0002						
Hf				2.2					
Fe	0.005	0.003	0.007	<0.002	0.010	0.005	0.010	0.010	0.010
Pb	0.002	0.002							
Mg	0.001	0.002	0.0001				0.001		
Mn	0.001	0.002	0.0002						
Mo	99.95		0.0025	0.0015	99.93	0.030	87.0 ± 1	0.030	99.20
Ni	0.001	0.003	0.0001	<0.001		0.002	0.001	0.002	0.001
K			0.0001						
Re			99.97				13.0 ± 1	26.0 ± 2	
Si	0.003	0.002	0.0003		0.003	0.003	0.003	0.003	0.003
Sn	0.003	0.002	0.0002						
Ta				Bal.					
Ti	0.002	0.002	0.0002						0.4-0.6
W		99.95		8.2	0.030	99.95	0.010	74.0 ± 2	0.030
V				<0.001					
Zr			0.0001	<0.050					0.50-0.99
C	0.005	0.005	0.002	0.005	0.003	0.003	0.003	0.003	0.050
H			0.0005	0.00025	0.0005	0.0005	0.0005	0.0005	0.002
N			0.001	<0.0005	0.001	0.001	0.001	0.001	0.002
O			0.004	<0.005	0.005	0.003	0.005	0.003	0.050
S					0.002	0.0005	0.002	0.0005	0.002
P					0.002	0.005	0.002	0.005	0.002

Table 2
Recrystallization Conditions

Alloy	Temperature°C	Time/Hours
Ta-10W	1177	1.0
T-111	1177	1.0
Mo	1100	0.5
Mo-13Re	1600	0.5
Mo-26Re	1600	0.5
Mo-41Re	1530	1.0
Re	1530	0.5
Re-5W	1530	0.5
TZM	1530	0.5
W	2000	0.5

Table 3

Average Notch Specimen Fracture Energy for All Material Exposed to Sodium and for Material in the As-Received Condition

Alloy	Recrystallized and Exposed To Sodium		As-Received
	Notch Specimen Fracture Energy	Standard Deviation	Notch Specimen Fracture Energy
	joules/cm ²	joules/cm ²	joules/cm ²
Ta-10W	92.3	31.8	77.9
T-111	87.7	32.7	78.0
Mo(1)	58.2	18.9	71.3
Mo(2)	19.2	9.7	47.7
Mo-13 Re	33.3	12.8	57.0
Mo-26Re(1)	52.7	10.6	35.4
Mo-26Re(2)	60.9	25.9	108.8
Mo-41Re(1)	127.4	42.7	31.2
Mo-41Re(2)	158.9	40.5	155.0
TZM(1)	40.1	12.6	99.9
TZM(2)	48.9	12.6	63.9
Wrought Re	153.1	48.2	56.8
CVD Re	160.7	40.5	80.1
CVD Re-5W	161.6	39.7	105.5
W			7.3

Table 4

Average Notch Specimen Ultimate Tensile Strength for all Material Exposed to Sodium and for Material in the As-Received Condition

Alloy	Recrystallized and Exposed to Sodium		As Received
	Notch Specimen Ultimate Tensile Strength (UTS)	Standard Deviation	Notch Specimen (UTS)
	MPa	MPa	MPa
Ta-10W	768	22.1	813
T-111	764	52.4	809
Mo(1)	668	62.0	989
Mo(2)	368	74.4	646
Mo-13Re	442	40.7	759
Mo-26Re(1)	671	37.2	638
Mo-26Re(2)	645	153.0	1086
Mo-41Re(1)	1017	32.4	920
Mo-41Re(2)	1011	29.6	1360
TZM(1)	523	68.2	1053
TZM(2)	559	28.3	713
Wrought Re	955	48.3	826
CVD Re	842	27.6	827
CVD Re-5W	855	24.1	875

Table 5

Comparison of Notched and Smooth Specimen Fracture
Energy Before Exposure to Na

Alloy	Average Fracture Energy (joules/cm ²)	
	Notched	Smooth
Ta-10W	77.9	240.0
T-111	78.0	304.0
Mo(1)	71.3	289.0
Mo(2)	47.7	308.0
Mo-13Re	57.0	120.6
Mo-26Re(1)	35.4	81.4
Mo-26Re(2)	108.9	299.8
Mo-41Re(1)	31.2	312.8
Mo-41Re(2)	155.0	412.0
TZM(1)	99.9	198.2
TZM(2)	63.9	179.1
Wrought Re	56.8	-
CVD Re	80.1	320.5
CVD Re-5W	105.5	354.7
W	7.3	35.1

Table 6

Comparison of Notched and Smooth Specimen Ultimate Tensile Strength

Alloy	Average Ultimate Tensile Strength MPa	
	Notched	Smooth
Ta-10W	813	710
T-111	809	688
Mo(1)	988	878
Mo(2)	647	806
Mo-13Re	759	763
Mo-26Re(1)	638	632
Mo-26Re(2)	1086	999
Mo-41Re(1)	920	901
Mo-41Re(2)	1360	1201
TZM(1)	1053	1043
TZM(2)	713	643
Wrought Re	826	-
CVD Re	896	730
CVD Re-5W	875	718

Table 7

Average Rockwell A Hardness for all Sodium Exposure Conditions

Alloy	Recrystallized		As Received
	Average Hardness Rockwell A	Standard Deviation	Average Hardness Rockwell A
Ta-10W	58.2	1.1	59.1
T-111	58.2	1.2	58.5
Mo(1)	52.6	1.8	61.5
Mo(2)	51.2	1.7	53.7
Mo-13Re	49.9	1.6	62.0
Mo-26(1)	57.8	1.0	58.9
Mo-26(2)	57.8	1.8	65.9
Mo-41Re(1)	61.9	1.4	64.1
Mo-41Re(2)	62.2	1.3	70.0
Re (Wrought)	63.7	1.1	61.4
TZM(1)	53.4	1.4	64.0
TZM(2)	53.4	1.5	54.9

Table 8

Average Weight Change for all Sodium Exposure Conditions

Alloy	Average Weight Change mg	Standard Deviation mg
Ta-10W	-0.19	4.2
T-111	+0.75	3.9
Mo(1)	-0.83	4.0
Mo(2)	-3.5	1.8
Mo-13Re	-2.6	1.6
Mo-26Re(1)	+4.3	2.9
Mo-26Re(2)	-1.9	1.4
Mo-41Re(1)	+3.8	2.0
Mo-41Re(2)	-0.1	0.6
Re (CVD)	-2.4	1.1
Re (Wrought)	-1.8	0.8
Re-5W (CVD)	-2.8	1.7
TZM(1)	-4.7	3.3
TZM(2)	-2.3	1.9

Table 9
Fracture Energy Regression Survey

Alloy	R ²	F*	σ (j/cm ²)
Ta-10W	0.99	288.7	2.88
T-111	0.97	56.7	6.95
Mo(1)	0.45	1.16	19.17
Mo(2)	0.86	6.72	5.25
TZM(1)	0.78	5.2	8.00
TZM(2)	0.85	7.8	6.80
Mo-13Re	0.73	3.93	8.97
Mo-26Re(1)	0.71	3.58	7.73
Mo-26Re(2)	0.51	1.48	23.71
Mo-41Re(1)	0.91	13.4	16.91
Mo-41Re(2)	0.95	24.9	11.82
WRGT Re	0.94	27.0	14.64
CVD Re	0.92	13.8	15.69
CVD Re-5W	0.98	74.2	7.25

* Degrees of Freedom

Regression 7
Residuals 12
Total 19

Table 10

Notched Ultimate Tensile Strength Regression Survey

Alloy	R ²	F*	σ (MPa)
Ta-10W	0.90	12.77	9.1
T-111	0.91	18.40	19.1
Mo(1)	0.20	0.43	69.0
Mo(2)	0.59	2.03	67.7
TZM(1)	0.69	3.89	47.2
TZM(2)	0.35	0.90	29.1
Mo-13Re	0.68	3.62	28.9
Mo-26Re(1)	0.56	2.21	31.1
Mo-26Re(2)	0.30	0.75	160.1
Mo-41Re(1)	0.71	3.92	22.2
Mo-41Re(2)	0.73	4.62	19.4
WRGT Re	0.50	1.69	42.9
CVD Re	0.20	0.36	31.7
CVD Re-5W	0.49	1.62	21.6

* Degrees of Freedom

Regression 7
Residuals 12
Total 19

Table 11
Hardness Regression Survey

Alloy	R ²	F*	σ(R _A)
Ta-10W	0.52	1.52	0.99
T-111	0.75	5.21	0.76
Mo(1)	0.50	1.73	1.64
Mo(2)	0.45	1.18	1.62
TZM(1)	0.51	1.76	1.26
TZM(2)	0.46	1.46	1.40
Mo-13Re	0.47	1.55	1.49
Mo-26Re(1)	0.61	2.64	0.77
Mo-26Re(2)	0.61	2.64	1.42
Mo-41Re(1)	0.57	2.08	1.20
Mo-41Re(2)	0.24	0.55	1.50
WRGT Re	0.17	0.36	1.22
CVD Re	-	-	-
CVD Re-5W	-	-	-

* Degrees of Freedom

Regression 7
Residuals 12
Total 19

Table 12
Weight Change Regression Survey

Alloy	R ²	F*	σ (mg)
Ta-10W	0.87	9.24	2.5
T-111	0.79	6.50	2.2
Mo(1)	0.37	1.00	4.0
Mo(2)	0.96	31.26	0.5
TZM(1)	0.30	0.73	3.5
TZM(2)	0.98	75.10	0.4
Mo-13Re	0.96	37.26	0.4
Mo-26Re(1)	0.64	3.06	2.2
Mo-26Re(2)	0.57	2.29	1.1
Mo-41Re(1)	0.99	176.6	0.2
Mo-41Re(2)	0.37	1.00	0.6
WRGT Re	0.98	106.4	0.1
CVD Re	0.98	77.7	0.2
CVD Re-5W	0.75	5.17	1.1

* Degrees of Freedom

Regression 7
Residuals 12
Total 19

Table 13

Fracture Energy as a Function of Oxygen Potential
Normalized to Recrystallized Fracture Energy

Alloy	$\bar{Y}_{\text{As Rec'd}}$	$\bar{Y}_{\text{Recrystallized}}$	$\frac{\Sigma \bar{Y}\{2\text{ppmw}\{O\}\}}{\bar{Y}_{\text{Recrystallized}}}$	$\frac{\Sigma \bar{Y}\{50\text{ppmw}\{O\}\}}{\bar{Y}_{\text{Recrystallized}}}$	$\frac{\Sigma \bar{Y}\{100\text{ppmw}\{O\}\}}{\bar{Y}_{\text{Recrystallized}}}$
TA-10W (A)	77.9	80.0	0.81	1.80	1.27
T-111 (B)	78.0	76.9	0.78	1.84	1.15
Mo (C ₁)	71.25	49.2	1.42	1.24	1.31
Mo (C ₂)	47.7	17.1	0.84	1.61	1.29
Mo-13Re (E)	57.0	19.5	1.20	2.39	1.88
Mo-26Re (F ₁)	35.4	27.9	1.63	2.15	2.01
Mo-26Re (F ₂)	108.9	53.2	1.11	1.09	1.34
Mo-41Re (G ₁)	31.2	24.5	3.96	6.17	6.07
Mo-41Re (G ₂)	155.0	114.1	1.15	1.50	1.58
TZM (N ₁)	99.9	32.9	1.05	1.74	1.13
TZM (N ₂)	63.9	40.5	0.95	1.52	1.30
ReWRGT (K)	56.8	52.7	2.02	3.32	3.59
Re(CVD) (J)	80.1	77.5	1.64	2.27	2.37
Re-5W(CVD) L	105.5	87.0	1.46	2.01	2.19

Y = Fracture Energy Joules/cm²

Table 14

**Ta-10W Alloy Mechanical Properties and Weight
Change as a Function of Exposure to Sodium at Different
Oxygen Potentials**

I.D.	INDEPENDENT VARIABLES				DEPENDENT VARIABLES				
	T E M P.	T I M E	[O]	C O N D.	YST. C 0.2% OFFSET MPa	UTS MPa	FRACTURE ENERGY JOULES/CM ²	HARDNESS ROCKWELL A	WEIGHT CHANGE g x 10 ³
A23	-	-	-	A		823	66.8	56.2	-
A28	-	-	-	A		803	88.9	56.2	-
A27	-	-	-	A	616	715	195.4	56.2	-
A30	-	-	-	A	629	705	284.5	56.2	-
A25	+	+	-	A		770	72.2	55.1	+0.8
A29	+	+	-	A		776	74.3	56.4	+1.5
A5	+	+	-	R		775	76.3	57.6	+1.3
A15	+	+	-	R		77g	74.3	56.8	+1.5
A4	+	-	-	R		74g	4g.1	57.9	+3.3
A10	+	-	-	R		745	47.6	58.1	+2.2
A1	-	+	-	R		770	52.4	59.8	+0.9
A2	-	+	-	R		773	58.9	58.6	+0.6
A21	-	-	-	R		773	86.3	57.6	+0.7
A22	-	-	-	R		773	75.3	60.8	
A3	+	+	+	R		722	111.4	56.6	-16.1
A20	+	+	+	R		743	110.2	57.9	-13.4
A12	+	-	+	R		756	83.4	57.4	-0.7
A13	+	-	+	R		763	86.2	57.4	+1.8
A9	-	+	+	R		744	90.9	59.4	+1.6
A7	-	-	+	R		776	114.2	59.1	+0.6
A18	-	-	+	R		791	113.9	58.1	+1.3
A17	0	0	0	R		802	147.0	59.5	+0.5
A19	0	0	0	R		782	145.5	57.3	+1.3
A6	0	0	0	R		808	138.9	58.2	-1.9

----- = no exposure, R = recrystallized, A = as-received
 ◇ = smooth bar

	TEMPERATURE	TIME	[O] POTENTIAL	
+	800°C	130 hrs.	100 ppmw	$\bar{w} = 5.047 \text{ g} \pm 0.043 \text{ g}$
0	550	70	50	$\frac{Na}{A} = \frac{3.73 \text{ g Na}}{\text{cm}^2}$
-	300	10	2	$\frac{Na}{V} = \frac{50.1 \text{ g Na}}{\text{cm}^3}$

Table 15

T-111 Alloy Mechanical Properties and Weight
Change as a Function of Exposure to Sodium at Different
Oxygen Potentials

I. D.	INDEPENDENT VARIABLES				DEPENDENT VARIABLES				
	T E M P.	T I M E	[O]	C O N D.	YST. C 0.2% OFFSET MPa	UTS MPa	FRACTURE ENERGY JOULES/CM ²	HARDNESS ROCKWELL A	WEIGHT CHANGE g x 10 ³
B23	-	-	-	A		813	75.0	57.8	-
B24	-	-	-	A		804	81.0	57.1	-
B28	-	-	-	A	611	686	300.0	57.2	-
B29	-	-	-	A	646	689	308.0	57.6	-
B26	+	+	-	A		814	78.8	55.5	+0.2
B33	+	+	-	A		830	77.1	55.9	+0.2
B7	+	+	-	R		855	74.8	55.8	+1.3
B20	+	+	-	R		796	78.9	56.1	+1.3
B3	+	-	-	R		701	38.0	57.7	+1.0
B6	+	-	-	R		734	39.4	57.9	+1.1
B1	-	+	-	R		722	53.9	58.6	+0.4
B2	-	+	-	R		764	53.4	59.8	+0.5
B16	-	-	-	R		645	74.6	59.2	+1.3
B17	-	-	-	R		670	66.5	59.7	+1.3
B5	+	+	+	R		762	86.7	56.5	-5.0
B19	+	+	+	R		767	90.9	58.1	-11.6
B12	+	-	+	R		742	87.3	57.5	-2.6
B14	+	-	+	R		759	84.1	59.0	-10.6
B4	-	+	+	R		780	83.3	59.4	+0.3
B9	-	+	+	R		771	79.3	59.8	+0.7
B13	-	-	+	R		782	109.9	56.9	+0.6
B18	-	-	+	R		760	86.9	59.0	+0.6
B10	0	0	0	R		807	136.3	57.5	+0.3
B11	0	0	0	R		827	152.9	58.0	+0.8
B8	0	0	0	R		827	141.0	58.5	+0.4
B15	0	0	0	R		807	135.8	58.6	+0.2

----- = no exposure, R = recrystallized, A = as-received

◇ = smooth bar

$$\bar{w} = 4.716 \text{ g} \pm 0.034 \text{ g}$$

	TEMPERATURE	TIME	[O]	POTENTIAL	
+	800°C	130 hrs.	100 ppmw		$\frac{\text{Na}}{A} = \frac{4.88 \text{ g Na}}{\text{cm}^2}$
0	550	70	50		
-	300	10	2		

$$\frac{\text{Na}}{V} = \frac{53.7 \text{ g Na}}{\text{cm}^3}$$

Table 16

Hydrogen Concentration of Selected Ta-10W Specimens

Specimen I.D.	Exposure Conditions			[H] _{ppmat}
	T(°C)	t(hours)	[O] _{Na} (ppmw)	
A21	300	10	2	1167, 1041, 1831
A1	300	130	2	1759, 1921, 1759
A10	800	10	2	808, 682, 646
A5	800	130	2	108, 144, 108
A17	550	70	50	<18, <18, <18
A3	800	130	100	126, 108, 126

Table 17

Carbon Concentration of Selected Ta-10W Specimens

Specimen I.D.	Exposure Conditions			C_{ppmat}
	T(°C)	t(hours)	[O] _{Na} (ppmw)	
A28	-	-	-	753, 151
A21	300	10	2	<151
A10	800	10	2	301, 452
A5	800	130	2	452, 151
A6	550	70	50	603, 151
A13	800	10	100	753, 753

Table 18

Oxygen Concentration of Selected Ta-10W and T-111 Specimens

Specimen I.D.	Exposure Conditions			O_{ppmat}	\bar{O}_{ppmat}
	T(°C)	t(hours)	[O] _{Na} (ppmw)		
A23	-	-	-	339,226	282
A2	300	130	2	339,452	395
A19	550	70	50	905,1130	1018
A18	300	10	100	565	565
A12	800	10	100	678	678
A20	800	130	100	226, <111	168
A20+	800	130	100	2814	2814
A2+	300	130	2	1662	1662
A18+	300	10	100	2487, 1922	2205
A12+	800	10	100	2375, 2601	2488
B24	-	-	-	570, 792	736
B1	300	130	2	679, 792	681
B11	550	70	50	1357, 1357	1357
B5	800	130	100	792, 1130	961

+ Unetched samples

Table 19

Ta-10W and T-111 Ultimate Notched Tensile Strength and Fracture Energy as a Function of Crucible Material⁺

Specimen I.D.	UTS (mPa)		Fracture Energy (j/cm ²)	
	Nickel	316SS	Nickel	316SS
A24	773		82.4	
A26	812		103.1	
A4		749		49.1
A10		745		47.6
B25	796		108.3	
B27	742		82.9	
B3		701		38.0
B6		734		39.4

⁺ All specimens were recrystallized and exposed at 800°C, 10 hours in Na with low oxygen potential.

Table 20

Mo Mechanical Properties and Weight Change as a Function of Exposure to Sodium at Different Oxygen Potentials (Source 1)

I.D.	INDEPENDENT VARIABLES				DEPENDENT VARIABLES			HARDNESS ROCKWELL A	WEIGHT CHANGE g x 10 ³
	T E M P.	T I M E	[O]	C O N D.	YST. C 0.2% OFFSET MPa	UTS MPa	FRACTURE ENERGY JOULES/CM ²		
C6	-	-	-	A		989	70.9	61.5	
C8	-	-	-	A		989	71.6	61.5	
C11	-	-	-	A	811	879	303.8	61.3	
C12	-	-	-	A	802	876	275.0	61.7	
C34	+	+	-	A		982	79.5	57.2	+0.3
C9	+	+	-	A		945	72.7	57.7	+3.2
C19	+	+	-	R		715	60.4	51.6	-2.6
C10	+	+	-	R		695	44.6	53.1	-2.6
C7	+	-	-	R		671	42.8	49.5	+0.5
C18	+	-	-	R		664	42.3	49.3	+2.2
C1	-	+	-	R		701	57.9	50.5	+0.3
C3	-	+	-	R		677	44.9	52.6	+0.8
C35	-	-	-	R		685	62.5	52.7	+3.8
C37	-	-	-	R		666	50.2	51.5	+4.1
C13	+	+	+	R		691	68.7	53.6	+3.1
C22	+	+	+	R		607	41.6	50.8	+3.4
C26	+	-	+	R		682	69.8	53.0	+3.3
C28	+	-	+	R		682	28.4	53.5	-14.0
C20	-	+	+	R		677	62.1	54.9	+0.7
C25	-	+	+	R		665	62.5	54.6	+1.0
C14	-	-	+	R		696	107.8	53.3	+4.1
C24	-	-	+	R		701	73.6	51.1	+0.9
C30	0	0	0	R		687	73.7	54.7	+3.2
C31	0	0	0	R		684	73.7	54.7	+3.2
C5	0	0	0	R		698	70.5	55.9	+0.6
C21	0	0	0	R		422	25.7	51.8	+0.6

----- = no exposure, R = recrystallized, A = as-received
 ◇ = smooth bar

$$\bar{w} = 2.732 \text{ g} \pm 0.015 \text{ g}$$

	TEMPERATURE	TIME	[O] POTENTIAL
+	800°C	130 hrs.	100 ppmw
0	550	70	50
-	300	10	2

$$\frac{Na}{A} = \frac{4.94 \text{ g Na}}{\text{cm}^2}$$

$$\frac{Na}{V} = \frac{56.0 \text{ g Na}}{\text{cm}^3}$$

Table 21

**Mo Mechanical Properties and Weight
Change as a Function of Exposure to Sodium at Different
Oxygen Potentials (Source 2)**

I.D.	INDEPENDENT VARIABLES				DEPENDENT VARIABLES				
	T E M P.	T I M E	[O]	C O N D.	YST. C 0.2% OFFSET MPa	UTS MPa	FRACTURE ENERGY Joules/cm ²	HARDNESS ROCKWELL A	WEIGHT CHANGE g x 10 ³
C63	-	-	-	A		855	76.7	53.7	-
C70	-	-	-	A		439	18.6	53.7	-
C58	-	-	-	A	696	788	302.0	53.5	-
C60	-	-	-	A	744	823	331.9	53.6	-
C62	+	+	-	A		581	41.2	53.4	+3.6
C75	+	+	-	A		554	38.0	48.0	+4.4
C64	+	+	-	R		419	17.6	50.4	+0.3
C56	+	+	-	R		357	10.7	51.1	+0.4
C59	+	-	-	R		204	2.4	47.2	+1.1
C73	+	-	-	R		419	16.1	48.6	+1.0
C53	-	+	-	R		292	9.1	51.3	+1.9
C51	-	+	-	R		338	12.2	50.1	+4.0
C67	-	-	-	R		347	18.7	50.9	+5.0
C82	-	-	-	R		432	27.7	52.3	+4.7
C57	+	+	+	R		454	31.8	50.8	+6.4
C81	+	+	+	R		380	23.1	51.1	+6.4
C74	+	-	+	R		437	29.9	53.2	+4.3
C77	+	-	+	R		460	38.3	52.4	+4.8
C78	-	+	+	R		280	8.5	51.6	+3.6
C80	-	+	+	R		277	9.1	54.0	+3.7
C54	-	-	+	R		354	21.2	49.4	+3.7
C76	-	-	+	R		301	14.3	52.9	+3.6
C65	0	0	0	R		422	25.7	51.4	+3.6
C79	0	0	0	R		451	28.6	52.8	+3.8

----- = no exposure, R = recrystallized, A = as-received
 ◇ = smooth bar

$$\bar{w} = 4.301 \text{ g} \pm 0.029 \text{ g}$$

	TEMPERATURE	TIME	[O] POTENTIAL	
+	800°C	130 hrs.	100 ppmw	$\frac{Na}{A} = \frac{4.19 \text{ g Na}}{\text{cm}^2}$
0	550	70	50	
-	300	10	2	$\frac{Na}{V} = \frac{35.6 \text{ g Na}}{\text{cm}^3}$

Table 22

TZM Alloy Mechanical Properties and Weight Change as a Function of Exposure to Sodium at Different Oxygen Potentials (Source 1)

I.D.	INDEPENDENT VARIABLES				DEPENDENT VARIABLES				
	T	T	[O]	C	YST.	UTS	FRACTURE	HARDNESS	WEIGHT
	E	I		O	C 0.2% OFFSET		ENERGY	ROCKWELL	CHANGE
M	M		N	MPa	MPa	JOULES/CM ²	A	g x 10 ³	
P.	E		D.						
N23	-	-	-	A		1014	90.5	64.0	-
N29	-	-	-	A		1091	109.2	64.0	-
N24 ◊	-	-	-	A	941	1062	190.7	64.0	-
N25 ◊	-	-	-	A	913	1024	205.6	64.0	-
N32	+	+	-	A		449	57.1	57.4	+0.1
N34	+	+	-	A		449	19.1	61.7	-4.2
N6	+	+	-	R		649	44.6	52.5	+2.9
N20	+	+	-	R		567	27.8	51.2	+2.7
N8	+	-	-	R		566	27.9	52.9	+2.8
N15	+	-	-	R		598	36.7	51.1	+2.9
N1	-	+	-	R		512	27.4	52.8	+5.8
N2	-	+	-	R		527	30.7	51.5	+5.7
N17	-	-	-	R		552	47.1	52.5	+6.2
N18	-	-	-	R		434	34.5	55.0	+6.3
N3	+	+	+	R		429	26.9	52.8	+8.5
N19	+	+	+	R		391	25.9	55.9	+8.0
N11	+	-	+	R		540	45.8	54.5	+6.1
N12	+	-	+	R		447	30.6	53.7	+6.0
N7	-	+	+	R		530	52.1	53.8	+5.7
N9	-	+	+	R		557	50.7	54.2	+5.7
N10	-	-	+	R		416	26.1	54.5	+5.7
N14	-	-	+	R		480	38.9	55.1	+5.7
N13	0	0	0	R		569	49.6	51.7	+6.1
N16	0	0	0	R		551	48.7	53.6	+5.8
N4	0	0	0	R		573	64.6	53.5	+5.5
N5	0	0	0	R		556	65.6	55.5	+5.5

----- = no exposure, R = recrystallized, A = as-received
 ◊ = smooth bar

					$\bar{w} = 4.452 \text{ g} \pm 0.063 \text{ g}$
	TEMPERATURE	TIME	[O] POTENTIAL		
+	800°C	130 hrs.	100 ppmw		$\frac{Na}{A} = \frac{4.08 \text{ g Na}}{\text{cm}^2}$
0	550	70	50		
-	300	10	2		$\frac{Na}{V} = \frac{34.4 \text{ g Na}}{\text{cm}^3}$

Table 23

TZM Alloy Mechanical Properties and Weight Change as a Function of Exposure to Sodium at Different Oxygen Potentials (Source 2)

I.D.	INDEPENDENT VARIABLES				DEPENDENT VARIABLES				WEIGHT CHANGE g x 10 ³
	T E M P.	T I M E	[O]	C O N D.	YST. C 0.2% MPa	UTS MPa	FRACTURE ENERGY JOULES/CM ²	HARDNESS ROCKWELL A	
N76	-	-	-	A		716	68.6	54.9	-
N83	-	-	-	A		709	59.2	54.9	-
N79◇	-	-	-	A	503	673	251.5	54.9	-
N80◇	-	-	-	A	532	613	106.6	54.9	-
N75	+	+	-	A		691	51.8	54.5	+1.7
N81	+	+	-	A		673	47.5	52.8	+1.9
N55	+	+	-	R		496	30.4	50.4	-0.8
N66	+	+	-	R		585	31.7	53.6	-0.9
N58	+	-	-	R		572	30.9	53.8	-0.6
N67	+	-	-	R		564	28.4	50.2	-0.9
N51	-	+	-	R		573	42.7	53.4	+0.7
N52	-	+	-	R		547	40.3	54.3	+0.9
N53	-	-	-	R		565	53.9	53.0	+3.1
N62	-	-	-	R		532	50.0	50.7	+3.3
N61	+	+	+	R		558	51.2	54.2	+4.9
N69	+	+	+	R		483	36.8	53.0	+5.1
N59	+	-	+	R		564	49.7	52.1	+3.0
N60	+	-	+	R		579	52.6	54.5	+3.3
N68	-	+	+	R		581	58.5	55.2	+3.1
N70	-	+	+	R		575	59.2	54.1	+3.0
N63	-	-	+	R		554	51.2	54.5	+2.9
N64	-	-	+	R		576	62.9	54.2	+2.9
N56	0	0	0	R		578	61.1	53.4	+3.0
N57	0	0	0	R		552	49.3	53.4	+2.7
N54	0	0	0	R		546	63.5	54.6	+4.0
N65	0	0	0	R		602	72.7	55.7	+2.6

----- = no exposure, R = recrystallized, A = as-received
 ◇ = smooth bar

$$\bar{w} = 4.282 \text{ g} \pm 0.027 \text{ g}$$

	TEMPERATURE	TIME	[O] POTENTIAL	
+	800°C	130 hrs.	100 ppmw	$\frac{Na}{A} = \frac{4.16 \text{ g Na}}{\text{cm}^2}$
0	550	70	50	
-	300	10	2	

$$\frac{Na}{V} = \frac{35.7 \text{ g Na}}{\text{cm}^3}$$

Table 24

Mo-13Re Alloy Mechanical Properties and Weight Change as a Function of Exposure to Sodium at Different Oxygen Potentials

I.D.	INDEPENDENT VARIABLES				DEPENDENT VARIABLES			HARDNESS ROCKWELL A	WEIGHT CHANGE g x 10 ³
	T E M P.	T I M E	[O]	C O N D.	YST. C O.2% OFFSET MPa	UTS MPa	FRACTURE ENERGY JOULES/CM ²		
E74	-	-	-	A		753	54.9	62.0	-
E87	-	-	-	A		764	59.1	62.0	-
E75	-	-	-	A	712	779	145.9	62.0	-
E76	-	-	-	A	689	747	95.3	62.0	-
E77	+	+	-	A		859	78.1	55.2	+0.3
E79	+	+	-	A		811	74.3	54.6	+0.8
E57	+	+	-	R		441	25.8	48.3	-0.1
E62	+	+	-	R		441	26.3	50.8	-0.7
E53	+	-	-	R		429	22.2	45.7	-0.4
E67	+	-	-	R		433	20.9	49.3	-0.2
E51	-	+	-	R		422	20.6	49.8	+2.7
E52	-	+	-	R		387	16.4	49.6	+2.9
E68	-	-	-	R		420	30.9	51.1	+3.9
E69	-	-	-	R		398	24.1	49.7	+4.0
E54	+	+	+	R		441	34.7	51.6	+4.3
E70	+	+	+	R		480	43.1	51.2	+4.9
E59	+	-	+	R		479	43.6	48.8	+3.6
E60	+	-	+	R		525	56.2	48.0	+2.6
E55	-	+	+	R		40g	29.3	50.0	+2.9
E56	-	+	+	R		428	33.6	51.6	+3.0
E61	-	-	+	R		390	24.3	49.9	+3.4
E65	-	-	+	R		408	28.6	50.4	+3.4
E63	0	0	0	R		444	33.5	51.0	+2.2
E64	0	0	0	R		435	33.8	52.6	+3.6
E58	0	0	0	R		516	59.3	50.7	+3.0
E56	0	0	0	R		514	59.4	47.4	+3.4

----- = no exposure, R = recrystallized, A = as-received
 ◇ = smooth bar

	TEMPERATURE	TIME	[O]	POTENTIAL	
+	800°C	130 hrs.	100 ppmw		$\bar{w} = 4.545 \text{ g} \pm 0.037 \text{ g}$
0	550	70	50		$\frac{Na}{A} = \frac{4.19 \text{ g Na}}{\text{cm}^2}$
-	300	10	2		$\frac{Na}{V} = \frac{38.3 \text{ g Na}}{\text{cm}^3}$

Table 25

Mo-26Re Alloy Mechanical Properties and Weight Change as a Function of Exposure to Sodium at Different Oxygen Potentials (Source 1)

I.D.	INDEPENDENT VARIABLES				DEPENDENT VARIABLES				
	T E M P.	T I M E	[O]	C	YST. C 0.2% OFFSET MPa	UTS MPa	FRACTURE ENERGY JOULES/CM ²	HARDNESS ROCKWELL A	WEIGHT CHANGE g x 10 ³
F16	-	-	-	A		648	34.5	58.9	-
F23	-	-	-	A		627	36.2	58.9	-
F28	-	-	-	A	512	657	105.5	58.7	-
F29	-	-	-	A	535	606	57.3	58.9	-
F11	+	+	-	A		660	46.8	56.4	+0.4
F26	+	+	-	A		673	42.4	57.4	+0.3
F5	+	+	-	R		710	44.8	55.0	-1.0
F18	+	+	-	R		690	37.3	57.1	-1.0
F13	+	-	-	R		719	46.6	57.4	0
F21	+	-	-	R		734	45.9	58.1	-0.8
F2	-	+	-	R		662	37.3	57.8	-5.4
F3	-	+	-	R		673	41.7	57.7	+3.3
F22	-	-	-	R		638	57.9	56.8	-5.4
F27	-	-	-	R		643	52.8	58.0	-5.1
F7	+	+	+	R		689	65.4	58.4	-4.5
F24	+	+	+	R		714	69.4	58.2	-4.4
F8	+	-	+	R		631	48.3	58.4	-5.6
F14	+	-	-	R		729	69.0	58.7	-5.4
Fg	-	+	+	R		635	43.2	58.5	-5.7
F12	-	+	+	R		643	49.6	58.7	-5.8
F10	-	-	+	R		618	50.1	56.5	-5.7
F25	-	-	+	R		658	53.5	57.4	-5.8
F15	0	0	0	R		668	59.4	57.3	-6.0
F19	0	0	0	R		625	51.5	57.0	-6.0
F4	0	0	0	R		708	74.6	58.9	-5.6
F20	0	0	0	R		642	54.6	59.1	-9.7

----- = no exposure, R = recrystallized, A = as-received

○ = smooth bar

	TEMPERATURE	TIME	[O]	POTENTIAL	
+	800°C	130 hrs.	100 ppmw		$\bar{w} = 3.786 \text{ g} \pm 0.029 \text{ g}$
0	550	70	50		$\frac{Na}{A} = \frac{4.62 \text{ g Na}}{\text{cm}^2}$
-	300	10	2		$\frac{Na}{V} = \frac{51.5 \text{ g Na}}{\text{cm}^3}$

Table 26

Mo-26Re Alloy Mechanical Properties and Weight Change as a Function of Exposure to Sodium at Different Oxygen Potentials (Source 2)

I.D.	INDEPENDENT VARIABLES				DEPENDENT VARIABLES			HARDNESS ROCKWELL A	WEIGHT CHANGE g x 10 ³
	T E M P.	T I M E	[O]	C O N D.	YST. C 0.2% OFFSET MPa	UTS MPa	FRACTURE ENERGY JOULES/CM ²		
F74	-	-	-	A		1099	110.1	65.9	-
F81	-	-	-	A		1073	107.6	65.9	-
F73◇	-	-	-	A	866	993	299.3	65.9	-
F76◇	-	-	-	A	888	1004	300.2	65.9	-
F75	+	+	-	A		1048	103.5	61.3	+0.4
F83	+	+	-	A		1071	112.5	62.0	+0.9
F59	+	+	-	R		733	52.8	56.1	-0.2
F65	+	+	-	R		170	1.7	54.0	+0.8
F53	+	-	-	R		760	61.2	58.6	-0.1
F69	+	-	-	R		757	57.8	54.9	0.0
F51	-	+	-	R		536	23.1	57.1	+2.2
F52	-	+	-	R		693	49.5	57.9	+1.8
F58	-	-	-	R		736	85.2	59.5	+2.7
F63	-	-	-	R		715	84.6	58.1	+2.7
F60	+	+	+	R		751	93.8	60.0	+3.1
F70	+	+	+	R		720	84.4	60.0	+3.0
F54	+	-	+	R		707	67.7	56.1	+2.0
F57	+	-	+	R		532	32.1	58.1	+2.0
F67	-	+	+	R		676	70.1	58.8	+1.6
F68	-	+	+	R		722	84.7	59.7	+1.6
F55	-	-	+	R		652	59.1	59.3	+1.7
F64	-	-	+	R		695	77.0	59.4	+1.8
F61	0	0	0	R		618	55.3	56.8	+6.3
F56	0	0	0	R		716	85.4	57.0	+1.9
F64	0	0	0	R		687	77.3	59.4	+1.8
F62	0	0	0	R		318	14.6	55.3	+1.7

----- = no exposure, R = recrystallized, A = as-received
 ◇ = smooth bar

	TEMPERATURE	TIME	[O] POTENTIAL	$\bar{w} = 4.852 \text{ g} \pm 0.092 \text{ g}$
+	800°C	130 hrs.	100 ppmw	$\frac{Na}{A} = \frac{4.19 \text{ g Na}}{\text{cm}^2}$
0	550	70	50	
-	300	10	2	$\frac{Na}{V} = \frac{40.2 \text{ g Na}}{\text{cm}^3}$

Table 27

Mo-41Re Alloy Mechanical Properties and Weight
Change as a Function of Exposure to Sodium at Different
Oxygen Potentials (Source 1)

I.D.	INDEPENDENT VARIABLES				DEPENDENT VARIABLES			HARDNESS ROCKWELL A	WEIGHT CHANGE g x 10 ³
	T E M P.	T I M E	[O]	C O N D.	YST. C 0.2% OFFSET MPa	UTS MPa	FRACTURE ENERGY JOULES/CM ²		
G26	-	-	-	A		909	34.7	64.1	-
G30	-	-	-	A		931	27.7	64.1	-
G23 ◊	-	-	-	A	682	896	316.7	64.1	-
G25 ◊	-	-	-	A	735	906	308.9	64.1	-
G24	+	+	-	A		955	88.9	61.9	+1.1
G29	+	+	-	A		957	85.5	62.0	+0.8
G10	+	+	-	R		1040	59.9	61.1	-0.4
G16	+	+	-	R		979	76.8	57.1	-0.2
G9	+	-	-	R		980	72.4	62.1	-0.3
G14	+	-	-	R		1021	78.4	61.4	+0.1
G1	-	+	-	R		1085	108.3	62.1	-4.9
G2	-	+	-	R		1027	48.6	61.1	-5.3
G17	-	-	-	R		1040	157.9	61.8	-4.6
G18	-	-	-	R		1051	172.9	61.7	-4.1
G3	+	+	+	R		1006	153.2	63.2	-4.1
G19	+	+	+	R		971	126.4	63.6	-3.6
G6	+	-	+	R		975	112.8	61.6	-4.8
G12	+	-	+	R		991	116.5	61.5	-4.8
G4	-	+	+	R		1060	184.9	62.0	-5.1
G5	-	+	+	R		1044	166.5	62.5	-5.2
G8	-	-	+	R		1034	165.1	63.0	-5.3
G20	-	-	+	R		1040	164.3	61.1	-4.8
G15	0	0	0	R		1006	160.2	62.9	-5.2
G7	0	0	0	R		995	150.3	62.6	-5.2
G11	0	0	0	R		991	143.0	63.7	-5.3

----- = no exposure, R = recrystallized, A = as-received
◊ = smooth bar

	TEMPERATURE	TIME	[O] POTENTIAL	
+	800°C	130 hrs.	100 ppmw	$\bar{w} = 4.107 \text{ g} \pm 0.033 \text{ g}$
0	550	70	50	$\frac{Na}{A} = \frac{4.65 \text{ g Na}}{\text{cm}^2}$
-	300	10	2	$\frac{Na}{V} = \frac{53.4 \text{ g Na}}{\text{cm}^3}$

Table 28

Mo-41Re Alloy Mechanical Properties and Weight Change as a Function of Exposure to Sodium at Different Oxygen Potentials (Source 2)

I.D.	INDEPENDENT VARIABLES				DEPENDENT VARIABLES			HARDNESS ROCKWELL A	WEIGHT CHANGE g x 10 ³
	T E M P.	T I M E	[O]	C O N D.	YST. C 0.2% OFFSET MPa	UTS MPa	FRACTURE ENERGY JOULES/CM ²		
G75	-	-	-	A		1346	152.8	70.0	-
G76	-	-	-	A		1370	157.2	70.0	-
G73 ◊	-	-	-	A	1093	1187	425.3	70.0	-
G74 ◊	-	-	-	A	1117	1214	398.6	70.0	-
G78	+	+	-	A		1330	154.0	64.4	-0.5
G83	+	+	-	A		1316	154.6	63.6	-0.1
G62	+	+	-	R		1027	108.9	61.4	+1.3
G70	+	+	-	R		1046	118.2	59.5	0.0
G56	+	-	-	R		1009	92.8	60.4	+0.5
G68	+	-	-	R		998	89.5	65.0	+1.1
G51	-	+	-	R		1054	124.6	61.4	-0.1
G52	-	+	-	R		1031	110.6	62.0	-0.2
G63	-	-	-	R		1017	183.7	60.7	+0.5
G65	-	-	-	R		1047	224.3	62.0	+0.1
G66	+	+	+	R		986	174.0	62.9	+1.5
G69	+	+	+	R		944	149.6	64.1	-1.1
G57	+	-	+	R		975	149.1	60.6	+0.4
G58	+	-	+	R		982	159.3	62.6	+0.4
G53	-	+	+	R		1030	202.4	61.8	0.0
G55	-	+	+	R		1030	199.7	62.6	-0.4
G59	-	-	+	R		1000	183.0	63.6	-0.3
G64	-	-	+	R		1055	223.3	63.8	-0.3
G60	0	0	0	R		1013	177.3	61.7	-0.4
G61	0	0	0	R		1009	169.3	62.6	-0.2
G54	0	0	0	R		980	173.9	63.4	-0.1
G67	0	0	0	R		994	164.9	62.6	-0.4

----- = no exposure, R = recrystallized, A = as-received
 ◊ = smooth bar

	TEMPERATURE	TIME	[O] POTENTIAL	$\bar{w} = 5.357 \text{ g} \pm 0.076 \text{ g}$
+	800°C	130 hrs.	100 ppmw	$\frac{Na}{A} = \frac{4.20 \text{ g Na}}{\text{cm}^2}$
0	550	70	50	
-	300	10	2	
				$\frac{Na}{V} = \frac{41.0 \text{ g Na}}{\text{cm}^3}$

Table 29

Oxygen Concentration of Selected Mo and Mo Alloy Specimens

Specimen I.D.	Exposure Conditions			Oxygen Conc.* ppm at
	T(°C)	t(hours)	[O] _N ppmw	
C6	-	-	-	<59, 119
C1	300	130	2	<59, <59
C13	800	130	100	<59, <59
C63	-	-	-	<59, <119
C51	300	130	2	<59, <59
C57	800	130	100	<59, <59
E74	-	-	-	<67, <67
E51	300	130	2	<67, <67
E70	800	130	100	<67, <67
F16	-	-	-	150, <75
F2	300	130	2	<75, <75
F7	800	130	100	<75, <75
F74	-	-	-	<75, 150
F51	300	130	2	<75, <75
F70	800	130	100	<75, 150
G30	-	-	-	83, <83
G1	300	130	2	<83, <83
G3	800	130	100	<83, <83
G75	-	-	-	<83, 332
G52	300	130	2	<83, 250
G66	800	130	100	83, 83
N23	-	-	-	<59, <59
N2	300	130	2	599, 659
N3	800	130	100	1318, 719
N83	-	-	-	839, 958
N52	300	130	2	1857, 1677
N61	800	130	100	1617, 1617

*All samples etched.

Table 30

Wrought Re Mechanical Properties and Weight Change as a Function of Exposure to Sodium at Different Oxygen Potentials

I.D.	INDEPENDENT VARIABLES				DEPENDENT VARIABLES			HARDNESS ROCKWELL A	WEIGHT CHANGE g x 10 ³
	T E M P.	T I M E	[O]	C O N D.	YST. C 0.2% MPa	UTS MPa	FRACTURE ENERGY Joules/cm ²		
K23	-	-	-	A		840	57.4	61.4	-
K25	-	-	-	A		812	56.2	61.4	-
K24	+	+	-	A		913	90.4	63.2	0.0
K26	+	+	-	A		926	82.8	63.4	-0.3
K4	+	+	-	R		984	77.6	64.3	+0.2
K13	+	+	-	R		894	83.0	61.9	+0.4
K8	+	-	-	R		940	79.6	63.4	+0.4
K18	+	-	-	R		953	87.0	63.8	+0.3
K1	-	+	-	R		927	89.1	65.6	+2.1
K2	-	+	-	R		949	95.3	63.0	+2.3
K17	-	-	-	R		966	189.6	64.3	+2.6
K19	-	-	-	R		858	149.4	64.6	+2.7
K3	+	+	+	R		989	207.4	63.0	+2.4
K20	+	+	+	R		989	198.7	64.9	+2.5
K15	+	-	+	R		883	169.1	62.7	+1.9
K16	+	-	+	R		931	190.4	63.1	+2.0
K10	-	+	+	R		1037	203.3	62.2	+2.1
K11	-	+	+	R		1006	178.1	65.1	+2.0
K9	-	-	+	R		997	189.3	62.6	+1.8
K12	-	-	+	R		897	176.4	64.5	+2.0
K5	0	0	0	R		944	175.3	64.5	+2.1
K7	0	0	0	R		957	189.4	63.2	+1.7
K6	0	0	0	R		959	144.0	65.1	+2.0
K14	0	0	0	R		1033	190.7	62.9	+1.8

----- = no exposure, R = recrystallized, A = as-received
 ◊ = smooth bar

	TEMPERATURE	TIME	[O] POTENTIAL	
+	800°C	130 hrs.	100 ppmw	$\bar{w} = 6.767 \text{ g} \pm 0.076 \text{ g}$
0	550	70	50	$\frac{Na}{A} = \frac{4.61 \text{ g Na}}{\text{cm}^2}$
-	300	10	2	$\frac{Na}{V} = \frac{46.5 \text{ g Na}}{\text{cm}^3}$

Table 31

CVD Re Mechanical Properties and Weight Change as a Function of Exposure to Sodium at Different Oxygen Potentials

I.D.	INDEPENDENT VARIABLES				DEPENDENT VARIABLES			HARDNESS ROCKWELL A	WEIGHT CHANGE g x 10 ³
	T E M P.	T I M E	[O]	C O N D.	YST. C 0.2% MPa	UTS MPa	FRACTURE ENERGY JOULES/CM ²		
J26	-	-	-	A		851	69.9		-
J35	-	-	-	A		941	90.2		-
J23	-	-	-	A	452	735	335.7		
J24	-	-	-	A	487	725	305.2		
J29	+	+	-	A		862	103.2		0.0
J30	+	+	-	A		872	110.7		-0.1
J15	+	+	-	R		855	95.2		+0.2
J10	+	-	-	R		853	100.0		+0.3
J12	+	-	-	R		844	95.1		+0.1
J1	-	+	-	R		821	100.5		+2.7
J2	-	+	-	R		843	115.8		+2.9
J19	-	-	-	R		851	190.9		+3.2
J20	-	-	-	R		860	191.8		+3.0
J7	+	+	+	R		829	190.1		+3.5
J3	+	+	+	R		817	193.9		+3.4
J14	+	-	+	R		849	185.2		+2.5
J9	-	+	+	R		873	213.6		+2.9
J11	-	+	+	R		875	193.8		+2.7
J17	-	-	+	R		813	141.1		+2.8
J8	-	-	+	R		823	170.1		+3.1
J16	0	0	0	R		847	185.9		+2.4
J18	0	0	0	R		815	185.0		+2.5
J5	0	0	0	R		781	144.8		+2.8
J13	0	0	0	R		895	189.0		+2.5

----- = no exposure, R = recrystallized, A = as-received
 ◇ = smooth bar

	TEMPERATURE	TIME	[O] POTENTIAL	
+	800°C	130 hrs.	100 ppmw	$\bar{w} = 2.426 \text{ g} \pm 0.039 \text{ g}$
0	550	70	50	$\frac{Na}{A} = \frac{6.05 \text{ g Na}}{\text{cm}^2}$
-	300	10	2	$\frac{Na}{V} = \frac{130 \text{ g Na}}{\text{cm}^3}$

Table 32

CVD Re-5W Alloy Mechanical Properties and Weight
Change as a Function of Exposure to Sodium at Different
Oxygen Potentials

I. D.	INDEPENDENT VARIABLES				DEPENDENT VARIABLES			HARDNESS ROCKWELL A	WEIGHT CHANGE g x 10 ³
	T E M P.	T I M E	[O]	C O N D.	YST. C 0.2% OFFSET MPa	UTS MPa	FRACTURE ENERGY JOULES/CM ²		
L25	-	-	-	A		862	96.0		-
L32	-	-	-	A		889	114.9		-
L24◇	-	-	-	A	441	740	365.4		-
L26◇	-	-	-	A	246	695	343.9		-
L23	+	+	-	A		881	84.9		0.0
L30	+	+	-	A		889	85.8		+0.1
L3	+	+	-	R		867	106.9		+0.4
L14	+	+	-	R		880	100.3		+0.2
L7	+	-	-	R		863	93.2		+0.4
L18	+	-	-	R		849	101.8		+0.5
L1	-	+	-	R		854	111.2		+3.1
L2	-	+	-	R		834	114.7		+8.0
L19	-	-	-	R		867	190.2		+3.8
L20	-	-	-	R		869	194.3		+3.9
L5	+	+	+	R		868	207.5		+3.7
L12	+	+	+	R		867	196.3		+2.7
L4	+	-	+	R		874	183.5		+3.0
L13	+	-	+	R		825	175.2		+2.8
L10	-	+	+	R		835	181.1		+3.2
L15	-	+	+	R		898	193.6		+3.4
L6	-	-	+	R		893	202.6		+2.9
L8	-	-	+	R		844	182.6		+3.1
L11	0	0	0	R		816	181.4		+3.2
L16	0	0	0	R		822	169.6		+2.9
L17	0	0	0	R		851	171.2		+2.8
L9	0	0	0	R		820	175.7		+2.7

----- = no exposure, R = recrystallized, A = as-received

◇ = smooth bar

	TEMPERATURE	TIME	[O] POTENTIAL	
+	800°C	130 hrs.	100 ppmw	$\bar{w} = 2.384 \text{ g} \pm 0.119 \text{ g}$
0	550	70	50	$\frac{Na}{A} = \frac{6.00 \text{ g Na}}{\text{cm}^2}$
-	300	10	2	$\frac{Na}{V} = \frac{132 \text{ g Na}}{\text{cm}^3}$

Table 33

W Mechanical Properties and Weight Change as a Function of Exposure to Sodium at Different Oxygen Potentials

I. D.	INDEPENDENT VARIABLES				DEPENDENT VARIABLES			HARDNESS ROCKWELL A*	WEIGHT CHANGE g x 10 ³
	T E M P.	T I M E	[O]	C O N D.	YST. C 0.2% OFFSET MPa	UTS MPa	FRACTURE ENERGY JOULES/CM ²		
D12	-	-	-	A		549	26.4		-
D16	-	-	-	A		1129	67.3		-
D11 \diamond	-	-	-	A		497	53.9		-
D1	+	+	-	A		221	3.3		+1.7
D28	+	+	-	A		152	0.8		+1.5
D3	+	+	-	R		0	0		+0.8
D24	+	+	-	R		16	0		0.1
D26	-	+	-	R		0	0		
D2	+	+	+	R		0	0		+0.3
D29	+	+	+	R		20	2.4		-0.5
D23	+	-	+	R		30	0.1		-2.1
D27	+	-	+	R		171	2.9		-2.5
D8	-	+	+	R		0	0		
D31	-	+	+	R		78	0.5		-0.6
D6	-	-	+	R		123	0.9		-1.3
D25	-	-	+	R		26	0.4		-2.2
D32	0	0	0	R		32	0.3		-2.7
D33	0	0	0	R		128	4.9		-2.7
D20	0	0	0	R		52	0.3		-3.2

----- = no exposure, R = recrystallized, A = as-received
 \diamond = smooth bar * hardness not tested because of brittle nature of material

	TEMPERATURE	TIME	[O]	POTENTIAL	
+	800°C	130 hrs.	100 ppmw		$\bar{w} = 5.419 \text{ g} \pm 0.088 \text{ g}$
0	550	70	50		$\frac{Na}{A} = \frac{4.83 \text{ g Na}}{\text{cm}^2}$
-	300	10	2		$\frac{Na}{V} = \frac{53.4 \text{ g Na}}{\text{cm}^3}$

Table 34

Posttest Hardness of Tube Outer Surface
as a Function of Distance and Temperature
from the Bottom

Distance from Bottom (mm)	Hardness R _A					Approximate Temperature°C
	T-111	Ta-10W	Mo-41Re	CVD Re	Re-5W	
3.18		57.8				2000°C
6.35	61.0	57.9	61.8			2000°C
9.53	60.2	58.5	61.7			2000°C
12.70	63.1	58.6	61.9	30.0		2000°C
15.88	63.2	55.5	65.2	37.5	38.2	
19.05	61.2	58.9	64.8	50.0	40.9	
22.23	59.6	58.9	65.0	49.8	38.5	
25.40	62.2	58.5	65.0	45.1	41.3	1600°C
28.58	65.3	56.3	64.3	44.4	47.6	
31.75	67.0	57.2	66.0	44.9	51.2	1440°C
34.93	65.4	58.1	65.6	42.5	49.4	
38.10	65.1	58.0	65.5	45.8	51.0	1295°C
41.28	63.7	60.0	65.8	45.1	50.2	
44.45	56.9	60.0	65.9	50.1	49.5	1155°C
47.63	63.9	61.2	64.3	62.0	51.5	
50.80	61.9	58.0	64.0	61.8	50.9	1045°C
53.98	58.1	56.1	63.5	53.2	52.3	
57.15	62.1	55.2	62.5	49.8	57.0	970°C
60.33			63.0	55.3	58.4	
63.50				57.1	59.8	900°C

DISTRIBUTION:

Division of Reactor Safety Research (7)
Office of Nuclear Regulatory Research
U.S. Nuclear Regulatory Commission
Washington, DC 20555
Attn: C. N. Kelber
M. Silberberg
R. W. Wright (5)

Joint Research Center (10)
Ispra Establishment
21020 Ispra (Varese)
Italy
Attn: R. Klersy
H. Holtbecker
P. Fasoli-Stella
O. Simoni
P. Schiller (5)
H. Meister

Power Reactor & Nuclear Fuel
Development Corporation (PNC) (5)
Fast Breeder Reactor Development Project (FBR)
9-13, 1-Chome, Akasaka
Minato-Ku, Tokyo
Japan
Attn: A. Watanabe (2)
H. Nakamura
M. Saito
K. Takahashi

Monsieur A. Schmitt
IPSN/DSN
CEN Fontenay-aux-Roses
B. P. 6
92260 Fontenay-aux-Roses
France

Safety Studies Laboratory/DSN (3)
Commissariat a L'Energie Atomique
Centre d'Etudes Nucleaires de Cadarache
B. P. 1, 13115 Saint-Paul-lex-Durance
Bouches-du-Rhone
France
Attn: M. Bailly
M. Meyer Heine
G. Kayser

DISTRIBUTION (Continued)

Centre d'Etudes Nucleaires de Grenoble
B. P. 85-Centre de Tri
38401 Grenoble Cedex
France
Attn: D Rousseau/Pi-SEDTI

UKAEA (2)
Safety and Reliability Directorate
Wigshaw Lane
Culcheth
Warrington, WA3 4NE
England
Attn: M. Hayns
R. S. Peckover

Atomic Energy Establishment (2)
Winfrith, Dorchester
Dorset
United Kingdom
Attn: R. Potter (2)

Battelle Pacific Northwest Laboratories
Battelle Boulevard
Richland, WA 99352
Attn: F. E. Panisko

Kernforschungszentrum Karlsruhe (9)
Postfach 3640
D-75 Karlsruhe
West Germany
Attn: A. Fiege
G. Heusener (PSB)
P. Hoffmann (PSB)
H. Werle (INR)
L. Barleon (IRB)
G. Hoffman (IRM)
K. Thomauske (IRB)
U. Muller (IRM)
G. Fieg (INR)

Argonne National Laboratory (3)
Reactor Analysis and Safety Division
9700 South Cass Avenue
Argonne, IL 60439
Attn: L. Baker, Jr.
J. D. Gabor
R. D. Pedersen

DISTRIBUTION (Continued)

Westinghouse Hanford Co. (2)
337 Bldg., 300 Area
P. O. Box 1970
Richland, WA 99352
Attn: G. R. Armstrong
C. P. Cannon

EG&G Idaho (3)
P. O. Box 1625
Idaho Falls, ID 83415
Attn: E. Anderson
R. W. Miller
B. J. Buescher

Mass. Inst. of Tech. (1)
Mech. Eng. Dept.
Cambridge, MA 02139
Attn: P. Griffith

Westinghouse Electric Co. (1)
P. O. Box 10864
Pittsburg, PA 15236
Attn: A. Pieczynski
R. W. Buckmann

Cabot Corp. (1)
County Line Road
Boyertown, PA 19512
Attn: J. H. Chen

Department of Metallurgical Engr. (1)
Colorado School of Mines
Golden, CO 80401
Attn: G. Edwards

Special Metals Corp. (1)
New Hartford, NY 13413
Attn: W. H. Sutton

Teledyne (1)
Wah Chang Albany
1600 N.E. Old Salem Rd.
P. O. Box 460
Albany, OR 97321
Attn: P. M. O'Larey

DISTRIBUTION (Continued)

Metallurgical and Materials Engr. (1)
University of Pittsburg
848 Benedum Hall
Pittsburg, PA 15261
Attn: H. Brody

College of Engineering
1012 Engineering Bld.
University of California
Santa Barbara, CA 93106
Attn: R. Mehrabian

Martin Marietta Energy Systems, Inc. (4)
P. O. Box X
Oak Ridge, TN 87831
Attn: T. Kress
R. Cooper
G. M. Goodwin
J. De Van

Martin Marietta Energy Systems, Inc. (3)
Y-12 Plant
P. O. Box Y
Oak Ridge, TN 37831
Attn: J. Koger
G. Northcutt
B. Reis

Los Alamos National Laboratory (11)
Attn: C. A. Anderson J-576
M. Merrigan
L. Lundberg
W. Kirchner K-551
D. Sandstrom G-756
H. Casey
T. J. Trapp E-561
Roy Feber C-348 (4)

Rhenium Alloys Inc.
Elyria, OH 44035
Attn: J. Kish

Brookhaven National Laboratory
Upton, Long Island
New York, NY 11973
Attn: J. Weeks

DISTRIBUTION (Continued)

General Electric
Knolls Atomic Power Lab.
River Road
Schnectedy, NY
Attn: Richard Lupi

Rockwell International--Rocky Flats
Box 464
Golden, CO 80401
Attn: C. Edstrom

U. S. Department of Energy
Oak Ridge, TN 37831
Attn: Gene Chapman

1830	M. J. Davis	6420	J. V. Walker
1820	R. E. Whan	6421	T. R. Schmidt (5)
1832	W. B. Jones	6421	D. N. Cox
1832	R. J. Salzbrenner	6421	G. W. Mitchell
1832	J. W. Munford	6421	C. A. Ottinger
1832	J. Stephens	6422	D. A. Powers
1832	J. A. Van Den Avyle	6422	J. Gronager
1833	J. L. Jellison	6423	P. S. Pickard
1833	M. J. Cieslak	6423	A. Furutani
1833	F. M. Hosking	6425	W. J. Camp
1833	R. W. Fisher	6427	M. Berman
1833	A. A. Netz	6427	J. T. Hitchcock
1833	J. P. Maroone	6430	N. Ortiz
1833	F. J. Zanner (30)	6433	L. Cropp
1841	R. B. Diegle	6433	W. McCulloch
1841	W. R. Cieslak	6440	D. A. Dahlgren
1846	R. K. Quinn	6450	J. A. Reuscher
1846	W. F. Hammetter (2)	6451	T. F. Luera
1846	R. A. Sallach	6452	M. F. Aker
2520	N. J. Magnani	6452	J. Philbin
2523	N. A. Godshall	6454	G. L. Cano
2526	W. A. Averill	8024	M. A. Pound
3141	C. M. Ostrander (5)	8310	R. W. Rohde
3151	W. L. Garner (3)	8312	J. A. Brooks
6400	A. W. Snyder	8343	W. A. Swansiger
6410	J. W. Hickman	8347	K. Wilson
3154	C. H. Dalin (28)		